ROMA TRE
UNIVERSITÀ DEGLI STUDI

Dottorato in Scienze della Terra

XXXI CICLO

Tectonic evolution of northeastern Iran deduced by paleomagnetic investigations

Andrea Leonardo Visconti

Tutor: Prof. Francesca Cifelli

Co-tutor: Prof. Massimo Mattei

Table of contents

ABSTRACT

In this thesis, an extensive paleomagnetic sampling (70 sites) was carried out in north-eastern Iran along the Allah Dagh, Binalud and Kopeh Dagh mountain belts, with the aim of reconstructing the rotation history and evaluating oroclinal processes of this portion of the Eurasia-Arabia collision area, as well as assessing whether the studied sediments have a magnetic fabric dominated by sedimentary or tectonic processes. I sampled the red beds units from the Lower Cretaceous Shurijeh Fm. and from the Middle-Upper Miocene Upper Red Fm (URF). Paleomagnetic results from all the sampled areas show a homogeneous amount of CW rotations measured in both the Lower Cretaceous Shurijeh Fm. and Middle-Late Miocene URF. These paleomagnetic results suggest that the oroclinal bending process that caused the curvature of mountain belts in northern Iran after the Middle-Late Miocene, also extended to the northeastern border of the Arabia-Eurasia deforming zone.

AMS data has been integrated with paleomagnetic results, confirming the predominance of Arabia-Eurasia collision process as fundamental tectonic element which drove all the magnetic fabric configuration detected on the red beds units. The integration with previous paleomagnetic results and GPS, seismological, geomorphological and structural data available in the area, allowed to propose a hypothesis of tectonic evolution of the north Iran-Caspian Sea area, from Middle-Late Miocene to Present.

In the proposed model, the initiation of the oroclinal bending processes in northern Iran occurred about 6-4 Myr ago, related to the impinging of Central Iran between the South Caspian block and the southern margin of the Turan platform, caused by the northward subduction of the South Caspian basement under the Apsheron-Balkan Sill. As paleomagnetic results are inconsistent with the present-day kinematics of the northern Iranian blocks, as depicted by seismicity and GPS data, this suggests that the tectonic processes responsible for the bending of northern Iran mountain chains are no longer active. Moreover, data suggest that the westward motion of the South Caspian block, accommodated by the opposite strike-slip motion along the Ashkhabad and Shahrud faults, occurred very recently (~2 My ago).

In conclusion, data from this thesis helped to better understand the recent tectonic evolution of Northern Iran. In particular, paleomagnetic data were used to speculate that the initiation of the northward subduction of the South Caspian basin below the Apsheron-Balkan Sill and the westward extrusion of the South Caspian block did not occur at the same time, with the former occurring between the late Miocene and the Pliocene, and the latter during the Pleistocene.

1. INTRODUCTION

1.1. Introduction to the scientific topic

The study of crustal deformation is one of the most fascinating aspect of the geosciences, for this reason the interesting results acquired in the last decades on the importance of the continental crustal rotations around a vertical axis, have acquired a fundamental meaning for the interpretation of continental deformation.

Along the plate margin, in the arc-shaped mountain belts, passive rotations may be common and are generally detected by studying of structural rotated markers, such as thrust, beds, fold axes, faults (Freund, 1970; Marshak, 1988; Schreurs, 1994). The development of paleomagnetic analysis supported a rapid evolution of the knowledge about such rotations. In fact these studies, combined with structural analysis, are fundamental in the comprehension of the tectonic evolution of several continental deforming zones. During the past few decades, paleomagnetism has been used as a fundamental tool to assess kinematic models of curved orogenic systems around the world because of its great potential in quantifying vertical axis rotations. The combination of structural and paleomagnetic data represents a traditional approach for determining whether the curvature of a mountain belt has a primary or secondary origin and, in general, for constraining its tectonic evolution. Paleomagnetic data reveal rotations comparing the resulting paleomagnetic declinations within the deforming region with those found in coeval rocks collected in the regions outside the deforming zone (e.g., Eldredge et al., 1985; Lowrie and Hirt, 1986; Nur et al., 1989; Oldow et al., 1990; Pierre et al., 1992; Ron et al., 1984; Tait et al., 1996; among many others).

Ferromagnetic minerals are the basic elements of each paleomagnetic study, being able, to record the geomagnetic field at the time of formation of rocks. In all sedimentary rocks there are ferromagnetic minerals with varying concentrations (parts per billion in limestones), enough to provide in many cases a measurable characteristic magnetic signal.

Among the different structural markers, the anisotropy of magnetic susceptibility (AMS) has been increasingly used in association with paleomagnetic analyses to investigate the origin of curved orogens (e.g., Weil and Yonkee, 2012). In fact, in curved fold and thrust belts the orientation of the magnetic lineation often strictly follows the curvature of the orogen, being therefore representative of its structural trend. Therefore, AMS studies represent a unique instrument, which may provide significant markers of the strain patterns that affect the stratigraphic series during the time. However, is important taken into account that the results obtained from AMS can be affected by other factors, which may overprint the primary syn-sedimentary tectonic imprint.

Early sedimentary processes, such as paleocurrents or differential compaction structures, are able to influence the rock magnetic fabric (e.g., Felletti et al., 2016; Lowrie and Hirt, 1987; Piper et al., 1996; Pueyo Anchuela et al., 2013; Rees, 1965).

In addition, there are other aspects of magnetic behaviour that can mislead the interpretation of magnetic fabrics. Among these, as shown by Ihmlé et al. (1989), the inverse magnetic fabrics in magnetite, as well as all those processes that allow the crystallization of new magnetic phases. New minerals in fact, can develop in association with significant variations of thermal/pressure condition, for example fluids circulation, plutonic rocks intrusion or metamorphism processes.

The preliminary characterization of magnetic minerals is therefore a fundamental step, useful to identify those minerals responsible of secondary magnetizations. In fact the occurrence of remagnetizations in sedimentary contexts has occurred often (e.g., Kent, 1985), usually associated to frequent processes as fluids circulation (e.g., Van Der Voo and Torsvik, 2012; Witte and Kent, 1991), organic matter maturity (e.g., Blumstein et al., 2004) or any other mechanisms correlated with sedimentary burial (Aubourg et al., 2012; Banerjee et al., 1997; Katz et al., 1998).

Northern Iran represents a unique tectonic framework to use paleomagnetism for reconstructing the history of intracontinental deformation within plates, being characterized by a complex history of deformation, dominated by the long-standing convergence history between Eurasia and Peri-Gondwana Terranes. Kopeh Dagh region is a crucial area, which today represents the northeastern side of the Arabia-Eurasia collision zone, where the convergence is divided into compressional and strike-slip components as discussed by several authors which have mainly investigated active tectonics in the central and eastern part of the chain (Bretis et al., 2012; Hollingsworth et al., 2010, 2008, 2006; Robert et al., 2014; Shabanian, 2012; Shabanian et al., 2009b, 2009a). Although the Kopeh Dagh region was considered part of stable Turan block, it's seem clear that was affected by important deformation processes, which have modified its structural configuration at different times; for this reason, the study area represent a good target for understanding the Post Cimmerian evolution of northeastern part of the iranian region and for better comprehend the main tectonic processes of the area

The recent study about the oroclinal bending in the Alborz Mountains (Mattei et al., 2017) outlined how this important range can be considered a secondary arc that originated as a linear mountain belt and that progressively acquired its present day curved shape by means of opposite vertical axis rotations occurring along its strike. Kopeh Dagh mountain chain is the eastern prosecution of this oroclinal system, despite being a linear fold and thrust belt with a moderate

curvature. As argued by Mattei et al. (2017), the curvature of Alborz arc was entirely acquired after the middle-late Miocene, which is the age of the Upper Red Formation (URF).

In the recent years, paleomagnetic research in Iran has mainly been focused on the reconstruction of the late Paleozoic–early Mesozoic northward drift of the Cimmerian blocks (Besse et al., 1998; Muttoni et al., 2009b, 2009a). Conversely, few paleomagnetic data are available from Jurassic to Cenozoic units (Ballato et al., 2008; Cifelli et al., 2015; Mattei et al., 2014, 2012; Soffel et al., 1996; Wensink, 1982, Bina et al., 1986) leaving the post-Cimmerian history of central Iran poorly constrained. In this thesis, the study has focused on the Post-Cimmerian evolution of the Kopeh Dagh in order to understand if the deformation history of Kopeh Dagh belt was interested by a similar evolution during the Post Cimmerian phase. The role of paleomagnetic rotations in the origin and tectonic evolution of Kopeh Dagh mountain chain was never investigated, with the exception of the northwestern part of the belt, in Turkmenistan, where Bazhenov (1987) carried out a paleomagnetic study of the Cretaceous and Paleogene sedimentary successions.

In order to fill this gap in paleomagnetic information, the thesis was focused on an integrated AMS and paleomagnetic study from the Kopeh Dagh range, in a wide area between 57° and 60° of longitude where suitable Cretaceous and Miocene formations crop out.

1.2. Objectives and methodological strategy

During the past few decades, paleomagnetism and magnetic fabric studies were increasingly used in tectonic studies as tools for defining the deformational history of rocks (e.g., Borradaile and Henry, 1997; Cifelli et al., 2005; Jackson and Tauxe, 1991; Kissel, 1986; Mattei et al., 1997; Rochette et al., 1992; Tarling and Hrouda, 1993), the latitudinal drift of continental blocks (Besse and Courtillot, 2002; Kent and Irving, 2010; Muttoni et al., 2013, 2009b, 2009a), and the role of crustal block rotations in the evolution of curved tectonic structures (e.g., Carey, 1955; Eldredge et al., 1985; Marshak, 1988; Van der Voo et al., 1997; Cifelli et al., 2015, 2008; Lowrie and Hirt, 1986; Mattei et al., 2017; Tait et al., 1996; Weil and Sussman, 2004)

Paleomagnetism has been shown to be a powerful tool to gauge the amount and sense of vertical-axis block rotations in different tectonic settings (e.g., Cifelli et al., 2008; Mattei et al., 2004; McKenzie and Jackson, 1986; Nur and Ron, 1987; Ron et al., 1990; Terres and Luyendyk, 1985; Wells and Hillhouse, 1989). The spatial and temporal relationship between deviations in structural trend and the vertical axis rotations that took place within the belt, arcuate belts have been interpreted as primary, secondary or composite features (Weil and Sussman, 2004).

Besides paleomagnetism, numerous studies have shown that the Anisotropy of Magnetic Susceptibility (AMS) can be related to mineral and tectonic fabrics and that it can be successfully employed in the field of structural geology as a powerful tool for fabric analysis in different rock types (e.g., Borradaile and Henry, 1997; Cifelli et al., 2005; Jackson and Tauxe, 1991; Kligfield et al., 1981; Mattei et al., 1997; Rochette et al., 1992; Tarling and Hrouda, 1993).

In this thesis, AMS and paleomagnetic analyses were used for deciphering the origin of magnetic lineation in weakly deformed sedimentary rocks and for reconstructing the tectonic rotations which affected the northeastern part of Iran since the Cretaceous time, evaluating possible oroclinal processes within the Arabia-Eurasia collision zone. Paleomagnetic and fabric magnetic measurements on the rock collection from the Kopeh Dagh range were carried out with a 2-fold purpose: evaluating oroclinal processes within the Arabia-Eurasia collision zone, and assessing whether the studied sediments have a fabric dominated by sedimentary or tectonic processes. In particular, the Cretaceous sediments of the Shurijeh Formation and the Miocene Upper Red Formation (URF) were analyzed to test for the first time with paleomagnetic data the origin (primary versus secondary) of this orogenic arc.

1.3. Outline of the thesis

This thesis is structured in eight chapters. After the present chapter, focused on introducing the study and the pursued objectives, the second chapter describes the geological framework in which the study is focused, the Kopeh Dagh Range. A general overview on the geologic evolution of Cimmerian microcontinents drift is reported as well as a detailed description of stratigraphic sequence of Kopeh Dagh Basin. In this chapter, a detailed description of the sampled sedimentary units and a characterization of the present tectonic setting are also reported.

The third chapter includes the descriptions of all methods adopted during the development of this study together with a synthetic overview of the paleomagnetic studies related to the thesis topic. Besides a specific description of the selection and sampling of study area, the paleomagnetic and non-paleomagnetic techniques involved to collect the main information about the magnetic mineralogy, the magnetic anisotropy and the paleomagnetic components of the sampled units.

The second part describes the main results obtained starting with the fourth chapter. In this chapter the magnetic mineralogy characteristics are accurately described highlighting the different contribution of magnetic minerals for the two sampled formations, besides within each sampling sites, depending to the geographic position and alteration conditions.

The subsequent two chapters constitute the main block of the results in this dissertation, through the AMS and paleomagnetic studies developed in the study area.

The fifth chapter tackles the tectonic deformation evolution of study area using the Anisotropy of Magnetic Susceptibility results. Using AMS data has been possible to obtain a magnetic fabric characterization for each sampling sites as well as for the sedimentary units studied around the range. The sixth chapter has been focused on the paleomagnetic analysis of rotational history of study area and other around, as well as together with recent work has been reconstruct the evolution of oroclinal bending of Alborz-Kopeh Dagh mountain system. This chapter has been published as: *Clockwise paleomagnetic rotations in northeastern Iran: Major implications on recent geodynamic evolution of outer sectors of the Arabia-Eurasia collision zone in Gondwana Research* 71 (2019), pages 194–209.

Finally in the third part of the thesis results presented along this dissertation are summarized in a general discussion. Chapter eight conclude this thesis, showing the main approached points.

2. GEOLOGICAL SETTING

The wide continental deformation driven by the Arabia-Eurasia collision, makes the Iranian plateau one of the largest regions of convergent deformation on the Earth. The iranian intracontinental deformation is concentrated in several mountain belts, which surround the northern and southern border of Iran. This region is, in fact, the result of the various tectonic processes, including continental collision (Zagros, Greater Caucasus, Alborz, Kopeh Dagh and Talesh), subduction of oceanic lithosphere (Makran and Apsheron Balkan Sill) and an abrupt transition between a young orogen (Zagros) and a subduction zone (Makran) (Allen et al., 2006; Vernant et al., 2004) (Fig. 2.1).

Iran is characterized by a complex history of deformation, dominated by the long-standing convergence between Eurasia and Perigondwanan terranes. During Middle to Late Triassic, the northward drift of Gondwanan terranes caused the closure of the Paleotethys Ocean, separating the Eurasian Plate from Central Iranian blocks, and their collision against the southern margin of Eurasia, with the developing of the Eo-Cimmerian orogeny (e.g., Zanchetta et al., 2013). This process also caused the progressive opening of the Neotethys ocean on the southern margin of the Central Iranian blocks, that starting in the Permian, it covered all the Triassic time. The subsequent northward subduction and the progressive closure of the Neotethys ocean were accompanied by the opening of small back-arc basins during the Early Cretaceous, and during the Late Cretaceous, testified by the presence of several ophiolitic units surrounding Central Iran (Agard et al., 2011, as show in Fig.2.1). These oceanic basins started to subduct during the Late Cretaceous (Bröcker et al., 2013; Saccani et al., 2010) and were closed during Paleocene to Eocene times (Agard et al., 2011). This phase was followed during Late Tertiary to present-day by intracontinental deformation related to the closure of the Neotethys ocean and to the Arabia-Eurasia continental collision (Allen et al., 2003; Ballato et al., 2013, 2011; Berberian, 1983; Ganser and Huber, 1962; Guest et al., 2006a, 2006b; Jackson et al., 2002; Rezaeian et al., 2012; Stöcklin, 1974; Zanchi et al., 2009b, 2006). This latter orogenic phase is testified by intracontinental mobile belts (Talesh, Zagros, Alborz, and Kopeh Dagh ranges) that surround moderately aseismic crustal blocks (Central Iran, South Caspian and Lut blocks), which accommodated a relative small amount of shortening, by subduction beneath the central Caspian Sea (Aspheron-Balkhan Sill) and Makran, and by N–S right-lateral and E-W left lateral fault systems in Central and Eastern Iran (Fig. 2.1).

The overall convergence between the Eurasian and Arabian plates, is the result of a combination of Africa-Eurasia and Arabia-Eurasia motion, that is approximately N-S; the GPS-derived velocity for the northern margin of the Arabia plate is 18±2mm/yr relative to Eurasia at longitude 48°E (McClusky et al., 2000). The convergence rate increases eastward because the Arabia-Eurasia Euler pole lies in the Mediterranean area and is roughly 10mm/yr higher in eastern Iran than in the western part (Allen et al., 2004; Vernant et al., 2004). East of 58°E most of the total shortening (26 mm/yr) is accommodated by the Makran subduction zone (19.5 ± 2 mm/yr) and less by the Kopeh Dagh (6.5 ± 2 mm/yr) (Vernant et al., 2004). GPS data (Fig.2.2) show that shortening rates across the Turkish-Iranian plateau, between the Alborz and Zagros mountains, are only ~2 mm/yr at the most (Vernant et al., 2004). Active strike-slip faults deform parts of the plateau, especially in eastern Anatolia and NW Iran west of 48°E, with ~NE-SW trending left-lateral and ~NW-SE trending right lateral faults (Allen et al., 2011).

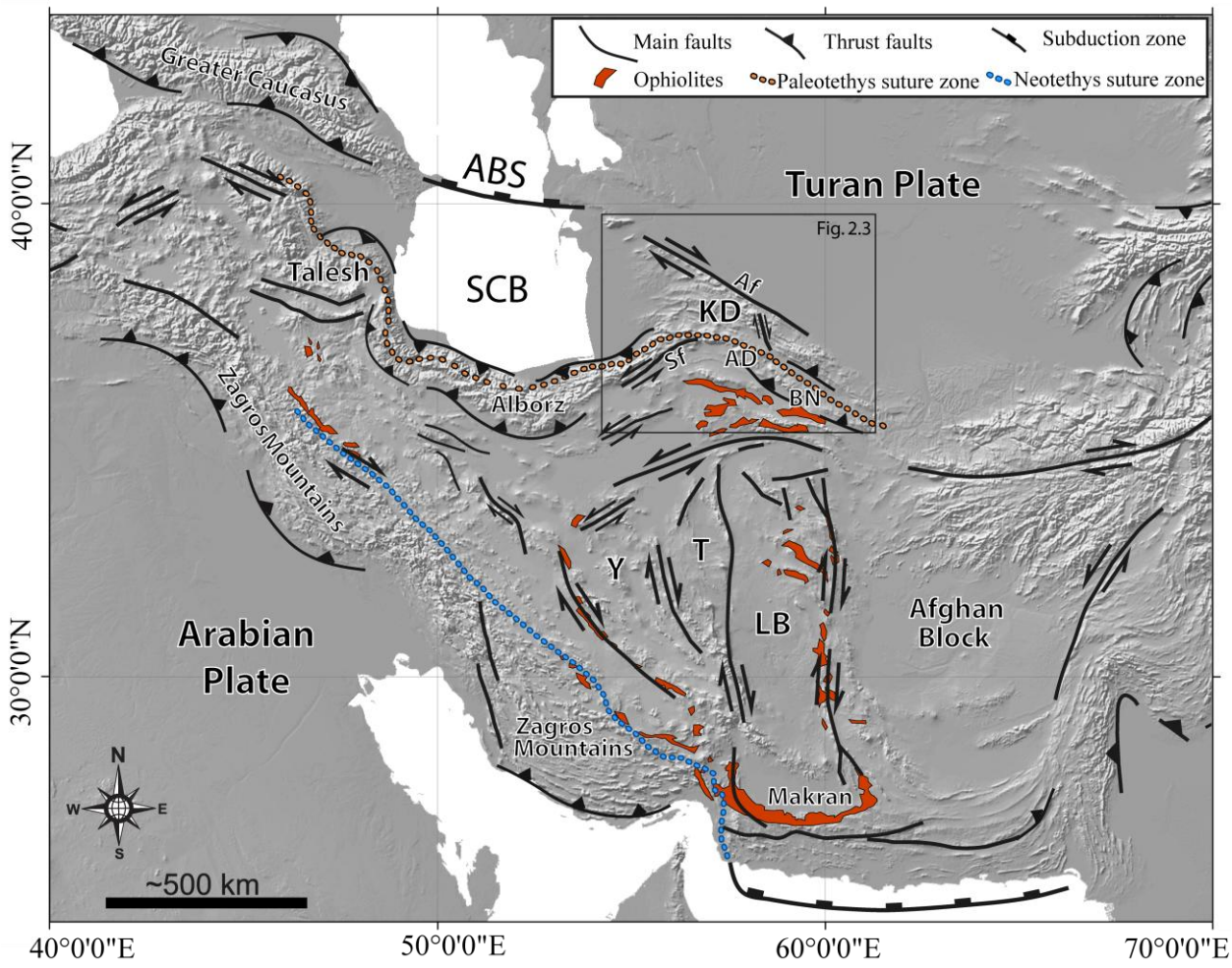

Fig.2.1. *Schematic tectonic map of Iran. The main present day tectonic features are reported together with ophiolites and the Paleotethys and Neotethys sutures. Af = Ashgabat Fault; BN = AD = Allah Dagh; Binalud Mts.; KD = Kopeh Dagh; LB =Lut Block; Y= Yazd Block; T= Tabas Bloc; SCB= South Caspian Basin; ABS= Apsheron-Balkan Sill; Sf = Shahrud Fault.*

North-eastern Iran represents a key area for the understanding of these geodynamic processes, being interested by both the Cimmerian orogeny and by Tertiary to present-day deformation related to Arabia-Eurasia collision. In fact, the Paleotethys suture zone corresponds to the boundary between the Kopeh Dagh fold-and-thrust belt to the NE, and the eastern prolongation of the Alborz range to the NW (Fig. 2.1). Remnants of the Paleotethys Ocean are located within the Binalud Mountains where the Cimmerian event was characterized by collision during the Late Triassic/Early Jurassic (Sheikholeslami and Kouhpeyma, 2012), followed by the deposition of sedimentary units of Kopeh Dagh Basin on the southern margin of the Eurasian Plate, from Jurassic to the Tertiary (Brunet et al., 2003).

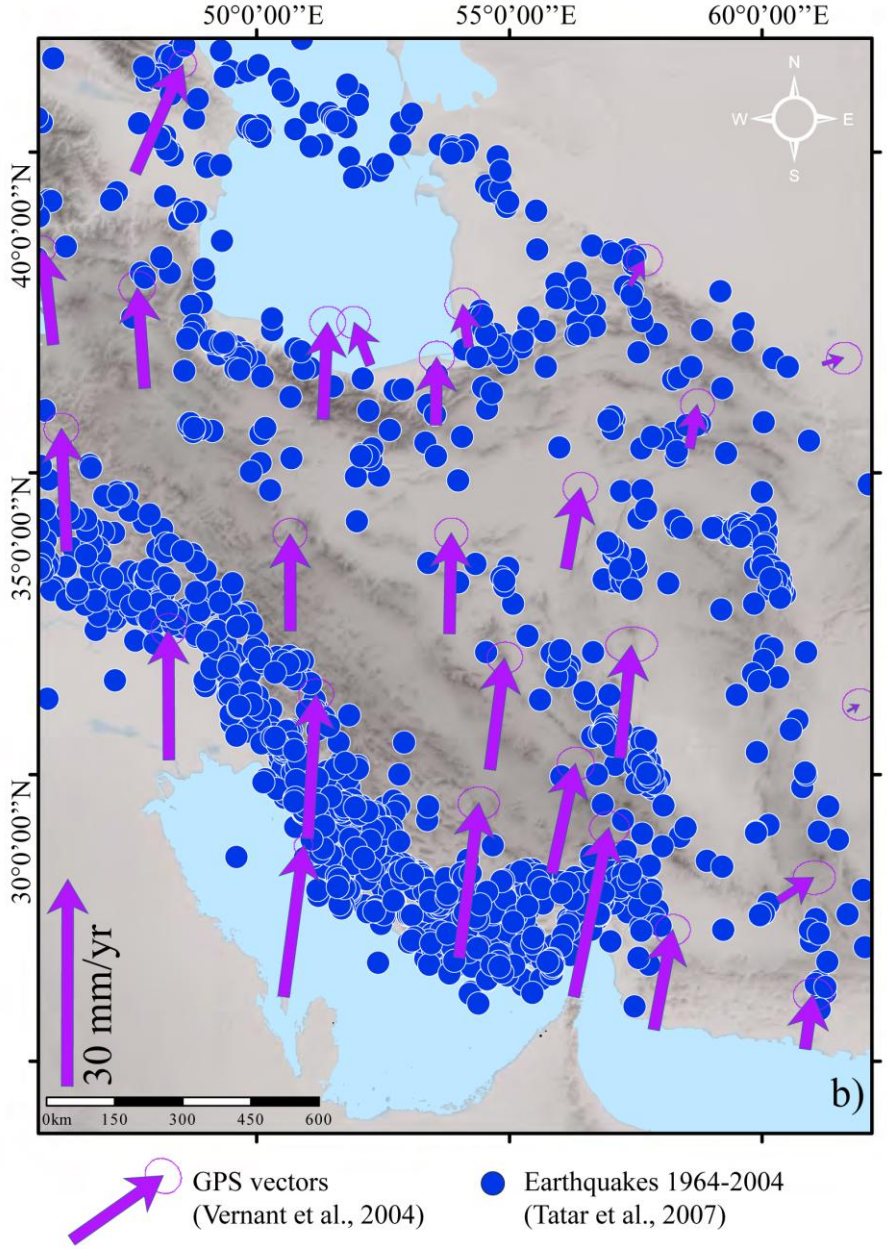

Fig.2.2 *Location of tele-seismically recorded earthquakes in a period of 1964–2004 from Tatar et al. (2007) and GPS-derived velocity field of the collision zone, with respect to stable Eurasia (Vernant et al., 2004). Af = Ashgabat Fault; BN = AD = Allah Dagh; Binalud Mts.; KD = Kopeh Dagh; LB =Lut Block; Sf = Shahrud Fault.*

The area object of this thesis ranges from the edge of the Eastern Alborz to the eastern part of Kopeh Dagh mountain, near Mashhad-Fariman ophiolitic-melange complexes and Agdarband Triassic tectonic window (Fig. 2.3). In the Iranian region the Post-Cimmerian phase was interested by a long stable sedimentation stage, which allow the deposition of several hundred meters of Late Jurassic, Cretaceous and Cenozoic sedimentary units, along the narrow oceanic basins opened during the Cretaceous. This long sedimentation stage was abruptly interrupted with the beginning of the Arabia-Eurasia collision, which interest the study area at the end of Paleogene.

2.1. Evolution of Cimmerian orogeny

As described by several authors, the iranian region started its long and complex geological evolution during the closure of Paleo-Tethys Ocean and the consequent opening of Neo-Tethys Ocean at the end of the Paleozoic (e.g., Muttoni et al., 2009; Ruttner, 1993; Sengor, 1979; Şengör et al., 1984; Soffel et al., 1989; Stampfli and Borel, 2002; Stöcklin, 1974; Zanchetta et al., 2009; Zanchi et al., 2009a). The Iran microplate rifted off Gondwana in the Early Permian and collided with Eurasia at the beginning of the Late Triassic after the final consumption of the Paleotethys Ocean (e.g., Muttoni et al., 2009; Zanchi et al., 2015). The collision with Laurasia of several Gondwanaland's fragments, concluded a long-living Late Paleozoic convergence due to the northward subduction of the Paleotethys Ocean beneath the southern Eurasia margin (Zanchetta et al., 2009). This diachronous compressional event which interested the entire southern Eurasian margin from Turkey to Thailand, affected the Iranian microplate during the Carnian-Norian time in the Alborz mountains (Stöcklin, 1974; Zanchi et al., 2015, 2009a) and in the Kopeh Dagh range (Horton et al., 2008; Ruttner, 1993, 1991; Zanchetta et al., 2013) forming the Eo-Cimmerian orogen. The orogen is discontinuously exposed along the Eastern Alborz near Gorgan (Neka Valley) and in Talesh mountains as show by Zanchi et al. (2009b), as well as in the Kopeh Dagh range near Mashhad (Fariman and Darreh-Anjir metamorphic complexes) (Fig. 2.3).

The deposition of the Upper Triassic-Jurassic Shemshak Formation constrained the age of the collision in the Alborz; in the Kopeh Dagh, Ala-Dagh, Binalud and Fariman Mts. the equivalent successions of Shemshak Fm. is represented by the Kashafrud Formation, which unconformably covers the Cimmerian deformational structures generated by the continental collision that closed Paleo-Tethys Ocean in this region (Horton et al., 2008; Sengor, 1979; Wilmsen et al., 2009b; Zanchi et al., 2009a). Deposition of these units was the result of the uplift of the Cimmerian mountain chains, with their consequent denudation which produced large quantities of sediments that collected in an extensive foreland basin situated to the south (Fürsich et al., 2009a).

In Early-Middle Jurassic time the so-called Mid-Cimmerian tectonic phase occurred. This phase has developed in particular during the Bajocian time and it probably represents the onset of fragmentation and differentiation of the Iran Plate into a number of individual microplates and blocks of variable sizes (Fürsich et al., 2009b; Seyed-Emami et al., 2003). Two unconformities at the base and top of the syn-orogenic units of Shemshak and Kashafrud formations are the sedimentary expressions of rapid basin shallowing due to the uplift and erosion for the lower unconformity, and an indication of a rapid subsidence pulse for the Upper Bajocian unconformity at the top. All these events took place within a short time interval, between the Early and Late Bajocian (Fürsich et al., 2009b). In particolar, as shown by Fürsich et al. (2009b), the area studied in this thesis was characterized by the presence of an important unconformity which separates the marine, siliciclastic sediments of the Upper Bajocian-Bathonian Kashafrud Formation from older underlying Triassic rocks. This unconformity was interpreted as the result of the main collision phase between the Iran and Turan plates, which started around the Triassic-Jurassic boundary (Wilmsen et al., 2009c). Zanchi et al. (2016) show that the Triassic Eo-Cimmerian structures exposed in Agdarband basin are sealed by the Middle Jurassic Kashafrud Formation, which marks the beginning of a new geodynamic cycle, characterized by a marked rifting event probably related to the opening of the Proto-Caspian Basin.

The Post-Cimmerian phase, which commonly started at the end of the Jurassic, was characterized by an important paleogeographic evolution of the iranian blocks. As shown by Mattei et al. (2015), during the Middle Jurassic the Central-East Iranian Microcontinent (CEIM), attached to Eurasia, was placed in the middle latitude (~40°N) temperate belt, but during the Jurassic shifted to the low latitude tropical arid belt (~15°N). This latitudinal shift explains the restoration of carbonatic sedimentary condition during the Middle-Late Jurassic time with the switch from coal-bearing sedimentation to carbonate platform deposition in the late Middle Jurassic (Fürsich et al., 2003; Mattei et al., 2015). The Middle-Late Jurassic stratigraphic units, which characterized the CEIM, are in good agreement with the paleogeographic reconstruction made by several authors (Dercourt et al., 1986; Fürsich et al., 2003; Wilmsen et al., 2005, 2009a) which previously suggested that, during the Late Jurassic, Yazd, Tabas and Lut blocks of the CEIM, were oriented east-northeast/west-southwest. In particular the stratigraphy and facies distribution demonstrate that the Yazd Block was emerged for most of the Jurassic period, while the marine influence increased from Tabas to the Lut blocks (Mattei et al., 2015). The paleomagnetic studies on the Late Jurassic Garedu Formation (Cifelli et al., 2013; Mattei et al., 2015, 2014), which is made of several hundred meters of red conglomerates, sandstones and

siltstones in the CEIM, allowed the estimation of paleogeographic dislocation of the Cimmerian blocks during the beginning of Post-Cimmerian phase. The results from upper Jurassic units of the CEIM confirmed the latitude drop which affected the entire Eurasian region during the so-called Jurassic massive polar shift (JMPS) (Mattei et al., 2014; Muttoni et al., 2005). The Upper Jurassic-Early Cretaceous period was identified as a crucial phase for the evolution of CEIM configuration. In fact, as said below, the estimated orientation for the Yazd, Tabas and Lut blocks until Middle-Late Jurassic were E-NE/W-SW, with the Lut Block bordered to the south by the Neotethys Ocean and to the southeast by the Neo-Sistan oceanic seaway (Mattei et al., 2015). The paleomagnetic rewiew from Mattei et al. (2015) demonstrated as starting from post Triassic time the CEIM was interested by a total amount of counter clockwise (CCW) rotation between 45° and 82°, with a mean value of 66° (±13°) respect to Eurasia. During the Early Cretaceous, the CEIM was detached from Eurasia and surrounded by small oceanic basins (Sistan, Sabzevar, Nain Baft oceans) which probably opened and closed in response to the counter-clockwise rotational movements (Dercourt et al., 1986; Wilmsen et al., 2013). Drove by the Late Jurassic-Early Cretaceous northward propagation of the Sistan Ocean rifting-spreading, the CEIM underwent another counter-clockwise rotation (34°±15°) during Early Cretaceous (Mattei et al., 2015).

Starting from the end of the Cretaceous, the progressive closure of the Neotethys and peri-Tethys oceans drove the paleogeographic setting of the entire iranian region. Most of the reconstructions on the closure of the Neotethys propose that the formation of the active margin along the Eurasian margin started since the Late Triassic-Early Jurassic (Bagheri and Stampfli, 2008; Stampfli and Borel, 2002). This oceanic subduction was followed by formation of a cordilleran-type margin along the Sanandaj-Sirjan Zone during the Jurassic-Cretaceous (Ghasemi and Talbot, 2006) and by formation of various marginal oceans in the back-arc domain. As proposed by Rossetti et al. (2010), these oceanic basins were formed in two major periods, during Late Jurassic-Early Cretaceous and the Late Cretaceous. The various small oceans, today represented by the ophiolitic domains which surround the CEIM (as showed in Fig.2.1), were subsequently closed starting from the end of Early Cretaceous to Late Cretaceous and in part during the Paleogene, in connection with the closure of the Neotethys Ocean and consequent convergence of Arabian Plate respect to Eurasia (Agard et al., 2005; Dercourt et al., 1986; Wilmsen et al., 2013).

2.2. The Arabia-Eurasia collision

The closure of various small oceans around CEIM, developed during the late Cretaceous and in the Paleogene, was probably the first warning of the northward drift of Arabian plate and correlated closure of the Neotethys (Dercourt et al., 1986; Rossetti et al., 2010; Stampfli and

Borel, 2002; Wilmsen et al., 2015).The Arabia-Eurasia convergence took place first in southern Iran with the Zagros fold and thrust belt that started as early as the late Eocene (Vernant et al., 2004). Estimates for the age of the initial collision between Arabia and Eurasia vary from ~65 Ma (Berberian and King, 1981), using the end of ophiolitic obduction, to ~5 Ma (Philip et al., 1989), taking the onset of coarse clastic sedimentation around parts of the Greater Caucasus. Deformation and syn-tectonic sedimentation took place on the northern side of the Arabian Plate in the early Miocene (~16-23 Ma, Robertson, 2000), related to the overthrusting of allochthonous nappes originating on the Eurasian side of Neo-Tethys (Allen et al., 2004). Today the shortening is mainly accommodated by distributed faulting in high mountain ranges in the south (the Zagros mountains) and the north (the Alborz and Kopeh Dagh mountains); these deforming regions are separated by relatively aseismic desert areas which appear not be deforming (Walker et al., 2003; Walker and Jackson, 2004).

2.3. The Kopeh Dagh range

Iran is pushed against its northeastern (Turan Shield) and eastern (Afghan Block) boundaries, causing considerable crustal shortening in Kopeh Dagh region (~15mm/yr, Vernant et al., 2004).

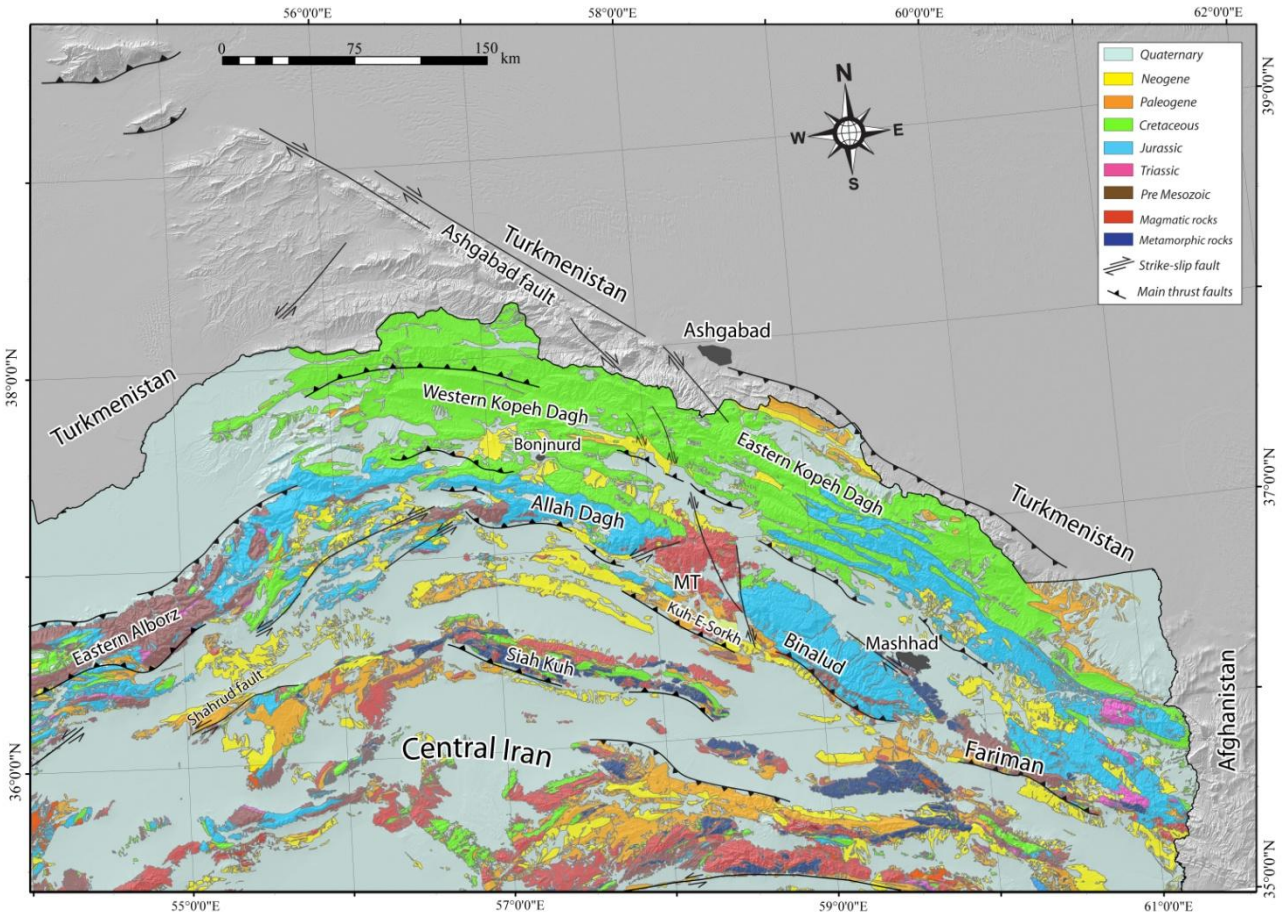

Fig.2.3 *Schematic geological map of north-eastern Iran. MT = Meshkan triangle.*

The current regional setting is the result of two major events: the Cimmerian orogeny, consequence of the closure of the Paleotethys Ocean, as testified by ophiolitic domains located within the Binalud mountains; and the Alpine-Himalayan orogeny occurred after the closure of the Neotethys Ocean(e.g., Sheikholeslami and Kouhpeyma, 2012; Stöcklin, 1974; Wilmsen et al., 2009b, c; Zanchi et al., 2009a). The eastern part of the chain, the Fariman complex and the Agdarband region, are interpreted as remnants of a magmatic arc and related basins developed at the southern Eurasia margin (Zanchetta et al., 2013; Zanchi et al., 2016).

The Kopeh Dagh range, which stretches over nearly 700 km from Turkmenistan to Afghanistan, is composed of gently folded rock sequences of Lower Jurassic to Neogene sedimentary deposits. Following the closure of Paleotethys, in the Middle Triassic (Ruttner, 1993; Zanchi et al., 2016, 2009a) over 10.000 m of sediments were deposited in the Kopeh Dagh Basin, an elongate subsiding back-arc basin located along the southern margin of the Eurasian Plate (Brunet et al., 2003; Ferré et al., 2016; Kalanat et al., 2017; Lasemi, 1995).

This orogen represents the product of the Late Cenozoic deformation in northeastern Iran and it forms the northeastern side of the Arabia-Eurasia collision zone. The Kopeh Dagh, Ala-Dagh, Binalud and Fariman Mts. accommodating part of Arabia-Eurasia convergence not absorbed by the Makran subduction. South of the northeastern mountain chains, the Lut Block is bordered to the west and east by large strike-slip faults (Vernant et al., 2004). Like the Alborz and the Zagros, the Kopeh Dagh, Ala-Dagh, Binalud and Fariman display partitioning of the overall convergence into compressional and strike-slip components, with right lateral slip on the Ashgabat fault on the northern side of the range and a series of shorter faults segments within it (Allen et al., 2006; Vernant et al., 2004).

As argued by Allen et al. (2004) and by Walker & Jackson (2004), if the north-south convergence rate in the eastern Zagros is at least the same as the central part (~10mm/yr), it implies that the Kopeh Dagh convergence may be ~16mm/yr at maximum, for a total N-S shortening that it would take ~5 million years to achieve the ~75 km of total crustal shortening estimated for the western sector of the range.

2.3.1. The Agdarband/Kashafrud/Kopeh Dagh Basins evolution

The Kopeh Dagh Basin was formed on Hercynian to Early Cimmerian basement, following the northeast Iran collision with the Turan Plate in the early Mesozoic (Garzanti and Gaetani, 2002;

Poursoltani et al., 2007). The basin, located at the southern margin of Turan Platform, was opened after the Middle Triassic orogeny as a result of the closure of the Hercynian Ocean in northeast Iran (Alavi et al., 1997; Berberian and King, 1981; Ruttner, 1993; Zanchi et al., 2016, 2009a); together with Amu-Darya Basin (southern part of Turkmenistan), form a large intracontinental basin filled by thick post-Triassic sequence of mostly marine sediments as limestones, marls and sandstones (Bretis et al., 2012).

As proposed by several authors (Ruttner, 1993, 1991; Zanchetta et al., 2013; Zanchi et al., 2016, 2009a), the study area is characterized by the presence of different Paleozoic magmatic and metamorphic complexes which were interpreted both as the remnants of Paleotethys Ocean, both as remnants of a magmatic arc and related basins developed at the southern Eurasia margin, on top of the north directed Paleotethys subduction zone, before the collision of Cimmerian blocks with Eurasia (Zanchetta et al., 2013). In particular the Paleotethys remnants are well exposed close to Mashhad, in the Binalud Mountains, where an accretionary wedge with ophiolitic fragments rests below the not well dated conglomerates and sandstones, probably deposited in the Late Triassic-Early Jurassic time interval (Alavi, 1991; Zanchi et al., 2009a). The Fariman and the Darreh Anjir complexes, which do not include ophiolites, instead indicate a supra-subduction zone setting, characterized by several episodes of arc-splitting and basin opening. As shown by Zanchetta et al. (2013), these two complexes were probably formed on the southernmost active margin of the Turan domain of Eurasia, under which the Paleotethys Ocean subducted during Permian and Triassic times.

The base of the Mesozoic sedimentary succession is only exposed in the eastern part of the range; in fact, in Agdarband area exists an anticline, which has been eroded down to pre-Jurassic basement. In this erosional window are well exposed the marine Triassic Cimmerian units which testified that the Agdarband basin, probably a branch of the Kopeh Dagh Basin, was formed in an arc setting along the southern Eurasia margin in the frame of an extensional-transtensional tectonic regime (Alavi et al., 1997; Ruttner, 1993; Zanchetta et al., 2013; Zanchi et al., 2016).

The Triassic-Jurassic sedimentary succession of Agdarband basin is more than 1 km thick and was deposited between the Olenekian and the Rhaetian; Zanchi et al. (2016) show as the basin was filled by four main sedimentary units: the basal continental conglomerates and sandstones, follows by the Early Triassic marine shallow water Sefid-Kuh Limestones, which in turn is overlain by the Middle Anisian deep water cherty limestones of the Zazar-Kardeh Formation. The deposition of the Carnian continental Miankuhi Formation, which unconformably overlain the Early Triassic marine beds of the basin, signed the end of marine sedimentation as well as the volcanism in the

Agdarband area. The unconformity at the base of this continental shales marks the collision of the Iran plate with Eurasia and may be coeval to the one at the base of the Shemshak Group in the Alborz mountains (Zanchi et al., 2016).

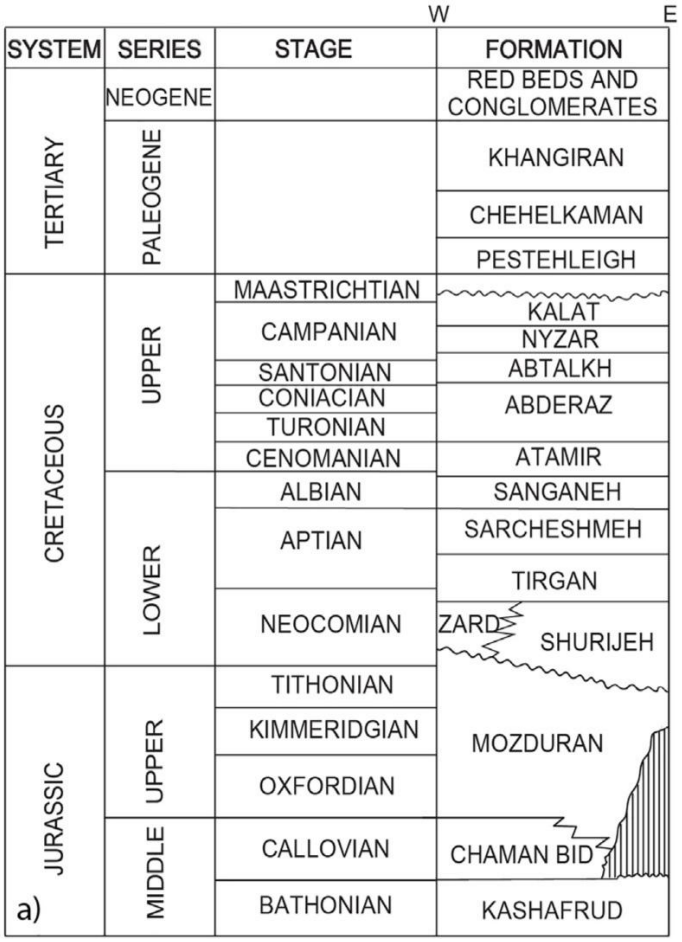

Fig.2.4 *– Schematic stratigraphic section sedimentary units outcropping in north-eastern Iran (modified from Kavoosi et al., 2009; Kavoosi, 2015; Moussavi-Harami and Brenner, 1990)*

As described by Zanchi et al. (2009a), the continental sandstones, shale and coal of the Shemshak Group, unconformably covered the Paleozoic basement and the Triassic succession, which from CEIM to Alborz mountains reflect the onset of Eo-Cimmerian deformation in Northern Iran (Wilmsen et al., 2009a). In the study area the deposits of the Shemshak Group have not been directly recognized, but as showed by Wilmsen et al. (2009c) the Lower-lower Middle Jurassic non-marine sedimentary succession of the Binalud Mountains (near Mashhad), may be correlated with the Jurassic part of the Shemshak Group of the Alborz Mountains. In the Binalud Mountains the coeval deposits of the Shemshak Group are interpreted as Cimmerian molasse, which are overlain by marine siliciclastic of the Kashafrud Formation (Upper Bajocian-upper Bathonian) (Taheri et al., 2009) (Fig. 2.4).In the eastern sector of Kopeh Dagh Mountains, starting from the Late Bajocian, a strongly subsiding rift basin was opened; the Kashafrud Basin was affected by

the accumulation of more than 2000 m of Upper Bajocian-Upper Bathonian siliciclastic sediments (Taheri et al., 2009).

Considering the entire region of Kopeh Dagh, the Mesozoic sedimentary succession was deposited starting from the eastern sector in the Kashafrud Basin, which was progressively evolved in the so-called Kopeh Dagh Basin. In fact the Kashafrud Basin, as argued by Taheri et al. (2009), may be considered as the eastern extension of the South Caspian Basin, which entered the rifting stage in the late Early Jurassic and the spreading stage in the Late Bajocian. The Mid Jurassic sedimentation in the Kashafrud/Kopeh Dagh Basin on the southern Turan Plate, probably reflecting back-arc extension associated with northward subduction (Poursoltani et al., 2007).

The Middle Jurassic clastic deposits of the Kashafrud Formation, which sealed the units and deformation structures of Eo-Cimmerian orogenic stage, may be considered not only a consequence of Mid Cimmerian compressional events, but probably a syn-rifting deposits influenced by the extensional regime active during that period (Poursoltani et al., 2007; Zanchi et al., 2016). This sedimentary formation was deposited in a large, rapidly subsiding intracontinental basin characterized by a northward paleoflow direction from the southern basin margin (Poursoltani et al., 2007). Coeval rock units as the Bashkalateh Formation of the easternmost Alborz and Dalichai Formation of the central and eastern Alborz provide links between the Kashafrud Basin and the South Caspian Basin (Brunet et al., 2003) that started to open earlier during Toarcian-Aalenian times (Fürsich et al., 2005; Taheri et al., 2009)

The Kashafrud Formation is disconformably overlain by the marine carbonates of the Mozduran Formation, which started their deposition during the Oxfordian, suggesting a Callovian hiatus (Aghanabati, 2004) (Fig.2.3). After a general regression which affected the Callovian time as testified by the paleosol horizons, formed at the top of Kashafrud Formation (Zand-moghadam et al., 2016), the deposition of Mozduran Formation marks a marine transgression from NW, starting from the end of Callovian (Lasemi, 1995). The contact between the Mozduran and Kashafrud Formations, which in the eastern Kopeh Dagh is unconformable, to the west is conformable and gradational with deeper-marine Bathonian to Oxfordian carbonates and shale/marls of the Chaman Bid Formation (Kavoosi et al., 2009; Kavoosi, 2015; Zand-moghadam et al., 2016). As showed by Kavoosi et al. (2009), the Mozduran Formation becomes younger from west to east and this trend is also accompanied by their eastward transition to evaporites and siliciclastic sediments with a decrease in thickness in the eastern part of the Kopeh Dagh Mountains. The nannofossils investigations carried out by Moheghy & Hadavi (2014) and by Hadavi & Khodadadi (2013) in different study sections, confirm that the age of boundary between the Mozduran and Shurijeh

Formations is diachronous with a variable age between Early Berriasian-Late Valanginian for the eastern sections and Early Hauterivian for the western section.

The red siliciclastic beds of Shurijeh Formation disconformably overlay the Mozduran Formation, marking the marine carbonatic sedimentation, which affect the Kopeh Dagh Basin during the Late Jurassic time (Kavoosi et al., 2009; Zand-moghadam et al., 2016) . In fact at the end of the Jurassic and through the Early Cretaceous, the epicontinental sea regressed toward the northwest and a 230 to 900 m thick interval of redbed siliciclastic sediments was deposited in fluvial systems (Moussavi-Harami and Brenner, 1992, 1990). The inclusion of Upper Jurassic fossils in the limestone pebbles, which forming the lower conglomeratic member of Shurijeh Formation, indicating that nearby Upper Jurassic carbonates were eroded during the Early Cretaceous (Moussavi-Harami and Brenner, 1992). The period of uplift and erosion which allowed the deposition of the Shurijeh Formation marked a change in sedimentary style, from carbonate dominance to siliciclastic dominance, that lasted through much of the Early Cretaceous time (Moussavi-Harami and Brenner, 1993).

2.3.2. The Shurijeh Formation

The Shurijeh Formation is one of the two lithologies sampled in this thesis for paleomagnetic analyses (Fig.2.5). This formation is made of mixed siliciclastic-carbonate-evaporite deposits that have been deposited in a variety of continental (fluvial, ephemeral lake depositional systems), coastal and marine environments during the Late Jurassic-Early Cretaceous times (Mortazavi et al., 2014). As illustrated by Moussavi-Harami & Brenner (1990), the Shurijeh fluvial deposits consist of six lithofacies with a vertical variations in sedimentary characteristics that allow to divide the interval in three parts: relatively coarse-grained the lower and middle parts, finer-grained the upper part. The lower part of the redbed interval is composed of coarse-grained sediment, which was deposited in a low-sinuosity, proximal, braided system; the Middle part is mainly composed of very coarse-grained to pebbly sandstone, deposited as a sheet-flood deposits in a distal braid-plain; finally the upper part of the interval consists mainly of finer-grained sediments interlayer by gypsum/anhydrite deposits that were deposited in a high-sinuosity, meandering stream system under arid condition as a consequence of the major marine regression at the Jurassic-Cretaceous transition (Moussavi-Harami et al., 2009; Moussavi-Harami and Brenner, 1990). Furthermore the paleocurrent analysis indicate that the fluvial system flowed from south and southwest to the north; in fact the petrographic analysis from Moussavi-Harami & Brenner (1990) indicated that more than 80% of the pebbles in the Lower Cretaceous rocks consist of quartz eroded from the Triassic redbed units which are primarily composed of volcanogenic

sediments and were exposed in the southern side of eastern Kopeh Dagh Basin. The recent petrographical analysis from Mortazavi et al. (2014) have shown as the Shurijeh values of SiO2 contents suggest that the source rocks were probably felsic igneous rocks. The thickness of the Shurijeh Formation ranges from 100 m above the paleo-high to about 1000 m (Fig.2.5) thick and moving in the western sector decrease they thickness until being completely replaced by the Zard Formation, which mainly consists of marine marls, calcareous shale with some sandstone beds (Afshar-Harb, 1994; Robert et al., 2014).

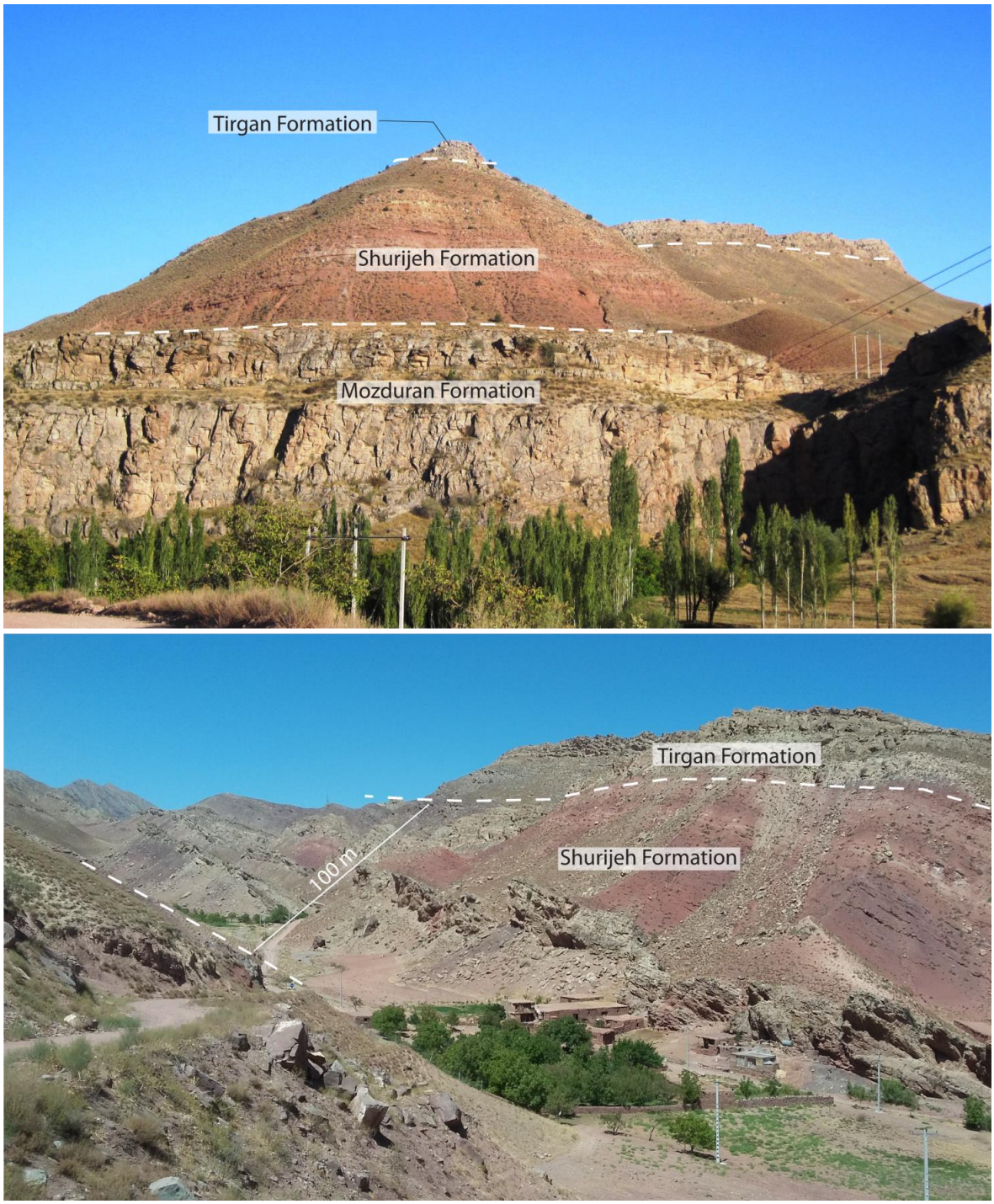

Fig.2.5 *Stratigraphic relationship of the fluvial Shurijeh Fm. with the limestones of Mozduran Fm. at the base and the limestones of Tirgan Fm. at the top.*

2.3.3. The late Early Cretaceous-Neogene deposition in the Kopeh Dagh Basin

The new transgression that affected the Kopeh Dagh Basin at the end of Barremian, led to shallow marine shelf conditions in which bioclastic and oolitic limestones of the Tirgan Formation were deposited conformably on the Shurijeh Formation (Raisossadat and Moussavi-Harami, 2000).

During the late Aptian, the Kopeh Dagh Basin subsided abruptly and relatively deep-water marlstones were deposited (Moussavi-Harami and Brenner, 1992), in fact that was marked by the deposition of several deeper marine marly shelf units as the Sarcheshmeh Formation, a silty marlstone characterized by an upper limestone member. This formation marks the beginning of deep water sedimentation, followed by a relative sea level fall, that was definitely testify by the appearance of the dark-grey and black shales of Sanganeh Formation, characterized by proximal shelf to mud-dominated sedimentation with suboxic conditions, which was dated Late Aptian-Early Albian (Heidari et al., 2015; Raisossadat, 2006) (Fig. 2.4). During Albian-Early Cenomanian time, the area was still affected by the relative fall of sea level, which caused the deposition of the glauconitic sandstone and green shales of the Atamir Formation (Sharafi et al., 2013) (Fig. 2.4).

As described by Moussavi-Harami & Brenner (1992), the orogenic activity was much greater in the western part of the basin, where an angular unconformity between the Cenomanian and Maastrichtian sediments was identified; otherwise in the eastern Kopeh Dagh Basin the subsidence rate again increased, as a result of both tectonic and sediment loading during the late Turonian through the Santonian. That allowed the continuity of deposition throughout the Late Cretaceous, in fact over the Aitamir Formation the pelagic chalky limestones of the Abderaz Formation were deposited, for a total of 540 m thick (Ardestani et al., 2012; Vahidinia and Ardestani, 2017) (Fig. 2.4). During the Late Cretaceous time, the Kopeh Dagh Basin was interested by a rising of sea level and consequently was covered by a shallow to deep sea (Stampfli and Borel, 2002) as outlined by the deposition, over the Abderaz Formation, of an alteration of shales, marly sandstones and shallow limestone units (Kalantari, 1987). The Abtalkh Formation, composed mainly of marls, shales and silty marls, overlies conformably on the last chalky limestone bed of the Abderaz Formation and itself conformably overlain by the sandy Nyzar Formation (Ferré et al., 2016). The Cretaceous sedimentation was closed by the deposition of the Kalat Formation during the ending of Campanian; this formation is a unit of limestone which contains subordinate sandstones intercalation (Moheghy et al., 2013; Moussavi-Harami and Brenner, 1992). Close to the end of Cretaceous period and beginning of Paleocene, the epicontinental sea regressed toward the northwest and a thick interval of red bed and siliciclasitic

fluvial sediments of the Pestehleigh Formation were deposited in disconformity on the Kalanat Formation (Rivandi et al., 2013) (Fig. 2.4). During the late Paleocene, the sea level rose rapidly with abrupt shifting of potential siliciclastic point sources toward the central and eastern parts of the basin; this transgression allowed the deposition of the Chehelkaman Formation, an alternation of limestone, dolomites and interbeds of marls, shales and evaporites sediments which conformably overlie the Pestehleigh red beds (Mahboubi et al., 2001; Rivandi et al., 2013) (Fig. 2.4). The transition to the Lower Eocene is characterized by the occurrence of some layers of marls followed by the deposition of alternating limestones and marls of the Khangiran Formation, which becomes sandier within the upper part (Kalantari, 1987; Robert et al., 2014). Along the outcrop belt, non-marine red beds lie disconformably above Eocene shoreline sediments, indicating that Kopeh Dagh sedimentation was dominantly non-marine during the Neogene time (Moussavi-Harami and Brenner, 1992). This unconformable change from marine Khangiran Formation to terrestrial continental red beds sedimentation occurring during the Oligocene-Early Miocene (34-20 Ma), marks the onset of uplift in the Kopeh Dagh Basin, which probably began after the early-to-middle Oligocene (Berberian and King, 1981; Robert et al., 2014).

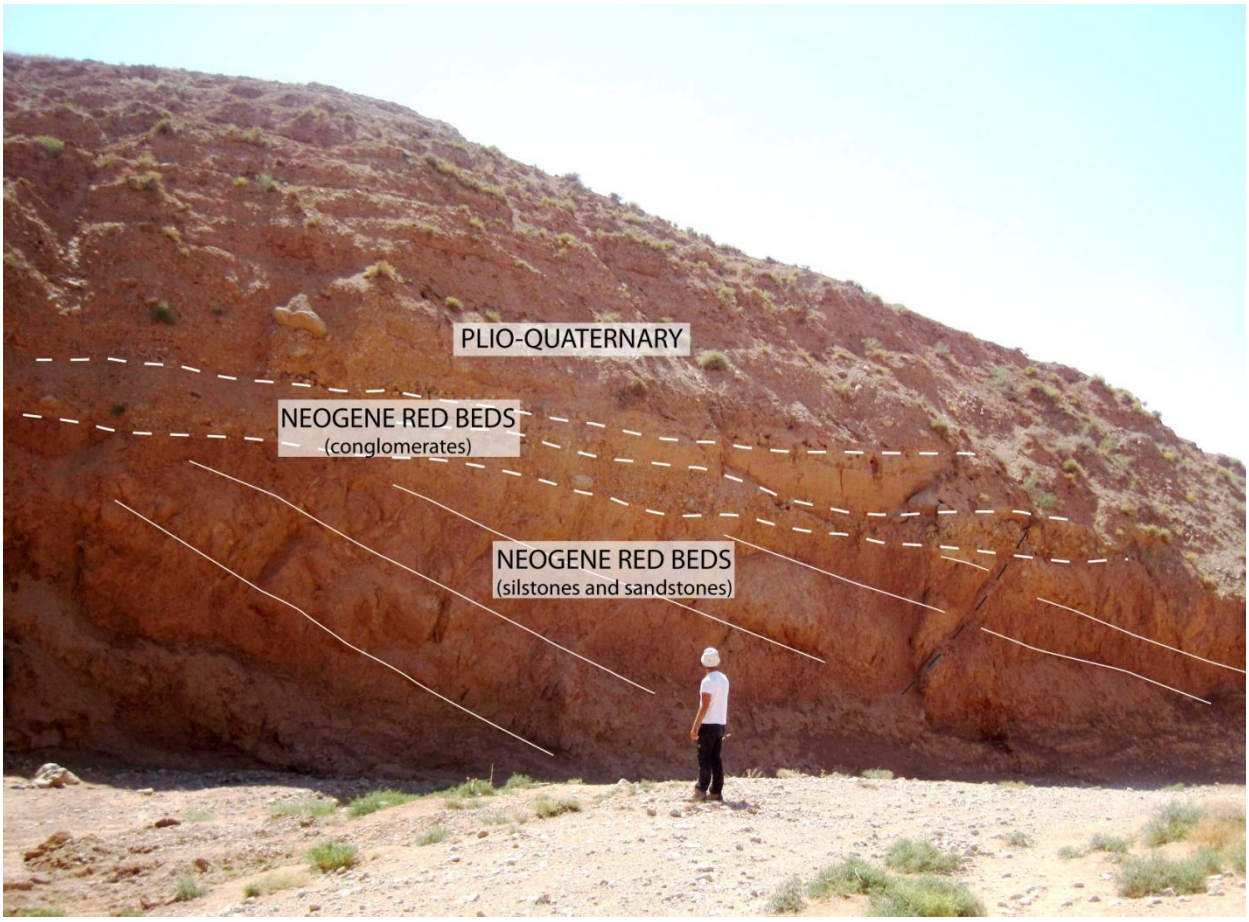

Fig.2.6 *Outcrop appearance of a URF sampling site. The Neogene red beds are disconformably covered by the Plio-Quaternary conglomeratic deposits*

The Neogene red bed deposits (red beds and conglomerates, Fig. 2.4) are similar to the post 20 Ma Upper Red Formation (URF) of the Central Alborz (Robert et al., 2014), although started their deposition earlier than their analogue in the Alborz/South Caspian Basin. Therefore the upper portion of the Kopeh Dagh Neogene red bed deposits can be correlated with the middle-late Miocene Upper Red Fm. (URF) of Central and Northern Iran, and for this reason from here onwards it will be call URF. The URF is the second lithology that I have sampled for the paleomagnetic analysis of this thesis (Fig.2.6-2.7).

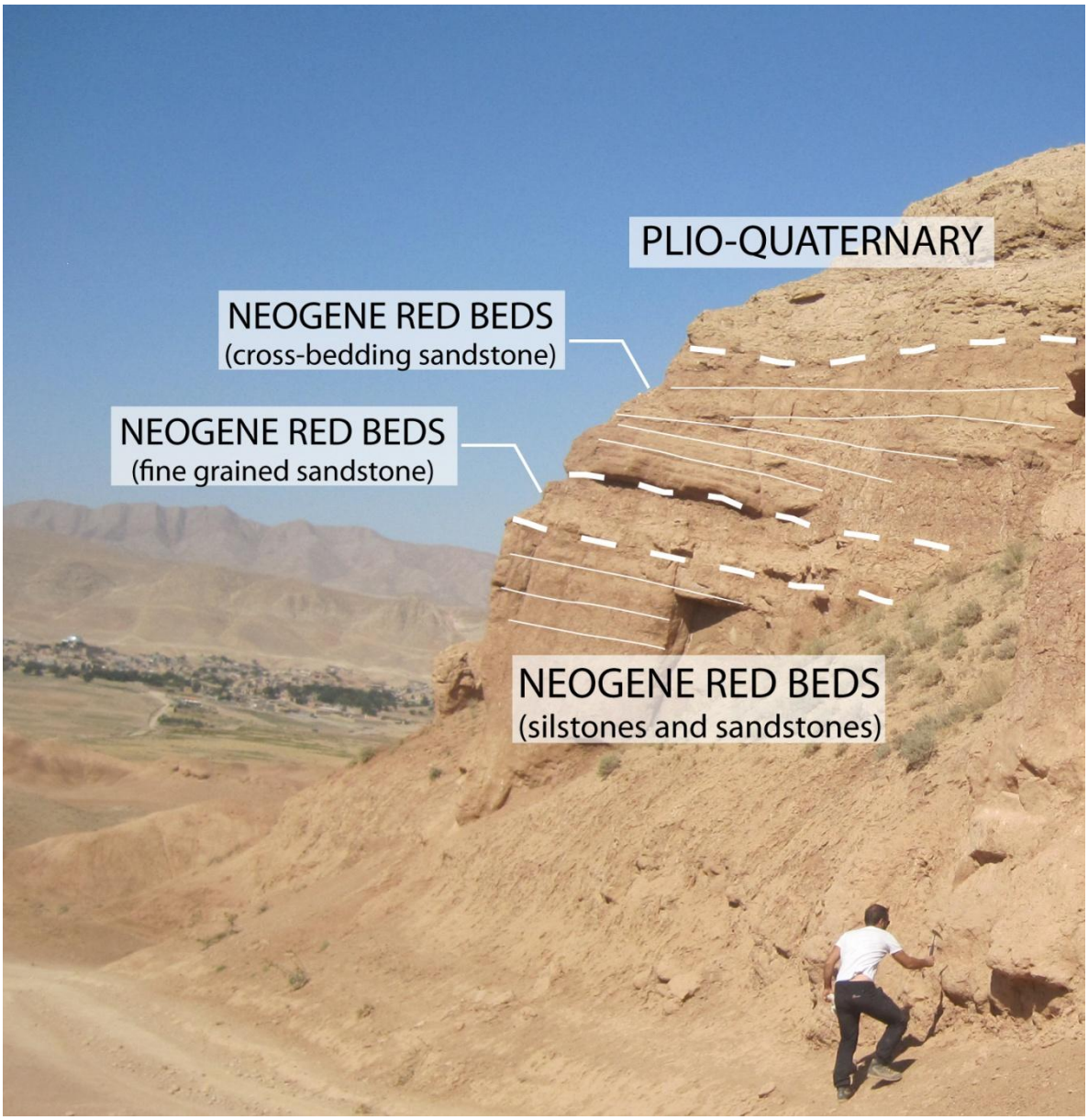

Fig.2.7 *Outcrop appearance of a URF sampling site. Neogene red beds deposits organization disconformably covered by the Plio-Quaternary conglomeratic deposits*

2.4. Structural configuration of Kopeh Dagh region

As described above, the N to NNE convergence between Arabia and Eurasia requires Iran to be compressed into NE corner where the Kopeh Dagh mountains developed (Hollingsworth et al., 2010). This region was interested by a general reactivation of old Paleozoic structures, that started since the middle Oligocene, at the beginning of the northward motion of the Arabian Plate.

The seismicity along the whole mountain range indicates strain partitioning of oblique right-lateral shortening in thrust and strike-slip components, taking place on spatially separated faults (Jackson et al., 2002; Walters et al., 2013). The fault system is offset both right- and left-laterally (Hollingsworth et al., 2008) and it includes both right-lateral strike-slip faults and reverse faults with the same southeast strike (Hollingsworth et al., 2008), evidence for strain partitioning (Yeats, 2012).

The Kopeh Dagh range is delimited to the north by the right-lateral Ashkhabad strike-slip fault which runs along the north-eastern edge of the mountain belt; the fault separates the Turkmenistan platform from the South Caspian region as well as from the deforming region of northeast Iran (Hollingsworth et al., 2010, 2008; Walters et al., 2013) (Fig. 2.1).

Style of deformation differs along the chain and Hollingsworth et al. (2006) define three distinct regions of the Kopeh Dagh; east, west and central. Walters et al. (2013) described as East of 59°E the Kopeh Dagh have their highest peaks responding to a N-S shortening of about 2 mm/yr, that appears to be subdivided into range-parallel thrust and right lateral strike-slip fault. In the Mashhad area in fact the main faults are the right-lateral Neyshabur and the Mashhad strike-slip faults at the southern and northern side of Binalud Mountain respectively. West of 57°E, the topography becomes gradually more subdued with the right-lateral Ashkhabad fault that is the dominant feature in the geomorphology, following the Kopeh Dagh range front. Here the Ashkhabad fault together with the left-lateral Shahrud fault system zone, has been suggested as facilitating the north-westward extrusion of the South Caspian Block (Jackson et al., 2002; Walters et al., 2013). The structural setting of the central part of the range, between 57°E and 59°E, is still much debated. Here the relative motion of the South Caspian Block away from north-east Iran causes to experience range-parallel extension in addition to the N-S convergence between Iran and Eurasia (Walters et al., 2013). Hollingsworth et al. (2006) suggest that both E-W extension and N-S compression are accommodated by anticlockwise rotation on a series of NNW-striking right-lateral strike-slip faults. This region, called the Quchan-Bakhardan Fault Zone, has been described by Shabanian et al. (2009) with an alternative model which suggests that the right-lateral strike-slip faults of the QBFZ do not rotate but instead accommodate the north-westward translation of Iran relative to Eurasia.

3. METHOD AND SAMPLING

3.1. Historical background

The ancient Greeks knew about “lodestones” (or loadstones), rare natural magnets, with the power to attract iron. One site where such stones were found was near the city of Magnesia in Asia Minor (now Turkey), and from that (perhaps) came the term “magnetism.” However, it may have been an unknown Chinese scholar around the year 1000 who first placed a lodestone on a “boat” floating in a bowl of water and observed that wherever and whenever the experiment was performed, the boat always rotated to face south (Stern, 2002)

The interaction between the geomagnetic field and the rocks was noted by the late 18th century. Already at the end of the 16th century William Gilbert published his book De Magnete, proposing that the Earth itself was a giant magnet, implying that it has a magnetic field, but only in the 1830s Carl Friedrich Gauss formulated a procedure which permitted to measure a magnetic field completely and analyze its characteristics with the spherical harmonic analysis (Lanza and Meloni, 2006).

The first studies of the direction of magnetization in rocks were made by Delesse in 1849 and Melloni in 1853, who concluded that volcanic rocks acquired a remanent magnetization during cooling. At the end of 19th century G. Folgerhaiter reached the same conclusion and suggested that the direction of remanent magnetization was that of the geomagnetic field during cooling, furthermore he noted that some rocks have a remanent magnetization opposite to the direction of the present day field (Lowrie, 2007).

The studies of David and Brunhes at the beginning of 20th century on the material backed by lava flows confirmed the speculation that the Earth's magnetic field had reversed its polarity in the past (McElhinny and McFadden, 1999). By the mid-1920s, several important aspects of paleomagnetism in rocks had been established, from the Mercanton (1926) and Matuyama (1929) studies on different lavas outcrops, confirmed that the Earth's magnetic field had reversed its polarity in the past, in fact reversal should be found in rocks from all parts of the world.

In 1922, a German meteorologist, geophysicist and polar explorer named Alfred Wegener proposed a radical new idea, the hypothesis of "continental drift", based on years of study of geological, paleontological and paleoclimatic indicators, such as the geographic distribution of coal deposits. At that time, there was no way of explaining the mechanism by which the continents drifted, only motions of the crust were considered, and idea of rigid continents ploughing through rigid oceanic crust was unacceptable to geophysicists. Subsequently, paleomagnetism give

important contributions to understanding continental drift by providing the means to trace past continental motions quantitatively (Lowrie, 2007; Stern, 2002).

The rapid evolution of the paleomagnetism analyses occurred in the '30s and '40s as led to a new type of stratigraphy based on the aperiodic reversal of polarity of the geomagnetic field, which in now known as magnetic polarity stratigraphy (Opdyke and Channell, 1996).

The numerous studies on recent lava deposits (Pleistocene-Quaternary) allowed understanding clearly the existence of aperiodic inversions of the geomagnetic field; in fact the modern era of studies on reversals of the geomagnetic field began with those of Hospers at the beginning of 1950s in Iceland and at the same time the studies of Roche in the Massif Central of France, which elaborated on the early work of Brunhes. As in Matuyama's studies, the new results indicated that rocks and sediments designated as Upper Pleistocene and Quaternary in age possessed normal directions of magnetization, whereas reverse directions of magnetization appeared in rocks of early Pleistocene or Pliocene age (Opdyke and Channell, 1996)

During this time ('50s and '60s) the paleomagnetic studies are focused on the hypothesis of geomagnetic field reversal with the reconstruction of a global geomagnetic polarity timescale.

Starting from the 40s, the development of magnetometers was able to measure the magnetization of igneous rocks; within a few years there was a rapid improvement of more sensitive equipment, which allowed measuring the natural remanence even in sedimentary rocks. Paleomagnetic study of sedimentary rocks began with the classic study of Creer et al. (1954) which documented 16 zones of alternating polarity of the Torridonian sandstone (Scotland).

The fact that the declination and inclination of the magnetic field vary widely over Earth's surface makes it difficult to compare paleomagnetic results from sites separated by thousands of kilometers.

Fisher (1953) had therefore developed statistics to deal with directions of magnetization obtained from rocks and showed that the vector mean (treating each direction as a unit vector) was the best estimate of the true mean direction, and he showed how to calculate the 95% circle of confidence. This method of analyzing the direction of magnetization by calculating pole positions provides a way of comparing directions from sampling sites separated by considerable distances, indeed even between continents (Opdyke, 1995).

In 1955, there were very few groups working in paleomagnetism. In England, besides Runcorn's group at Cambridge, there was P.M. S. Blackett's group at Imperial College, London; Thellier and his students in France, in South Africa, studies were initiated by A. Hales and his student I. Gough at the Bernard Price Institute of Witwatersrand University on Precambrian intrusives in South Africa (Gough, 1956). In Russia, Khramov had begun his studies but his work was almost

unknown in the West. In Japan, an innovative paleomagnetic group under the direction of T. Nagata at Tokyo University was very active particularly in rock magnetism, and N. Kawai had established another group at Kyoto University which began to address tectonic problems as well as magnetic mineralogy. An important contribution was given by Graham (1949), who had suggested several ways of testing whether directions of magnetization had remained unchanged over geological time. The first of these is the fold or tilt test which can be employed if a bed has been folded into a geological structure after the beds are deposited. If the directions of magnetization were acquired before folding, then the observed directions of magnetization will become better grouped after correcting for bedding tilt (Opdyke, 1995).

A major breakthrough in the understanding of the problems of crustal mobility were two papers published by Irving (1957, 1956). In Irving (1956) presented the first review of paleomagnetic results which resulted in the first paleomagnetic pole list, he also published the first polar wander curves to compare North American and European data and showing that climatically sensitive sediments occurred at the correct paleolatitude when compared with paleomagnetic results from the same continent but did not agree if compared with paleomagnetic results from other continents. He therefore concluded the following "these results suggest that prior to Tertiary times the pole has not only shifted its position with respect to certain land masses but also that these land masses have moved relative to one another" (Irving, 1956).

In general, in the second half of the 1950s the choice of paleomagnetists to study red sedimentary rocks for the high magnetic stability and relatively strong remanent intensity of hematite lead to a higher ratio of success, particularly in the absence of thermal and AF demagnetization. The other rock type which yielded good results were basaltic rocks, both extrusive and intrusive where magnetite was the main magnetic carrier. Sensitive magnetometers had been developed to measure these rocks as the Spinner magnetometers in South Africa as well as the astatic magnetometers in England and later in Australia.

In the early 1960s, a series of interdisciplinary studies were carried out in which K/Ar dating and the measurement of magnetization polarity were carried out on the same lavas (Cox et al., 1963; McDougall and Tarling, 1963). These studies established that rocks of the same age had the same polarity and led to the establishment of the first radiometrically dated polarity time scale. The long intervals of constant polarity of the geomagnetic field were designated as magnetic epochs and named after the pioneers in the study of the geomagnetism (Brunhes, Matuyama, Gauss, and Gilbert); the shorter intervals (events) were named after the locality of discovery such as Jaramillo Creek in New Mexico and Olduvai Gorge in Tanzania. The developments which led to the first dated polarity time scale were soon followed by studies of magnetic stratigraphy in sediments and

investigations of oceanic magnetic anomalies (Opdyke and Channell, 1996).In 1964, Irving's (1964) book was published and widely distributed, and the formative years of paleomagnetism had essentially ended. The following were clear by this time:

1. If paleomagnetic data were interpreted in terms of the dipole hypothesis then the data were fully interpretable in terms of relative motion between the continents or as local rotations within orogenic zones.
2. The introduction of partial thermal demagnetization and AF demagnetization rapidly improved the quality of the database.
3. An improving database only strengthened these interpretations of continental motion.
4. New data from Africa, South America, India, and Eurasia became available, and in all cases, continental motion was supported by these data.

3.2. The Earth's magnetic field properties

Each point of the surface of the planet is affected by the Earth's magnetic field, where it can be represented by a vector whose orientation varies depending on the longitude and latitude of each considered point (Fig.3.1).

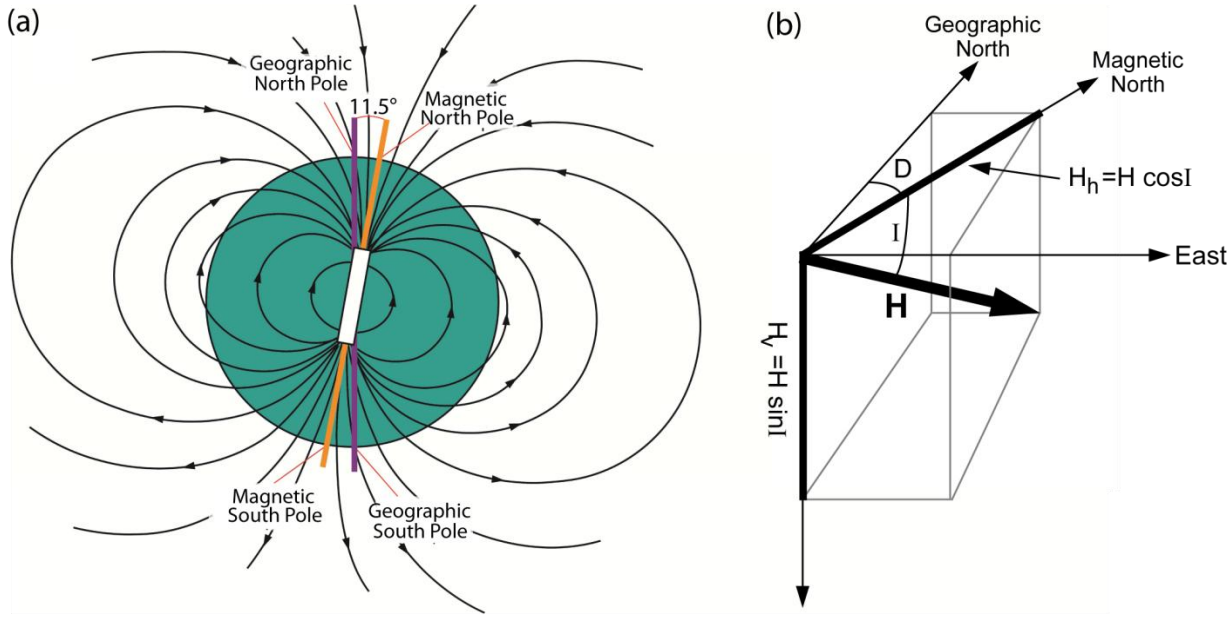

Fig. 3.1 (a) *Earth's magnetic field modelled as a magnetic dipole oriented around 11.5° with respect to the rotation axis of the planet.* ***(b)*** *Description of the direction of the magnetic field. The total magnetic field vector* ***H*** *can be subdivided into (1) a vertical component, Hv = H sin I and (2) a horizontal component, Hh = H cos I; inclination, I, is the vertical angle (= dip) between the horizontal and* ***H****; declination, D, is the azimuthal angle between the horizontal component of* ***H*** *(= Hh) and geographic north; the component of the magnetic field in the geographic north direction is H cos I cos D; the east component is H cos I sin D (Butler, 1998).*

This vector is defined by the *declination*, which is the angle from 0° to 360° that its horizontal component in local coordinates forms with respect to the geographic North; by the *inclination*, that corresponds to the angle that the vector forms with the horizontal plane, from 0° if it is horizontal,

to 90°/-90° if it is vertical, being positive downwards; and by the *intensity*, represented through a scalar magnitude of the vector and corresponding to the intensity of the magnetic field in each point. The Earth's magnetic field has undergone variations through time in its intensity, its orientation and its polarity, according to recurrence periods of very different duration (e.g. Opdyke and Channell, 1996). If the short-term variations are not considered to be representative (non-dipolar portion of geomagnetic field), only the variations of the dipole portion of geomagnetic field are measurable at geological scale. This premise supports the Geocentric Axial Dipole model (GAD; Fig.3.2), a model for which the orientation of the geomagnetic field corresponds to a perfect dipole aligned with the Earth rotation axis if it is averaged for a lapse about 10^5 years (e.g. Opdyke and Henry, 1969). The GAD model assumes that the time-averaged geomagnetic field can be modelled by a single magnetic dipole at the centre of the Earth which is aligned along the rotation axis. The magnetic field inclination in this model is related to geographic latitude by the dipole equation: $\tan I = 2 \tan \lambda$. The declination of the field is zero everywhere. This best fitting inclined dipole accounts for approximately 90% of the present geomagnetic field at the surface. The remaining ~5% is called the nondipole field. The palaeomagnetic records spanning the last 5 million years show that the average position of the geomagnetic pole is indistinguishable from the rotation axis. Thus, over periods sufficient to average out secular variation (~10^5 years) the geomagnetic field appears to be adequately described by the GAD model. The GAD assumption is equally valid for periods of normal and reversed polarity of the geomagnetic field, but does not apply to periods when the field is transitional between the two polarity states (Morris, 2003).

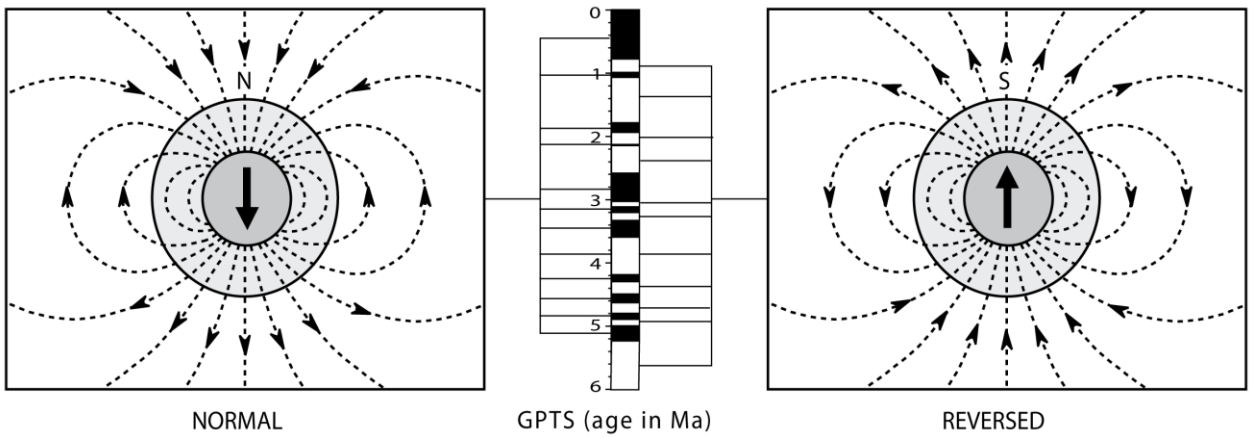

Fig.3.2 *Schematic representation of the geomagnetic field as a geocentric axial dipole (GAD). In a period of normal polarity (right), the average magnetic north pole is at the geographic north pole, and a compass aligns along magnetic field lines; inclination is positive (downwards) in the northern hemisphere and negative (upwards) in the southern hemisphere. Conversely, during reversed polarity (left), both poles (geographic and magnetic) are oriented oppositely and the compass needle points south; inclination is negative in the northern and positive in the southern hemispheres. In the geomagnetic polarity time scale (centre), normal polarity is represented in black and reverse polarity in white (Langereis et al., 2010).*

Large-scale variations especially useful in geology are magnetic polarity changes. A magnetic inversion consists on the switch of both North and South poles (Fig. 3.2). In its present disposition, magnetic field shows its negative pole (i.e. North magnetic pole) matching with the North geographic pole. This disposition is termed *normal polarity* as well as the periods in which North magnetic pole coincided with the South geographic pole are termed as periods of *reverse polarity*. The performance of the *Geomagnetic Polarity Time Scale* was possible by dating these variations along the history of the planet, firstly based on paleomagnetic data from rocks of the oceans floors (Heirtzler et al., 1968). In this absolute time-scale, periods with normal polarity are represented in black whereas periods with reverse polarity are represented in white (Fig. 3.2).

3.3. Fieldwork strategies and sampling procedures

According to Butler's (1998) a *site* is an exposure of a particular bed (or beds) from a sedimentary sequence, which can be considered as a single spot in terms of AMS or paleomagnetic conditions. Therefore, each site is a singular field locality, generally constituted by only one lithology, containing the same potential magnetic carriers that probably have undergone similar sedimentary, diagenetic and tectonic process. Special attention was paid to an even geographical distribution of sampling sites, more grouped in presence of fold structures (fold test).

The PhD work has been based on a collection of new paleomagnetic data, more than 800 samples, most of them from the Early Cretaceous red-beds of the Shurijeh Formation and, secondarily, from the Neogene red-beds of the "Upper Red Formation", which are distributed in a large area from longitude 57°E to 61°. The preliminary detection of the potentially suitable outcrops has been crucial at the beginning of any field trip. In fact, all the sampling sites were selected and identified before the expedition on the field, using an integrated Google Earth images analysis and Iranian geological maps investigations. This "procedure" has allowed to selecting the Cretaceous and Neogene outcrops which were more accessible, overlying the geological maps on the relative Google Earth areas and applying the transparency tool to the maps, has been possible define if the outcrops had the expected characteristics (colour, extension, accessibility) and were also located in the corrected geographic position (Fig.3.3). This preparatory phase has been fundamental not only to identify the well exposed and accessible outcrops, but also to select, from bibliography, the sedimentary formations which were potentially related to the research topic.

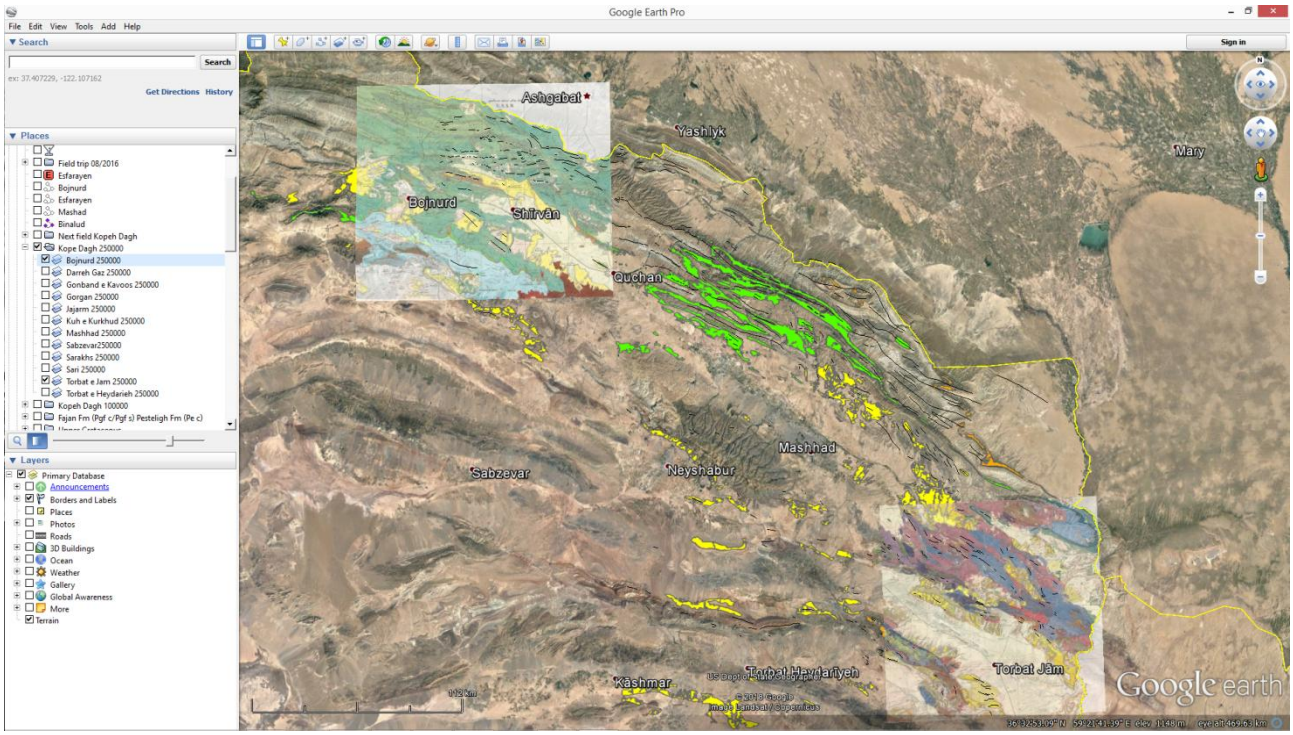

Fig.3.3 *Example of preliminary investigation on Google Earth in order to identify the potential outcrops suitable for our paleomagnetic investigations*

During the field trips, a total of 822 samples were sampled. In total, 70 sites were collected, 45 sites from Early Cretaceous redbeds, 23 sites from Neogene redbeds and 2 sites from Paleogene (Fig. 3.6). These samples, cover a very huge area from the Central to the Eastern part of Kopeh Dagh (from 57°E to 61°E), which represent an important improvement in the areal coverage of paleomagnetic sampling in Iran. Samples were taken from the outcrops using a hand-held gasoline-powered drill. After drilling, the cylindrical cores were oriented *in situ* with an inclinometer attached to a compass. Each measure was corrected to account for a local ~ 4° magnetic declination according to the NOAA National Geophysical data center.

In each sampling site the bedding was measured, as well as any fractures, faults or grain size variations; in general the sampling was performed in fresh fine-grained (mudstones-silstones) intervals, avoiding the coarse and conglomeratic members (Fig.3.4).

Fig.3.4 *Core sample collection procedure. Sampling techniques include the use of a gas-powered drill machine with diamond drilling bit. Cores are signed and oriented in situ with an inclinometer attached to a compass.*

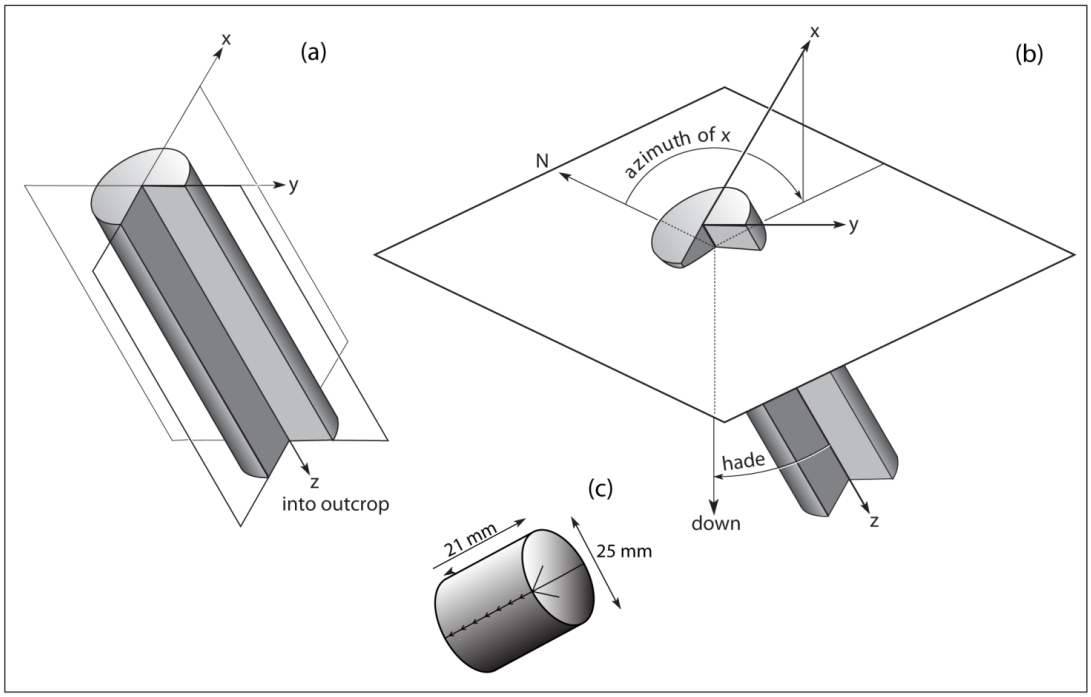

Fig.3.5 *Orientation system for sample collected by portable core drill.* ***(a)*** *Schematic representation of core sample in situ. The z axis points into outcrop; the x axis is in the vertical plane; the y axis is horizontal.* ***(b)*** *Diagram which shows the orientation angles for core samples. The angles measured are the hade of the z axis (angle of z from vertical) and geographic azimuth of the horizontal projection of the +x axis measured clockwise from geographic north.* ***(c)****Schematic representation of a single specimen ready for the measurement.*

Each sample was cut in order to obtain standard cylindrical paleomagnetic specimens (25 mm base × 22 mm height, ~11 cc) (Fig.3.5). The cutting process was performed using a double-disc cutting machine available at the Laboratory of Paleomagnetism at the University of Roma Tre (Fig.3.6). The cutting procedure was performed using water for hard lithologies and in dry conditions for soft lithologies. For several specimens it was necessary to use a specific non-magnetic glue.

Fig.3.6 *Specimens preparation procedure. Cutting process was performed using a double-disc cutting machine, in order to obtain standard cylindrical paleomagnetic specimens around 10,3cm^3 in volume.*

The sampling area has been divided into three main sampling areas, one in the central part of the region, which is part of the Eastern Alborz mountains, precisely the so called Allah Dagh Mountains; the second one at north of Mashhad with few sites in the Binalud Mountains very close to Mashhad. This area represents the central-eastern sector of Kopeh Dagh chain, finally the third area, which interest the eastern part of Kopeh Dagh range, between the Fariman metamorphic complex and the Triassic Agdarband tectonic window.

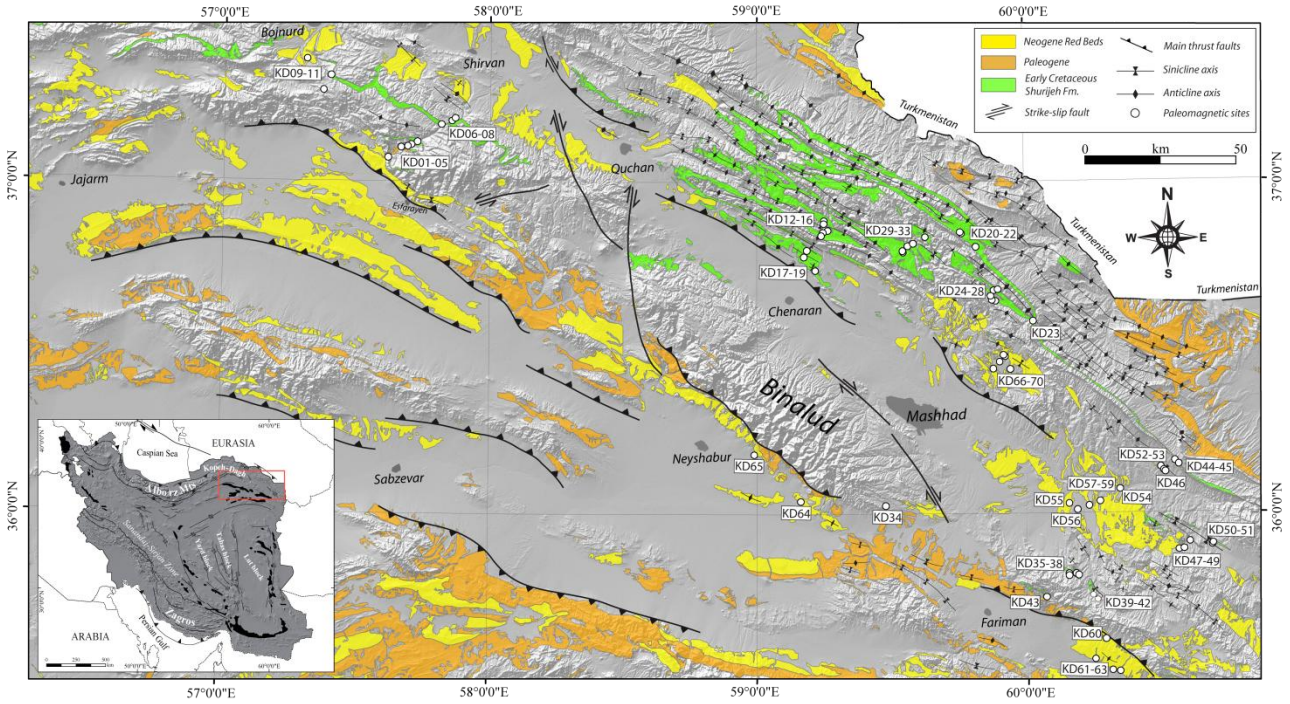

Fig. 3.7 *Main outcrops of Shurijeh Fm. and Neogene sediments of the URF and location of paleomagnetic sampling sites (KD).*

In the first area ~80 samples of Shurijeh Formation were collected, in 6 sampling sites (KD01, KD02, KD03, KD06, KD07, KD08, KD11), 2 sites of Neogene red beds (KD09, KD10) and 2 sites of Paleogene Peistaleigh Formation (KD04, KD05) (Fig.3.7). This area is located in the so-called Allah Dagh Mountains, part of the Eastern Alborz Mountains.

In the second area most of the Early Cretaceous samples were collected, 237 core in 22 sampling sites (from KD12 to KD33 shown in Fig.3.7) and ~80 samples were collected in 8 Neogene sampling sites. The Neogene sites are placed in two different sectors, one near Mashhad (sites from KD66 to KD70, as show in Fig.3.7), along the southern margin of Kopeh Dagh which is bordered by the Ahmadabad thrust fault, part of the huge thrust system that interests the southern side of the central-east Kopeh Dagh range, and the second one along the southern side of Binalud Mountains (KD34, KD64 and KD65, as show in Fig.3.7). In the northern part of this area the alternation of several syncline and anticline folds allows the cropping out of the entire Cretaceous succession, with Shurijeh Formation at the base.

The third area interests the eastern sector of the range, where the shortening still active in the Kopeh Dagh range, die out eastward into Afghanistan. Here, in a total of 29 sampling sites were collected ~350 samples, 193 of which from 16 Early Cretaceous outcrops and the other 157 from 13 Neogene sites (Fig.3.8). In this area the Cretaceous succession are very scarce, characterized by few hundred meters which crop out in small structures strongly deformed. The fragments of Shurijeh Formation are included in the small fold systems which deform the Cretaceous

succession in this sector of the belt. The Neogene outcrops are widely diffuse in this area, placed in a gently hills sector limited by the Fariman metamorphic complex at south and the Agdarband Basin at north.

3.4. Magnetic Mineralogy

Determining the presence of the magnetic minerals, their amount and their characterization in the sampled rocks is fundamental, in order to obtain a robust paleomagnetic information that will be considered for tectonic interpretation. For this reason in this study a detailed magnetic minerals characterization has been carried out. The different mineral phases, their crystallographic structure and their grain size give different responses when subjected to a magnetic field. Considering the coexistence in the same rock, of several ferromagnetic phases, it is possible that they develop in different stages of its geological history and thus may carry different paleomagnetic components each acquired during those different stages. Therefore, a characterization of the magnetic mineralogies present in a rock is a crucial starting point in studies based on AMS and paleomagnetism. The methodologies used in these studies and their specific purposes are described in detail in the following paragraphs.

Rock magnetic experiments were performed on selected samples to determine the nature of ferromagnetic and paramagnetic contributions to total AMS, the shape and the orientation of the magnetic fabric; if for the AMS analysis I defined indirectly the abundance of a mineralogy group on the other (e.g. ferromagnetic vs. paramagnetic) using the anisotropy parameters, for the paleomagnetic analysis I detected the nature and the abundance of the magnetic minerals within the samples using specific magnetic methods. Among them the demagnetization of isothermal remanent magnetization (IRM), thermal demagnetization of three-component IRM and measurement of hysteresis properties have allowed the quantification and identification of the magnetic minerals.

3.4.1. Acquisition of isothermal remanent magnetization (IRM) curves

Isothermal remanent magnetization (IRM) refers to the magnetization acquired by a rock sample when exposed to external magnetic field of certain intensity. In the laboratory, IRM is imparted by exposure (usually at room temperature) to a magnetizing field generated by an electromagnet. IRM is the form of remanence produced in hysteresis experiments and is acquired by ferromagnetic grains with coercive force less than the applied field (Butler, 1998).

Applying more intense magnetic fields to a sample in the same direction and measuring the remanent magnetization of the rock after each step, it's possible to obtain the IRM curve of each

sample. The geometry of this curve may help in identifying the ferromagnetic phase or phases present in the sample, by means of their specific coercivity values (Dunlop, 1972). The shape of the curve of acquisition of IRM with increasing magnetizing field is measure of the coercivity spectrum of magnetic minerals present in the sample. SD magnetite, MD magnetite, fine SD hematite, coarse SD hematite, and goethite are the common magnetic phases present in sediments which show rather characteristic and distinct coercivity spectra and IRM acquisition curves (Dunlop, 1972; Opdyke and Channell, 1996).

For this study, a representative suite of samples was subjected to rock magnetic analysis using IRM acquisition curves up to 2.7 T field, imparted by a 2G Enterprise Pulse Magnetizer model 660; the stepwise acquisition of IRM was applied starting from 20 mT stopping to 2700 mT for a total amount of 12 different magnetization steps, as shown in Fig 4.1. After each step, the values of the isothermal remanent magnetization were measured on a 2G DC-SQUID cryogenic magnetometer placed in a magnetic-shielded room at the Paleomagnetism Laboratory of INGV (Roma).

3.4.2. Thermal demagnetization of the composite IRM

Thermal demagnetization of a composite 3-axis IRM (Lowrie, 1990), is very useful for determine magnetic mineralogy. This analysis combines coercivity values and unblocking temperatures, in order to differentiate ferromagnetic contributors present in the same specimen. Low coercivity minerals (e.g. magnetite or phyrrotite) are magnetically saturated under a magnetic field of low intensity, whereas high coercivity minerals (e.g. hematite and goethite) do not reach the complete saturation when subjected to the maximum magnetic field (e.g. Dunlop and Özdemir, 2001).

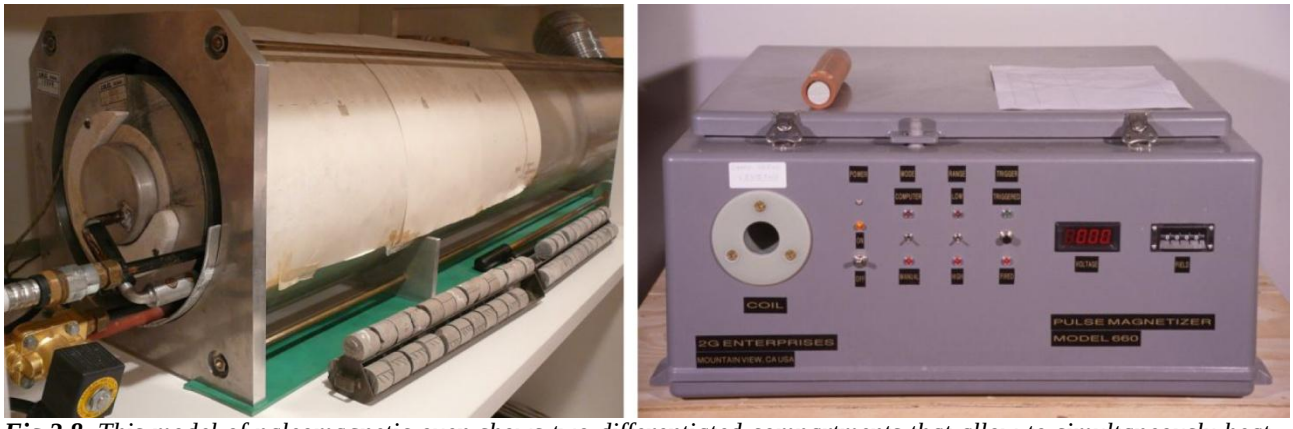

Fig.3.8. *This model of paleomagnetic oven shows two differentiated compartments that allow to simultaneously heat and cool two groups of samples. Around 45 samples can be processed in one compartment.*

Three different magnetic fields were applied in decreasing order of intensity along samples' orthogonal axes (x, y, z) with an ASC pulse magnetometer and thermally demagnetized (Fig. 3.8). following the Lowrie's (1990) procedure. The intensity of the applied fields imparted were 2700,

600 and 120mT, respectively. This procedure generates a remagnetization of the ferromagnetic minerals in specimens according to their coercivity and oriented parallel to each of the three orthogonal directions The following step was to develop a thermal stepwise demagnetization of the remagnetized samples; all the samples were subjected to thermal demagnetization adopting 11 demagnetization steps from room temperature to 680°C. The steps of demagnetization were: room temperature, 150, 350, 440, 480, 530, 560, 580, 630, 660 and 680 °C. Remanent magnetization was measured at each step on a DCSQUID (Direct current Superconducting Quantum Interference Device) cryogenic magnetometers (2G Enterprises, USA) available at the INGV Laboratory of Paleomagnetism. This technique was applied on the representative set of samples already analyzed using IRM acquisition curves, in this way a complete magnetic minerals characterization was achieved, giving the specific indication about the magnetic minerals within the analysed samples.

3.4.3. Backfield procedures

The procedure to obtain backfield IRM curves is linked to the previous IRM acquisition curves performance, involving again the application of increasing magnetic fields, but in these cases, in a direction opposed to that applied to obtain the IRM acquisition curve. Backfield curves allow determining the coercivity of remanence (Hcr), which is the magnitude of magnetic field necessary to demagnetize the sample. The methodology to measure backfield IRM curves was applied to few representative URF samples: powdered samples were measured on MICROMAG Princeton Measurements Corporation 3900 vibrating sample magnetometer (VSM), at the INGV laboratory (Fig. 3.9).

Fig.3.9. *Micromag 3900 Vibrating Sample Magnetometer from Princeton Measurement Corp. (USA) available at the Paleomagnetic Laboratory of the INGV. Used to perform IRM acquisition curves, backfield curves and hysteresis loops in powdered samples*

The coercivity of remanence (Hcr) of selected powders/fragments were measured on MICROMAG Princeton Measurements Corporation 3900 vibrating sample magnetometer (VSM), in fields up to 1T, at the INGV laboratory (Fig. 3.9). The powders were located in pharmaceutical gel caps suitable for vibrating in the VSM. The coercivity of remanence (B_{cr}) values have been extrapolated from backfield remagnetization curves up to -1 T, following forward magnetization in a +1T field.

3.4.4. Hysteresis loops

The advent of the alternating gradient force magnetometer (MICROMAG) allows hysteresis loops to be generated for small (~50mg) samples, even for weakly magnetized sediments (Opdyke and Channell, 1996). Hysteresis loops result from applying progressively higher magnetic fields to a rock and subsequently decreasing fields in the opposite directions; the induced magnetization is measured at each step. The shape of the obtained cycle is conditioned by the mineralogy that characterises the sample. The hysteresis properties of selected powders/fragments were measured

on MICROMAG Princeton Measurements Corporation 3900 vibrating sample magnetometer (VSM), in fields un to 1 T, at the INGV laboratory (Fig. 3.9). The powders were located in pharmaceutical gel caps suitable for vibrating in the VSM, that allow to determine, after subtracting the high field linear trend, the coercive force (B_C), the saturation remanent magnetization (M_{rs}), which is the magnetization that remains in the sample when the applied magnetic field disappears; the coercivity, *Hc*, that is the magnitude of applied magnetic field necessary to magnetically saturate certain substance, and the saturation magnetization (Ms), which is the maximum magnetization acquired by the sample and thus depends on its characteristic coercivity (Dunlop and Özdemir, 2001). The effect of this procedure in a paramagnetic mineral is reflected into a straight line with constant positive slope. Only ferromagnetic phases describe a hysteresis loop when exposed to an external magnetic field, from which the parameters characterizing minerals can be calculated.

3.5. Anisotropy of Magnetic Susceptibility (AMS)

Anisotropy of magnetic susceptibility is a rock magnetic study method which analyse the preferred orientation of magnetic minerals in a rock or unconsolidated sediments. Magnetic susceptibility is the physical property that defines the capacity of any material to magnetize when subjected to an external magnetic field.

In a volume of natural rock several variables can shape the magnetic susceptibility, such as the different magnetic phases present, their grain size and grain geometry, their relative abundance and their distribution within the sample and with respect to the applied magnetic field (Tarling and Hrouda, 1993). The spatial variations in magnetic susceptibility constitute the anisotropy of magnetic susceptibility (AMS). In other words, AMS constitutes the property of materials whereby identical magnetic fields applied in different directions produce different intensities of induced magnetization (Morris, 2003).

A natural rock contains a variety of minerals with ferromagnetic, paramagnetic or diamagnetic properties. Depending on the magnetic properties, each grain contributes to the total susceptibility and its anisotropy. When ferromagnetic minerals exceed 0.1 volume percentage of the whole rock, they control the magnetic properties, otherwise the susceptibility of paramagnetic minerals tends to dominate the diamagnetic minerals provided they constitute more than 1% of the rock (Dubey, 2014) . For isotropic substance the magnetic susceptibility is represented by a single constant K, while for anisotropic substance its represented by a set of constants (K_{11}; K_{22}; K_{33}) that are the eigenvalues of the symmetric tensor; they are called the principal susceptibilities and are indicated with K_1, K_2 and K_3 ($K_{11} \geq K_{22} \geq K_{33}$) (i.e. K_1 or maximum, K_2 or intermediate, and K_3 or minimum

axes (Fig.3.10). This tensor is represented by tri-axial ellipsoid whose axes coincide with the principal directions. In this way the anisotropy of a specimen can be represented visually by the shape of the ellipsoid. If $K_{11}=K_{22}>K_{33}$, the ellipsoid is oblate (disc-shaped). If $K_{11}>K_{22}=K_{33}$, the ellipsoid is prolate (cigar-shaped). Oblate susceptibility ellipsoids are commonly observed in sedimentary rocks and in rocks with a significant foliation, with K_3 oriented perpendicular to the bedding and foliation, respectively. Prolate ellipsoids can be observed in volcanic lava flows and current-deposited sediments, where K_1 is aligned parallel to the paleoflow direction (Morris, 2003).

The K_1 axis is parallel to the magnetic lineation whereas the K_3 axis is perpendicular to the magnetic foliation plane.

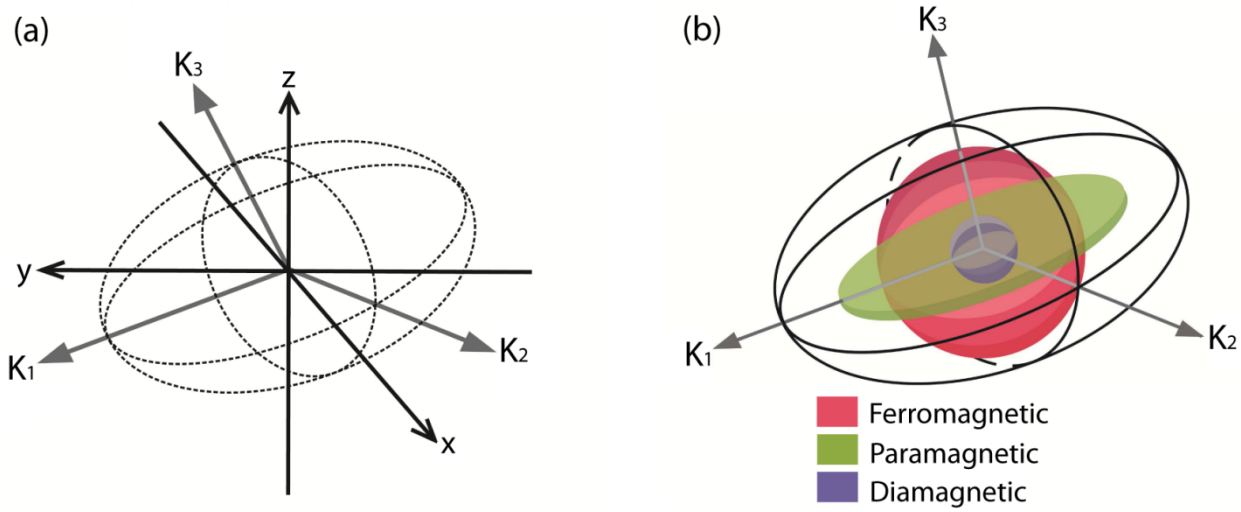

Fig. 3.10. (a) *Graphic representation of the magnetic susceptibility ellipsoid, defined by the susceptibility values in its three main axes: maximum (K_1), intermediate (K_2), and minimum (K_3). Modified from Tarling and Hrouda, (1993).* ***(b)*** *The resultant magnetic fabric is the sum of contributions from all the magnetic carriers present in a sample: dia-, para- and ferromagnetic materials.*

Considering the bulk magnetic anisotropy of a certain volume of rock, as the sum of the contributions from all the magnetic phases present in it, the single phase diamagnetic, paramagnetic and ferromagnetic show individually, different magnetic behaviour depending on the temperature conditions, their capacity to retain a remanent magnetization or the intensity of the applied magnetic field. These differences allow recognizing mineral species within rocks. Several studies concerning with natural materials stated the necessity to separate the contribution of each magnetic phase to the total AMS (e.g. Owens and Bamford, 1976; Rochette and Fillion, 1988; Tarling and Hrouda, 1993).

In sedimentary rocks, an evolution of the magnetic fabric has been observed with the increasing of deformation. In undeformed sediments the ellipsoid is spherical ($K_{11}=K_{22}=K_{33}$), the specimen has

an isotropic magnetic susceptibility and the magnetic foliation is parallel to the bedding plane; this fabric is attributed to depositional and/or compaction processes.

Several parameters have been defined both for the quantification of the magnitude of anisotropy and for defining the shape of the ellipsoid (Hrouda, 1982; Tarling and Hrouda, 1993). Combining K_{11}, K_{22}, K_{33} in different way it's will possible calculate several parameters which describe the shape of the ellipsoid: $P = K_1/K_3$ $L = K_1/K_2$ $F = K_2/K_3$

The degree of anisotropy P is a measure of how marked anisotropy is, instead the magnetic lineation and foliation (L, F) describe the shape of the ellipsoid. L prevails when the ellipsoid is prolate ($K_{11}>K_{22}=K_{33}$) while F prevails when it's oblate ($K_{11}=K_{22}>K_{33}$) (Lanza and Meloni, 2006).

The magnetic lineation L (K_1/K_2) is defined by the orientation of K_1, while the magnetic foliation F (K_2/K_3) is defined as the plane perpendicular to K_3. The T-shape parameter varies from -1 (perfect prolate ellipsoid, $K_1 > K_2 = K_3$) to 1 (perfectly oblate ellipsoid, $K_1 = K_2 > K_3$), while a value of 0 corresponds to a triaxial ellipsoid; this parameter is preferable to most other overall shape parameters as includes all three principal susceptibilities in its calculation and symmetrical in its distribution of values over the full range of ellipsoid shapes (Tarling and Hrouda, 1993). Oblate shapes correspond to $0< T \leq 1$, while negative values, $-1\leq T <0$, correspond to prolate shape.

The mean susceptibility ($K_{mean} = (K_1 + K_2 + K_3)/3$) is the main parameter used in the literature to quantitatively describe the intensity of AMS; furthermore this parameter gives a relative estimation of the amount of magnetic minerals in the samples, in fact high values of K_{mean} outline a sufficient concentration of magnetic minerals in the analysed specimen.

A parallelism between the orientations of the magnetic fabric and the petrofabric in natural rocks has been largely demonstrated allowing AMS to be used as a petrofabric marker and hence as a strain marker (Borradaile, 1988; Borradaile and Henry, 1997; Borradaile and Jackson, 2004; Fuller, 1969; Graham, 1966, 1954; Jelinek, 1981; Jezek and Hrouda, 2004; Kligfield et al., 1983; Kissel et al., 1986; Tarling and Hrouda, 1993). The magnetic fabric registered in natural rocks results from the sum of contributions from all the magnetic minerals present in them, whatever is their behaviour: dia-, para- and ferromagnetic. The first works relating the AMS orientation with the petrofabric of rocks were mainly focused on the AMS associated with the ferromagnetic fraction (e.g. Fuller, 1969; Graham, 1966). Magnetic fabrics in sedimentary rocks are thought to develop very early after deposition and during sediment compaction (i.e. the called *primary magnetic fabrics* as defined by Tarling and Hrouda, 1993). If the sediments undergo tectonic deformation, progressively a tectonic AMS sub-fabric will develop modifying the primary sedimentary magnetic fabric, according to the nature and extent of deformation. When the

deformation is low to moderate, the principal maximum axis K_1 (magnetic lineation) will align perpendicular to the shortening direction. This early development provides them the capacity to reflect the strain pattern controlling the tectonic evolution of the area during deposition and early diagenesis (e.g. Cifelli et al., 2013, 2005; Kissel et al., 1986; Larrasoaña et al., 2004; Moussaid et al., 2013; Soto et al., 2012, 2009), that for these reasons have motivated the use of AMS in structural studies. The accuracy and reliability of this technique were demonstrated even when applied to rocks that apparently underwent weak or none deformation (e.g. Cifelli et al., 2009, 2005, 2004; Kissel et al., 1986; Lowrie and Hirt, 1987; Mattei et al., 1999, 1997; Parés, 2004).

Fig.3.11. *KLY-3S Kappabridge susceptometer from AGICO Inc. (Czech Republic) available at the Paleomagnetism Laboratory of the University of Roma Tre.*

AMS data have been often used in association with paleomagnetic analyses to investigate the origin of curved orogens (Mattei et al., 2017; Weil and Yonkee, 2012). In curved fold and thrust belts the orientation of the magnetic lineation often follows the curvature of the orogen, being therefore representative of its structural trend; generally AMS has been well established as an important indicator of rock fabric that has been used to gain information on the depositional regime of sediments and to reconstruct their deformation history (Tarling and Hrouda, 1993); probably its first applications was the identification of paleoflow directions in detrital sediments (Hrouda, 1982).

For this thesis the low-field AMS was measured for individual specimens at room temperature with an AGICO Kappabridge KLY-3 susceptibility bridge (Spinning Specimen Magnetic Susceptibility Anisotropy Meter), which operates at a frequency of 875 Hz and as a typical sensitivity of ~2.0 x 10^{-8} SI. The analyses for all samples were conducted at the Paleomagnetism Laboratory of Roma Tre University (Fig.3.11). This instrument has a hollow, cylindrical

measurement coil in which the sample is located during measurement. This coil produces an alternating-current field of low intensity, 300A/m, and constant frequency, 875Hz (Jelínek and Pokorný, 1997). The instrument was provided with a diamagnetic spinning holder in which samples were situated in three perpendicular positions; the rotation of the robotic arm around a plane allows to register multiple measurements in each position of the sample. In summary, the 3+1 measurement positions (i.e. three perpendicular positions of the sample and a fourth to obtain its bulk magnetic susceptibility) allow to obtain a magnetic susceptibility ellipsoid (Fig.3.11). The software controlling the apparatus (i.e. Susar, AGICO Inc.) subtracts the empty holder value from results and provides errors in measurements, which contributes to the accuracy in the ellipsoid definition. The standard procedure to measure AMS at room temperature under a low magnetic field is considered the fastest, cheapest and conservative method for the magnetic characteristics of samples, which allowing their use in subsequent procedures, such as thermal demagnetization of the NRM.

3.6. Paleomagnetism

Paleomagnetic techniques constitute a methodological approximation that allows quantifying geological movements with respect to an external, global and absolute reference, that is the Earth's magnetic field. It is a fundamental tool to study plate-tectonics, since it provides absolute time references for relative movements between tectonic plates. Paleomagnetism exploits the fact that all rocks in the Earth surface present a variable amount of ferromagnetic minerals, able to maintain a remanent magnetization. Therefore, all rocks are potential carriers of a paleomagnetic signal, which under the necessary conditions can be used as a continuous marker of tectonic processes. One of the fundamental conditions to be considered is the age of the primary remnant magnetization with respect to the age of the rock containing it.

3.6.1. Relaxation time

The relaxation time (τ) is the capacity of ferromagnetic grains to maintain a magnetic remanence for a certain period of time (e.g. at geological-scale). It is defined as the time necessary to reorient the magnetic moments of a mineral grain with respect to a new applied magnetic field, i.e. to acquire a new remanent magnetization (e.g. Tarling and Hrouda, 1993; Tauxe, 2010).

Thermal vibrations of atomic magnetic moments can overcome internal (magnetostatic and magnetocrystalline) energy barriers in single-domain grains and cause their magnetizations to flip backwards and forwards along the 'preferred axes' (Morris, 2003). The relaxation time depends on several factors, such as temperature, grains size and composition (Opdyke and Channell, 1996).

In an assemblage of SD grains whose preferred axes are randomly distributed, thermal processes will result in a randomization and cancelling out of the individual magnetizations, thereby producing no net externally observed magnetization (Morris, 2003). At room temperature, most minerals show geological-scale relaxation times. However, when thermal energy increases (i.e. at higher temperatures), the time to erase the original magnetization (i.e. relaxation time) diminishes drastically. The remanent magnetization therefore decays exponentially with time.

3.6.2. Natural Remanent Magnetization (NRM)

It is known that the three fundamental assumptions of paleomagnetism are: the existence of the Earth's magnetic field which was able to affect all the rocks of the Earth's crust along the geological history, the capacity of ferromagnetic minerals contained in the rocks to record the Earth's magnetic field during rock formation, and the capacity of these minerals to retain the stable paleomagnetic signal through time. Natural remanent magnetization (NRM) is remanent magnetization present in a rock sample prior to laboratory treatment. NRM depends on the geomagnetic field and geological processes during rock formation and during the history of the rock. NRM typically is composed of more than one component. The NRM component acquired during rock formation is referred to as primary NRM, secondary NRM components can be acquired subsequent to rock formation and can alter or obscure primary NRM. The secondary components of NRM add vectorially to the primary component to produce the total NRM:

$$\boldsymbol{NRM = primary\ NRM + secondary\ NRM}$$

The primary component is called the *Characteristic Remanent Magnetization* (ChRM): the highest-stability component of NRM isolated during demagnetization (Morris, 2003).

The three basic forms of primary NRM are (1) thermoremanent magnetization, acquired during cooling from high temperature; (2) chemical remanent magnetization, formed by growth of ferromagnetic grains below the Curie temperature; and (3) detrital remanent magnetization, acquired during accumulation of sedimentary rocks containing detrital ferromagnetic minerals. Secondary NRM can result from chemical changes affecting ferromagnetic minerals, exposure to nearby lightning strikes, or long-term exposure to the geomagnetic field subsequent to rock formation (Morris, 2003).

3.6.3. Thermal demagnetization

Thermal demagnetization is a method related to the relaxation time reduction of ferromagnetic minerals with temperature. This technique involves heating a specimen to an elevated temperature and then cooling to room temperature in zero magnetic field. The magnetizations of all

ferromagnetic grains within the specimen with unblocking temperatures less than or equal to the demagnetization temperature are randomised upon heating. In the absence of a magnetic field, the magnetizations retain this random distribution upon subsequent cooling (Butler, 1998; Morris, 2003). This process obliterates the remanent magnetization to all minerals whose unblocking temperature is below the specific applied high temperature and, in presence of an external magnetic field, a thermo-remanent magnetization is induced to them. Since the external magnetic field acting during the procedure is zero, NRM is erased but no other magnetization is imprinted in the 'unblocked' minerals, which remain randomized. A stepwise demagnetization procedure is usually followed, with successively increasing temperatures demagnetizing successively higher unblocking temperature fractions. The last thermal step will depend on the Curie or Neel temperatures of the mineral phases present in each sample, until the NRM is completely erased.

3.6.4. Paleomagnetic measurements and analyses

The orientation and intensity of paleomagnetic components naturally registered in these samples were measured in the DCSQUID (Direct current Superconducting Quantum Interference Device) cryogenic magnetometers (2G Enterprises, USA) available at the Laboratory of Paleomagnetism at the Istituto Nazionale di Geofisica e Vulcanologia, INGV (Fig.3.12).

In order to isolate the cryogenic magnetometers and the ovens from the effect of the present Earth's magnetic field, the Laboratory is equipped by a magnetically shielded room which avoid samples to acquire a viscous remagnetization during the laboratory procedure (Fig.3.12). Sensors in DC-SQUID magnetometers are made of superconductive materials that need to remain refrigerated with liquid helium (4K) in order to maintain their properties. The equipments allow measuring rock samples with the standard dimensions. The thermal demagnetization process consists in applying heating-cooling cycles to samples, each with increasing temperature in absence of magnetic field.

Fig.3.12. *DC-SQUID cryogenic magnetometers from 2G Enterprises at the Laboratory of Paleomagnetism of the INGV-Rome Institute. Two Cryogenic magnetometers are installed in a shielded room.*

The analysis of a group of the Shurijeh Formation and URF samples were composed by 13 steps of increasing temperature: NRM (room temperature), 150, 250, 350, 440, 480, 530, 560, 580, 600, 620, 640, 660, 680ºC; for another group of samples 14 steps of increasing temperature were adopted: NRM (room temperature), 150, 230, 280, 340, 400, 440, 510, 580, 615, 630, 645, 660, 680 ºC. Steps above 610 °C were applied only in the rocks were the intensity of magnetization was still significant. Heating intervals were longer as the required temperature was higher, ranging from 30 minutes during the first stages to 50 minutes for higher temperatures.

3.6.5. Analysis of principal magnetic components

The obtained results were subjected to an analysis of the principal components, by plotting them in orthogonal vector diagrams known as Zijderveld diagrams (Zijderveld, 1967). These representations allow calculating the linear regression of directions of paleomagnetic components (Fig.3.13).

The mean magnetic components per site were calculated by means of Remasoft 3.0 software (Chadima and Hrouda, 2006), which applies Fisher statistics (Fisher, 1953). A *Fisherian distribution* of points within a sphere is a statistical approximation that represents the most probable orientation of the demagnetization points on a stereo-plot (Morris, 2003).

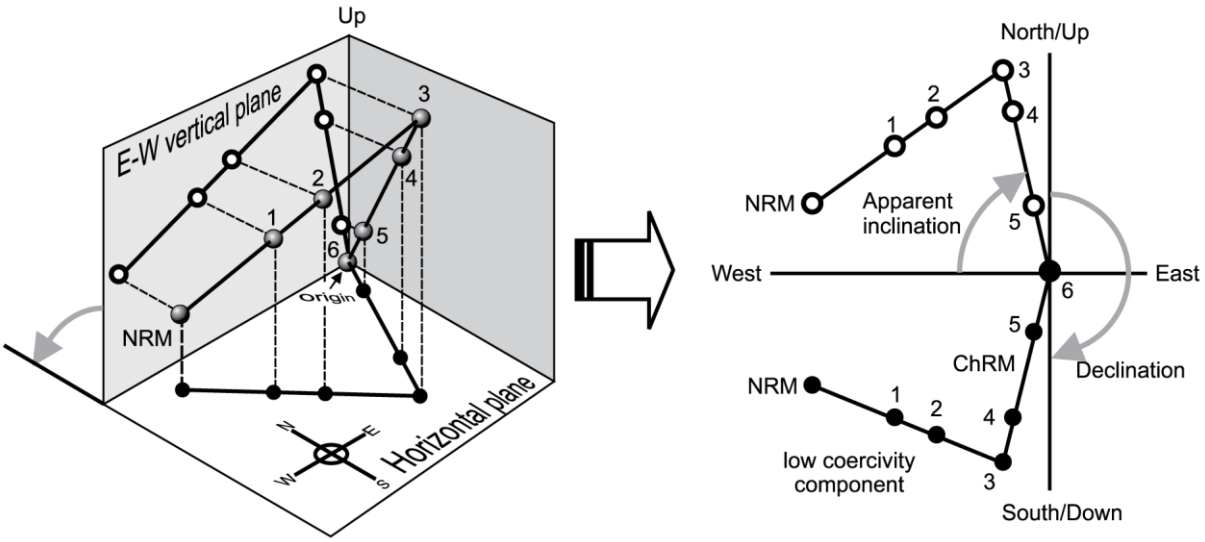

Fig.3.13. *Schematic representation of demagnetization data on an orthogonal demagnetization diagram (Zijderveld, 1967). Straight line segments of the demagnetization path define discrete components of magnetization, and best-fitting vectors are calculated using principal component analysis. Low coercivity components (that most frequently represent secondary magnetizations) are removed first leaving a more stable characteristic component (ChRM), that represents the primary magnetization. These changes are represented by projecting the magnetization vector (left) on to the horizontal plane and either the N–S or E–W vertical plane. The two projections are then combined (right) to give a single demagnetization diagram. The declination can be read directly from the diagram, whereas the inclination must be calculated from the apparent inclination. Numbers (1– 6) represent progressively higher demagnetization levels; solid black circles = projection of the magnetization vector on to the horizontal plane; open circles = projection of the magnetization vector on to (in this example) the E–W vertical plane (modified after Morris, 2003).*

This probabilistic description allows defining several parameters that inform about the representativeness and accuracy of the obtained data. The most important of these parameters are given by Remasoft 3.0: the mean direction of the magnetic components, defined by their declination and its inclination; *R* is the length of the mean result obtained from *N* components, always being *R*<*N*; the accuracy parameter, *k*, describes the dispersion of points and can directly relate *R* and *N* (k=N-1/N-R), being larger when *R* and *N* are more similar, and thus the dispersion of points is lower; the confidence limit, α_{95}, estimates the precision of the obtained mean direction, i.e. there is a 95% of possibilities of the true direction to be contained within the calculated α_{95} (Morris, 2003).

3.6.6. Tests of paleomagnetic stability

Sedimentary rocks acquire a detrital primary magnetization during sediment deposition and the earliest stage of diagenesis. Therefore the age of this primary magnetization can be considered as equivalent to that of the rocks, when the layers can be considered to remain horizontal in that acquisition moment (Butler, 1998; Tauxe, 2010).

During the time the rocks a remagnetization event can occur at any moment during diagenesis and exhumation. The directions of the mean components do not directly reveal the origin of the

magnetization; in this way, the obtained ChRMs (one or several per sample), need to be evaluated to determine if they are primary or if they belong to a subsequent remagnetization process.

Laboratory tests cannot prove that the ChRM is primary. Field tests of paleomagnetic stability can provide crucial information about the timing of ChRM acquisition. In studies of old rocks in orogenic zones, field test(s) of paleomagnetic stability can be the critical observation (Butler, 1998)

Several tests have been designed and adapted to fieldwork strategies in order to give a relative temporal order to the obtained ChRMs (Graham, 1949).

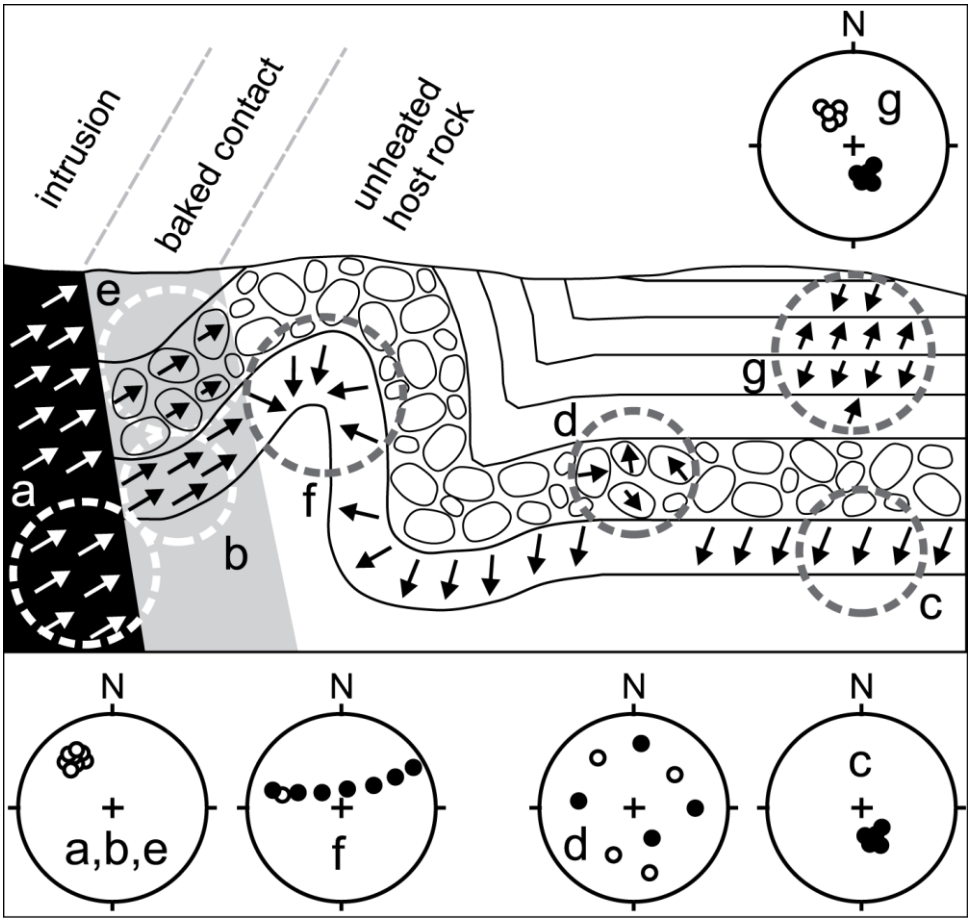

Fig.3.14. *Schematic geological section illustrating four field tests of palaeomagnetic stability: (**a, b, c**) the baked contact test; (**d, e**) the conglomerate test; (**c, f**) the fold test; and **(g)** the reversal test. See glossary entries for details. Arrows represent magnetization directions. Solid symbols on stereonets are downward remanence directions, open symbols are upward directions.*

- The *fold test* (Graham, 1949; Fig.3.14c-f). Samples are collected from beds with different present structural orientations (e.g., from around a fold). The distribution of ChRM directions before and after correcting for bedding tilt are compared. If ChRM directions become more closely grouped after untilting (Fig. 3.14c), this indicates that the ChRM was acquired before folding (Morris, 2003). In these cases, the result from the fold test is positive. Increased dispersion of ChRM

directions after untilting indicates that the magnetization is postfolding in age. In these cases, the fold test is negative (Fig. 3.14f).

A third response to the test can occur if the largest convergence between both sets of vectors does not occur BTC nor ATC, but in an intermediate position. This result will point to a syn-folding remagnetization of the rocks. For this thesis, the fold test was applied at the regional scale in the paleomagnetic studies performed (Fig.3.7) basically in the Jurassic- Cretaceous thrust-fault system northern of Mashhad where some sites has been collected on the opposite flank of fold structure (e.g. KD17-KD19, KD12-KD16, KD24-KD28 as show in Fig.3.7).

- The *reversal test* (e.g. Van der Voo, 2005, Fig. 3.14g).

If a suite of paleomagnetic sites affords adequate averaging of secular variation during both normal- and reversed-polarity intervals, the average direction of primary NRM for the normal-polarity sites is expected to be antiparallel to the average direction of primary NRM for the reversed-polarity sites. However, acquisition of later secondary NRM components will cause resultant NRM vectors to deviate by less than 180°. ChRM directions are said to "pass the reversals test" if the mean direction computed from the normal-polarity sites is antiparallel to the mean direction for the reversed-polarity sites. Passage of the reversals test indicates that ChRM directions are free of secondary NRM components and that the time sampling afforded by the set of paleomagnetic data has adequately averaged geomagnetic secular variation. Furthermore, if the sets of normal- and reversed-polarity sites conform to stratigraphic layering, the ChRM is probably a primary NRM.

The reversal test was performed in this thesis in order to verify if components with different polarities are perfectly antipodal (considering their statistical error), which is a sign of their primary origin (Fig. 3.14g).

- The *conglomerate test* (Fig. 3.14d-e).

If ChRM in clasts from a conglomerate has been stable since before deposition of the conglomerate, ChRM directions from numerous cobbles or boulders should be randomly distributed (= passage of conglomerate test). A non random distribution indicates that ChRM was formed after deposition of the conglomerate (= failure of conglomerate test). Passage of the conglomerate test indicates that the ChRM of the source rock has been stable at least since formation of the conglomerate. A positive conglomerate test from an intra formational conglomerate provides very strong evidence that the ChRM is a primary NRM (Butler, 1998). For

this thesis, the conglomerate test was performed on the Neogene URF deposits in the KD54 (Fig.3.15) and KD63 site.

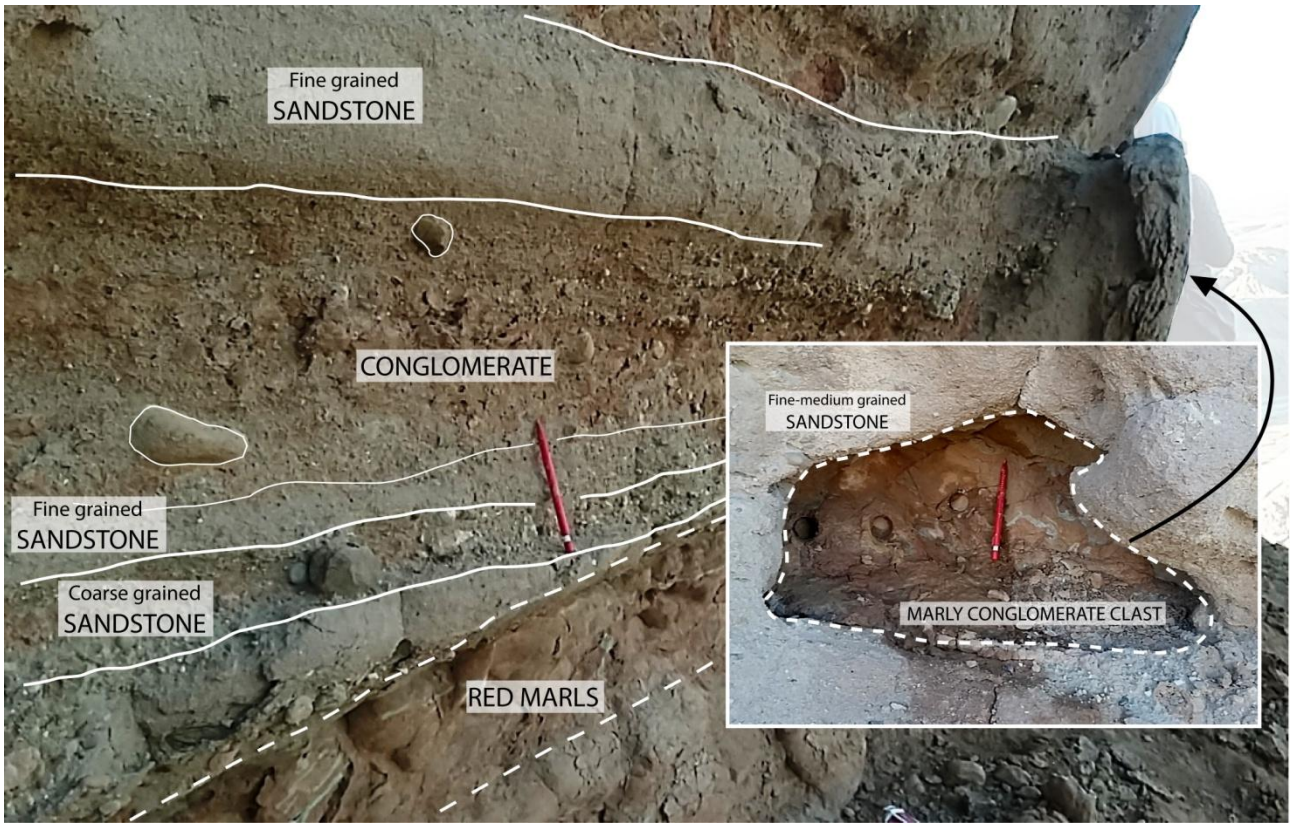

Fig.3.15. *Schematic representation of the Neogene KD54 site where the samples were collected in order to performed the conglomerate test.*

4. MAGNETIC MINERALOGY

4.1. Magnetic mineralogy results

To identify the magnetic mineralogy and characterize the ferromagnetic minerals of the studied samples, different methods were used.

The stepwise acquisition of an isothermal remanent magnetization (IRM) was imparted using a pulse magnetizer up to 2.7 T fields. As shown in Fig.4.1a, the IRM acquisition curves of the Early Cretaceous samples present a homogenous trend. In fact most of the 30 representative analysed samples show a progressive increase of IRM that does not reach saturation up to 2.7 T, suggesting the presence of a dominant high coercivity ferromagnetic mineral. The IRM increases initially steeply up to applied fields of 0.02-0.9 T and than starts climbing gently without reaching saturation up to 2.7 T. This information suggests the presence of variable amounts of low and high coercivity components.

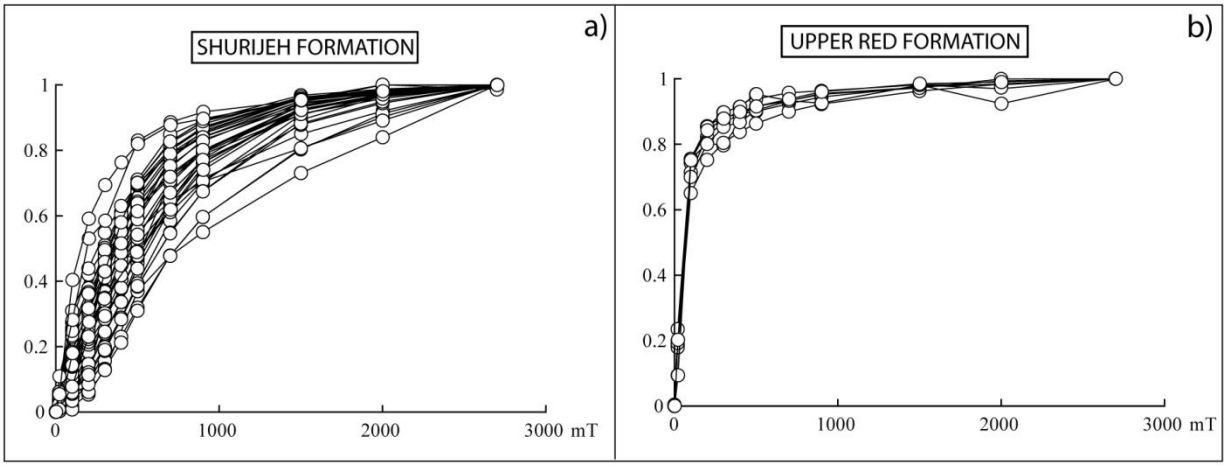

Fig.4.1 *Magnetic mineralogy of the analysed samples. a) For the Shurijeh sites IRM acquisition curves showing the prevalence of high-coercivity minerals in the analysed samples; b) For the URF sites IRM acquisition curves showing the coexistence of high and low-coercivity minerals in the analysed samples.*

The IRM of Neogene Red Beds increase initially more steeply in a shorter stepwise interval from 0.02 to ~0.3 T and than continues to climb gently without reaching saturation up to 2.7 T (Fig.4.1b). In this case, the 8 samples analyzed show a perfect fitting and their trend suggests the prevalence of the low coercivity components with a minor amount of the high coercivity components.

In order to detect which kind of magnetic mineral characterizes the samples I used thermal demagnetization (ThD) of a three component IRM imparted in 2.7, 0.6 and 0.12 fields along three orthogonal directions (Lowrie, 1990). The ThD of each IRM component is plotted separately in Fig.4.2-4.3-4.4 for the Shurijeh Fm. samples and in Fig.4.5 for the Neogene samples.

The ThD curves of the Early Cretaceous Shurijeh Formation show that the medium (0.6 T) and the hard (2.7 T) coercivity components are the largest, and that the soft (0.12 T) component is negligible. The mid-high coercivity (0.6 and 2.7 T) curves show maximum unblocking temperatures of 650-680°C consistent with the occurrence of hematite; the presence in these curves of an inflection between ~300 and 440°C suggests that at least part of this hematite may derive from the transformation of an original maghemite phase during thermal demagnetization treatment (Fig.4.2g-4.3e). In all the analyzed samples the scarce presence of low coercivity component (revealed by the 0.12 T curve) with maximum unblocking temperatures of ~570°C interpreted as magnetite, suggest the coexistence of hematite and magnetite minerals that probably characterized the entire Shurijeh Formation.

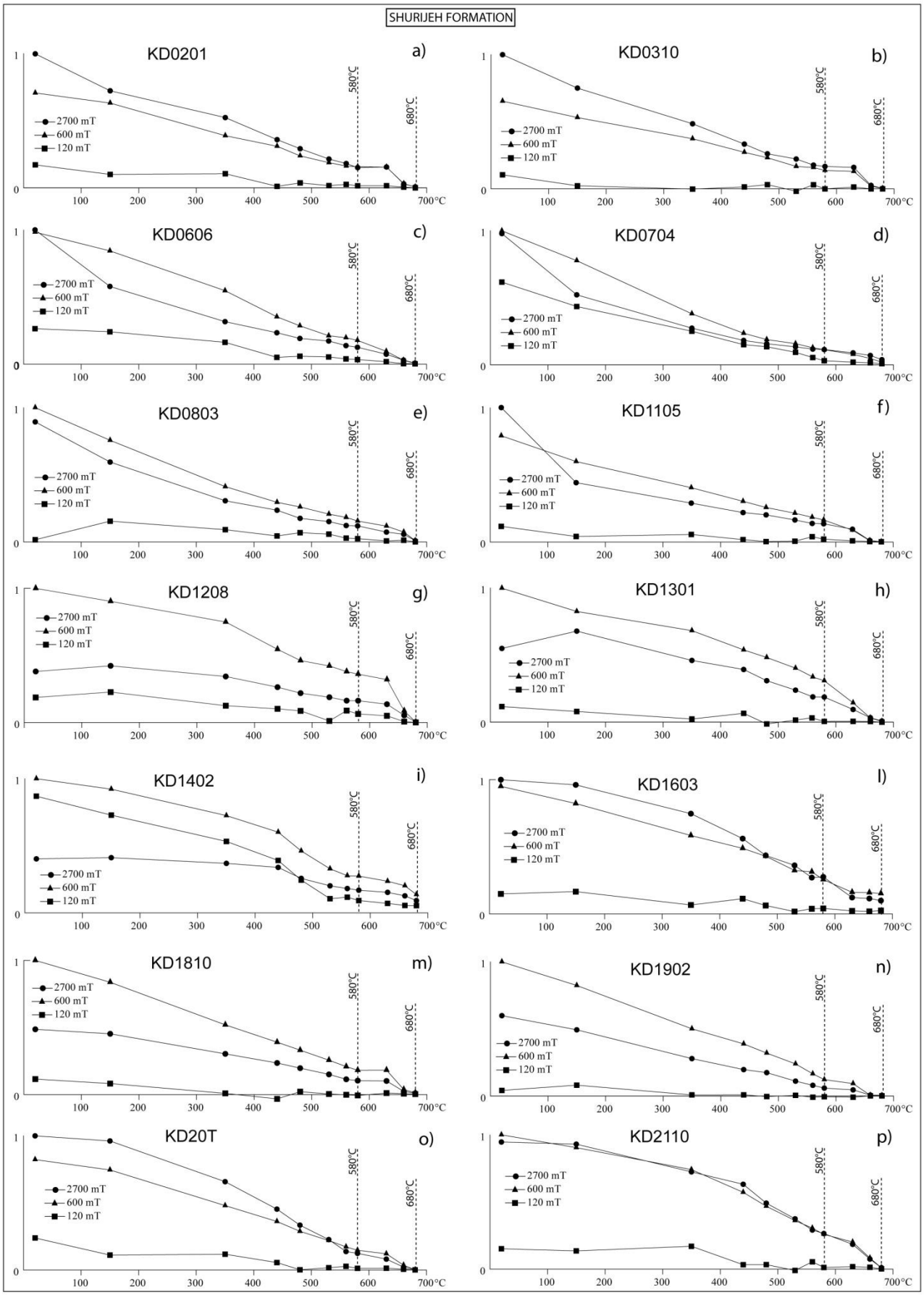

Fig.4.2 *Thermal demagnetization curves of a three-component (hard, medium, soft) IRM (Lowrie, 1990) of some representative samples from Shurijeh Fm.*

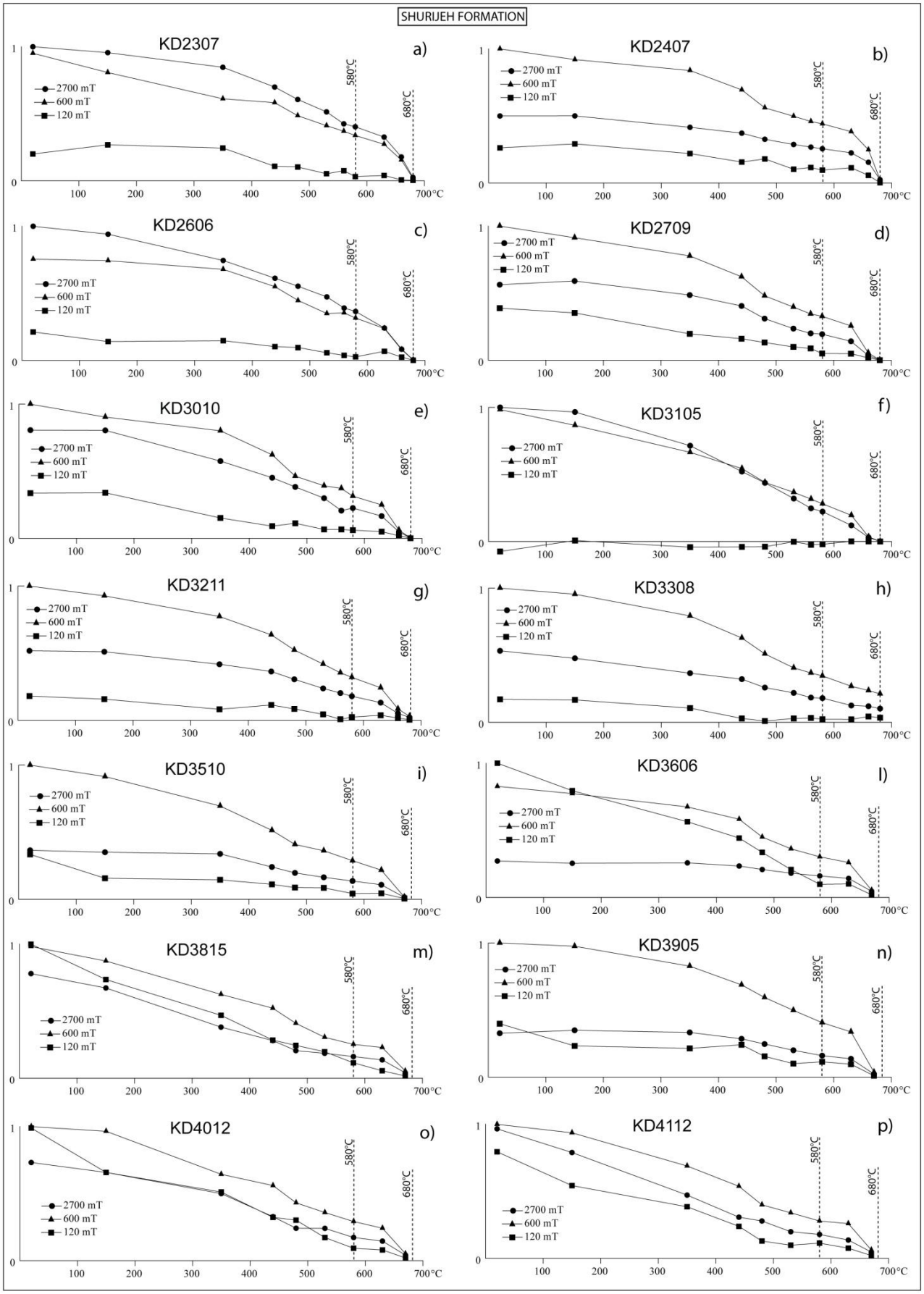

Fig.4.3 *Thermal demagnetization curves of a three-component (hard, medium, soft) IRM (Lowrie, 1990) of some representative samples from Shurijeh Fm.*

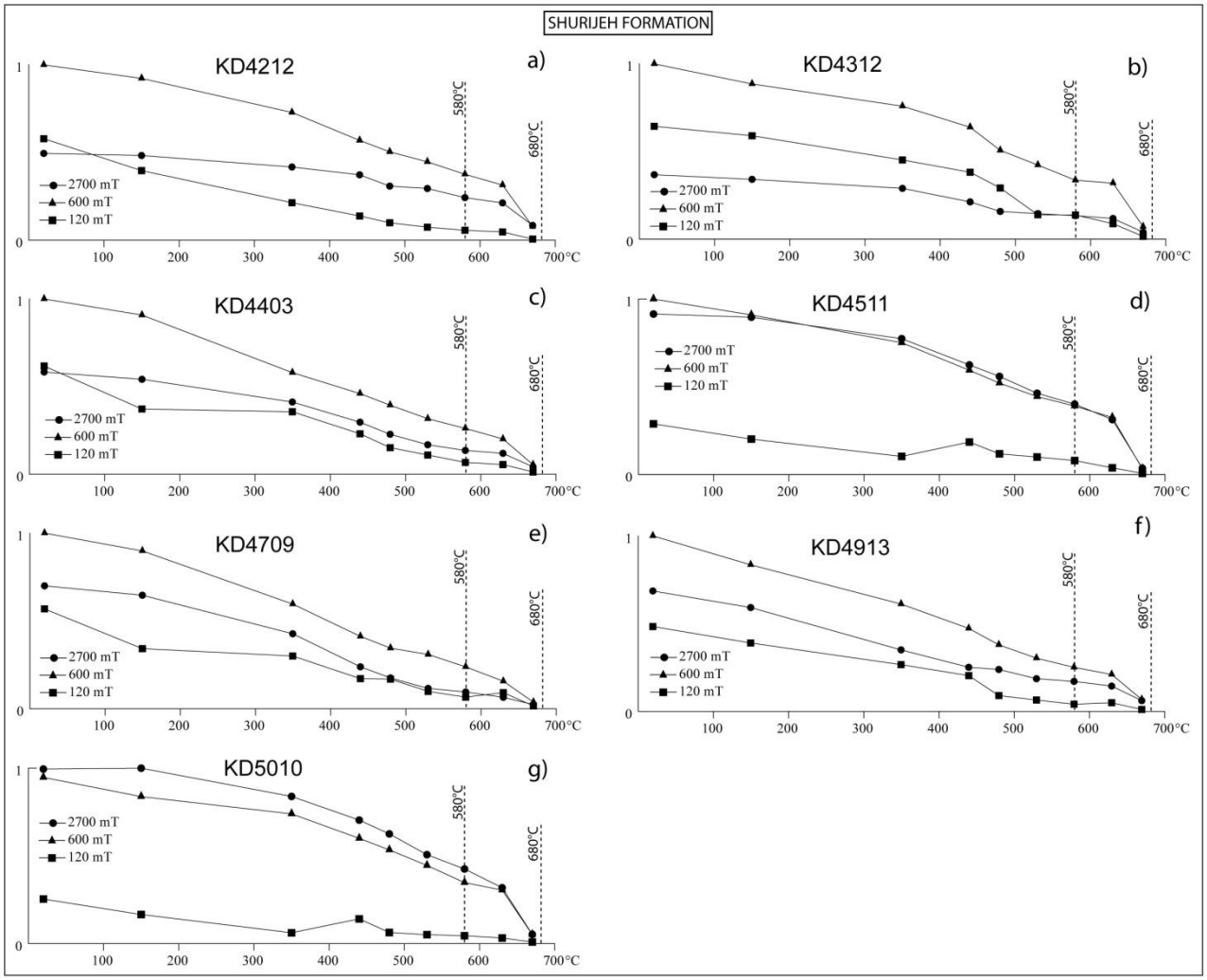

Fig.4.4 *Thermal demagnetization curves of a three-component (hard, medium, soft) IRM (Lowrie, 1990) of some representative samples from Shurijeh Fm.*

The ThD curves of the Neogene Upper Red Formation show that the low coercivity (0.12 T) component prevail respect to the hard (2.7 T) and mid coercivity components suggesting the presence of hematite, though the decay in intensity of all three components up to 570°C suggests also the presence of magnetite (Fig.4.5).

The analysis of further 5 representative samples of Upper Red Formation were carried out using a MICROMAG magnetometer. The results are mainly consistent with a coexisting of low coercivity component (magnetite), as evidenced by B_{cr} values generally lower than 50 mT, and high coercivity component (hematite), as suggest by the hysteresis loops that doesn't reach the saturation. The exception is sample KD6809, whose B_{cr} value is considerably higher (96.05 mT) that indicating the prevalence of high coercivity component (hematite). In general, for most of the Neogene Upper Red Formation samples has been detected the prevalence of hematite because the hysteresis loop and IRM acquisition curve are not saturated up to 1 T (Fig.4.6).

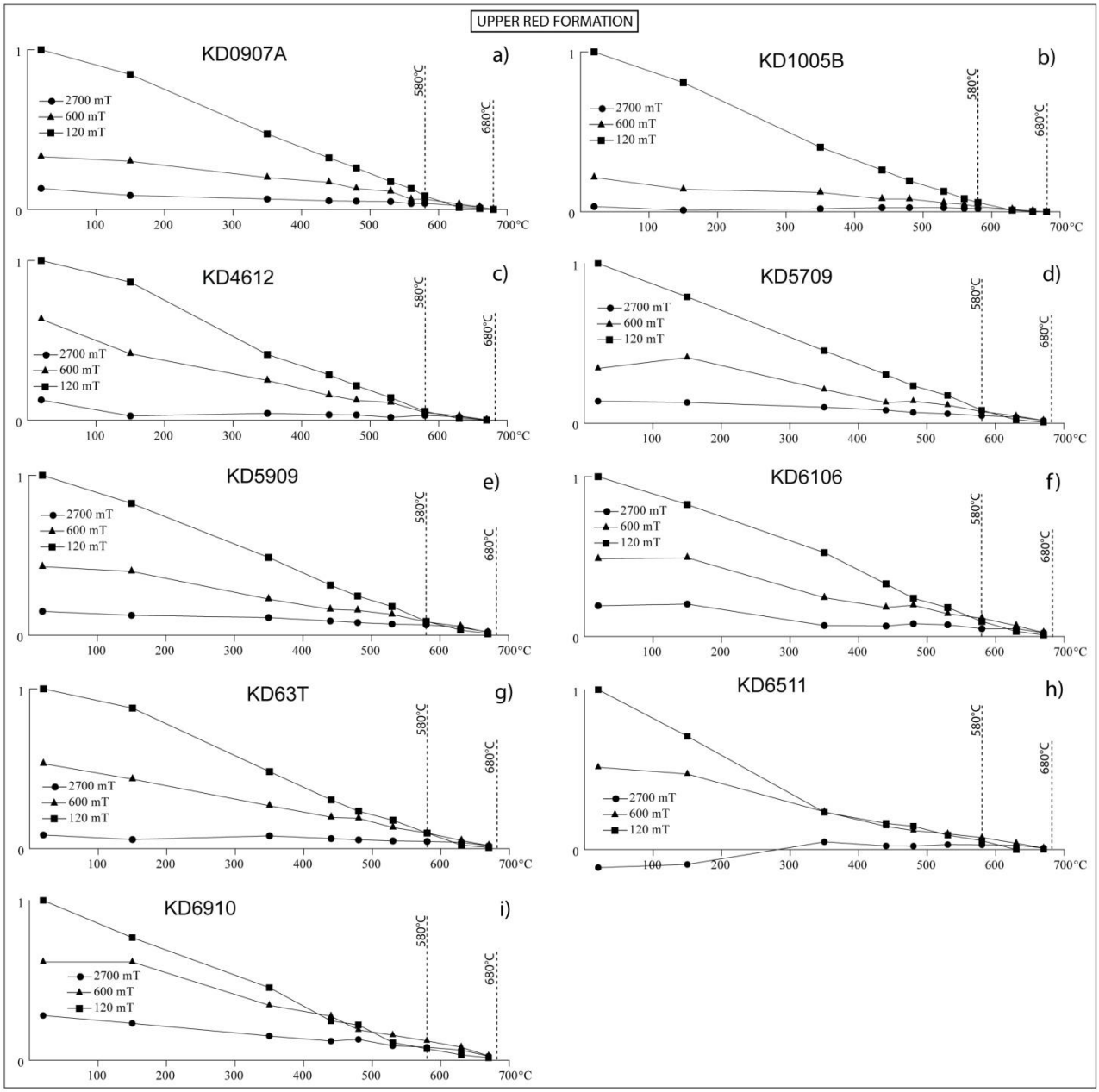

Fig.4.5 *Thermal demagnetization curves of a three-component (hard, medium, soft) IRM (Lowrie, 1990) of some representative samples from URF.*

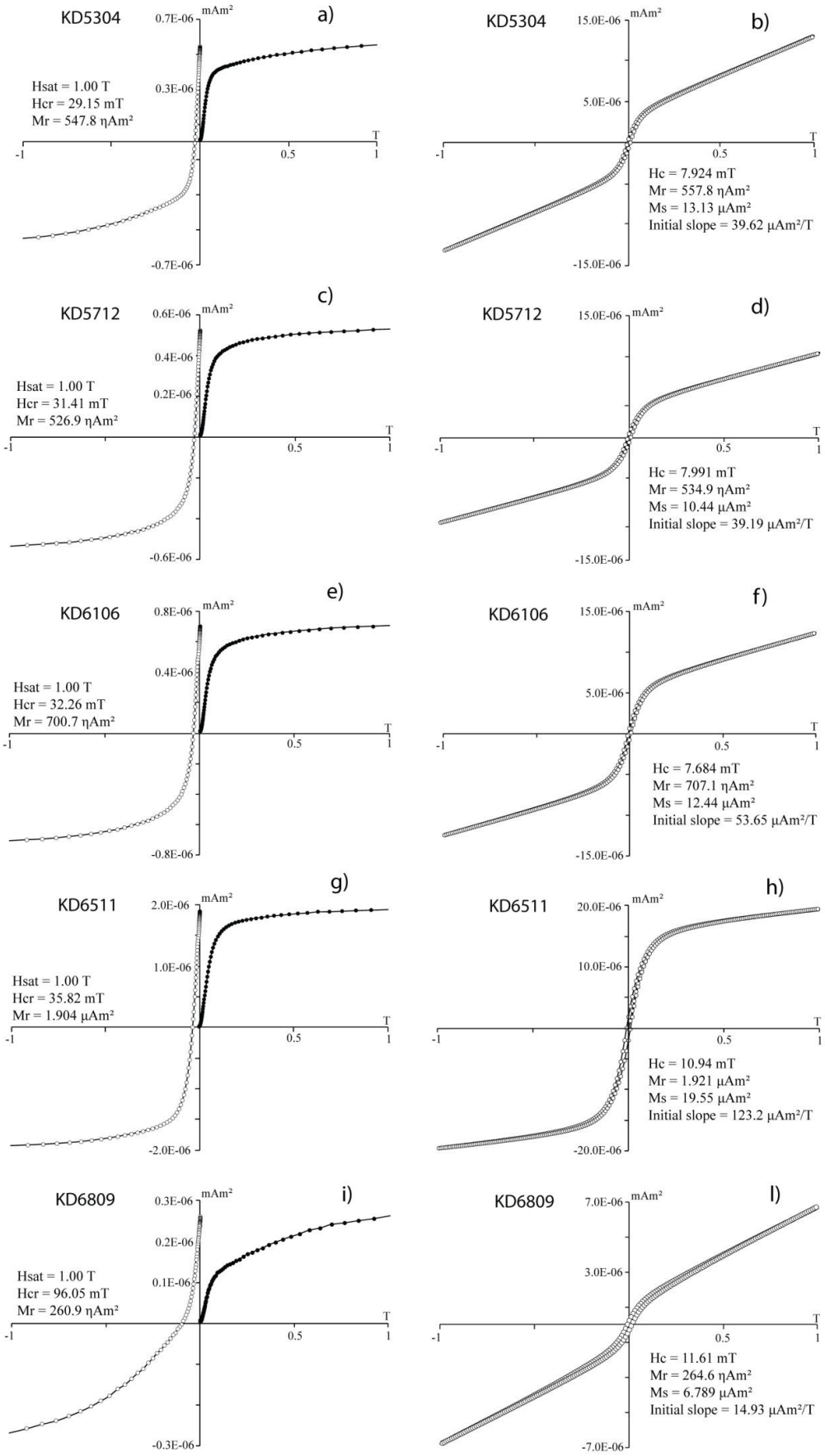

Fig.4.6 *IRM acquisition curves (a, c, e, g, i – black circles), backfield applications (a, c, e, g, i – white circles) and hysteresis loops (b, d, f, h, l), for some representative samples of URF.*

5. MAGNETIC FABRIC RESULTS

AMS parameters defined by Jelinek (1981) and Tarling and Hrouda (1993), including corrected anisotropy degree P' and shape parameter T, which varies from -1.0 to 1.0 for prolate to oblate ellipsoids, were calculated for each site.

In the Kopeh Dagh mountain range the structural trend of the sampling sites has been evaluated using the orientation of the magnetic lineation defined as the axis of maximum magnetic susceptibility K_{max} determined by mean of AMS analyses.

5.1. The Early Cretaceous Shurijeh Formation

As shows in Fig.5.1a, in the Kopeh Dagh Mts. sites, the mean magnetic susceptibility ($K_m=[K_1+K_2+K_3]/3$) values of the Shurijeh Fm. are well defined in a relatively short interval, with most of the samples showing K_m values in the range of 60 and 210 x 10^{-6} SI units and a median value of 144 x 10^{-6} SI.

The low magnetic susceptibility values of the Shurijeh Fm. cores are typical of sediments with a low ferrimagnetic mineral content, whose susceptibility and magnetic fabric are mostly determined by paramagnetic minerals, such as biotite, as well as these low values of magnetic susceptibility could be due to an important contribution of diamagnetic minerals such as quartz, which decrease the mean susceptibility values (Rochette, 1987; Sagnotti et al., 1998).

The main magnetic susceptibility parameters calculated for the Shurijeh Fm. samples show that most of the results from different sites are coherent; the corrected degree of anisotropy parameter, P_j, shows a range of values between 1.025 and 1.271 and only one site with the peak value of 1.492. Anyway, as shown by the P_j vs. K_m diagram (Fig. 5.1c), there is no different contribution of the ferromagnetic component to the magnetic susceptibility; in fact the corrected degree of anisotropy is low (<1.1 for 31 sites) for most of the sampling sites and showing no correlation with the sites affected by low K_m values; also the other 14 sites characterized by growing corrected degree of anisotropy values don't show correlation with the higher K_m values, suggesting that there is no contribution of the ferromagnetic fraction in the sites with high mean susceptibility values (Fig. 5.1c).

The magnetic lineation parameter, L (K_1/K_2), ranges between 1.01 and 1.098, while the magnetic foliation parameter, F (K_2/K_3), range between 1.014 and 1.189 and only one site with the peak value of 1.33 (Tab.5.1). Most of the site (42) mean values of the Shurijeh Fm. show a purely oblate (F>L, 0<T<1) ellipsoids and only 3 site mean values show a triaxial (F=L, T=0) ellipsoids, whereas no site mean values present a prolate ellipsoid (L>F, 0<T<-1) (Fig. 4.7e, Tab.5.1).

The magnetic foliation is well developed in almost all the Shurijeh red beds sites and is sub-parallel to the bedding plane. This could suggest that the magnetic foliation was formed as consequence of compaction. In almost all of these sites K_1 and K_2 have distinct orientations within the foliation plane, and K_1 shows a well-defined orientation.

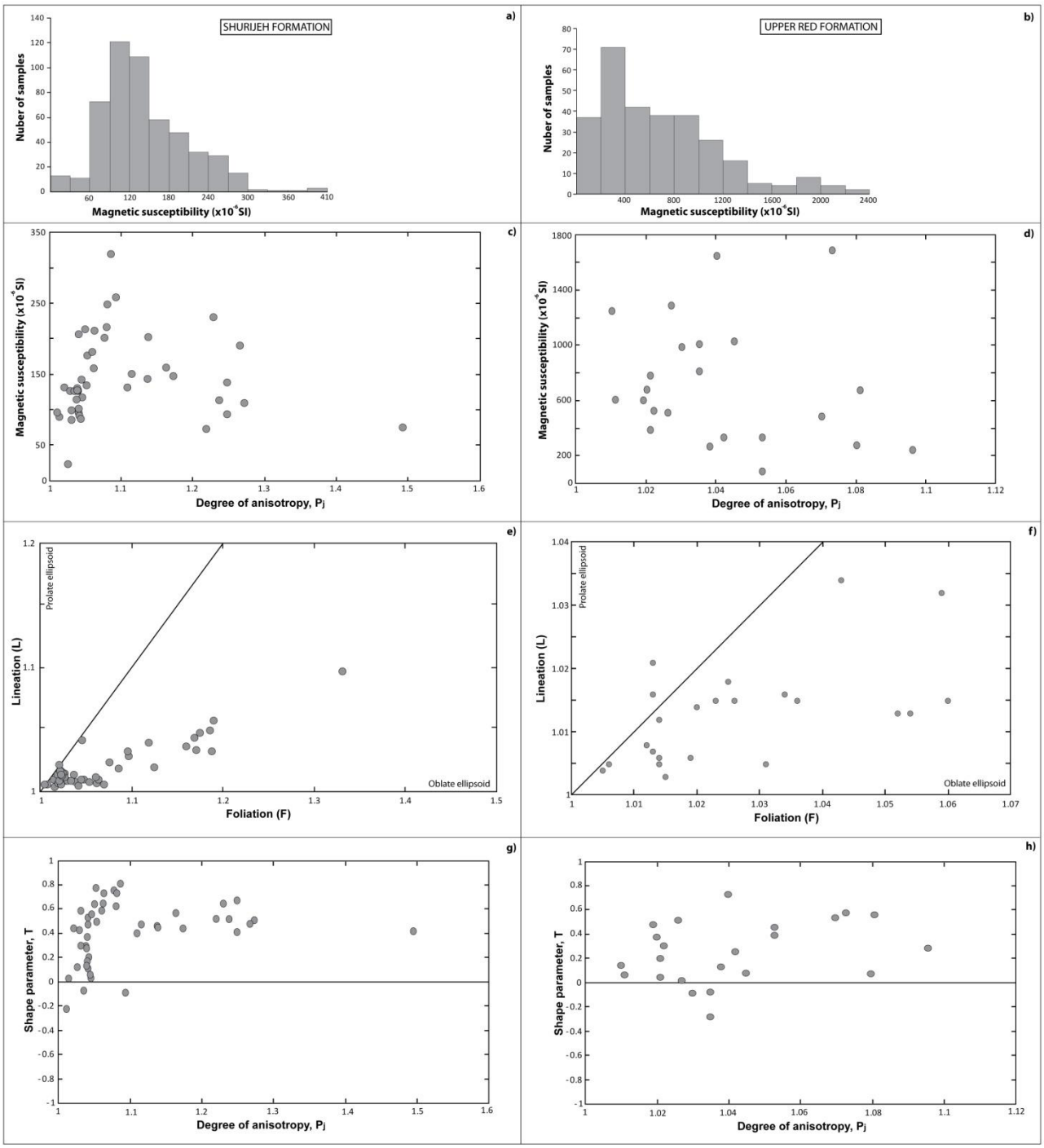

Fig.5.1. *Magnetic parameters for the entire set of 822 specimens of the Shurijeh Fm (left column) and URF Fm (right column). a)-b) Frequency distribution of the mean susceptibility (Km) values; c)-d) Plot of corrected anisotropy degree (Pj) versus mean susceptibility for site averages; e)-f) Flinn diagram of foliation ($F=K_2/K_3$) and lineation ($L=K_1/K_2$) AMS values for site averages; g)-h) degree of anisotropy Pj versus T diagram, calculated using mean site values.*

The magnetic lineation is well defined for most of the sites. The K_1 susceptibility directions for most of the sites are well grouped and e_{1-2} angles (the semi-angle of the 95% confidence ellipse in the K_1-K_2 plane), exceed 26° at only 18 sites (KD14-15-16, KD26, KD29, KD32, KD35, KD37-38-39-40-41, KD43-44-45, KD48-49, KD51).

The AMS directions of Shurijeh sampling sites show that the red fluvial deposits of Shurijeh Formation are characterized by different magnetic fabric types, which describe the degree of deformation of each sites and area sampled.

The first class of magnetic fabric, recognized at sites KD14 and KD29, is characterized by a well defined magnetic foliation parallel to the bedding plane with a sparse distribution of K_1 and K_2 axes along the foliation plane (Fig. 5.2).

In these sites the absence of a well defined magnetic lineation and the orientation of K_3 orthogonal to the bedding plane testify a purely sedimentary origin of the magnetic fabric which have not undergone a significant deformation, other than compaction.

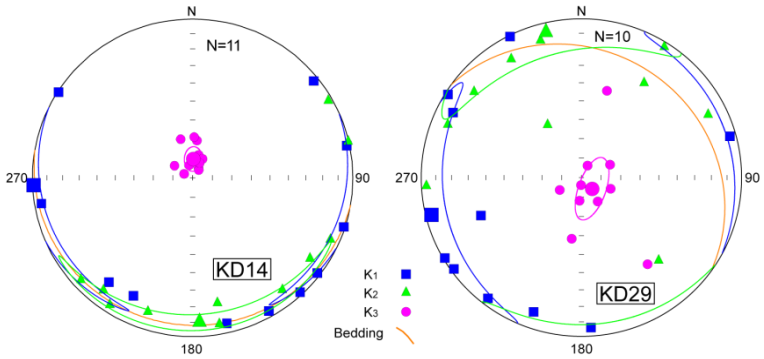

Fig.5.2 *AMS plots for sites KD014 and KD29. Data are plotted on lower hemisphere, equal-area projections, in geographic coordinates. Squares and circles represent maximum and minimum axes, respectively. Bedding planes are also represented.*

A second class of magnetic fabric has been observed in 27 sampling sites. In these sites, the magnetic foliation is well defined, with the K_3 axis orthogonal to the foliation plane and distinct orientation of K1 and K2 within the foliation plane(Fig. 5.3a-b). In these sampling sites the resulting AMS plots show a magnetic fabric configurations typical of a weak deformation regime characterized by a low shortening degree.

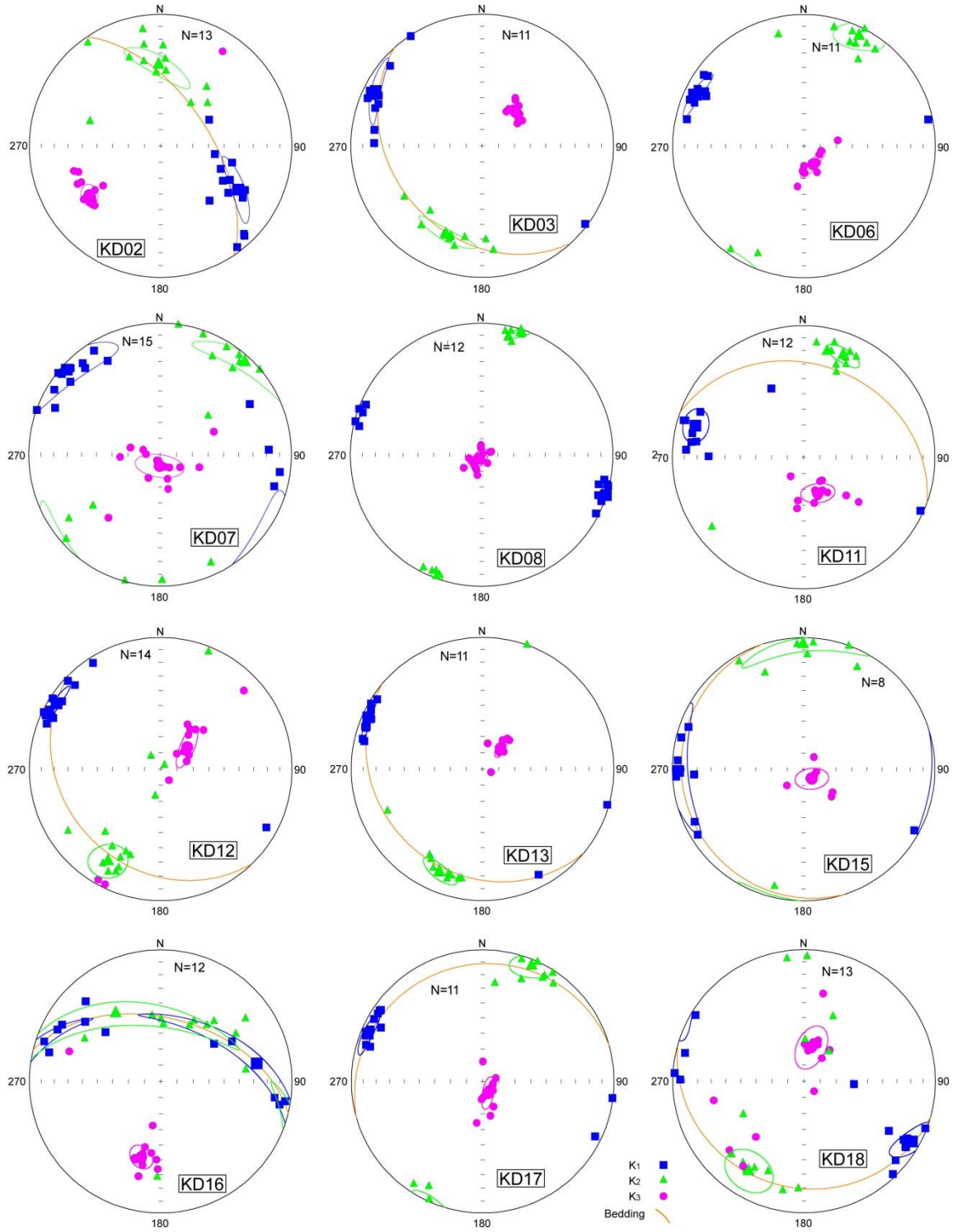

Fig.5.3a *AMS plots of Shurijeh Fm. sites. Data are plotted on lower hemisphere, equal-area projections, in geographic coordinates. Squares and circles represent maximum and minimum axes, respectively. Bedding planes are also represented.*

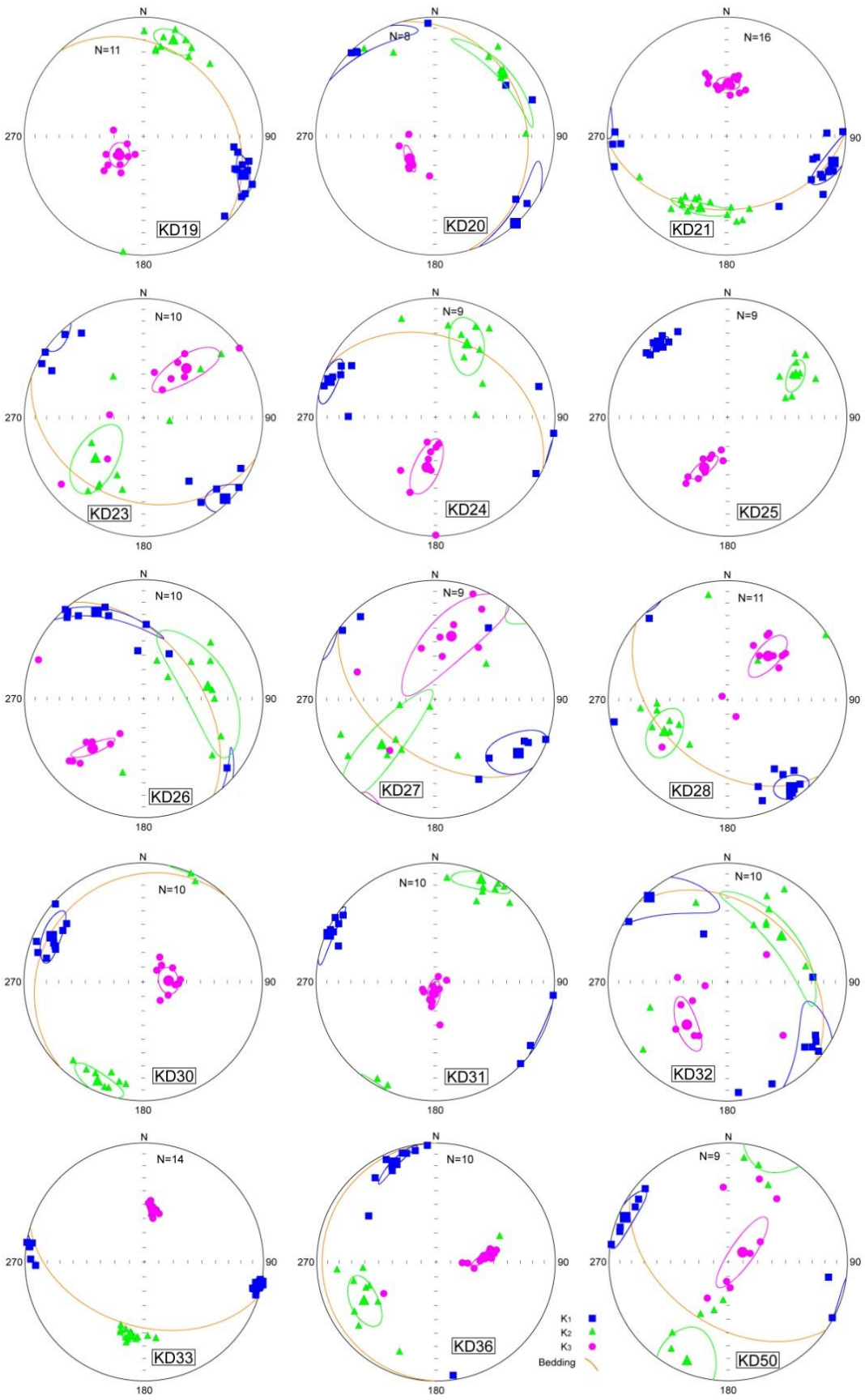

Fig.5.3b *AMS plots of Shurijeh Fm. sites. Data are plotted on lower hemisphere, equal-area projections, in geographic coordinates. Squares and circles represent maximum and minimum axes, respectively. Bedding planes are also represented.*

A third class of magnetic fabric has been observed in 11 sites, (Fig.5.4), which are characterized by K3 dispersed along a girdle orthogonal to the bedding plane or by a well defined magnetic foliation orthogonal to the bedding plane. This magnetic fabric does not show any relationships with the bedding plane, suggesting that the sedimentary fabric has been completely erased and the fabric has a pure tectonic origin. In most of the sites the magnetic lineation is well defined and lies at the intersection between the magnetic foliation and the bedding plane, suggesting that the lineation is an intersection lineation between the bedding plane and a tectonic foliation plane (cleavage), sub-orthogonal to the bedding.

Finally, in Fig. 5.5 five sites (KD01, KD22, KD37, KD49 and KD51) are shown, which show poorly defined magnetic fabric, probably due to the coarser granulometry of the sampling units or to complex magnetic mineralogy.

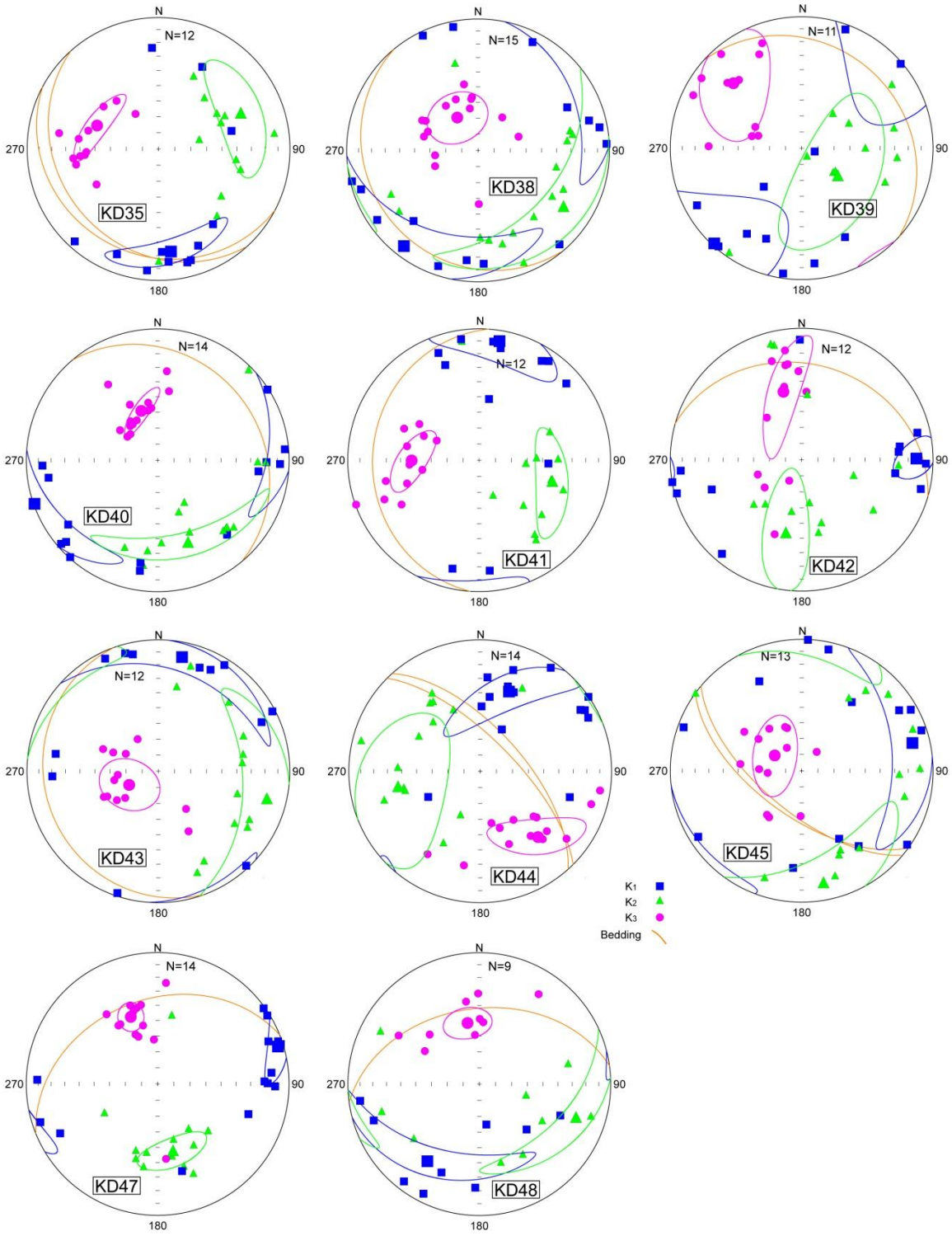

Fig.5.4 *AMS plots for Shurijeh Fm. sites. Data are plotted on lower hemisphere, equal-area projections, in geographic coordinates. Squares and circles represent maximum and minimum axes, respectively. Bedding planes are also represented*

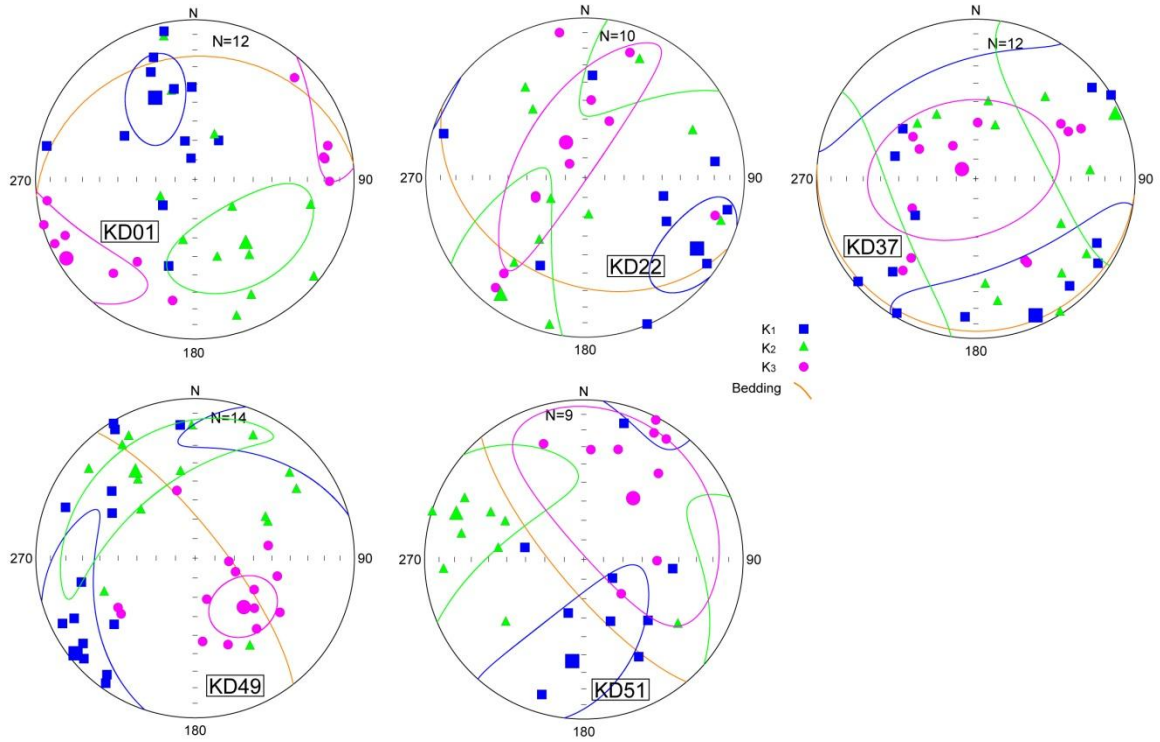

Fig.5.5 *AMS plots for Shurijeh Fm. sites. Data are plotted on lower hemisphere, equal-area projections, in geographic coordinates. Squares and circles represent maximum and minimum axes, respectively. Bedding planes are also represented.*

Summarizing, three different types of magnetic fabric can be recognized for the Shurijeh red beds, characterized by an increase of deformation rate (Fig 5.6). The first type of magnetic fabric has been observed only in 2 sites (4%) and is characterized by a well-defined magnetic foliation, parallel to the bedding plane, with the magnetic lineation dispersed within the magnetic foliation plane (Fig 5.6a). This magnetic fabric type represents the predominance of a sedimentary fabric, without evidences of tectonic overprint. The second type of magnetic fabric has been observed in 27 sites (60%). Here all the magnetic susceptibility directions are well grouped, with the magnetic foliation well defined and parallel to the bedding plane (Fig.5.6b). This fabric represents an initial stage of deformation, with the magnetic foliation related to sedimentary compaction and the magnetic lineation formed as a consequence of tectonic shortening. Finally the third type of magnetic fabric which has been observed in 11 sites (24%), is characterized by a magnetic foliation well defined on the cleavage plane and the lineation developed at the intersection between the bedding plane and the magnetic foliation plane, showing a tectonic control on the magnetic fabric (Fig.5.6c).

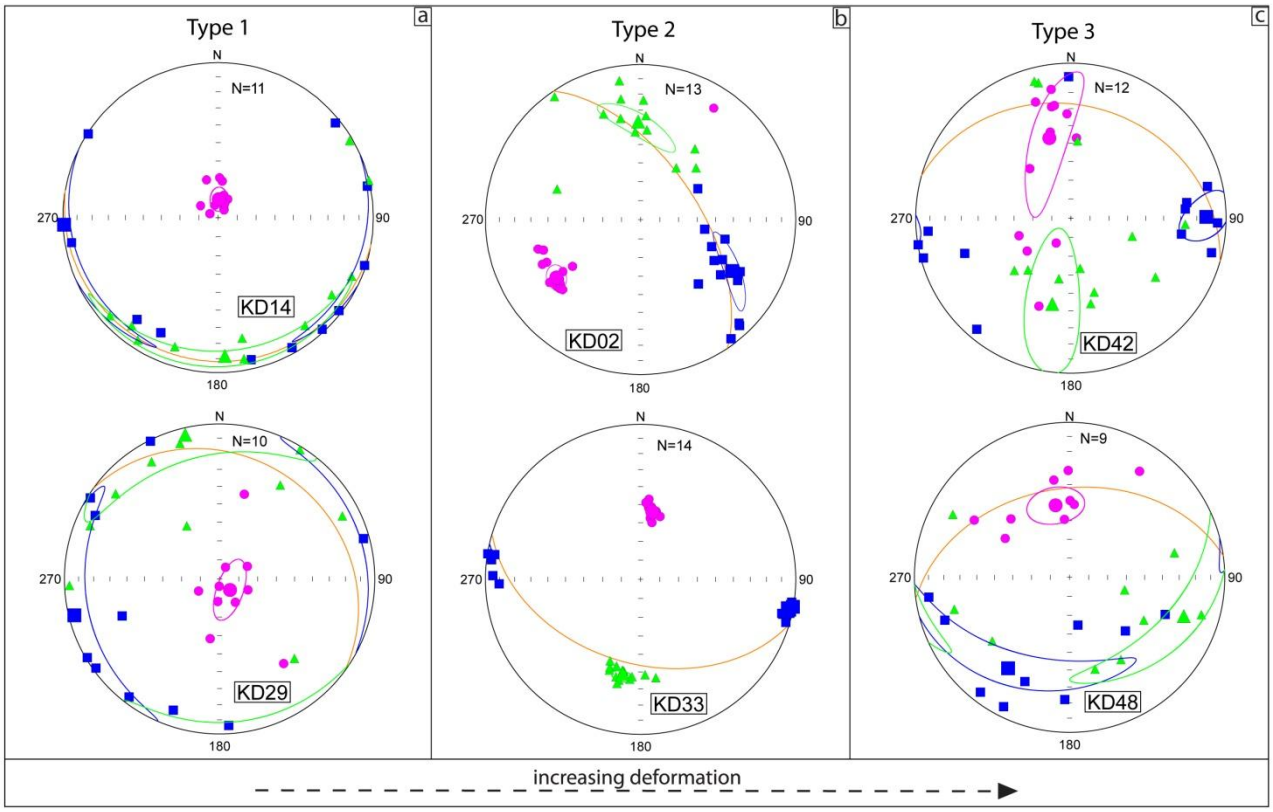

Fig.5.6 *AMS plots (a–c) for six sites representative of the different types of magnetic fabric observed in the study sites. Data are plotted on lower hemisphere, equal-area projections, in geographic coordinates. The ellipses indicate the 95% region around the principal susceptibility axes.*

5.2. The Neogene Upper Red Formation (URF)

The results from the Neogene Upper Red Formation show that the mean magnetic susceptibility (K_m) values are highly variable, with most K_m mean site values between ~1 x 10^{-6} SI and 1000 x 10^{-6} SI and a median value of 739 x 10^{-6} SI (Fig.5.1b).

The highly variable values resulting from the analysed Upper Red Fm. samples, suggest a different magnetic contribution. Low values indicate prevailing significant contribution of paramagnetic and diamagnetic minerals other than the presence of ferromagnetic minerals. Conversely the samples and sites which exhibit higher susceptibility values (up to 1200 x 10^{-6} SI units) suggest an higher contribution of the ferro-magnetic minerals to the magnetic fabric.

The magnetic parameters from the analyzed Upper Red Fm. show a large variability. The corrected degree of anisotropy parameter, P_j, shows a range of values between 1.01 and 1.096, while the shape parameter, T, shows a range of values from -0.27 to 0.739. The magnetic lineation parameter L (K_1/K_2), ranges between 1.003 and 1.034, while the magnetic foliation parameter F (K_2/K_3), range between 1.005 and 1.06 (Tab.2). Most of the sites (19) show a purely oblate (F>L, 0<T<1) ellipsoids, 2 sites show a triaxial (F=L, T=0) ellipsoids and 2 sites (KD62, KD64) have a prolate ellipsoids (L>F, 0<T<-1) (Fig. 5.1f, Tab.5.2). The P_j vs. T diagram (Fig. 5.1h) confirms that almost all sites have an oblate ellipsoid, with a strong variability in the corrected anisotropy

values (Fig.5.1f). The main magnetic susceptibility directions for most of the Neogene sites are well grouped and e_{1-2} angles (the semi-angle of the 95% confidence ellipse in the K_1-K_2 plane), exceed 26° only at 7 sites (Tab.5.2).

Different magnetic fabric has been observed in the URF sites, with a different contribution of tectonic deformation (Fig.5.7-5.8-5.9).

A first class of magnetic fabric has been observed only in two sites (KD10 and KD56, Fig.5.7), where a typical sedimentary fabric was found, with the K_3 axis well-grouped and the others forming a large girdle distributed along the bedding plane.

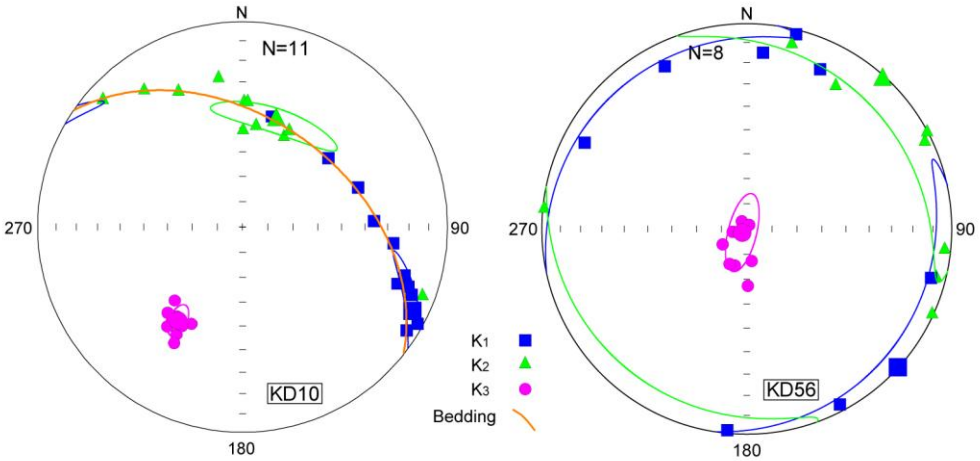

Fig.5.7*. AMS plots for URF Fm. KD56 and KD 58 sites. Data are plotted on lower hemisphere, equal-area projections, in geographic coordinates. Squares and circles represent maximum and minimum axes, respectively. Bedding planes are also represented.*

A second class of magnetic fabric has been observed in 16 sites (KD09, KD46, KD52-KD54, KD57-KD61, KD63-KD66, KD68 and KD70 sites, as show in Fig. 5.8a-b) and is characterized by the well defined principal axis, with K_3 orthogonal to the bedding plane and a well defined magnetic lineation, generally parallel to the bedding strike. In these sites the resulting AMS fabrics show a configurations typical of a weak deformation regime characterized by a low shortening degree.

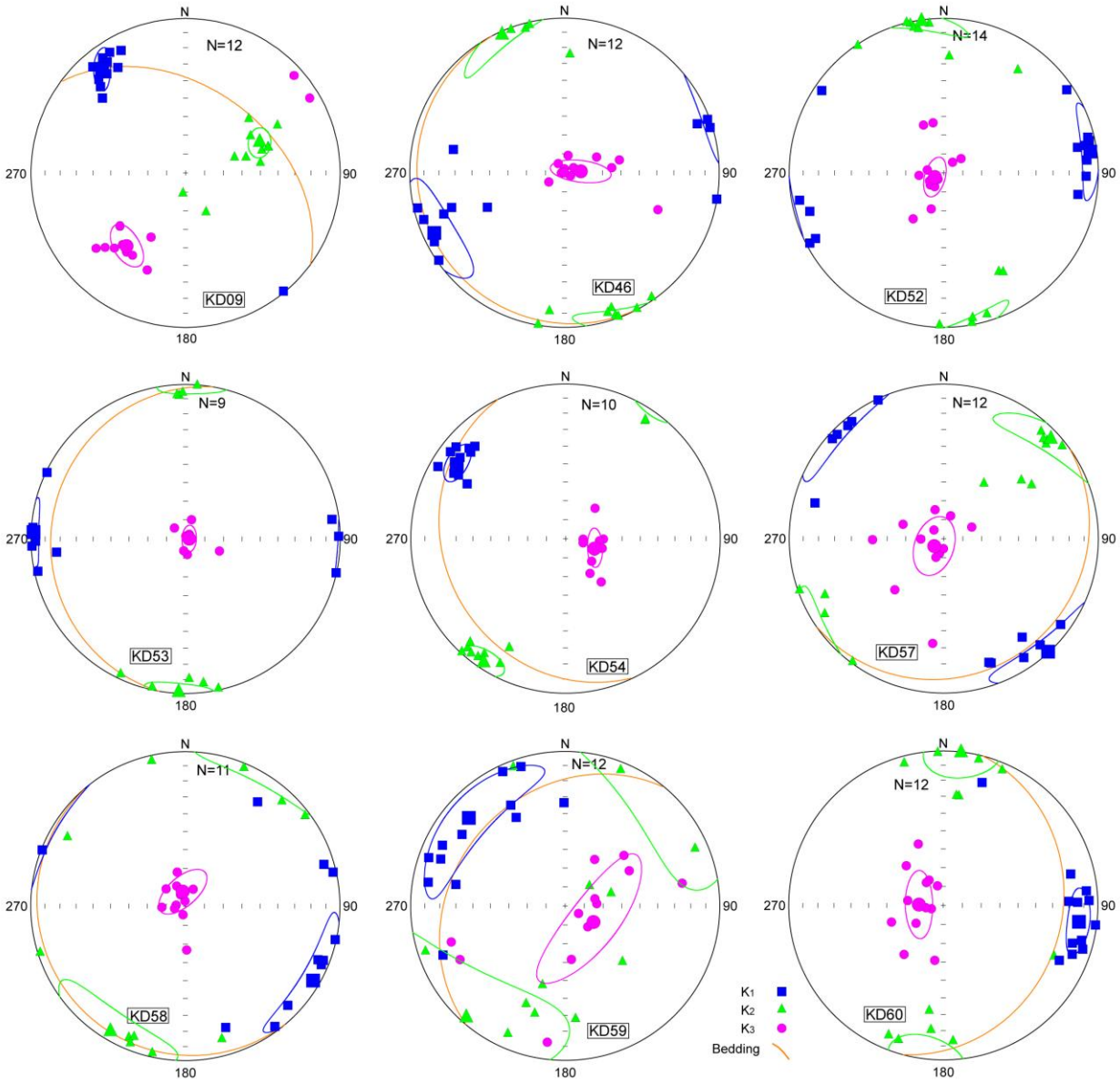

***Fig.5.8a**. AMS plots for URF Fm. sites. Data are plotted on lower hemisphere, equal-area projections, in geographic coordinates. Squares and circles represent maximum and minimum axes, respectively. Bedding planes are also represented.*

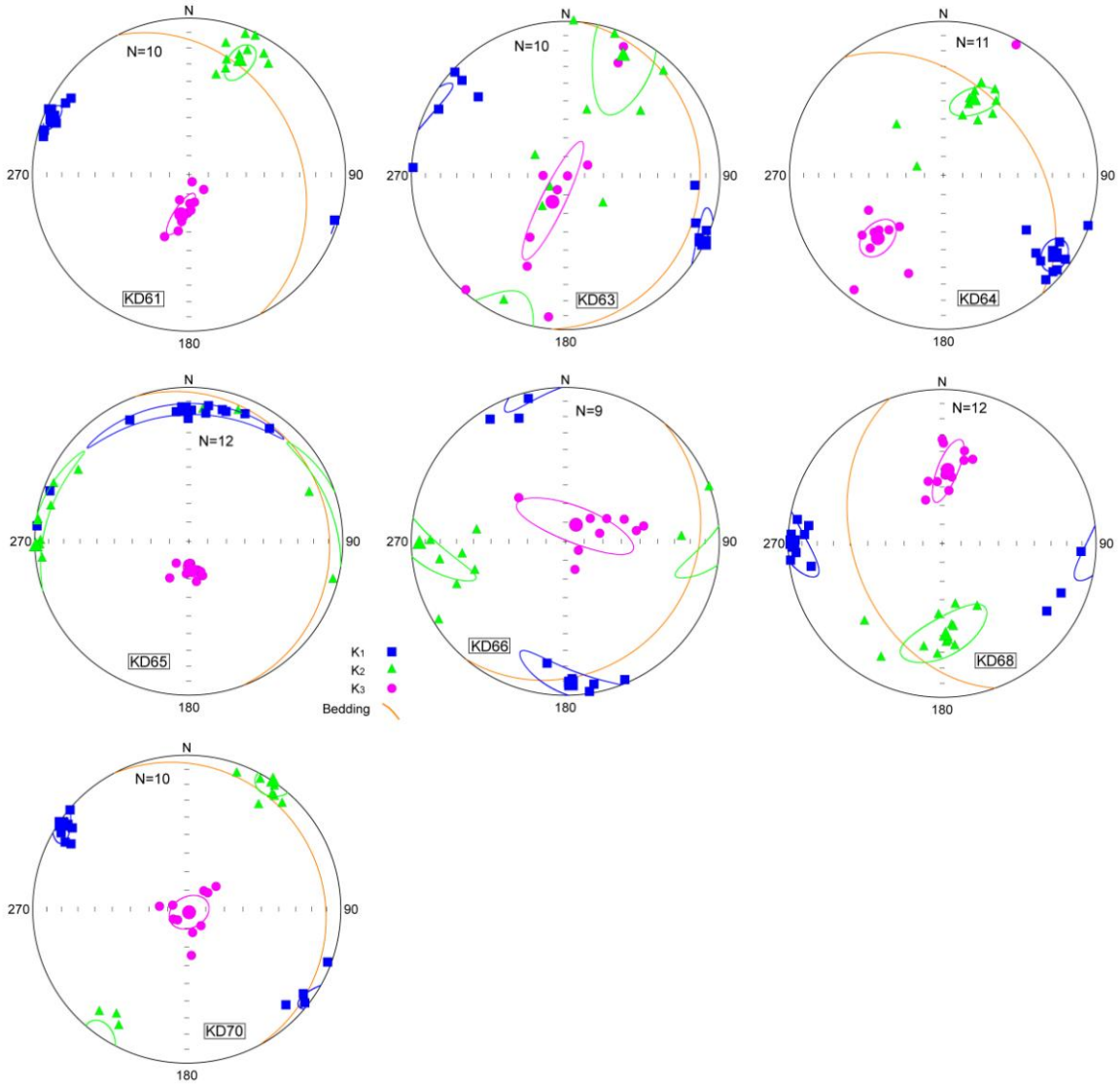

***Fig.5.8b**. AMS plots for URF Fm. sites. Data are plotted on lower hemisphere, equal-area projections, in geographic coordinates. Squares and circles represent maximum and minimum axes, respectively. Bedding planes are also represented.*

A third class of magnetic fabric (Fig.5.9) has been observed only in two sites (KD62, KD69), where the magnetic foliation is almost orthogonal to the bedding plane, whereas K_2 and K_1 are well defined and show distinct directions, with K_1 sub-parallel to the regional fold axes .

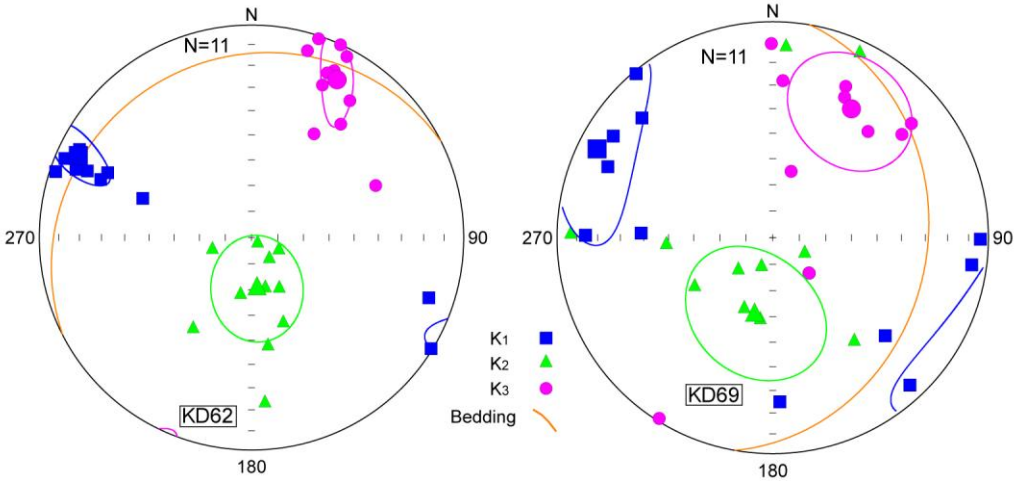

***Fig.5.9**. AMS plots for URF Fm. sites. Data are plotted on lower hemisphere, equal-area projections, in geographic coordinates. Squares and circles represent maximum and minimum axes, respectively. Bedding planes are also represented.*

Finally, in two sites (KD55 and KD67), as showed in Fig.5.10, the magnetic susceptibility configurations present a dispersed distribution of all magnetic axes, probably due to local structural configuration which could have deformed the magnetic fabric of the rocks or due to variations in the grain size of samples.

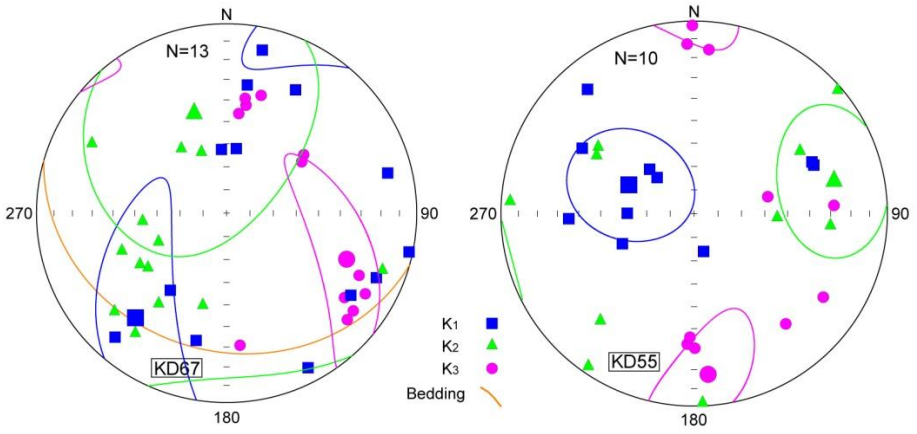

***Fig.5.10**. AMS plots for URF Fm. sites. Data are plotted on lower hemisphere, equal-area projections, in geographic coordinates. Squares and circles represent maximum and minimum axes, respectively. Bedding planes are also represented.*

As described below, the 22 Neogene red beds sites suggest the presence of three main magnetic fabrics relative to the geometric relationship between magnetic foliation and lineation. The first type has been observed in 2 sites (9%) and is characterized by a well defined magnetic foliation, parallel to the bedding plane, whereas the magnetic lineation is not well defined and dispersed within the foliation plane (Fig 5.11a). The second type of magnetic fabric has been observed in 16 sites (73%). Here the magnetic foliation is well defined, parallel to the bedding plane as well as the magnetic lineation, generally placed parallel to the strike direction of the bedding plane and to

the regional fold axis (Fig.5.11b). Finally the third type of magnetic fabric which has been observed in 2 sites (9%), is characterized by a magnetic foliation almost orthogonal to the bedding plane, suggesting the formation of a tectonic foliation not visible at the outcrop scale.

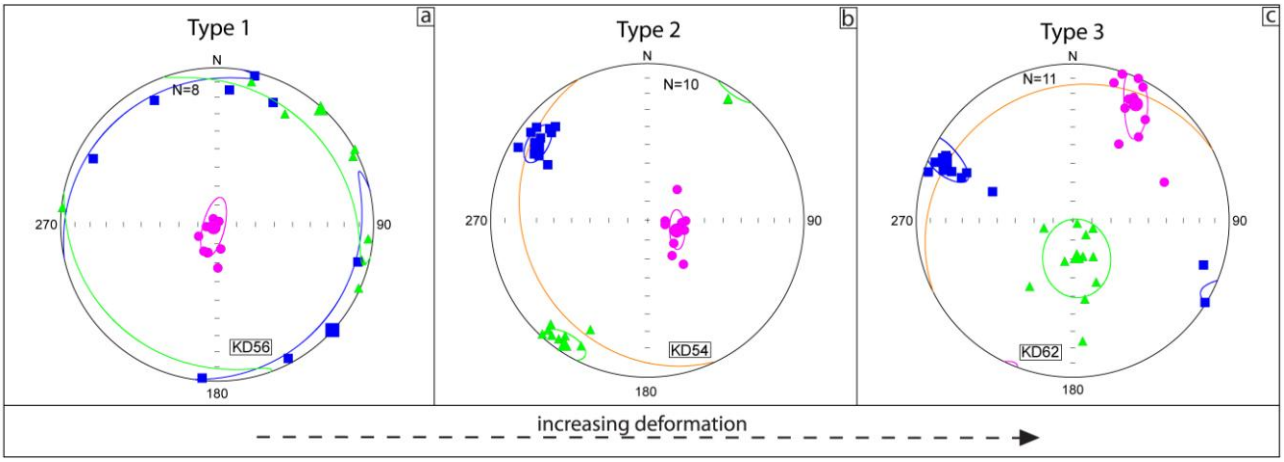

Fig.5.11. *AMS plots (a–c) for three sites representative of the different types of magnetic fabric observed in the study sites. Data are plotted on lower hemisphere, equal-area projections, in geographic coordinates. The ellipses indicate the 95% region around the principal susceptibility axes.*

The geographic distribution of magnetic lineations calculated both for Early Cretaceous and for Neogene samples, is shown in Fig.5.12. Most of the magnetic lineations, represented by the green and brown arrows in the map, show a homogenous trend parallel to the main tectonic structures which interest both the Early Cretaceous red beds and the Neogene red beds.

In Fig.5.12 and in the following three detailed maps (Fig. 5.13-5.14-5.15) were plotted only the data characterized by a value of $e_{1\text{-}2}$ lower than 45 (Tab.1-2); $e_{1\text{-}2}$ represents the semi-angle of the 95% confidence ellipse in the K_1-K_2 plane. This angle represents the parameter that measures the dispersion of the K_1-K_2 magnetic axes within each site in fact in several sites the resulting ellipsoid configuration is unreliable due to high values of $e_{1\text{-}2}$.

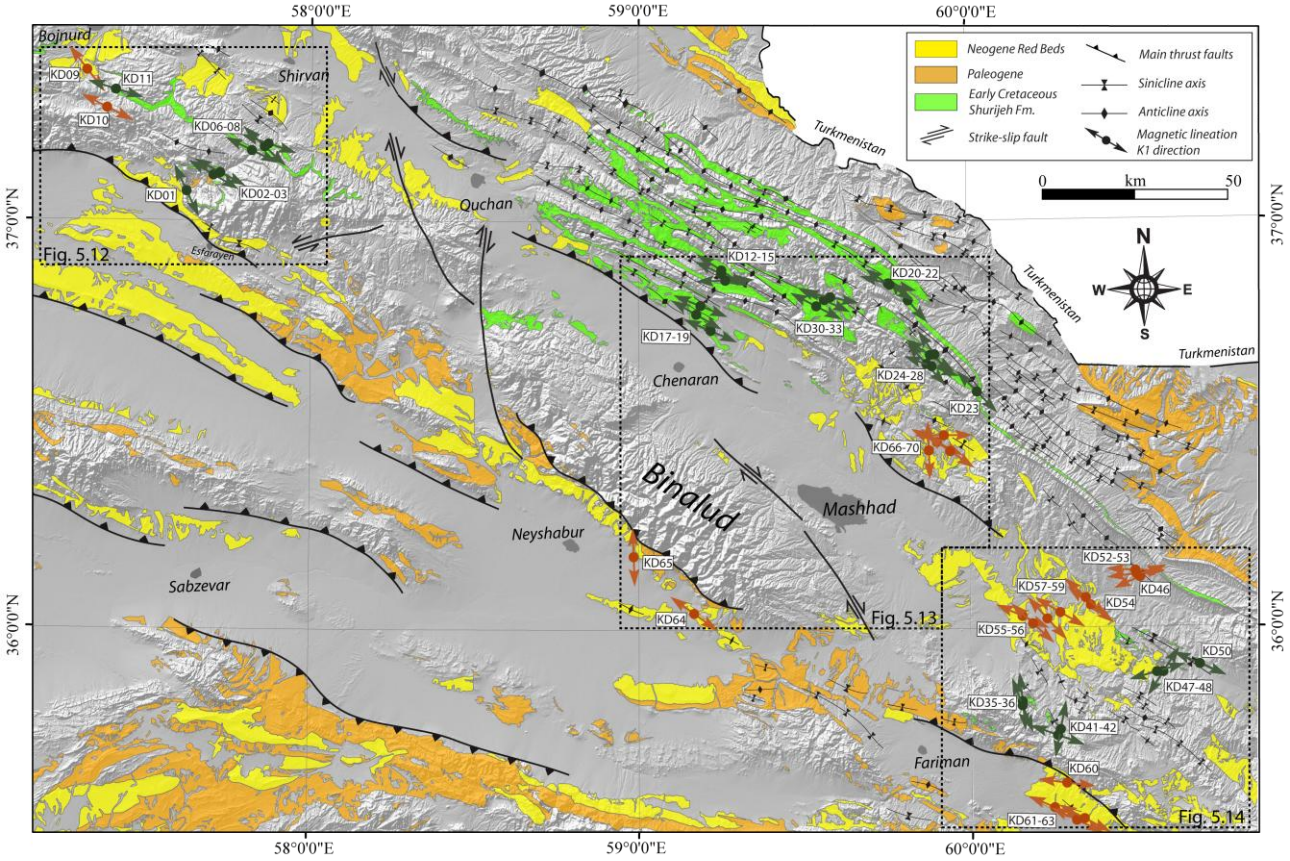

Fig.5.12. *Simplified geological map of the study area. AMS sampling sites and directions of in situ magnetic lineations from this study are also reported (green arrows for Early Cretaceous sites and brown arrows for Neogene sites).*

In the first area (Fig. 5.13) 6 sampling sites were collected from the Shurijeh Formation (KD01, KD02, KD03, KD06, KD07, KD08, KD11), and 2 sites from Neogene red beds of the URF (KD09, KD10) (Figure 5.13). Here the magnetic lineation of the Shurijeh sites is constantly oriented WNW-ESE, which is parallel to the main structural elements of the area represented by the regional fold axes, the Esfarayen and the North Esfarayen thrust faults (Hollingsworth et al., 2010), which outcrop along the southern margin of the Eastern Alborz Mountains. The only exception to these regional trend of magnetic lineation is represented by site KD01, which has been sampled along NNW-SSE oriented branch of the Esfarayen thrust system and that show a peculiar magnetic fabric, with a magnetic lineation parallel to the thrust fault and a sub-vertical magnetic foliation which indicates the development of a tectonic magnetic foliation, NNW-SSE oriented related to increasing amount of deformation in this site area(Fig.5.5).

In the second area (Fig. 5.14) 22 sites from the Early Cretaceous Shurijeh Fm. were collected, (from KD12 to KD33) and 5 sites in Neogene URF (from KD66 to KD70) (Fig.5.11), along the southern margin of Kopeh Dagh Mts.. In this part of the range, which is bordered by the Ahmadabad thrust fault, part of the long thrust system that interest the southern side of the central-

east Kopeh Dagh range, the presence of several syncline and anticline folds allows the exposure of the entire Cretaceous succession, with the Shurijeh Formation at the base.

In the Kopeh-Dagh Mts., north of Mashhad the magnetic lineation is oriented WNW-ESE in most of the sampling sites, parallel to the main fold axes and thrust faults, which characterize this sector of the range. In sites KD14, KD15 and KD16, located very close each other, magnetic lineation is slightly deviated toward a more W-E orientation (Fig.5.14), related to a local variation of the Amdurak Syncline trend.

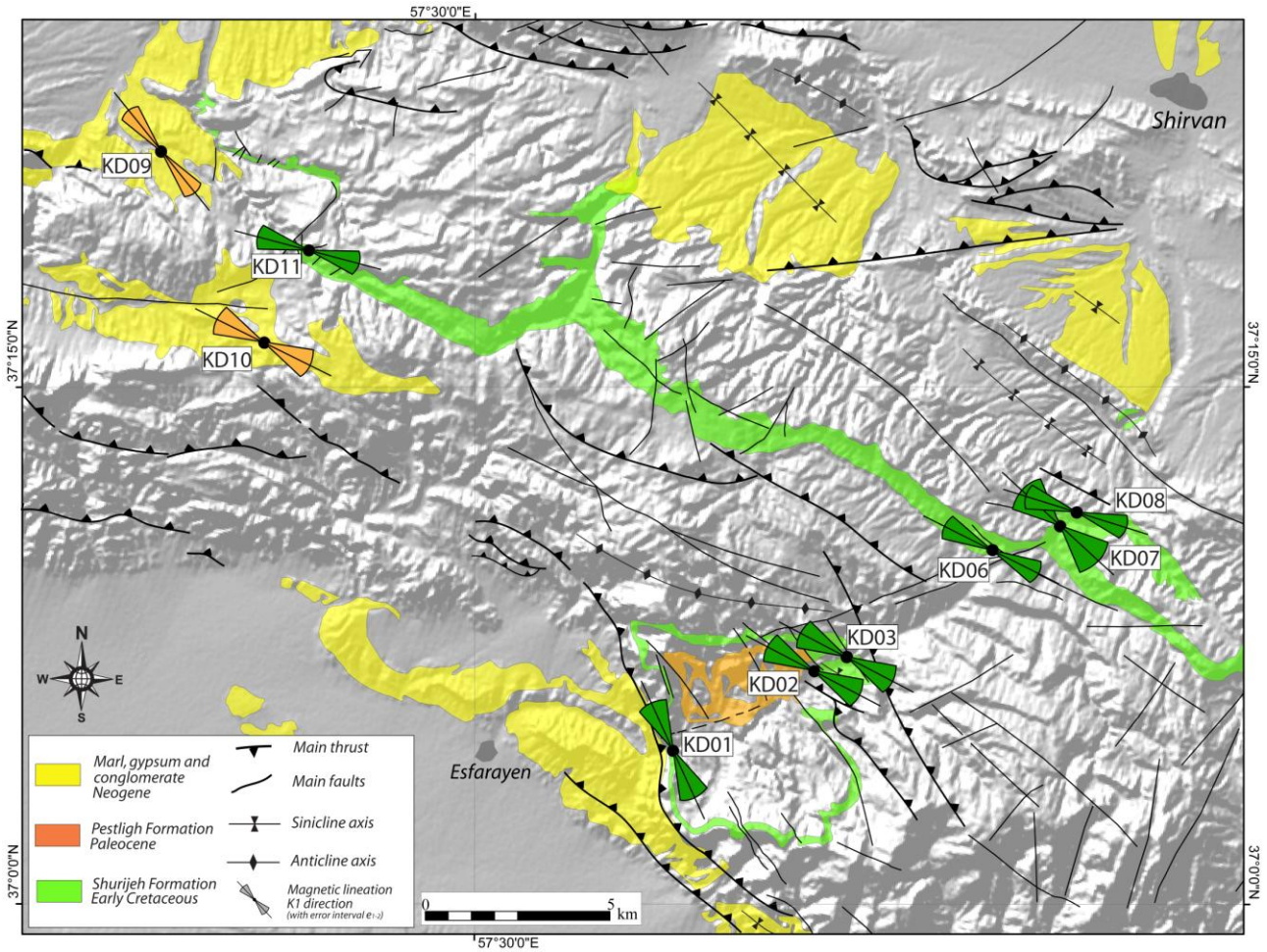

Fig.5.13 *Simplified geological map of the western sector, in the Allah Dagh mountains. Sampling sites and directions of in situ magnetic lineations from this area are also reported (green symbols for Early Cretaceous sites and brown symbols for Neogene sites).*

In most of the Neogene sites, sampled north-east of Mashhad and along the southern side of Binalud Mountains, the magnetic lineations are oriented WNW-ESE parallel to the main fold axes and to the main thrust fault systems, represented by the Neyshaber thrust fault, the Binalud thrust fault (Hollingsworth et al., 2010) along the southern side of Binalud Mountains and by the main thrust faults (Ahmadabad, Joghri and Manesar faults) which characterize the north-eastern part of the area (Mashhad Geological Map 1:100.000).The resulting values of magnetic lineation for sites

KD65 and KD66 show a N-S orientation due to the local structural deformation which probably has modified the magnetic fabric of the rocks; furthermore the resulting magnetic susceptibility values are characterized by high values of $e_{1\text{-}2}$, which indicate the low accuracy of the resulting magnetic susceptibility ellipsoids (Tab.5.1).

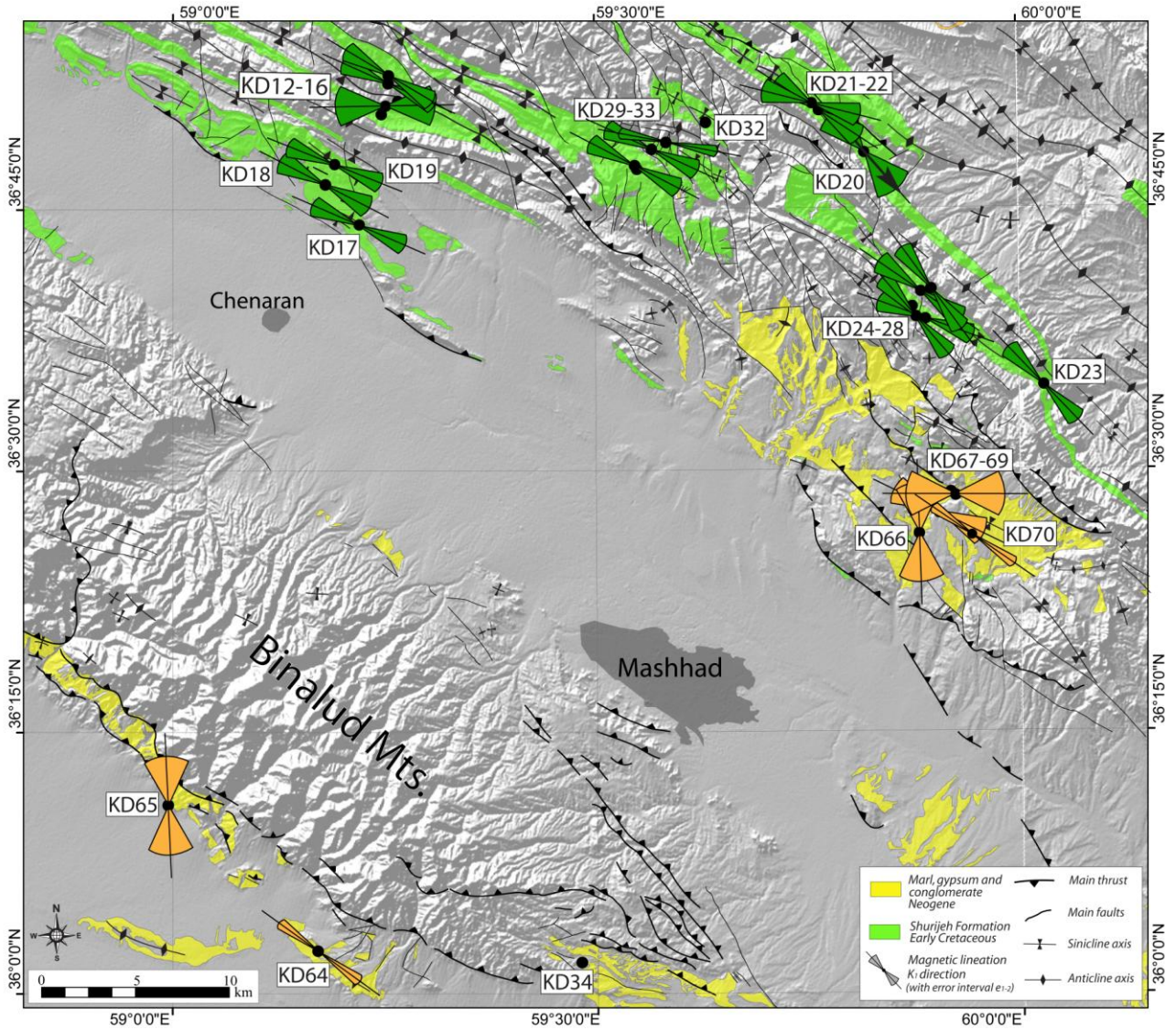

Fig..5.14 *Simplified geological map of the central sector of Kopeh Dagh range and Binalud Mountains. Sampling sites and directions of in situ magnetic lineations from this area are also reported (green symbols for Early Cretaceous sites and brown symbols for Neogene sites).*

The third area is located at the eastern sector of the study region. Here, I collected 16 sites from Early Cretaceous red beds of the Shurijeh Fm. and 13 sites from Neogene units of the URF (Fig.5.15). The distribution of the Cretaceous units in this area is quite dispersed and generally less diffuse than the central part of the chain (first and second areas, shown in Fig.5.12-5.13); in fact the Shurijeh deposits are characterized by a few hundred meters of thickness, which develop in small strongly deformed structures. The fragments of Shurijeh Formation are included in the small fold systems which deforms the Cretaceous succession in this sector of the belt.

In this area the measured magnetic fabric shows a variable shape and orientation, with a larger variability respect to the other areas. In several sites (KD41, KD42, KD47, KD48) the magnetic foliation is almost orthogonal to the bedding plane and is tectonically originated. (Fig.5.4) In few sites (KD44, KD47, KD48, KD49, KD50) the magnetic lineation shows a strict correlation with the regional structural trend oriented WNW-ESE. In all the other sites the magnetic lineation is poorly defined (high e1-2 angle) and shows a variable orientation, from N-S (KD35, KD36, KD37*, KD41, KD43*, KD51) to NE-SW (KD38*, KD39*, KD40*, KD42, KD45*) (Tab.1), which diverges from the regional structural trend, and possibly suggests the dominance of local deformation.

The 13 Neogene sites show, in general, a better correlation with the regional structural trend. In fact, most of the magnetic lineations are oriented WNW-ESE to NW-SE, parallel to the regional fold axes and to the main thrust fault systems (e.g. the Khairabad thrust fault which borders the western side of KD55 and KD56* sites sector) (Fig.5.15),. Close to these two sites, also KD54, KD57, KD58 and KD59 show a magnetic lineation parallel to the regional structural trend (Fig. 5.15). This parallelism between the magnetic lineations orientation and the regional tectonic structures can be also observed at sites KD60, KD61, KD62 and KD63, which are located along the southwestern side of the Fariman Complex range (Fig. 5.15). In these sites the magnetic lineation is oriented WNW-ESE, parallel to the orientation of the North Torbat-e-Jam thrust and the Torbat-e-Jam thrust (Hollingsworth et al., 2010), which define the southern margin of this sector of the range. Conversely, sites KD46, KD52 and KD53 sampled in a small syncline (Fig.5.15) located along the northern part of the sampling area (near Mozduran) show a well defined magnetic fabric, with a magnetic lineation oriented NE-SW at high angle with the WNW-ESE orientation of the regional structural trend (Fig.5.15) suggesting a local structural complexity in the area, or a sedimentary origin for the magnetic lineation in these sites.

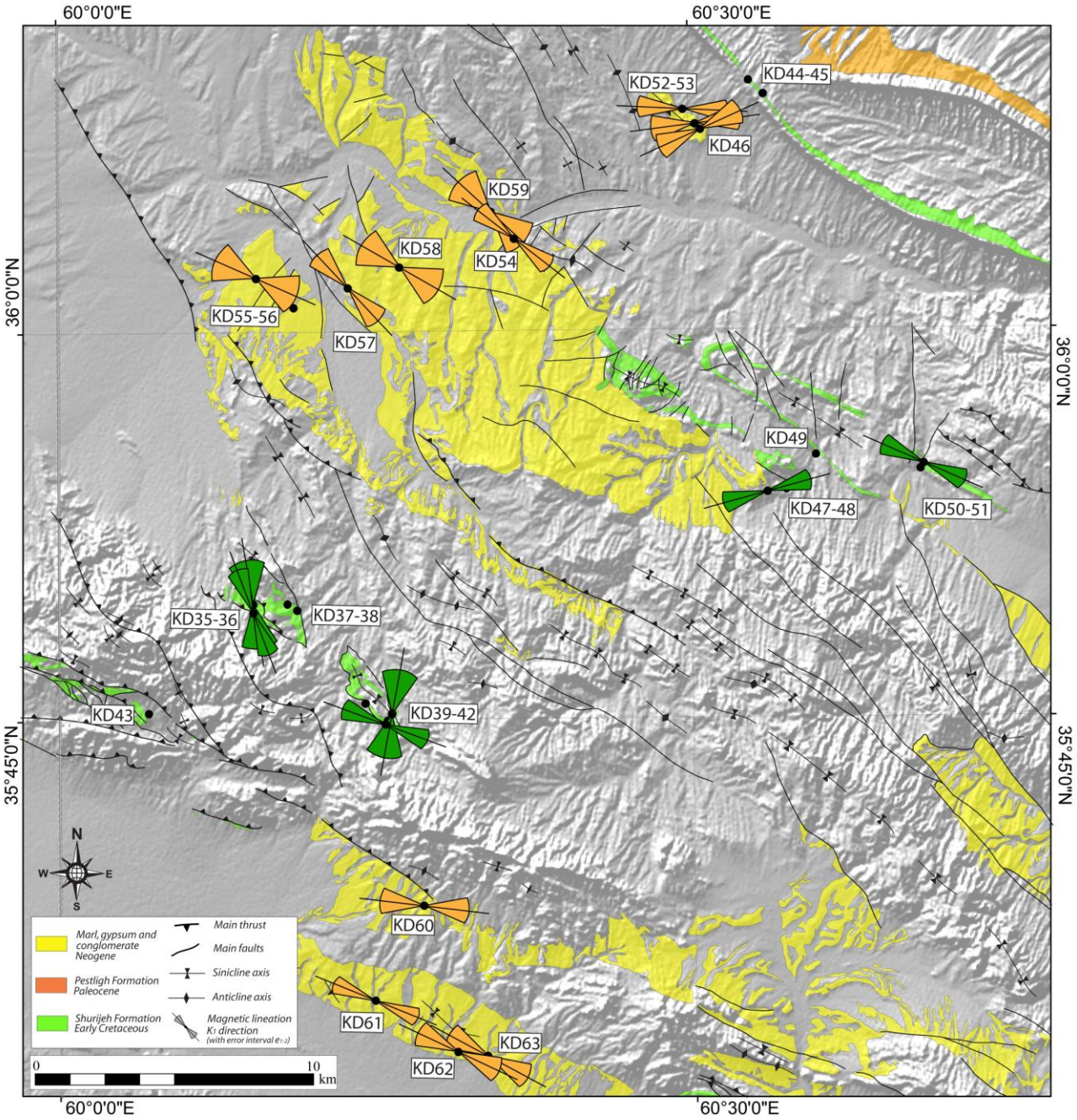

Fig.5.15. *Simplified geological map of the eastern sector along the Fariman metamorphic complex and near Agdarband tectonic window. Sampling sites and directions of in situ magnetic lineations from this area are also reported (green symbols for Early Cretaceous sites and brown symbols for Neogene sites).*

Site	Lat	Lon	S_o	N	K_m	L	F	P_j	T_j	D,I (K_1)	D,I (K_3)	e_{12}
KD01	37°04'28.30"	57°37'14.30"	354,24	12	23.9	1.010 (0.005)	1.014 (0.009)	1.025 (0.010)	0.121 (0.416)	334,42	238,6	24.9
KD02	37°06'46.00"	57°42'19.90"	56,60	13	132	1.004 (0.002)	1.015 (0.010)	1.020 (0.010)	0.441 (0.379)	119,33	235,34	22.8
KD03	37°07'12.80"	57°43'34.30"	228,32	11	202	1.007 (0.003)	1.061 (0.019)	1.076 (0.021)	0.754 (0.147)	297,10	45,60	17.4
KD06	37°10'16.90"	57°48'51.10"	338,18	11	214	1.008 (0.002)	1.038 (0.008)	1.049 (0.008)	0.641 (0.121)	295,10	153,77	12.7
KD07	37°10'58.10"	57°51'18.90"	0,0	15	127	1.007 (0.004)	1.019 (0.008)	1.028 (0.008)	0.426 (0.348)	312,4	182,83	27.6
KD08	37°11'21.30"	57°51'56.10"	0,0	12	159	1.010 (0.002)	1.047 (0.008)	1.061 (0.009)	0.646 (0.067)	108,1	209,87	5.5
KD11	37°18'59.90"	57°23'56.60"	20,30	12	207	1.009 (0.002)	1.028 (0.010)	1.040 (0.011)	0.472 (0.200)	286,15	158,66	10.0
KD12	36°52'41.40"	59°15'19.60"	226,26	14	127	1.014 (0.005)	1.018 (0.018)	1.034 (0.020)	-0.073 (0.450)	302,7	50,68	10.0
KD13	36°52'13.90"	59°15'19.60"	220,21	11	212	1.008 (0.003)	1.053 (0.015)	1.062 (0.017)	0.730 (0.078)	294,5	41,73	10.2
***KD14**	36°51'13.40"	59°15'59.90"	252,8	11	135	1.005 (0.002)	1.041 (0.009)	1.051 (0.011)	0.774 (0.113)	267,1	2,80	62.1*
KD15	36°50'56.30"	59°15'06.70"	29,28	8	320	1.006 (0.004)	1.069 (0.026)	1.085 (0.029)	0.809 (0.152)	269,5	139,82	31.5
***KD16**	36°50'28.00"	59°14'50.20"	14,50	12	86.2	1.006 (0.005)	1.022 (0.006)	1.030 (0.008)	0.586 (0.284)	79,26	194,40	76.6*
KD17	36°44'08.30"	59°13'14.20"	344,12	11	249	1.010 (0.002)	1.063 (0.009)	1.080 (0.011)	0.731 (0.056)	292,6	155,82	10.4
KD18	36°46'27.30"	59°10'51.00"	196,20	13	90.5	1.006 (0.003)	1.007 (0.004)	1.013 (0.006)	0.027 (0.298)	119,7	12,68	14.5
KD19	36°47'36.20"	59°11'30.80"	46,28	11	96.1	1.009 (0.003)	1.029 (0.007)	1.040 (0.009)	0.530 (0.156)	111,11	232,69	12.7
KD20	36°48'10.30"	59°49'09.20"	74,24	8	177	1.014 (0.008)	1.036 (0.014)	1.052 (0.020)	0.495 (0.242)	137,0	228,67	35.3
KD21	36°50'36.50"	59°45'57.10"	178,38	16	118	1.009 (0.004)	1.033 (0.008)	1.045 (0.010)	0.557 (0.141)	104,9	2,53	18.7
KD22	36°50'47.20"	59°45'42.50"	206,34	10	96.8	1.006 (0.004)	1.004 (0.002)	1.010 (0.004)	-0.224 (0.258)	122,18	332,70	24.3
KD23	36°34'48.70"	60°01'46.00"	200,30	10	143	1.015 (0.008)	1.026 (0.035)	1.044 (0.043)	0.031 (0.432)	135,4	41,44	14.6
KD24	36°38'37.80"	59°53'24.40"	26,34	9	115	1.012 (0.005)	1.024 (0.013)	1.037 (0.015)	0.295 (0.275)	289,6	190,55	12.5
KD25	36°38'45.50"	59°52'45.60"	25,39	9	127	1.012 (0.003)	1.026 (0.008)	1.039 (0.010)	0.370 (0.132)	317,17	205,51	6.0
***KD26**	36°39'19.40"	59°52'30.60"	54,52	10	102	1.017 (0.008)	1.022 (0.010)	1.040 (0.014)	0.110 (0.294)	331,18	226,40	47.6*
KD27	36°40'11.60"	59°53'06.50"	216,50	9	92	1.015 (0.006)	1.024 (0.010)	1.041 (0.013)	0.203 (0.300)	123,18	14,44	23.2
KD28	36°40'20.80"	59°53'49.70"	220,42	11	128	1.017 (0.011	1.021 (0.007)	1.039 (0.012)	0.169 (0.399)	144,10	43,48	11.9
***KD29**	36°47'14.90"	59°32'58.30"	36,22	10	99.8	1.009 (0.004)	1.020 (0.011)	1.030 (0.011)	0.298 (0.371)	256,4	137,82	52.7*
KD30	36°47'27.10"	59°32'52.70"	314,14	10	131	1.013 (0.009)	1.023 (0.010)	1.038 (0.006)	0.276 (0.464)	296,15	88,73	15.3
KD31	36°48'24.60"	59°34'02.90"	0,0	10	182	1.010 (0.004)	1.044 (0.020)	1.059 (0.025)	0.587 (0.144)	294,2	186,82	15.8
***KD32**	36°49'54.90"	59°37'53.80"	42,36	10	128	1.014 (0.009)	1.022 (0.014)	1.038 (0.014)	0.132 (0.506)	317,4	223,49	47.8*
KD33	36°48'47.30"	59°35'04.50"	197,45	14	217	1.012 (0.003)	1.060 (0.022)	1.079 (0.025)	0.623 (0.123)	100,0	10,54	5.3
KD35	35°49'31.73"	60°09'10.80"	208,20	12	160	1.020 (0.023)	1.124 (0.117)	1.162 (0.155)	0.567 (0.306)	173,22	291,48	34.0
KD36	35°49'11.68"	60°09'11.92"	270,5	10	151	1.019 (0.007)	1.085 (0.056)	1.114 (0.066)	0.473 (0.373)	338,11	84,56	16.3
***KD37**	35°49'30.18"	60°10'49.80"	185,5	12	231	1.034 (0.029)	1.170 (0.080)	1.228 (0.106)	0.645 (0.292)	156,7	305,81	57.1*
***KD38**	35°49'15.60"	60°11'16.33"	230,16	15	139	1.033 (0.018)	1.187 (0.073)	1.247 (0.093)	0.671 (0.158)	218,9	328,66	74.7*
***KD39**	35°45'39.20"	60°14'29.08"	42,22	11	144	1.029 (0.017)	1.096 (0.070)	1.136 (0.092)	0.460 (0.217)	223,2	314,29	52.2*
***KD40**	35°44'50.32"	60°15'26.03"	50,22	14	148	1.040 (0.022)	1.118 (0.076)	1.172 (0.103)	0.440 (0.204)	250,1	342,57	54.0*
KD41	35°45'15.62"	60°15'44.89"	274,20	12	114	1.044 (0.023)	1.168 (0.117)	1.236 (0.160)	0.517 (0.140)	10,9	270,47	33.8
KD42	35°44'59.14"	60°15'31.86"	16,28	12	203	1.033 (0.020)	1.095 (0.063)	1.137 (0.087)	0.448 (0.252)	89,14	345,45	17.8
***KD43**	35°45'18.83"	60° 4'13.66"	250,14	12	110	1.058 (0.022)	1.189 (0.063)	1.271 (0.091)	0.508 (0.091)	12,12	245,70	63.6*
***KD44**	36°09'7.99"	60°33'33.98"	48,64	14	132	1.024 (0.018)	1.075 (0.074	1.108 (0.099)	0.400 (0.370)	20,36	139,34	47.3*
***KD45**	36°09'40.03"	60°32'52.66"	220,65	13	75.6	1.098 (0.050)	1.330 (0.174)	1.492 (0.264)	0.417 (0.345)	76,14	300,71	57.7*
KD47	35°53'45.28"	60°33'36.18"	338,36	14	94.2	1.048 (0.029)	1.174 (0.133)	1.247 (0.185)	0.410 (0.251)	73,5	338,44	21.4
***KD48**	35°53'51.47"	60°34'29.96"	352,42	9	73.5	1.037 (0.020)	1.159 (0.137)	1.218 (0.182)	0.519 (0.147)	214,30	349,51	61.3*
***KD49**	35°55'09.34"	60°35'54.85"	52,76	14	191	1.050 (0.040)	1.185 (0.150)	1.265 (0.202)	0.478 (0.352)	232,5	135,54	66.2*
KD50	35°54'46.98"	60°40'58.80"	215,46	9	259	1.042 (0.016)	1.045 (0.041)	1.092 (0.043)	-0.090 (0.526)	293,6	56,78	17.3
***KD51**	35°54'35.03"	60°40'50.02"	230,76	10	87.7	1.022 (0.019)	1.020 (0.014)	1.043 (0.031)	0.059 (0.412)	186,36	39,49	58.5*

Tab.5.1 *List of magnetic anisotropy factors computed at each site of the sampled Shurijeh Fm. sites.*

Site	Lat	Lon	S_o	N	km	L	F	Pj	Tj	D,I (K_1)	D,I (K_3)	e_{12}
KD09	37°21'49.70"	57°18'34.50"	36,44	12	1010	1.014 (0.002)	1.020 (0.021)	1.035 (0.024)	-0.066 (0.407)	321,15	219,39	12.5
KD10	37°16'22.00"	57°22'22.10"	34,46	12	1650	1.005 (0.004)	1.031 (0.005)	1.040 (0.007)	0.739 (0.192)	116,8	214,44	24.2
KD46	36°07'46.81"	60°30'34.67"	242,6	12	513	1.006 (0.004)	1.019 (0.005)	1.026 (0.003)	0.526 (0.355)	245,8	85,81	23.0
KD52	36°07'59.66"	60°30'18.79"	0,0	14	486	1.013 (0.005)	1.052 (0.025)	1.070 (0.028)	0.547 (0.263)	82,5	245,85	19.3
KD53	36°08'33.47"	60°29'44.23"	280,14	9	676	1.015 (0.004)	1.060 (0.026)	1.081 (0.031)	0.571 (0.155)	272,2	88,88	13.1
KD54	36°03'36.11"	60°21'41.40"	244,22	15	334	1.015 (0.007)	1.036 (0.012)	1.053 (0.014)	0.402 (0.208)	308,13	164,74	13.4
KD55	36° 02'07.48"	60° 09'25.70"	0,0	10	1250	1.004 (0.003)	1.005 (0.003)	1.010 (0.005)	0.154 (0.404)	294,59	175,16	29.1
***KD56**	36°00'59.04"	60°11'12.70"	25,6	10	603	1.003 (0.002)	1.015 (0.011)	1.019 (0.013)	0.490 (0.423)	132,1	231,88	63.0*
KD57	36°01'43.86"	60°13'47.42"	145,12	12	782	1.007 (0.003)	1.013 (0.010)	1.021 (0.012)	0.211 (0.319)	137,1	232,84	25.2
KD58	36°02'31.52"	60°16'13.58"	170,8	12	680	1.005 (0.003)	1.014 (0.008)	1.020 (0.009)	0.387 (0.359)	120,5	351,82	27.7
KD59	36°04'38.32"	60°20'36.10"	310,28	12	607	1.005 (0.002)	1.006 (0.003)	1.011 (0.004)	0.076 (0.311)	312,17	120,73	37.9
KD60	35°37'49.37"	60°17'08.77"	105,24	12	334	1.015 (0.003)	1.026 (0.008)	1.042 (0.010)	0.267 (0.178)	97,13	272,77	13.9
KD61	35°34'11.17"	60°14'51.47"	11,21	11	1030	1.018 (0.002)	1.025 (0.013)	1.045 (0.012)	0.090 (0.288)	293,4	191,69	5.9
KD62	35°32'09.02"	60°18'43.16"	333,16	12	989	1.016 (0.005)	1.013 (0.004)	1.030 (0.007)	-0.075 (0.257)	295,11	28,17	18.5
KD63	35°31'59.81"	60°20'09.82"	95,14	16	1290	1.012 (0.006)	1.014 (0.008)	1.027 (0.007)	0.029 (0.508)	298,4	30,29	13.8
KD64	36°02'25.15"	59°10'14.56"	50,42	11	813	1.021 (0.003)	1.013 (0.008)	1.035 (0.008)	-0.270 (0.284)	126,12	226,41	8.9
KD65	36°10'50.38"	58°59'41.60"	15,15	12	1690	1.013 (0.007)	1.054 (0.015)	1.073 (0.016)	0.587 (0.241)	358,15	175,75	44.1
KD66	36°26'20.62"	59°52'51.17"	213,11	9	527	1.006 (0.003)	1.014 (0.012)	1.022 (0.014)	0.315 (0.373)	178,8	33,80	28.0
***KD67**	36°28'43.43"	59°55'7.79"	196,28	13	243	1.032 (0.028)	1.059 (0.039)	1.096 (0.052)	0.296 (0.406)	221,28	111,33	60.4*
KD68	36°28'31.40"	59°55'27.26"	184,37	13	268	1.015 (0.004)	1.023 (0.013)	1.038 (0.014)	0.142 (0.314)	270,3	4,50	20.7
KD69	36°27'31.72"	59°54'16.81"	100,29	11	277	1.034 (0.017)	1.043 (0.024)	1.080 (0.037)	0.085 (0.339)	297,8	31,30	30.7
KD70	36°26'13.34"	59°56'36.53"	62,12	10	388	1.008 (0.003)	1.012 (0.009)	1.021 (0.008)	0.056 (0.476)	304,2	144,88	10.1

Tab. 5.2 *List of magnetic anisotropy factors computed at each site of the sampled URF Fm. sites.*

6. PALEOMAGNETIC ANALYSIS

In the last years paleomagnetic studies have been largely used as a suitable tool for better understand how block rotation could contribute to the tectonic and geodynamic evolution of a continental region.

Several paleomagnetic studies focused on the reconstruction of the rotational history of Iranian region, in the Alborz mountains (Mattei et al., 2017), as well as in the so called Central Iranian Microcontinents (Mattei et al., 2015; Schmidt and Soffel, 1984; Soffel et al., 1996; Wensink, 1982)

The north-eastern sector of Iran, along the Allah Dagh, Binalud and Kopeh Dagh mountain belts represents a key area for the understanding of these geodynamic processes, being interested by both the Cimmerian orogeny and by Tertiary to present-day deformation related to Arabia-Eurasia collision. This area has never been investigated with paleomagnetic techniques excepted for very sparse data published by Bazhenov, (1987) in the Turkmenistan portion of Kopeh-Dagh and by Mattei et al., (2017) in the Rivand and Samghan folds, south of the Allah Dagh range. The extensive paleomagnetic sampling (70 sites) carried out for this PhD study, together with the available data, allow a new interpretation of the northward subduction of the South Caspian basin below the Apsheron-Balkan Sill and the westward extrusion of the South Caspian block, which will be discussed in the following.

This chapter consists of the published paper "Clockwise paleomagnetic rotations in northeastern Iran: Major implications on recent geodynamic evolution of outer sectors of the Arabia-Eurasia collision zone in Gondwana Research 71 (2019), pages 194–209".

Data relative to the paper are presented in Chapter 7 (page 101-104): Table1-2-3

6.1. CLOCKWISE PALEOMAGNETIC ROTATIONS IN NORTHEASTERN IRAN: MAJOR IMPLICATIONS ON RECENT GEODYNAMIC EVOLUTION OF OUTER SECTORS OF THE ARABIA-EURASIA COLLISION ZONE

Massimo Mattei[1], Andrea Leonardo Visconti[1], Francesca Cifelli[1*], Reza Nozaem[2], Aldo Winkler[3], Leonardo Sagnotti[3]

[1]Dipartimento di Scienze, Università Roma Tre, Largo San Leonardo Murialdo 1, IT-00146 Rome, Italy.

[2] School of Geology, College of Science, University of Tehran, Iran

[3] Istituto Nazionale di Geofisica e Vulcanologia, Via di Vigna Murata 605, IT-00143, Rome, Italy.

* corresponding Author (francesca.cifelli@uniroma3.it)

ABSTRACT

In this study, an extensive paleomagnetic sampling (70 sites) was carried out in north-eastern Iran with the aim of reconstructing the rotation history of the outer margin of the Eurasia-Arabia collision area represented by the Ala-Dagh, Binalud and Kopeh-Dagh mountain belts. We sampled the red beds units from the Lower Cretaceous Shurijeh Fm. and from the Middle-Upper Miocene Upper Red Fm (URF). Paleomagnetic results from all the sampled areas show a homogeneous amount of CW rotations measured in the above-mentioned Formations. These paleomagnetic results suggest that the oroclinal bending process that caused the curvature of Alborz mountain belt in north Iran after the Middle-Late Miocene, also extended to the Ala-Dagh, Binalud and Kopeh-Dagh mountain belts, at the north-eastern border of the Arabia-Eurasia deforming zone.

Based on our paleomagnetic results and on GPS, seismological, geomorphological and structural data available in the area, a hypothesis of tectonic evolution of the northern Iran-South Caspian Basin area, from Middle-Late Miocene to Present, is here proposed. In this model, the initiation of the oroclinal bending processes in northern Iran occurred about 6-4 myr ago, related to the impinging of North Iran between the South Caspian block and the southern margin of the Turan platform, driven by the northward subduction of the South Caspian basement under the Aspheron-Balkhan Sill. As paleomagnetic results from this study show a pattern of vertical axis rotations that is inconsistent with the present-day kinematics of the northern Iranian blocks as described by seismicity and GPS data, we suggest that the tectonic processes responsible for the bending of northern Iran mountain chains are no longer active and that the westward motion of the South Caspian basin, and therefore the initiation of opposite strike-slip motion along the Ashk-Abad and Shahrud faults, occurred very recently (~ 2 My ago). We therefore

propose that initiation of the northward subduction of the South Caspian basin below the Apsheron-Balkhan Sill and the westward extrusion of the South Caspian block did not occur at the same time, with the former occurring between the late Miocene and the Pliocene, and the latter during the Pleistocene.

1. INTRODUCTION

The Ala-Dagh, Binalud and Kopeh-Dagh mountains in north-eastern Iran represent the easternmost part of a curved mountain belt system that extends from north-western Iran to its Afghan border to the east (Fig. 1a). In north-eastern Iran, the mountain ranges are shaped in a series of linear fold and thrust belts oriented NW-SE between the stable Turkmenistan platform and Central Iran, and mark the northern limit of the continental deformation area related to the Arabia-Eurasia collision. The present-day tectonics of the area is characterized by the presence of different crustal blocks with different kinematics, whose origin and tectonic evolution has been largely debated in the last years (see Hollingsworth et al., 2008 and references therein). In particular, GPS and seismic data show that in north Iran the deformation pattern is related to the northward movement of Central Iran with respect to stable Eurasia, which decreases eastwards from Central Iran to the Turkmenistan border of Iran, and to the north-westward movement of the South Caspian Block with respect to stable Eurasia (Fig. 1b). This movement is accommodated by two strike-slip fault systems, the ENE-WSW oriented left-lateral Shahrud fault system and the WNW oriented right-lateral Ashk-Abad fault system, which represents the south and north boundary of the South Caspian Block, respectively (Fig. 1a). The present-day kinematics cannot explain the curvature of the northern Iran mountain belts, which has been acquired throughout oroclinal bending in a different tectonic regime (Mattei et al., 2017), suggesting a recent major tectonic reorganization of northern Iran (Ritz et al., 2006). In this framework, north eastern Iran represents a key area for defining the age of this major tectonic reorganization and for understanding the tectonic processes which have occurred at the boundary between the Iranian deforming zone and the southern margin of stable Eurasia.

In this work, we present new paleomagnetic results from the Lower Cretaceous Shurijeh Fm. and from the Middle-Upper Miocene URF from the Ala-Dagh, Binalud and Kopeh-Dagh mountain belts in north eastern Iran. Our new data define the history of vertical axis rotations of the area, which help to clarifying the tectonic evolution of this region and its role in accommodating the deformation related to the Arabia-Eurasia collision.

2. GEODYNAMIC AND TECTONIC SETTING

Iran is characterized by a complex history of deformation, dominated by the long-standing convergence between Eurasia and Cimmerian terranes. During Middle to Late Triassic, the northward drift of Gondwanan terranes caused the closure of the Paleotethys Ocean, separating the Eurasian Plate from

Central Iranian blocks, and their collision against the southern margin of Eurasia, with the developing of the Eo-Cimmerian orogeny (e.g., Zanchetta et al., 2013). This process was accompanied by the opening of the Neotethys ocean on the southern margin of the Central Iranian blocks during the Permian. The subsequent northward subduction and the progressive closure of the Neotethys ocean caused the opening of small back-arc basins during the Early and Late Cretaceous, testified by the presence of several ophiolitic units surrounding Central Iran (Agard et al., 2011) (Fig. 1a). These oceanic basins started to subduct during the Late Cretaceous (Bröcker et al., 2013; Saccani et al., 2010) and were closed during Paleocene to Eocene times (Agard et al., 2011). This phase was followed during Late Tertiary to present-day by intracontinental deformation related to the closure of the Neotethys ocean and to the Arabia-Eurasia continental collision (Allen et al., 2003a; Ballato et al., 2013, 2011; Berberian, 1983; Calzolari et al., 2016a, 2016b; Ganser and Huber, 1962; Guest et al., 2006a, 2006b; Jackson et al., 2002; Madanipour et al., 2013; Rezaeian et al., 2012; Stöcklin, 1974; Tadayon et al., 2018, 2017, Zanchi et al., 2009, 2006).

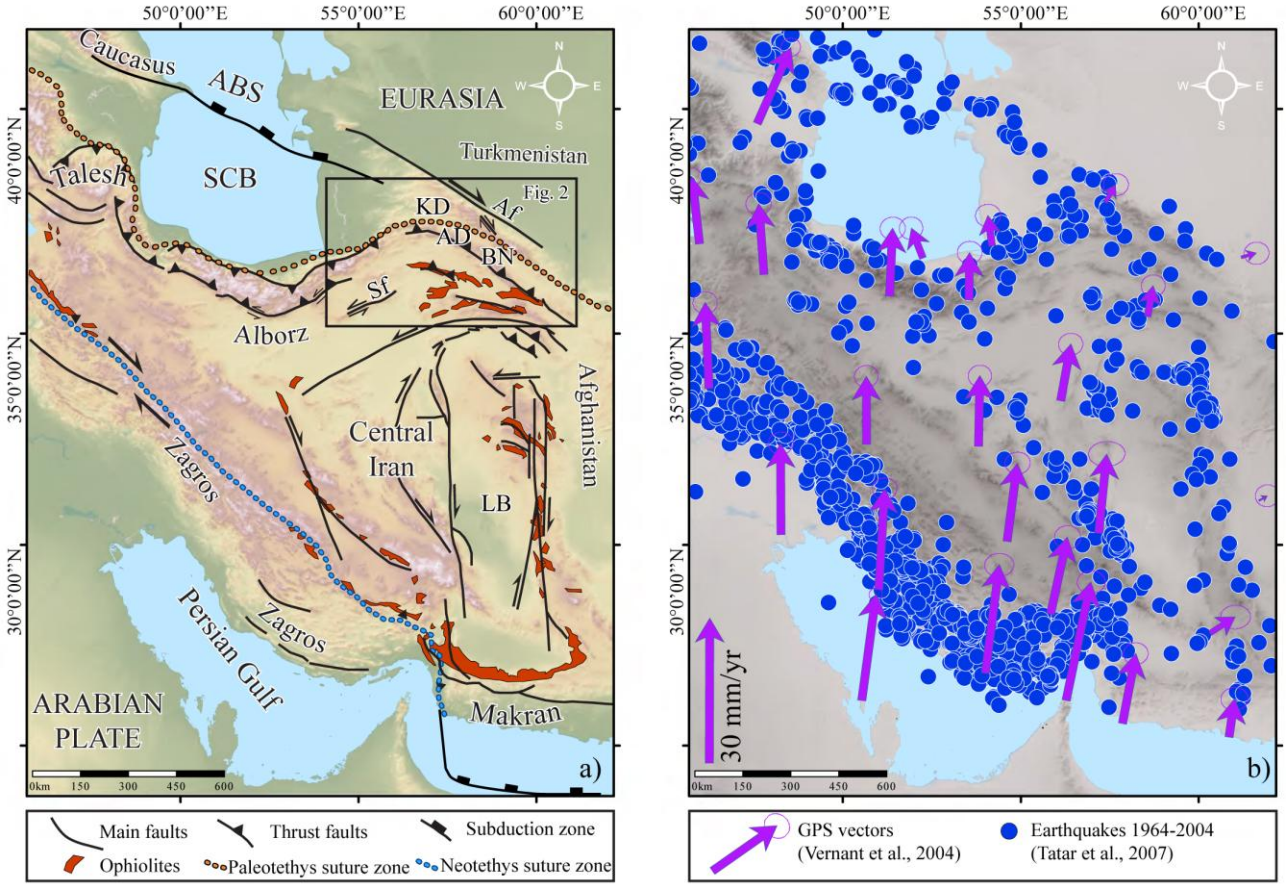

Fig. 1. a) Schematic tectonic map of Iran. The main present day tectonic features are reported together with ophiolites and the Paleotethys and Neotethys sutures; b) Location of teleseismically recorded earthquakes in a period of 1964–2004 from Tatar et al., (2007) and GPS-derived velocity field of the collision zone, with respect to stable Eurasia (Vernant et al., 2004). Af = Ashk-Abat Fault; AD = Ala-Dagh; BN = Binalud Mts.; KD = Kopeh-Dagh; LB =Lut Block; Sf = Shahrud Fault.

In Iran, this latter orogenic phase is testified by intracontinental mobile belts (Talesh, Zagros, Alborz, and Kopeh-Dagh ranges) that surround moderately aseismic crustal blocks (Central Iran, South Caspian

and Lut blocks) and accommodated a relative small amount of shortening, linked to subduction beneath the central Caspian Sea (Aspheron-Balkhan Sill) and Makran, and by N–S right-lateral and E-W left lateral fault systems in Central and Eastern Iran (Fig. 1a).

North eastern Iran represents a key area for understanding these geodynamic processes, being affected by both the Cimmerian orogeny and by Tertiary to present-day deformation related to Arabia-Eurasia collision. In fact, the Paleotethys suture zone corresponds to the boundary between the Kopeh-Dagh fold-and-thrust belt to the NE, and the eastern prolongation of the Alborz range to the SW (Fig. 1a). Remnants of the Paleotethys Ocean are located within the Binalud Mountains where the Cimmerian event was characterized by collision during the Late Triassic/Early Jurassic (Sheikholeslami and Kouhpeyma, 2012), followed by the deposition of sedimentary units of Kopeh-Dagh Basin on the southern margin of the Eurasian Plate, from Jurassic to the Tertiary (Brunet et al., 2003).

North of the Paleotethys suture the Cenozoic to present-day deformation is accommodated in the Kopeh-Dagh mountain belt, an approximately N120° oriented and 700 km long range, that extends from the Southern Caspian Sea to the Afghanistan border (Fig. 1). The Kopeh-Dagh mountain belt is made of Middle Jurassic to Late Tertiary and Quaternary sedimentary units deformed in large-scale folds, with a trend variable from ENE-WSW to NW-SE, west and east of 57° 00’ E longitude, respectively (Fig. 2). The right-lateral Ashk-Abad fault forms the northern boundary of the western Kopeh-Dagh and represents the northernmost edge of significant deformation related to Arabia-Eurasia collision. The fault corresponds to a major inherited crustal-scale structure, separating the Turan platform, which is part of stable Eurasia, from the South Caspian Region and from the deformed region of north eastern Iran. To the north-west, the deformation belt continues in the Apsheron-Balkhan belt, an active structure that represents the northern boundary of the South Caspian Sea Basin (Fig. 1a).

South of the Paleotethys suture, the Ala-Dagh and Binalud mountain belts accommodated the Tertiary to Present-day shortening (Fig. 2). The Ala-Dagh is made mostly of Jurassic and Cretaceous sedimentary units and forms NW to ENE trending folds. The most prominent structural feature of Ala-Dagh is given by the presence of north eastern dipping thrust faults associated with NW-SE oriented right-lateral and E-W oriented left-lateral strike-slip faults (Hollingsworth et al., 2006, 2008, 2010; Jackson et al., 2002; Shabanian et al., 2009a,b). North eastern dipping thrusts in this area have been responsible for the Neogene uplift of low relief ranges to the south of the Ala-Dagh that also show evidence of active deformation (Rivand and Samghan folds in Hollingsworth et al., 2010). The NW-oriented Binalud and Fariman mountain belts are a collection of the Paleotethys remnants, as well as Middle and Upper Mesozoic, and Cenozoic rocks that thrust southward over the Neogene and Quaternary units of Central Iran. The boundary between Ala-Dagh and Binalud mountain belt is represented by a complex area of deformation characterised by recent volcanism, by the presence of ENE-WSW oriented left-lateral strike-

slip fault systems and NNW-SSE oriented right-lateral faults, and bordered to the southwest by NW-SE oriented thrust faults (Meshkan triangle of Shabanian et al., 2009a, 2010) (Fig. 2).

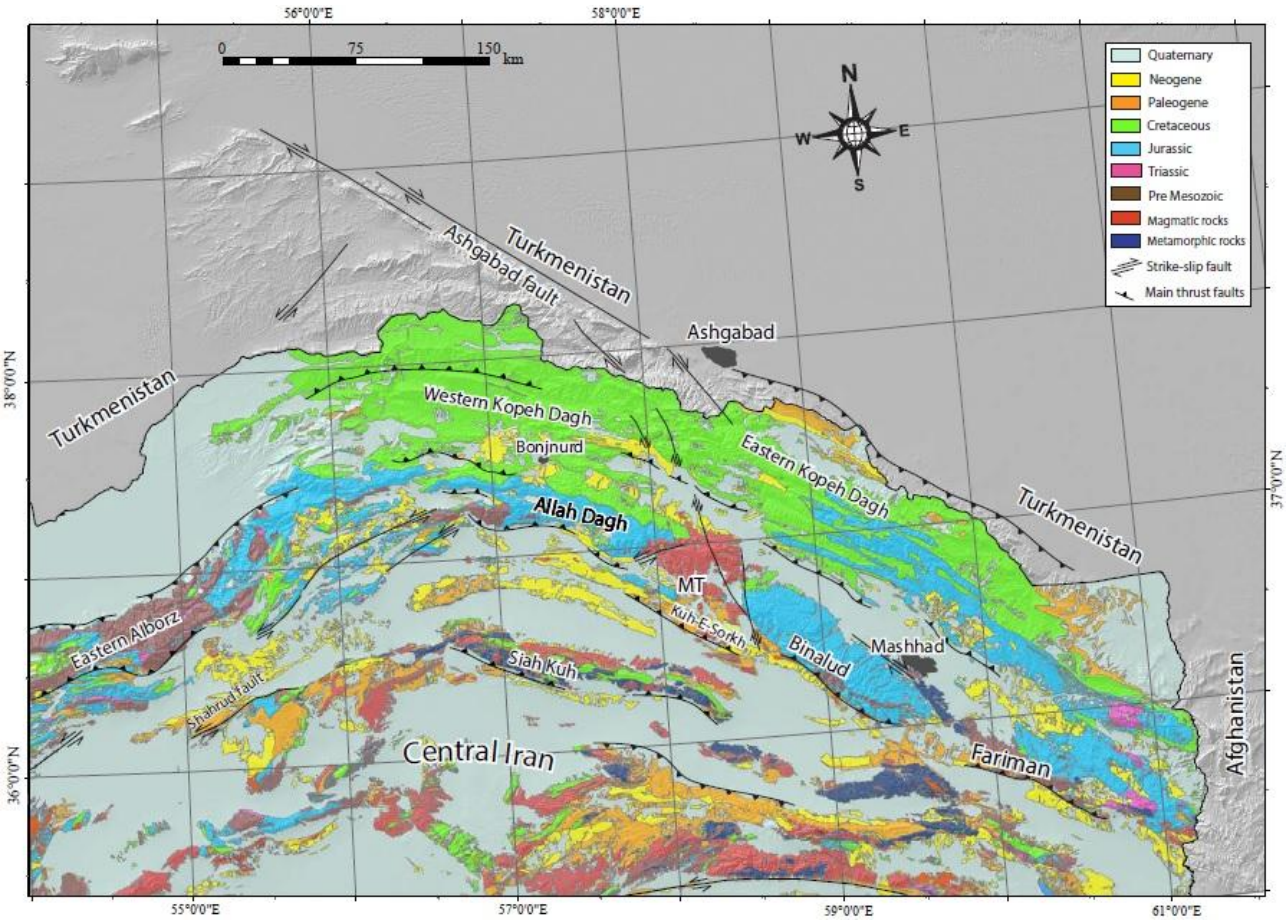

***Fig. 2**. Schematic geological map of northeastern Iran. MT = Meshkan triangle.*

Recent GPS measurements show that Arabia-Eurasia N-S convergence at the longitude of north eastern Iran (56°E-60°E) is around 25 mm/yr (Vernant et al., 2004) (Fig. 1b). These data evidence that most of deformation is taken up by the Zagros fold and thrust belt and by the Makran subduction zone in southern Iran, and that the Kuh-E Sorkh, Siah Kuh, Binalud, and Kopeh-Dagh mountain ranges of north eastern Iran only accommodate a fraction of this northward velocity. In particular, in north-eastern Iran the amount of shortening varies with longitude and decreases eastwards, with 4.5 ± 0.5 mm/yr of N–S shortening at longitude 59°E and reaching zero near the Afghan border (Mousavi et al., 2013).

South of 35°N, the N–S right-lateral shearing between western Afghanistan (which is part of stable Eurasia) and Central Iran is accommodated by N–S right-lateral faults within eastern Iran (Walker and Jackson, 2004). In north-eastern Iran, the pattern of faulting is more complex and involves thrusts and left-lateral faults and right-lateral strike-slip faults, west and east of ~57◦E, respectively. This pattern of faulting must also accommodate motion of the South Caspian Basin relative to its surroundings (e.g. Copley and Jackson, 2006; Djamour et al., 2010; Jackson et al., 2002). The South Caspian region moves independently of both north-eastern Iran and Eurasia and is suggested to be a rigid block based on a lack

of internal seismicity. From simple plate circuit closure models and GPS data, the South Caspian is thought to be moving to the NW at around 7–10 mm/yr, (Jackson et al., 2002; Mousavi et al., 2013). In particular, the NW motion of the South Caspian region is accommodated in northeast Iran by right-lateral slip on the Ashk-Abad fault and by left- lateral slip across the Shahrud left-lateral strike-slip fault system (Fig. 1 and 2).

3. REGIONAL STRATIGRAPHY AND PALEOMAGNETIC SAMPLING

In north-eastern Iran, after the completion of the Cimmerian orogeny, Middle Jurassic siliciclastic sediments, resting unconformably on folded Triassic or older rocks, deposited in deltaic and marine environments (Kashafrud Fm.) (Taheri et al., 2009) (Fig. 3a). The Kashafrud Fm. was overlain, in the western part of the basin, by the Upper Jurassic Chaman Bid Fm., which mostly consists of alternations of gray shales and marly limestones, deposited on the slope of a carbonate platform and in the adjacent basin (Kalantari, 1969).

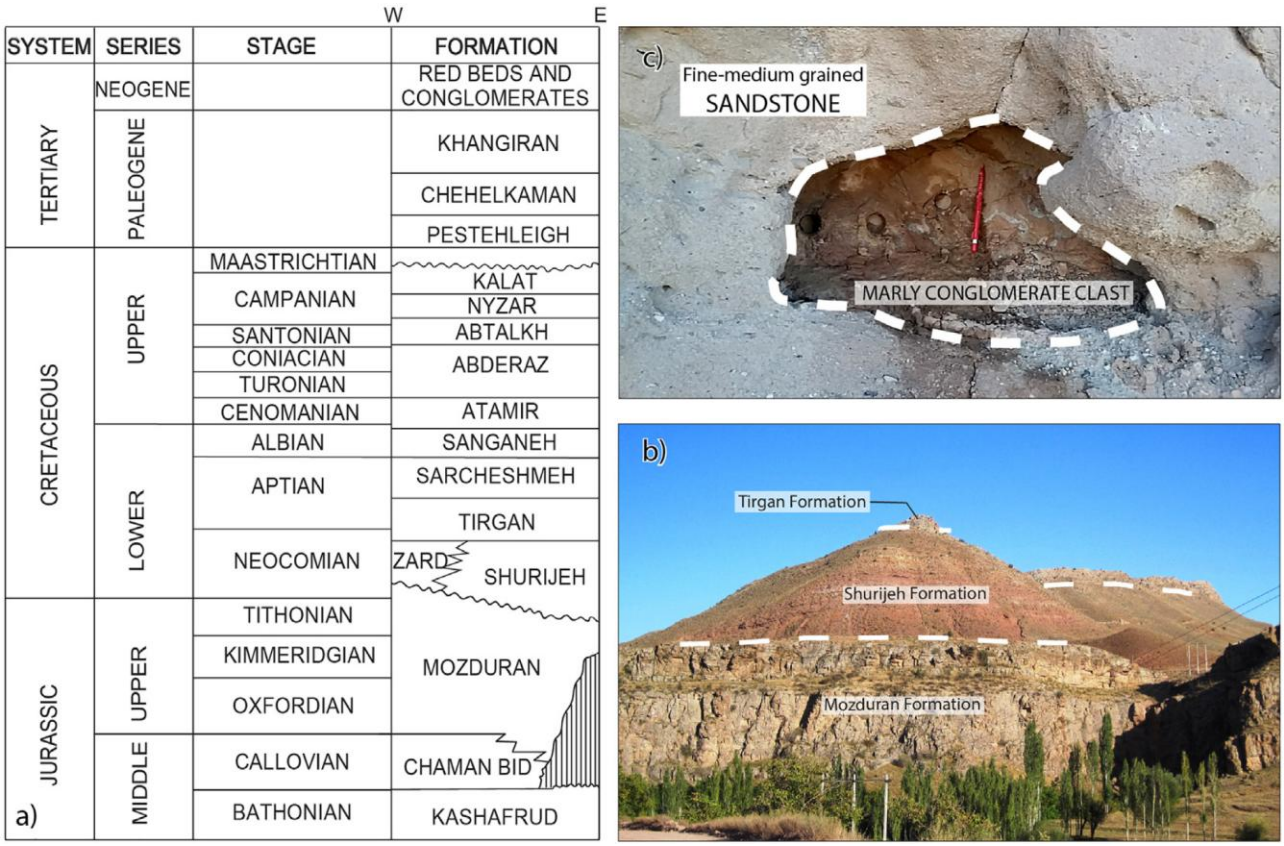

Fig. 3. *Schematic stratigraphic section of the sedimentary units outcropping in northeastern Iran (modified from Kavoosi et al., 2009; Kavoosi, 2015; Moussavi-Harami and Brenner, 1990); b) field outcrop of the stratigraphic section including the Shurijeh Fm (coordinates 36°50'1.87"N; 59°46'40.80"E); c) intraformational marly cobbles within conglomerates layers of the Neogene URF (coordinates 36° 3'36.11"N 60°21'41.40"E).*

In contrast, towards the east, the Kashafrud Fm is directly overlain by well-bedded marine limestone of the Mozduran Fm. whose facies varies towards the east to siliciclastic sediments (Taheri et al., 2009). At the end of Jurassic and during the Early Cretaceous (Neocomian), a marine regression occurred in the area

and red bed siliciclastic sediments were deposited in fluvial systems (Shurijeh Fm., Fig. 3b), whereas marine conditions persisted towards the northwest of the basin, in connection with Caspian Sea sedimentation (Afshar-Harb, 1979). During the Neocomian, a marine transgression brought back marine conditions in the area (Tirgan Fm.) that persisted through the Late Cretaceous, with several episodes of regional uplift testified by several hiatuses in the sedimentary succession (Afshar-Harb, 1979). A Late Cretaceous-Early Paleocene regression caused the deposition of continental red beds of the Pestehleigh Fm., followed by several episodes of marine incursions and regressions that occurred in the area though the Paleogene (Eocene), which is the age of the youngest marine sedimentation (Robert et al., 2014). Poorly dated continental conglomerates, sandstones and marls deposited during Late Paleogene (Oligocene)-Neogene times, marking the definitive continentalization and emersion of north-eastern Iran (Robert et al., 2014). The upper portion of this sequence can be correlated with the Neogene (middle-late Miocene) Upper Red Fm. (URF, Fig. 3c) of Central and Northern Iran, and for this reason from here onwards we will call them URF. These deposits are strongly discordant on the older sedimentary units, marking the onset of the compressional deformation in north-eastern Iran.

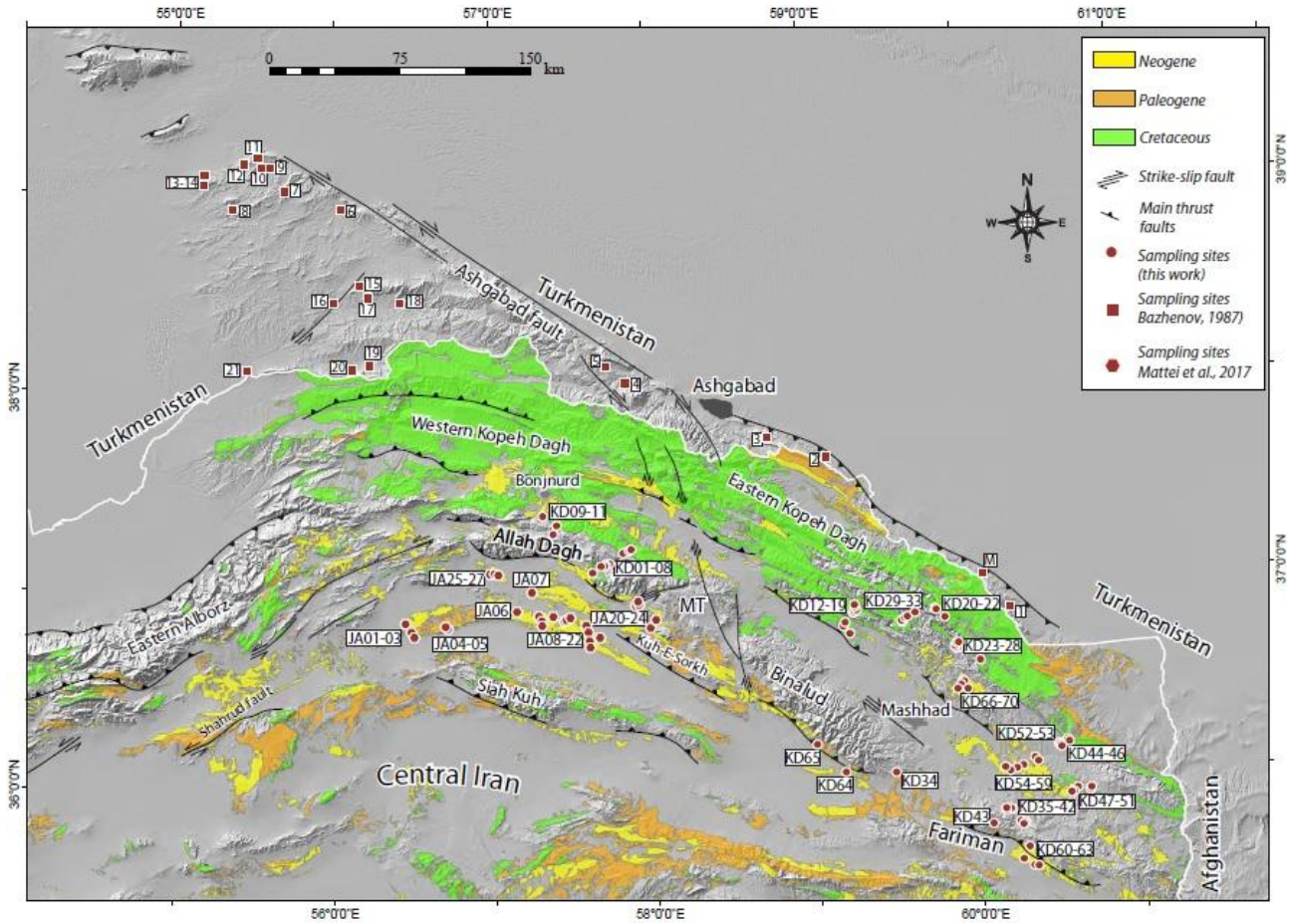

Fig. 4. Location of paleomagnetic sampling sites (KD). Numbers are referred to sampling by Bazhenov, 1987 whereas JA sites are from the work by Mattei et al., 2017.

Recent papers from Central and Northern Iran have shown that red beds units of Late Jurassic-Early Cretaceous (Garedu Fm.), almost equivalent to the Shurijeh Fm. of northeast Iran, and Middle-Late Miocene deposits of the URF have good magnetic properties and are very suitable for paleomagnetic analysis and tectonic reconstructions (Ballato et al., 2008, 2017; Cifelli et al., 2015; Mattei et al., 2012, 2015). The good magnetic properties of these deposits and their wide distribution in north-eastern Iran make the Shurijeh Fm. and the URF a valuable target for investigating vertical axis rotations in this region. Accordingly, paleomagnetic sampling was carried out in fine-grained sandstones, siltstones and red marls from these two units, and subordinately in the Paleocene clastic units of the Pestehleigh Fm (Fig. 4).

The sampling area extends along the Ala-Dagh, Binalud, and Fariman ranges and Kopeh-Dagh Mts., from longitude ~ 57°E to ~ 60°E (Fig. 4). Seventy sites were sampled using an ASC 280E petrol-powered portable drill with a water-cooled diamond bit. The cores were oriented *in situ* with a magnetic compass, corrected to account for a local ~4° magnetic declination. For each paleomagnetic site, nine to fifteen cores were taken from different stratigraphic levels in order to average secular variation of the geomagnetic field and to check for the occurrence of polarity reversals.

4. METHODS

The magnetic mineralogy of the sampled deposits was investigated using standard rock magnetic techniques. A stepwise acquisition of an isothermal remanent magnetization (IRM) was imparted on 45 representative specimens, using a pulse magnetizer up to a 2.7 T peak field. A three component IRM was also imparted on the same specimens by means of a 2G Enterprises mod. 660 pulse magnetizer at 2.7 T, 0.6 T, and 0.12 T fields along samples' orthogonal axes and thermally demagnetized according to the method by Lowrie (1990).

The hysteresis loops of powders from 5 representative Neogene samples were obtained on a Princeton Measurements Corporation 3900 vibrating sample magnetometer (VSM), in fields up to 1 T; the coercivity of remanence (B_{cr}) values have been extrapolated from backfield remagnetization curves up to −1 T, following forward magnetization in a +1 T field.

The NRM of one specimen per core was demagnetized by means of stepwise thermal demagnetization using small temperature increments (80-100 °C up to 300 °C and 30–50 °C above 300 °C) until the NRM decreased below the limit of the instrument sensitivity or random changes of the paleomagnetic directions appeared. Specimens were measured using a 2G Enterprises DC-SQUID (superconducting quantum interference device) cryogenic magnetometer located in a shielded room at the INGV Laboratory of Paleomagnetism (Rome, Italy). Data analysis was carried out using Remasoft 3.0 software (Chadima and Hrouda, 2006). The Characteristic Remanent Magnetization (ChRM) directions were computed using the principal component analysis (PCA) (Kirschvink, 1980), whereas the site-mean paleomagnetic directions were calculated using Fischer statistics (Fisher, 1953).

5. RESULTS

5.1 Magnetic mineralogy

Most of the 37 samples from the Lower Cretaceous Shurijeh Fm. are far from reaching IRM saturation at 2.7 T, suggesting the predominant presence of high coercivity minerals (Fig. 5a). Few samples acquire 60% of magnetic saturation at 300 mT, suggesting that low coercivity minerals are also present in some specimens. Thermal demagnetization of a three component IRM indicates that the high-coercivity magnetic phases show maximum unblocking temperatures of about 680° C, and were therefore ascribed to hematite (Fig. 5c). The low coercivity minerals, when present, are completely demagnetized at the 580°C or 630 °C steps, indicating magnetite, with possibly maghemite in oxidised rims, as main magnetic carriers (Fig. 5d).

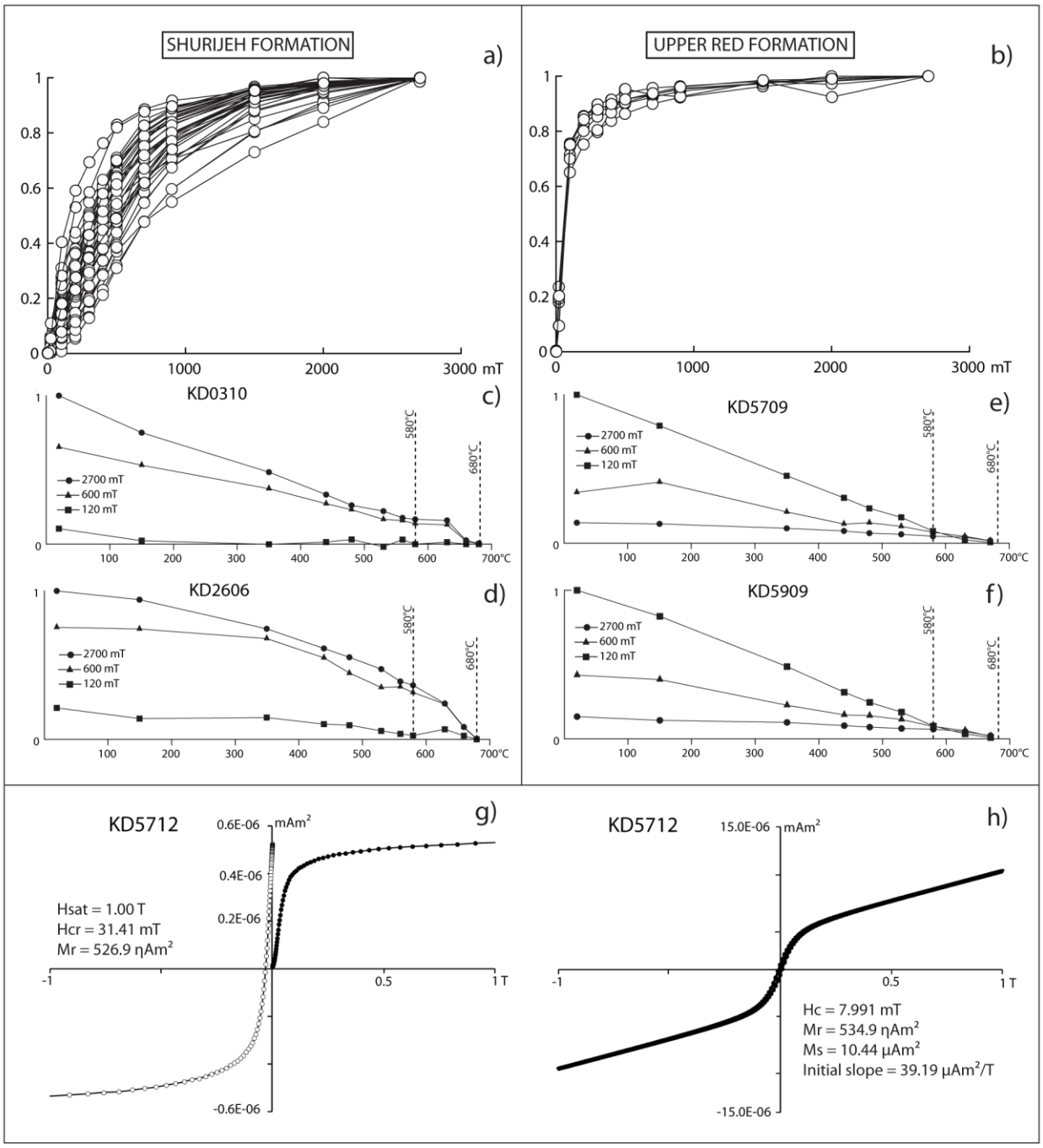

Fig.5. *Normalised Isothermal Remanent Magnetization (IRM) acquisition curves of representative samples from the Shurijeh Fm. (a) and URF deposits (b). c-f) Thermal demagnetization of a composite three-axis IRM (Lowrie, 1990) produced sequentially in magnetic fields of 2.7, 0.6, and 0.12 T in four representative specimens of Shurijeh Fm. (c-d) and URF deposits(e-f). g-h) Hysteresis data for representative samples: g) stepwise acquisition of an IRM in fields up to 1 T and back-field demagnetization curves for on representative specimen from URF; h) hysteresis loops for the same specimen.*

All the eight samples from Neogene Red Beds Fm. reach 80% of their saturation magnetization at 300 mT, suggesting the prevalence of the low coercivity components with a minor amount of high coercivity components (Fig. 5b). As for the Shurijeh Fm. samples, the high-coercivity magnetic phases show

maximum unblocking temperatures of about 680 °C, and were therefore identified as hematite (Fig. 5e), whereas the low coercivity phases are completely demagnetized at the 580°C or 630 °C steps, indicating magnetite and possibly maghemite as main magnetic carriers (Fig. 5f).

Further analyses on five representative samples of Upper Red Fm. were carried out using the VSM. Results are mainly consistent with the coexistence of low coercivity component (magnetite and maghemite), as evidenced by Hcr values generally lower than 50 mT, and high coercivity component (hematite), as suggested by IRM acquisition curves that don't reach magnetic saturation in the maximum applied field of 1 T (Fig. 5g,h).

5.2 Paleomagnetic behaviour and analysis of the ChRM

In the Shurijeh Fm., the Natural Remanent Magnetization (NRM) intensities range between 9.2 x 10^{-5} and 3.3 x 10^{-1} A/m. During thermal demagnetization, most of the samples underwent a very slight (generally less than 10%) decrease of NRM intensity between 20°C and 300°C, a significant decrease between 300° C and 580-630° C and a sharp decrease in NRM intensity between 630° and 680° C. For these samples, after removal of a viscous low temperature normal polarity component at 150°/240° C, the NRM vectors define a single linear path toward the origin of the demagnetization diagrams for both normal and reverse polarities (Fig. 6a-c). The ChRM directions were computed by principal component analysis (PCA) (Kirschvink, 1980) of the linear component between 150/320°C and 650/680°C (Fig. 6a-c).

In the URF, the Natural Remnant Magnetization (NRM) intensities range between 6.4 x 10^{-4} and 7.1 x 10^{-1} A/m. In most of the samples, after the removal of a viscous low temperature normal polarity component at 180°/240° C, the NRM vectors aligned along a single linear path toward the origin of the demagnetization diagrams for both normal and reverse polarities (Fig. 6 d-f). In these samples, the ChRM directions were computed by principal component analysis (PCA) (Kirschvink, 1980) by fitting a linear component between the 180/240°C and 580/670°C heating steps.

In the two Eocene red marls of the Pestehleigh Fm., we were not able to obtain reliable directions because most of the samples were too weakly magnetized, or gave scattered directions within a single site, or showed paleomagnetic direction parallel to the present day magnetic field in geographic coordinates, suggesting a recent magnetic overprint. For these reasons, sites from Eocene Fm. were not taken into account for tectonic interpretation.

In the Shurijeh and URF Fm. characteristic remanent magnetization (ChRM) was determined by PCA for 856 specimens. The maximum angular deviation (MAD) of the identified magnetic components was generally < 10°. The site-mean paleomagnetic directions are reported in Table 1. Bedding corrections were performed by progressively untilting bedding to horizontal using the Remasoft 3.0 software (Chadima and Hrouda, 2006).

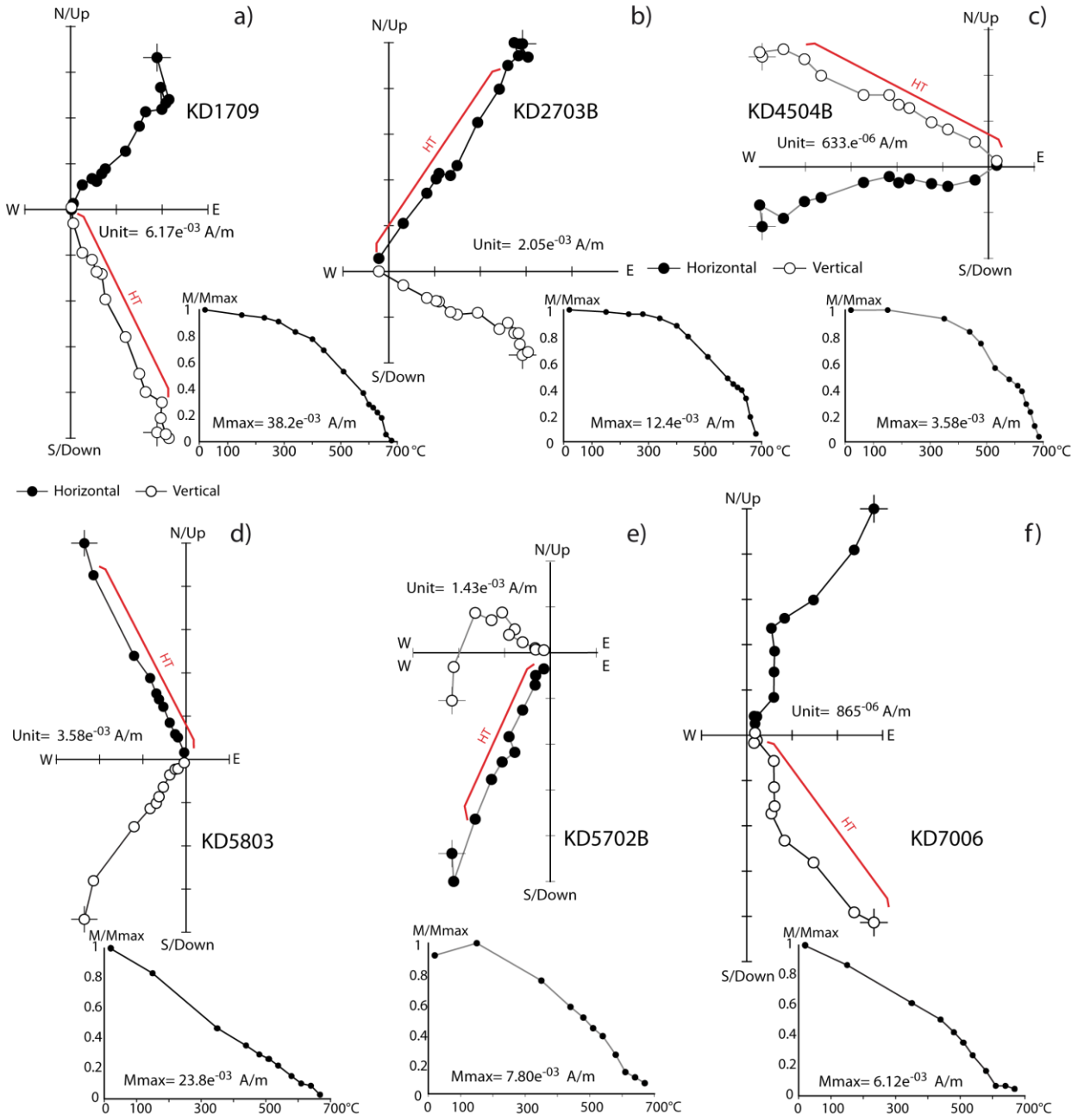

Fig. 6. *Orthogonal vector diagrams (before tectonic correction) for the progressive thermal demagnetization of representative samples. (a-c) Shurijeh Fm.; (d-f) URF. Open and solid symbols represent projections on the vertical and horizontal planes, respectively. N/UP, W, E, and S/DOWN indicate horizontal (north, south, west, and east) and vertical (up and down) projections combined into a single vector component diagram. For each sample, progressive thermal demagnetization data in Celsius degrees (°C) are reported. HT = High-temperature component.*

In the Shurijeh Fm. a stable and coherent ChRM was isolated in all the 45 sampled sites (Fig. 7; table 1). Most of these sites (41) show a normal polarity magnetization, whereas only 1 site (KD45) shows a reverse polarity magnetization and three sites (KD14, KD35, KD44) record mixed polarities, with most of the samples in these sites bearing normal polarity (Table 1). The 45 sites show well-grouped magnetic directions, with 40 sites having α_{95} values lower or equal to 10.0° and five sites with α_{95} values comprised

between 10.8° and 17.5°. Among these sites, one site (KD51) bears a normal polarity ChRM oriented along the present-day GAD field direction in geographic coordinates, which could indicate a recent magnetic overprint (Table 1). Furthermore, after tectonic correction this site show a WNW direction, which is very far from the mean direction obtained from all the other sites. Therefore, this site has been excluded from further tectonic interpretation. Since we obtained only one site with a reverse polarity ChRM, the bootstrap reversal test (Tauxe et al., 1991) was not applicable, whereas according to the reversal test of McFadden and McElhinny (1990), normal and reversed polarity site-mean directions are not antipodal and the reversal test is negative (γo = 32.3° and γc = 21.7°). On the other hand, the bootstrap fold test (Tauxe et al., 1991) is positive, showing that the degree of unfolding to produce the maximum τ_1 is included between 64-97% (Fig. 8a), suggesting that the ChRM for the Shurijeh Fm. has been acquired before folding and that ChRM directions can be used for tectonic interpretations.

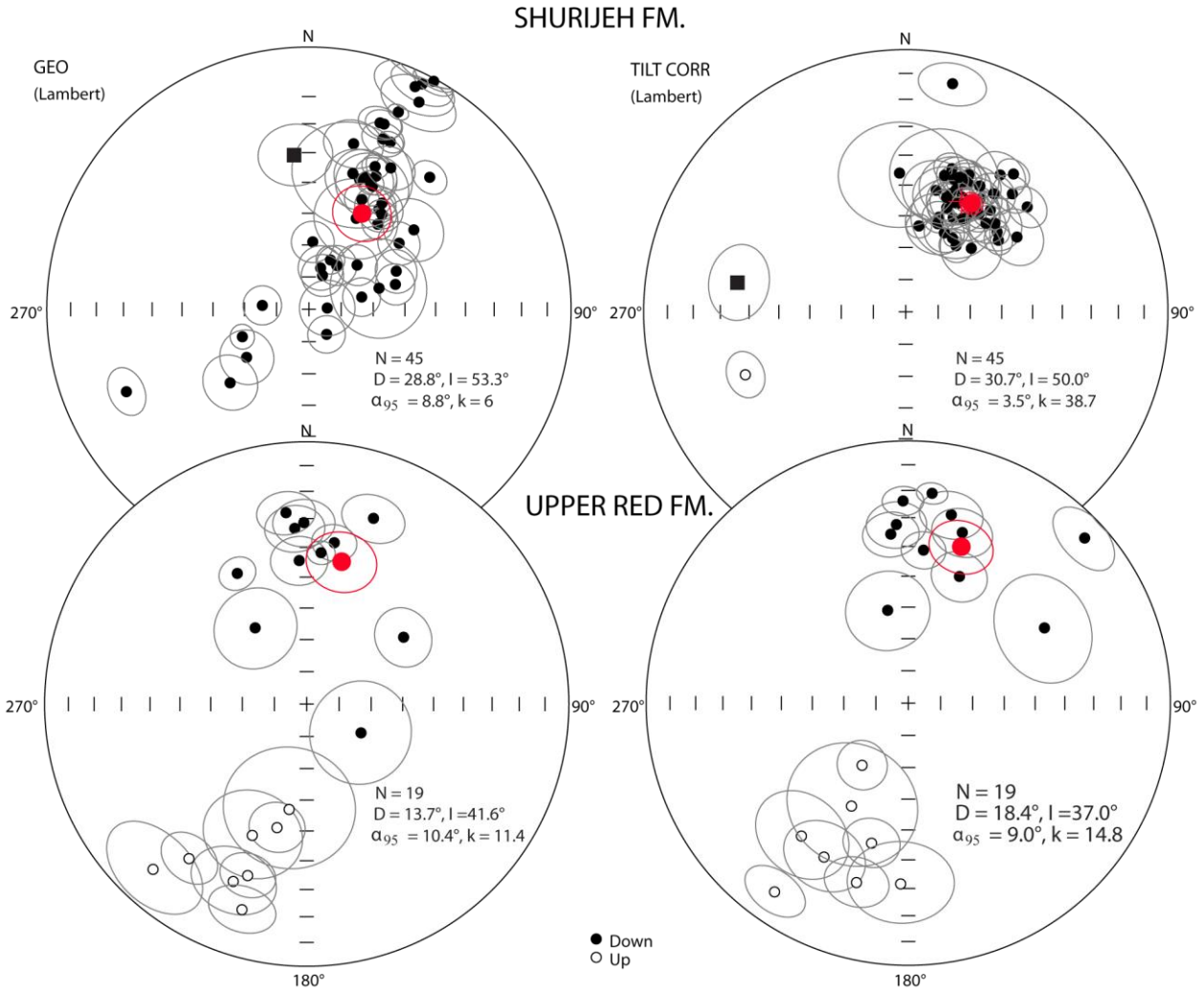

Fig. 7. Equal area projection of the site-mean directions from Shurijeh and URF. Solid and open circles represent projections on lower (normal directions) and upper (reverse directions) hemisphere, respectively. Square symbol represents site KD51, not considered for tectonic interpretation. Red symbols indicate the mean paleomagnetic directions for the analysed sites. Ellipses are the projections of the α_{95} cone about the mean directions.

When the 44 site mean directions are all reported in normal polarity, paleomagnetic directions are consistently oriented NNE and the mean direction for the Shurijeh Fm. is declination (Dec.) = 30.7°, inclination (Inc.) = 50.0°, k = 38.7, α_{95} = 3.5° (Fig. 7; Table 1).

In the URF a ChRM was isolated in 19 sampled sites, whereas site KD62 is characterized by scattered directions and has been not considered for further tectonic interpretation (Fig. 7; Table 1). Most of the sites show well defined ChRM direction, with α_{95} < 14.0°. Sites KD09, KD59, and KD63 show higher values of α_{95}, but their mean ChRM directions are similar to the other sites and have been also considered for tectonic interpretation (Table 1). Among the 19 sites, 11 record normal polarity and eight sites show reverse polarity (Fig. 7).

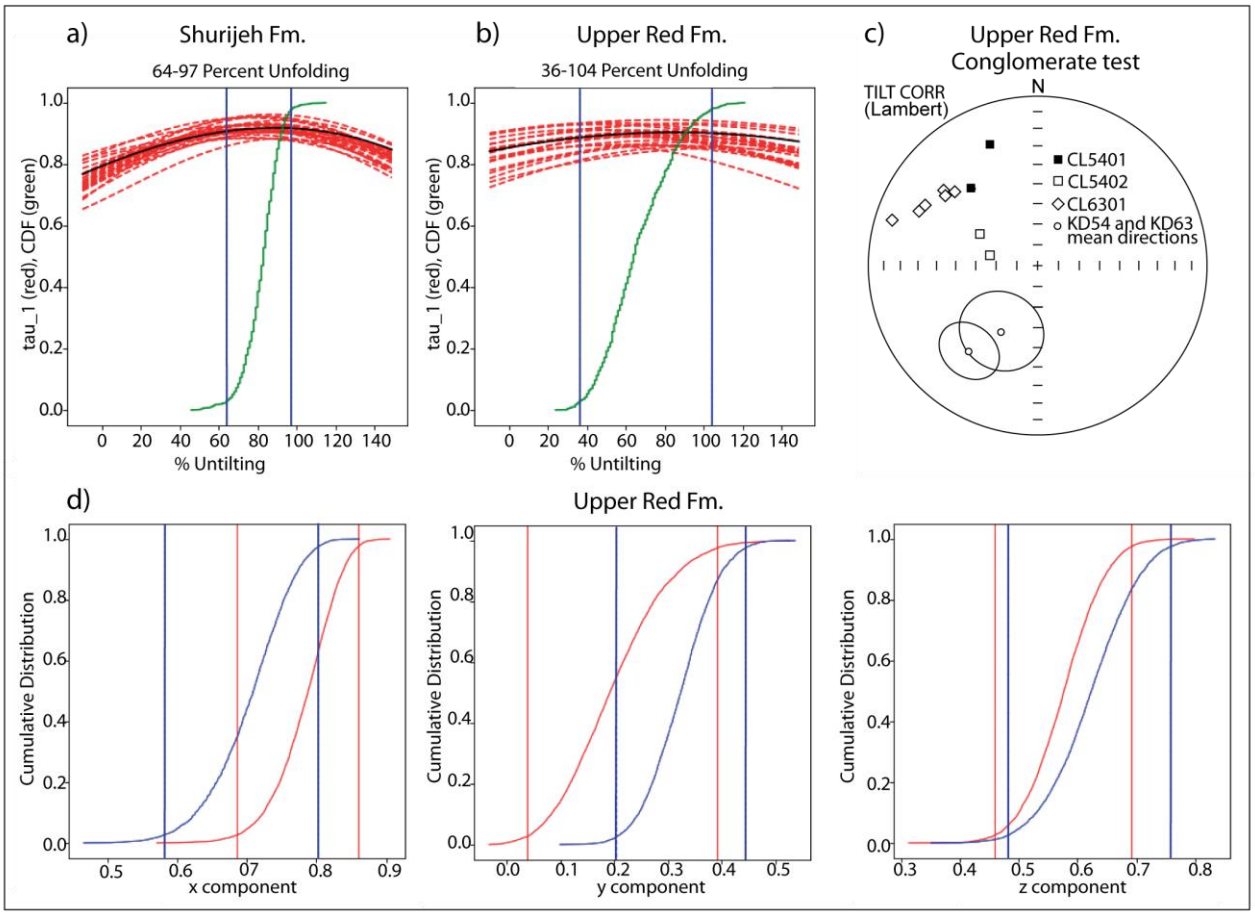

Fig. 8. *Field tests for URF and Shurijeh Fm. paleomagnetic results. a) and b): positive bootstrap fold tests (Tauxe et al., 1991) for the Shurijeh Fm. and URF, respectively. Red dashed lines represent the trends of the largest eigenvalues of the orientation matrices from representative data as they evolve during untilting. The directions are adjusted for tilt incrementally from -20% to 160%; c) equal area projection of the ChRM obtained from intraformational marly cobbles within conglomerates layers of the URF, compared with the mean ChRM obtained from the same sites. d) bootstraps reversal test for the URF. The graphics represent the cumulative distribution of Cartesian coordinates of data represented in a. The reverse polarity mode has been flipped to its antipode. The intervals containing 95% level of confidence of each set of components are also drawn (vertical line). The bootstraps reversal test (Tauxe et al., 1991) is positive, as the 95 % confidence intervals for the normal and reversed antipodes, overlap for X ,Y and Z.*

After tectonic correction, normal and reverse polarity site-mean directions group into two antipodal clusters with a positive bootstrap reversal test (Tauxe et al., 1991) (Fig. 8d). The bootstrap fold test (Tauxe

et al., 1991) is positive, showing that the degree of unfolding to produce the maximum τ_1 ranges between 36-104% (Fig. 8b), suggesting that the ChRM for the URF has been acquired before folding. Furthermore, in sites KD54 and KD63 we sampled some intraformational marly cobbles within conglomerates layers of the URF to perform a conglomerate test (Fig.3c). From these cobbles, we obtained well-defined ChRM, with coherent directions in samples from the same cobble, but randomly distributed in the different cobbles and far from the mean directions calculated for the sampled sites (Fig. 8c). These results indicate a positive conglomerate test for the URF intraformational conglomerate, providing very strong evidence that the ChRM is a primary magnetization. When all site mean directions are reported to normal polarity, paleomagnetic directions are consistently oriented N to NNE and the mean direction for the 19 ChRM directions from URF is declination (Dec.) = 18.4°, inclination (Inc.) = 37.0°, k = 14.8, α_{95} = 9.0° (Fig. 7; Table 1).

5.3 Paleomagnetic rotations

Since no Apparent Polar Wander Path (APWP) is available for Iran, the observed paleomagnetic directions must be compared with those expected for the Eurasian plate. Paleomagnetic rotations were then computed in relation to the fixed Eurasian plate using the coeval European paleopoles from Torsvik et al. (2012). Rotation values and associated 95% confidence limits were calculated according to the method of Demarest (1983) and reported in Table 1. The age of the isolated ChRM in the Shiurijeh Fm. is not precisely constrained. In fact, the ChRM directions in most of the sites (40 out of 44 sites) from the Shiurijeh Fm. have exclusively normal polarity directions. This prevalence of normal polarities is at odds with the Late Jurassic-Lower Cretaceous depositional age of the Shurijeh Fm., which is a time interval characterized by a high occurrence of magnetic reversal, with rapid alternation of periods with normal and reverse polarity. On the other hand, sites from Shurijeh Fm. show a positive fold test, indicating that the isolated ChRM has been acquired before the tectonic tilting of the sampled units. This suggests a post depositional magnetic overprint for the ChRM that occurred during a normal polarity chron before the Late Tertiary phase of folding related to the onset of the Alpine orogeny within the Kopeh-Dagh chain (Robert et al., 2014). These data, together with the inclination value comparable to that expected for the Eurasia APWP for 100 Ma, suggest that the magnetic overprint could have occurred during the Cretaceous long normal magnetic SuperChron 34 ranging between 124 and 84 My. It is worth to note that in red beds from Late Jurassic Garedu Fm. of Central Iran a normal polarity, high-inclination, paleomagnetic component has been also identified by Wensink, (1982) and Mattei et al., (2014). This component has been interpreted as the result of a post-folding magnetic overprint event of normal polarity, possibly associated with the Cretaceous deformation phase described in Central Iran by Ruttner (1968).

On this basis, the mean paleomagnetic directions from the Shurijeh Fm. has been compared with the 100 Ma reference pole (λ (°N) = -80.8°; ϕ (E) = 332.3°; A_{95} = 3.3°). Among the 44 reliable sites from the Shurijeh Fm, 34 sites show statistically significant CW rotations, and eight sites show mean declinations rotated clockwise with respect to the reference poles, but with error greater than rotation values (Table 1). Only two sites show a mean declination rotated CCW with errors greater than rotation values. At the regional scale the mean declination for the eastern Kopeh-Dagh is rotated 19.4° CW (± 5.2°) respect to the coeval Eurasia reference direction (Table 1).

ChRM directions from middle-late Miocene URF have positive reversal, fold and conglomerate field tests, indicating a primary origin of the isolated ChRM. On this basis, paleomagnetic directions have been compared with the 10 Ma reference pole (λ (°N) = -86.7°; ϕ (E) = 330.0°; A_{95} = 1.8°). Among the 19 sites from the URF, ten show statistically significant CW rotations, four sites show mean declinations rotated clockwise with respect to the reference poles, but with error greater than rotation values (Table 1). Five sites show a mean declination rotated CCW, two of them showing errors greater than rotation values. At the basin scale the mean declination for the URF in the eastern Kopeh-Dagh is rotated 14.3° CW (± 9°) respect to the coeval Eurasia reference direction (Table 1).

6. DISCUSSION

6.1 Previous paleomagnetic data in north-eastern Iran and Kopeh-Dagh range

Previous paleomagnetic results from north-eastern Iran and Kopeh-Dagh mountain belt are very sparse, being limited to data published by Bazhenov (1987) in the Turkmenistan portion of Kopeh-Dagh and in the Rivand and Samghan folds, south of the Ala-Dagh range (Mattei et al., 2017). Paleomagnetic data by Bazhenov, (1987) are from Lower Cretaceous to Paleocene units from the north-western part of the Kopeh-Dagh Mts. (Turkmenistan), comprised approximately between longitude 37°E and 39°E (Fig. 9a). In that study, samples were thermally demagnetized and interpreted using paleomagnetic directions after the final heating or using great circle intersection technique. Despite this statistical procedure does not fit modern standard analysis of paleomagnetic data, some site directions appear suitable for tectonic reconstruction, having positive reversal and fold tests. On this basis, we consider reliable data from sixteen sites yielding only linear directions, six from Cretaceous (Aptian-Cenomanian) units, and ten from Late Cretaceous-Paleocene deposits (Bazhenov, 1987; Table 2). The mean direction for the six Aptian-Cenomanian sites is declination Dec. = 21.0°, inclination (Inc.) = 54.5°, k = 138.6, α_{95} = 5.7°, whereas the mean direction for the ten Late Cretaceous-Paleocene sites is declination (Dec.) = 22.5°, inclination (Inc.) = 46.4°, k = 37.6, α_{95} = 8.0° (Table 2). In order to calculate paleomagnetic rotations, the Aptian-Cenomanian and Late Cretaceous-Paleocene sites have been compared with the 100 Ma (λ (°N) = -80.8°; ϕ (E) = 332.3°; A95 = 3.3°) and 70 Ma (λ (°N) = -79.2°; ϕ (E) = 355.7°; A95 = 2.5°) Eurasian reference poles, respectively

(Torsvik et al., 2012). The two sets of data show that, respect to the coeval Eurasia reference directions, the mean declination for the six Aptian-Cenomanian sites is rotated 9.6° CW (± 8.3°) whereas the mean declination for the ten Cretaceous-Paleocene sites is rotated 11.3° CW (± 5.2°) (Table 2).

Paleomagnetic results from Mattei et al., (2017) are from Middle-Late Miocene URF from the Rivand and Samghan fold structures, located to the southwest of Ala-Dagh mountain chain. These results show positive fold and reversal test with a mean regional direction (Dec.) = 21.5°, (Inc.) = 43.9°, k = 24.7, α_{95} = 6.9° that, when compared to the 10 Ma reference pole, indicates a CW rotation R = 17.4° (± 7.7°) respect to the coeval Eurasia reference direction (see Table 1 in Mattei et al., 2017 for further details).

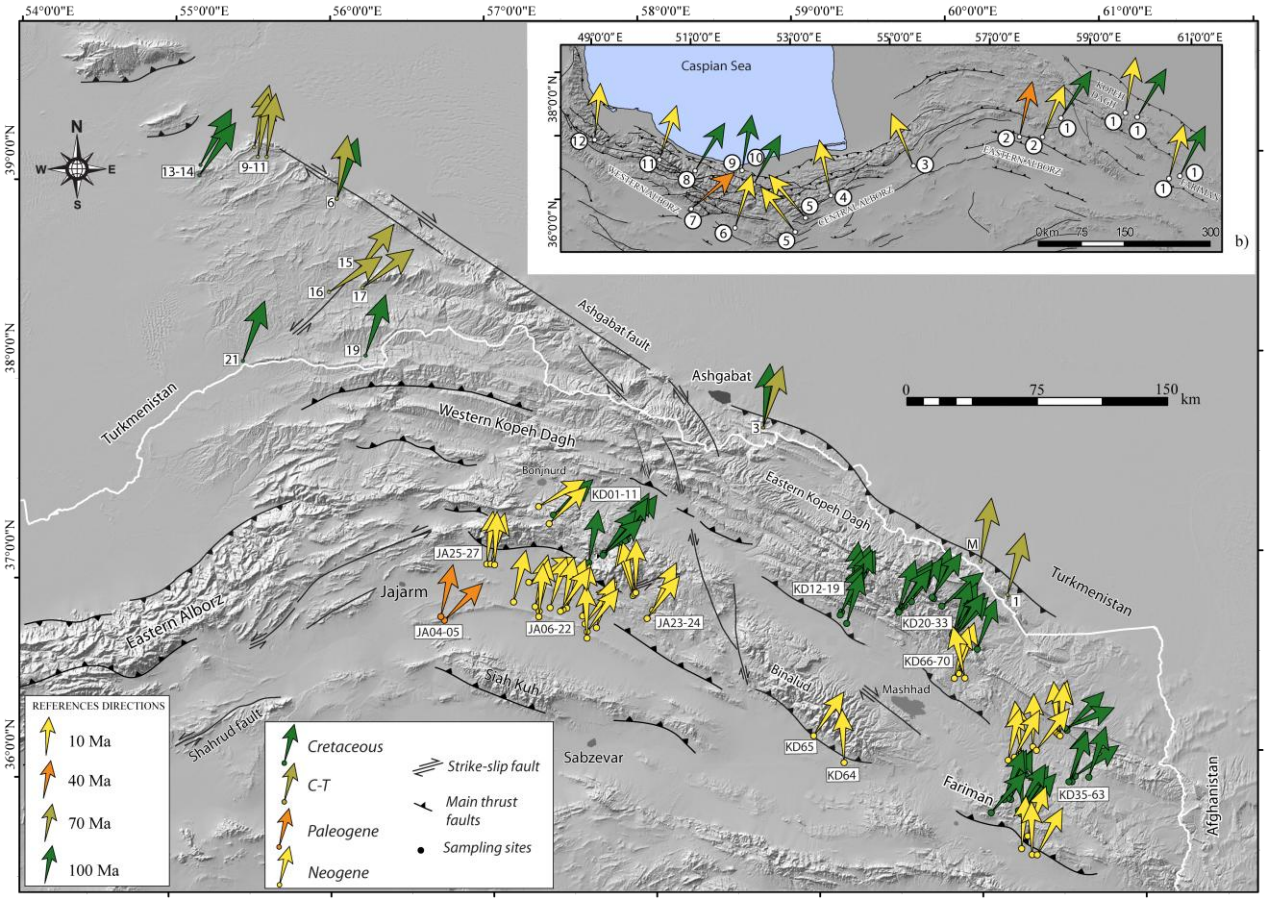

Fig. 9. *a) Paleomagnetic rotations from northeastern Iran and Turkmenistan, calculated comparing the obtained palaeodeclinations with the 10 Ma (URF), 40 Ma (Paleogene), 70 Ma (C-T) and 100 Ma (SHU and CRE) reference poles (see text and Tables 1 and 2 for details). Green arrows represent paleomagnetic declinations from Cretaceous rocks; orange arrows represent paleomagnetic declination from Eocene (Mattei et al., 2017) and Upper Cretaceous-Paleocene (Bazhenov, 1987) rocks; yellow arrows represent paleomagnetic declination from Middle-Late Miocene URF rocks. b) Mean paleomagnetic rotations from the different sectors of North Iran: 1) this work; 2) Jajarm (Mattei et al., 2017); 11) Alamut (Mattei et al., 2017); 12) Manjil (Mattei et al., 2017); 3-5) Semnan Basin (Mattei et al., 2017); 6) Eyvanikey (Ballato et al., 2011; Cifelli et al., 2015); 7) Karaj (Bina et al., 1986); 8-9 Chalus (Wensink and Varekamp, 1980); 10) Haraz River (Wensink and Varekamp, 1980). Arrows' colours are the same of Fig. 9a.*

6.2 Age and distribution of vertical axis rotations in Kopeh-Dagh, Ala-Dagh and Binalud-Fariman mountain belts

Paleomagnetic results from Iranian Kopeh-Dagh, Ala-Dagh and Binalud-Fariman mountains demonstrate that northeast Iran underwent CW vertical axis rotations. The amount of CW rotation is

statistically comparable in the Upper Jurassic-Lower Cretaceous Shurijeh Fm. (19.4° CW ± 5.2°) and in the Middle-Upper Miocene URF (14.3° CW ± 9°) (Table 1), suggesting that the entire amount of CW rotations measured in the Upper Jurassic-Lower Cretaceous units occurred after Late Miocene, and that northeast Iran did not undergo significant vertical axis rotations between Late Cretaceous and Late Miocene. It is worth to note that the amount of paleomagnetic rotations measured in the Shurijeh and URF is also statistically comparable with rotations obtained by Bazhenov, (1987) in the Aptian-Cenomanian (9.6° CW ± 8.3°) and Upper Cretaceous-Paleocene units (11.3° CW ± 5.2°) from Turkmenistan Kopeh-Dagh.

Paleomagnetic rotations are consistently distributed in the different geological structures of north-eastern Iran (Fig. 9a). The same directions are, in fact, observed in the Shurijeh Fm. sites from Ala-Dagh (D= 33.3°; I=47.0°; k=17.6; α_{95}=14.8°), Fariman (D= 27.2°; I=51.7°; k=53.1; α_{95}=5.7°), and Kopeh-Dagh (D= 31.2°; I=49.3°; k=44.97; α_{95}=4.5°) suggesting that these structures underwent a similar rotational history. URF sites show as well similar directions in Fariman (D= 14.9°; I=40.2°; k=25.9; α_{95}=10.3°) and Kopeh-Dagh (D= 9.8°; I=41.8°; k=19.2; α_{95}=14.1°) areas. These latter directions are also no statistically different from results obtained by Mattei et al., (2017) in the Rivand and Samghan fold structures (D = 21.5°, I = 43.9°, k = 24.7, α_{95} = 6.9°), south of Ala-Dagh (Fig. 9a).

6.2 Paleomagnetic constraints to geodynamic evolution of North Iran

6.2.1 Tectonic evolution of north-eastern Iran

The Cenozoic tectonic evolution of north-eastern Iran has been widely discussed in the last decades (Hollingsworth et al., 2010, 2008, 2006; Jackson et al., 2002; Shabanian et al., 2010; 2009a; 2009b). According to GPS, seismological, geomorphological and structural data two main features characterize the present-day kinematics of north-eastern Iran. The first feature is the northward motion of Central Iran with respect to Eurasia, which decreases linearly from ~11 mm/yr at the longitude of Tehran to zero at the eastern border of Iran (Vernant et al., 2004) (Fig. 1b). This velocity field is consistent with shortening accommodated by active folds and thrusts of north Iran and with distributed N–S right-lateral shear across northeastern Iran (Mousavi et al., 2013; Vernant et al., 2004). The second feature is represented by the westward extrusion of the South Caspian block, accommodated by dextral strike-slip faults along the northeast border of Iran (e.g. the Ashk-Abad Fault), and by left-lateral motion along its southern margin (e.g. the Shahrud fault system) (e.g., Hollingsworth et al., 2008) (Fig. 1).

Despite the general agreement on these first-order features that characterise the present-day kinematics of northeastern Iran, the tectonic evolution of the Kopeh-Dagh, Ala-Dagh and Binalud and how these structures accommodate the Arabia-Eurasia shortening and the westward extrusion of the South Caspian block, is much more debated and different models have been proposed (Fig. 10). A first class of models (Hollingsworth et al., 2010, 2008, 2006; Jackson et al., 2002) subdivides the Kopeh-Dagh range in three different regions, characterised by different kinematics and style of deformation (Fig. 10a). East of

59°E, mountains have the highest peaks and GPS data show 2 mm/yr N-S shortening between Central Iran and Eurasia, which appears to be partitioned into range-parallel thrusts and right-lateral strike-slip faults. West of 57°E, the topography across the Kopeh-Dagh decreases gradually and the range is progressively buried by sediments toward the Caspian coast (Lyberis and Manby, 1999; Robert et al., 2014), and the right-lateral Ashk-Abad Fault is the dominant tectonic feature of the region. In this area right-lateral slip and slip on range-parallel thrusts accommodates the motion between Eurasia and the South Caspian block (Jackson et al., 2002). Between 57° E and 59° E, the relative motion of the South Caspian block away from north-eastern Iran causes the central portion of the Kopeh-Dagh to experience range-parallel extension in addition to the N-S convergence between Iran and Eurasia that are accommodated by CCW rotation on a series of NNW-striking right-lateral strike-slip faults (Bakhardan-Quchan- Fault Zone) (Hollingsworth et al., 2006).

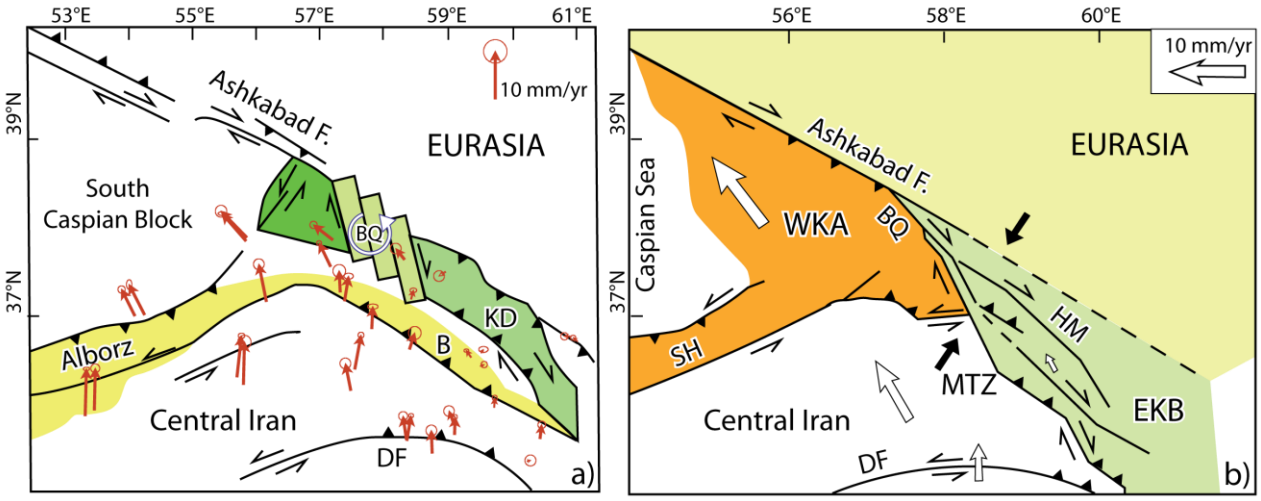

Fig. 10. *Tectonic models proposed for northeastern Iran (modified by Shabanian et al., 2009a). a) Simplified version of the kinematic model proposed by Hollingsworth et al., (2008). Red arrows represent GPS velocities in the Eurasian reference frame (Mousavi et al., 2013). b) model of the tectonic configuration in NE Iran proposed by Shabanian et al., (2009a). White arrows are GPS velocity vectors in the Eurasian reference frame. Black arrows show the direction of the σ_1 stress axis. B = Binalud; BQ = Bakharden-Quchan Fault system; DF = Doruneh Fault; EKB= eastern Kopeh-Dagh–Binalud tectonic domain; HM = Hezar Masjed Fault system; KD = Kopeh-Dagh; MTZ = Meshkan Transfer Zone; SH = Shahrud Fault system; WKA = western Kopeh-Dagh–Alborz tectonic domain. The inactive NE margin of the Kopeh-Dagh is marked by dashed line.*

A second class of models (Shabanian et al., 2009a) subdivides northeast Iran in two blocks with independent kinematics (Fig. 10b). The two blocks are separated by a NNW-SSE striking strike-slip fault system (Meshkan and Bakhardan-Quchan Fault Zones) that allows the northward movement of Central Iran relative to eastern Iran. In particular, the western Kopeh-Dagh movement toward the South Caspian Basin, is taken up by lateral motion on the Ashk-Abad Fault and the Shahrud Fault system. In this model, right-lateral strike-slip faults across the Kopeh-Dagh range do not rotate but instead accommodate the north-westward translation of Iran relative to Eurasia and represent the eastern border of the South Caspian Block (WKA in Fig. 10b).

Paleomagnetic data from north-eastern Iran show that Ala-Dagh, Binalud-Fariman Mts. and Kopeh-

Dagh underwent comparable amount of CW rotations in both Shurijeh and URF deposits. This pattern of paleomagnetic rotations is at odd with the present-day kinematics of northeast Iran as suggested by GPS data that highlight the existence of fault-bounded blocks with different kinematics. In particular, paleomagnetic data do not show differential rotations between Ala-Dagh, which belongs to the South Caspian block according to the Shabanian et al., (2010) model (Fig. 10b), and the eastern Kopeh-Dagh, Binalud and Fariman structures, which belong to the EKB block of Figure 10b.

On this basis, we propose that the measured pattern of paleomagnetic rotations has occurred in a tectonic regime different from the present-day one, and that the tectonic reorganization of north-eastern Iran is relatively young and therefore its rotational pattern cannot be detected using paleomagnetism. It is noteworthy that our sampling sites do not cover the Kopeh-Dagh region comprised between 57° and 59° E of longitude, where a CCW rotation of fault bounded blocks has been suggested (Fig. 10a) and therefore our data do not give any information on tectonic processes in this area.

6.2.2 Oroclinal bending in Northern Iran

Previous paleomagnetic results in north Iran (Ballato et al., 2008; Cifelli et al., 2015; Mattei et al., 2017) showed that the WNW-ESE oriented western Alborz and Rivand and Samghan fold belts rotated about 15–20° CW whereas the WSW-ENE oriented eastern Alborz Mts. rotated about 20°CCW. (Fig. 9b). This distribution of paleomagnetic rotations has been interpreted as the result of an oroclinal bending process that occurred in the Alborz Mts. after Late Miocene. Our paleomagnetic results from the Kopeh-Dagh, Ala-Dagh and Binalud-Fariman ranges confirm that the WNW-ENE oriented structure of north-eastern Iran underwent CW rotations after Late Miocene, supporting the oroclinal bending hypothesis of the whole mountain range. Furthermore, the absence of differential rotations in the Shurijeh Fm. and URF excludes that the oroclinal bending processes started earlier than Late Miocene, as suggested by Hollingsworth et al. (2010). Our paleomagnetic data also prove that oroclinal bending and CW rotation in north-eastern Iran are not limited to the Alborz Mts. but also extend to the east (Binalud Mts.) and to the outer margin of the deformation structures related to the Arabia-Eurasia convergence (Kopeh-Dagh Mts.).

In Figure 11, a paleotectonic reconstruction of North Iran from Miocene to Present is proposed, that takes into account the main constraints derived from paleomagnetic data. In Figure 11a we show a possible paleotectonic configuration of North Iran during the Middle-Late Miocene, before the beginning of the oroclinal bending process. The main features are: i) the presence along the southern Eurasia margin of two rigid blocks, with a high velocity and high-density mantle, separated by an embayment with low-density, low-velocity mantle (Maggi and Priestley, 2005; Kaban et al., 2016). These two blocks are the Turan platform to the east and the South Caspian Basin to the west, a trapped block of rigid (probably oceanic) crust today surrounded by active fold and thrust belts (e.g., Kadinsky-Cade et al., 1981); ii) the presence of the Alborz and Kopeh-Dagh orogenic systems whose existence during the Middle-Late

Miocene is testified by a Late Eocene-Oligocene regional unconformity in the western Kopeh-Dagh (Robert et al., 2014), by regional volcanic dikes dated to 8.7 to 6.7 Ma, cutting a regional thrust fault system in western Alborz (Guest et al., 2007), and by rapid exhumation of the Alborz Mts., as indicated by a strong cluster of apatite fission track ages around 10–20 Ma (Madanipour et al., 2013; Rezaeian et al., 2012); iii) the E-W orientation of the Alborz and Kopeh-Dagh mountain ranges derived by paleomagnetic data (Mattei et al., 2017 and results from this work).

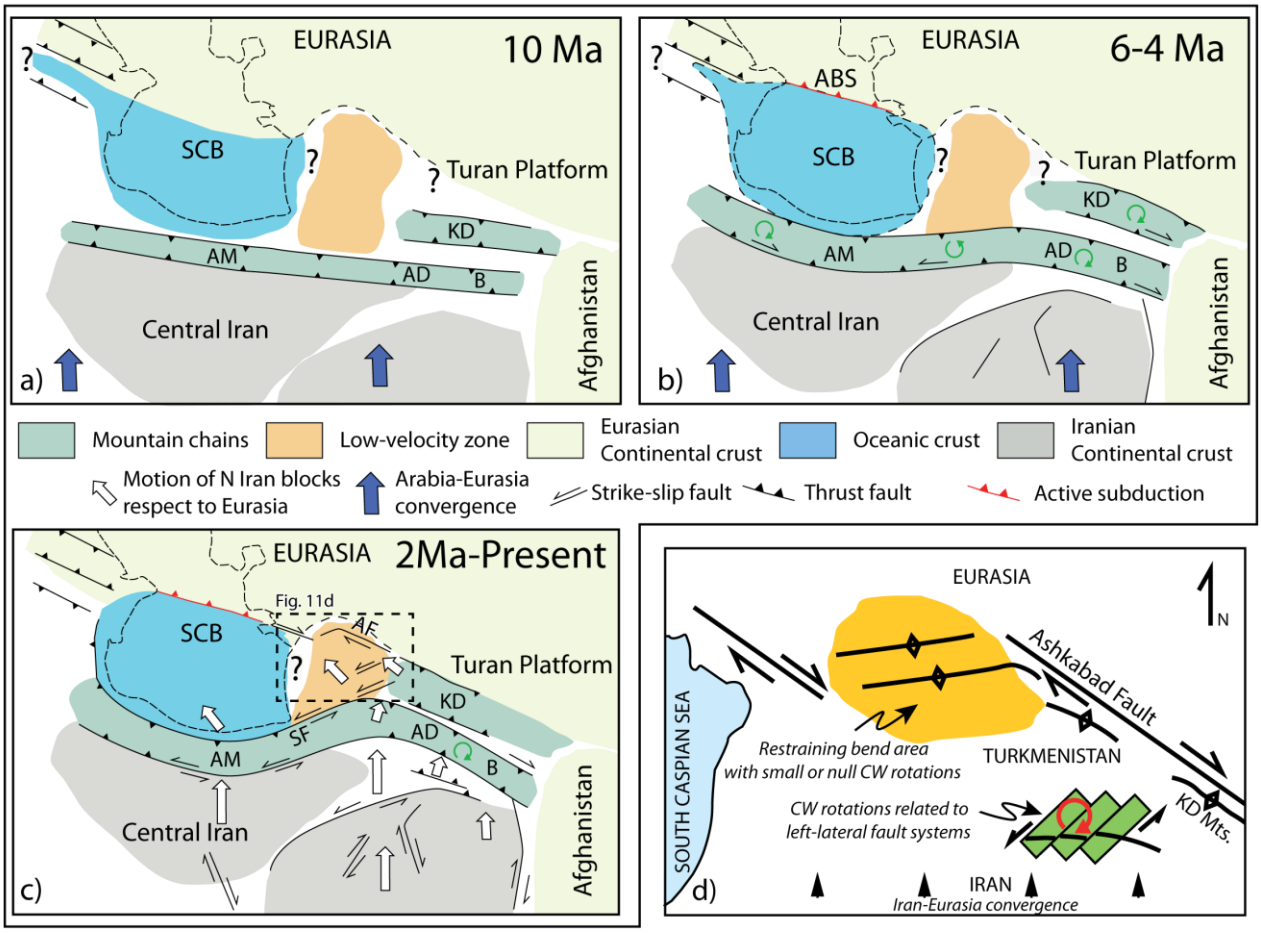

***Fig. 11. a-c**) Schematic cartoons of the tectonic evolution of Northern Iran from Late Miocene to Present (modified from Mattei et al., 2017): **a)** Linear W-E orientation of the North Iran mountain belts at 10 Ma, before the collision of the Central Iranian Blocks with the South Caspian Block and with the Turan Platform; **b)** collision of Central Iran with the South Caspian Block and with the Turan Platform, that caused the internal deformation and the outward migration of the mountain ranges, the initiation of the South Caspian subduction underneath the Aspheron Sill and was accompanied by large vertical axis rotations; **c)** recent to Present-day kinematics of North Iran with the westward extrusion of the South Caspian Block and the initiation of strike-slip tectonics in the area. **d)** Tectonic model of the Ashk-Abad area in Turkmenistan (inset in fig. 11c) explaining the origin of the differently oriented systems of fold and thrust structures and the CW rotations related to the presence of left-lateral strike slip fault system. AM = Alborz Mts.; B = Binalud Mts.; AD = Ala-Dagh Mts.; KD = Kopeh-Dagh; SCB = Sothern Caspian Basin; ABS = Aspheron-Balkhan Sill; AF = Ashk-Abad Fault*

In Figure 11b, the initiation of the oroclinal bending processes in North Iran is shown (about 6-4 Ma), related to the convergence of Central Iran with the South Caspian block and the southern margin of the Turan platform. In particular, the collision of Central Iran with the rigid South Caspian block has produced the present-day curved shape of the Western and Eastern Alborz mountain chain that progressively

wrapped around it with CW and CCW rotations, respectively (Allen et al., 2003; Cifelli et al., 2015; Hollingsworth et al., 2010; Mattei et al., 2017). At the same time, the interaction of Central Iran with the southern margin of the Turan platform caused the progressive CW rotation of the Ala-Dagh, Binalud and Kopeh-Dagh Mts. The age of the collision between Central Iran and the South Caspian block is suggested by several evidence, including: i) the incorporation of middle Miocene sedimentary sequences deposited in the Caspian Sea block (Red Marl Fm.) in the northern side of the Alborz orogenic wedge; ii) an important phase of exhumation in the Alborz Mts, accompanied by an increase of fold and thrust activities in the internal part of the chain during the late Miocene-Pliocene time (6–4 Ma) (Axen et al., 2001); iii) the outward migration of the orogenic wedge frontal thrusts along the southern and northern sides of the mountain range. In the South Caspian Basin this collisional event is recorded by an increase in the sedimentation rate, recorded by ≈2.4 km of tectonic subsidence since ≈ 5.5 Ma (Allen et al., 2002). This rapid accumulation of sediments is related to an increase in the basement subsidence, which testifies the beginning of northward subduction of the South Caspian basement under the Aspheron-Balkhan Sill, now imaged by the subcrustal earthquakes with depths down to 80 km (Allen et al., 2003, 2002; Jackson et al., 2002).

Finally, in Figure 11c the present-day tectonic configuration of North Iran is represented, highlighting the major changes in the tectonic regime of North Iran related to the initiation of the westward extrusion of the South Caspian block. According to GPS data we show that: i) Western and Eastern Alborz behave as a single block, moving toward the southwest with respect to Central Iran (Djamour et al., 2010; Mousavi et al., 2013); ii) the Western Kopeh-Dagh motion is coherent with the South Caspian Block and is presently moving toward northwest with respect to Eurasia, whereas the Binalud and Eastern Kopeh-Dagh Mts. behave substantially coherently and do not show significant movements with respect to Eurasia (Mousavi et al., 2013). The age of the beginning of this tectonic regime, associated to the initiation of left-lateral strike slip faulting in the Alborz Mts. (Shahrud Fault system), together with dextral movement along the Ashk-Abad fault at the NE boundary with the Eurasia plate has been largely disputed in the recent literature, being proposed at ~10 Ma (Hollingsworth et al., 2008), ~5 Ma (Allen et al., 2002), and ~1.8 Ma ago (Mattei et al., 2017; Ritz et al., 2006). Ritz et al., (2006) and Ritz (2009), on the basis of geomorphologic and structural data, suggested that the beginning of the westward motion of the South Caspian basin, and therefore the initiation of opposite strike-slip motion along the Ashk-Abad and Shahrud faults, occurred very recently (~ 2 Ma ago). Our paleomagnetic data, together with results from Mattei et al., (2017), fully confirm this tectonic scenario. In fact, our paleomagnetic results show a pattern of vertical axis rotations that is inconsistent with the present-day kinematics of the northern Iranian blocks as described by seismicity and GPS data. Therefore, we conclude that the oroclinal bending of northern Iran mountain chains is younger than ~7 Ma (younger age of URF) but is no longer active, as a consequence of a recent changing of the tectonic regime in North Iran. As a consequence, as suggested by

Ritz (2009), the initiation of the northward subduction of the South Caspian basin below the Apsheron-Balkan Sill (Fig. 11b) and the westward extrusion of the South Caspian block (Fig. 11c) did not occur at the same time, with the former starting between the late Miocene and the Pliocene, and the latter during the Pleistocene.

6.2.3 Reinterpretation of paleomagnetic rotations in the Turkmen Kopeh-Dagh Mts.

Paleomagnetic results from the Turkmenistan part of the Kopeh-Dagh Mts. have been published by Bazhenov, (1987). These data have been used in this study for calculating the relative vertical axis rotations of Bazhenov's sites with respect to coeval Eurasian poles (Torsvik et al., 2012) (Table 2). Sites were sampled in different fold structures whose strike ranges from WSW-ENE to NW-SE, almost orthogonal and parallel to the Ashk-Abad Fault, respectively (Fig. 9a). Paleomagnetic data show that about half of the sites are substantially not rotated, whereas half show a statistically significant CW rotation (Table 2). The oroclinal test applied on these paleomagnetic results is negative (Bazhenov, 1987), demonstrating that in this area there is no relationship between the fold axes orientation and the amount of vertical axis rotations, and that the curvature of the fold axis is primary. Therefore, an oroclinal bending mechanism is not applicable to this portion of the Kopeh-Dagh Mts. and the presence of fold and thrust structures with different orientation needs an alternative explanation.

The area investigated by Bazhenov, (1987) is located at the northwest termination of the right-lateral Ashk-Abad Fault, where the Kopeh-Dagh mountain belt is characterized by a series of E-W oriented large-scale folds. These folds are broadly convex northwards, and curve into the trend of the range-parallel, right-lateral Ashk-Abad Fault at the northern margin of the range (Allen et al., 2003; Lyberis et al., 1998; Lyberis and Manby, 1999). Toward the west, the fold axes plunge beneath the Quaternary cover bordering the southeastern margin of the Caspian Sea, where the E-W oriented set of folds continues into the eastern part of the Aspheron Sill (Fig. 11c-d) (Allen et al., 2003b; Bretis et al., 2012; Hollingsworth et al., 2008; Hinds et al., 2007; Jackson et al., 2002). In map view, fold and fault trends between the western end of the Ashk-Abad Fault and the eastern Apsheron Sill have the overall geometry of a right-lateral push-up structure. It is worth to note that in western Kopeh-Dagh upper Pliocene marine rocks are clearly folded with the Cretaceous-Paleogene rocks, and middle-upper Pliocene marine sediments are exposed at an altitude of 1100 m (Lyberis and Manby, 1999). Therefore, the age of the tectonic uplift and folding of these structure is post-Upper Pliocene and is almost coeval with the activity of the Ashk-Abad fault system. On this basis, we propose that these folds formed in a restraining bend in correspondence of the left step-over of the Ashk-Abad right-lateral fault system and eastern Apsheron Sill, with their fold axis trending at high angle respect to the WNW-ESE oriented main faults, showing no rotations or a limited amount of CW rotations (Fig. 11d and Table 2). On the other hand, significant CW rotations are measured by Bazhenov, (1987) at sites 15, 16 and 17 (Table 2, Fig. 9a), located in the northwest part of our study

area, at latitude 38°N, where the E-W oriented folds are dissected by a NNE-SSW oriented left-lateral strike-slip fault system (Fig. 3 in Lyberis and Manby, 1999). We hypothesise that such a large CW rotation could be related to the activity of such a fault system which rotates CW to accommodate the N-S component of shortening between the South Caspian Block and Eurasia and the along-strike elongation of the western Kopeh-Dagh respect to the South Caspian block (Fig. 11c-d).

7. CONCLUSIONS

Paleomagnetic results from the Kopeh-Dagh, Ala-Dagh, and Binalud mountain belts show a homogeneous amount of CW rotations measured in red bed units of both the Lower Cretaceous Shurijeh Fm. and Middle-Late Miocene URF. These paleomagnetic results show that the oroclinal bending process that occurred in North Iran after the Middle-Late Miocene, also extended to the north-eastern border of the Arabia-Eurasia deforming zone in Iran. The curvature of the Northern Iran mountain belts is due to the collision of Central Iran with two rigid blocks, the oceanic South Caspian Sea and the continental Turan platform, which represents the southern margin of Eurasia in the area. Paleomagnetic rotations occurred between ≈6-4 Ma and ≈2Ma, before the beginning of the westward extrusion of the South Caspian Block caused a drastic change in the tectonic regime of the area. In this reconstruction, the initiation of the northward subduction of the South Caspian Sea underneath the Aspheron Sill (≈ 6-4 Ma) preceded the initiation of strike-slip tectonics in north-eastern Iran (≈ 2Ma), which accompanies the westward movement of the South Caspian block (Ritz, 2009). In the Turkmenistan portion of the Kopeh-Dagh Mts. previous paleomagnetic data (Bazhenov, 1987) are reinterpreted in the framework of a new tectonic framework. The absence of a relationship between the fold axes orientation and the amount of vertical axis rotations is interpreted not as a primary curvature of the fold axes but as the consequence of the different tectonic location of the sampled sites. In particular, sites with no or limited amount of CW rotation are located in a restraining bend located between the western end of the Ashk-Abad Fault and the eastern Apsheron Sill, whereas larger CW rotations have been interpreted as the results of block rotations of a left-lateral strike-slip fault system which accommodate the N-S convergence between Iran and Eurasia and the E-W elongation due to the westward extrusion of the South Caspian Block.

7. GENERAL DISCUSSION

The paleomagnetic data collected, analysed and interpreted in this PhD project represent a further contribution for the comprehension of the post Cimmerian evolution of north-eastern sector of Iranian region. The Kopeh-Dagh, Ala-Dagh and Binalud-Fariman mountain belts representing the eastern prosecution of the Alborz oroclinal bending as well as the north-eastern accommodation of Arabia-Eurasia collision in Iran. In this key area, previous paleomagnetic results from north-eastern Iran and Kopeh-Dagh mountain belt are very sparse, being limited to data published by Bazhenov (1987) in the Turkmenistan portion of Kopeh-Dagh and in the Rivand and Samghan folds, south of the Ala-Dagh range by Mattei et al., (2017).

The extensive paleomagnetic sampling (70 sites) carried out, allowed to propose a new interpretation of the northward subduction of the South Caspian basin below the Apsheron-Balkan Sill and the westward extrusion of the South Caspian block, in order to better constrain the main events which interested this continental margin during the Arabia-Eurasia collision.

In this chapter the results of magnetic fabric and paleomagnetic analysis are discussed and interpreted in order to reconstruct the deformation history of the region.

7.1 The origin of the magnetic fabric

AMS technique was initially adopted, in the sedimentary rocks studies, for the identification of paleoflow directions in fluvial deposits (Baas et al., 2007; Hamilton and Rees, 1970; Hrouda, 1982; Ising, 1943); several studies demonstrated that there are many affinities between the shape and orientation of magnetic fabrics and the fluvial regime in which the sediments were deposited (Ellwood, 1980; Piper et al., 1996; Taira, 1989; Tarling and Hrouda, 1993). The natural and laboratory study cases evidenced how the magnetic fabric orientation was controlled by the direction of the long axes of magnetic grains, also aligned in the flow directions (Rees, 1965; Rusnak, 1957). For this reason in many cases the AMS data from sedimentary rocks and their relative magnetic fabric have been interpreted as associated to sedimentary processes, with the typical fabric configuration: the magnetic foliation parallel to the bedding plane and the magnetic lineation oriented parallel or orthogonal to the flow direction (Ellwood, 1980; Hamilton and Rees, 1970; Kissel et al., 1998).

Nevertheless, the AMS studies were related to the layer-parallel shortening (LPS) structures since the paper of Graham (1966), who described as the magnetic fabric could also reflect the tectonic evolution of softly deformed sediments (Kissel et al., 1986). Starting from these pioneering studies, several authors have been focused on this interaction and applying AMS technique in sedimentary rocks for kinematic analysis of fold-and-thrust belts, observing in many sedimentary

units a strict relationship between the evolution of magnetic fabric and the deformation history of rocks. If we consider an undeformed sediment, the magnetic foliation will be generally parallel to the bedding plane, defining the typical magnetic fabric attributed to depositional and/or compaction processes (Lee et al., 1990; Lowrie and Hirt, 1987; Paterson et al., 1995). The progressive tectonic deformation that this sediment can undergo, for example a horizontal shortening, would involve the developing of a tectonic AMS sub-fabric, which gradually modifies the original sedimentary magnetic fabric.

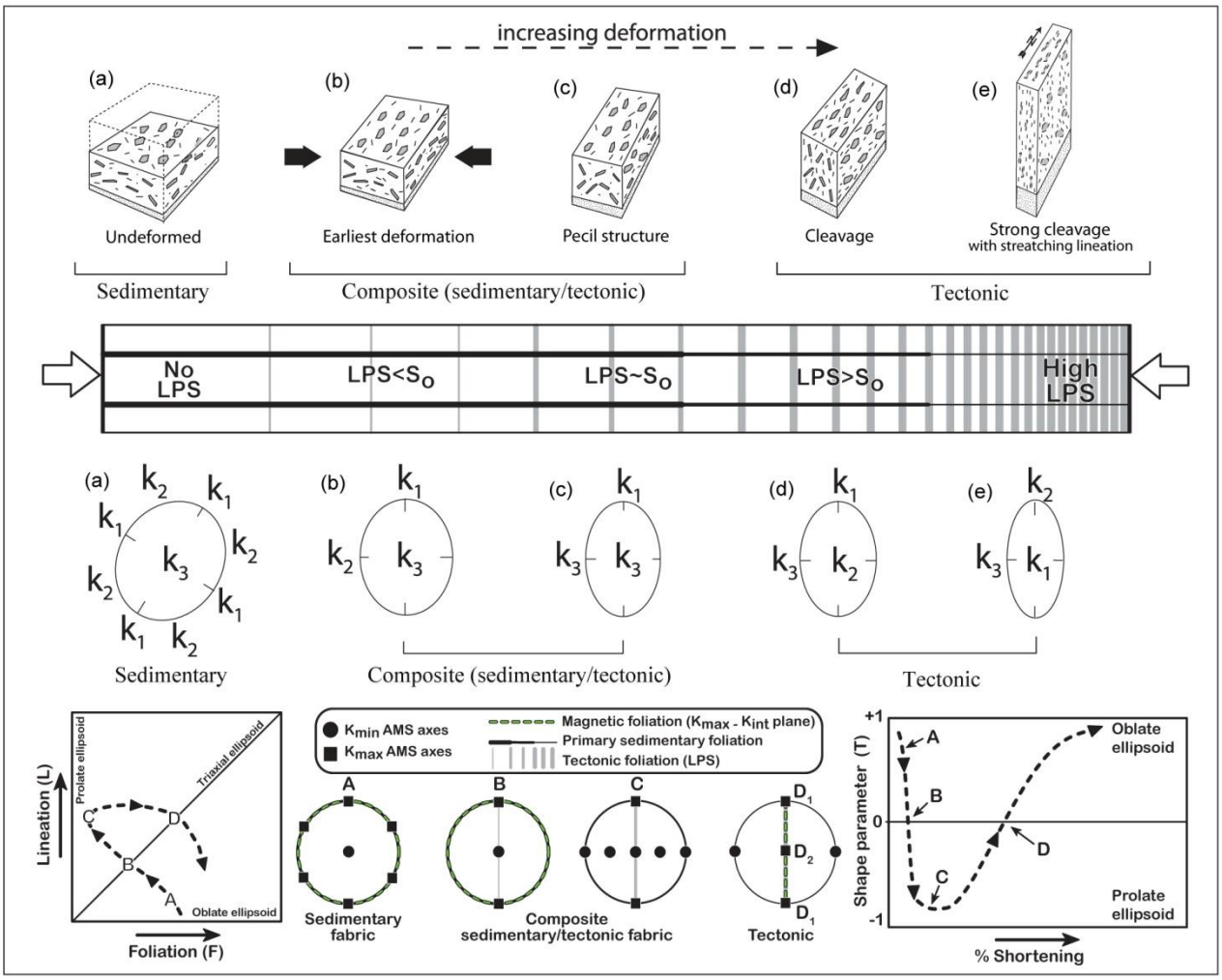

Fig.7.1. *Conceptual model for evolution of AMS fabrics in weakly to strongly deformed sedimentary rocks in fold-thrust belts. In the upper part are represent the evolution of the directional and shape characteristics of AMS and strain ellipsoids during progressive deformation (panels a–e; modified after Cifelli et al., 2013). In the lower part are represent the equal-area lower hemisphere projections, which show idealized changes in AMS ellipsoid directions (relative to horizontal bedding) from a dominant bed-parallel sedimentary fabric (stage A), to mixed layer-parallel shortening (LPS) and sedimentary fabrics (weak LPS in stage B and moderate LPS in stage C), to strong tectonic fabric (stage D, with K_{max} either parallel to structural trend, D_1, or down the dip of cleavage, D_2). Changes in lineation ($L = K_{max}/K_{int}$) and foliation ($F = K_{int}/K_{min}$) strength, and in ellipsoid shape parameter (T, which varies from +1 to −1 for oblate to prolate ellipsoids) also indicated. S_o—bedding fabric (modified after Weil and Yonkee, 2009).*

7.1.1 Paleocurrent processes

Through AMS analysis it is possible to establish the sedimentary or tectonic origin of the magnetic lineation; in fact the orientation of K_1 axis represent a good target for this interpretation. The purpose of our investigations was to define whether the fabric has maintained a primary sedimentary configuration or whether subsequent tectonic deformations have modified the magnetic fabric of the rocks.

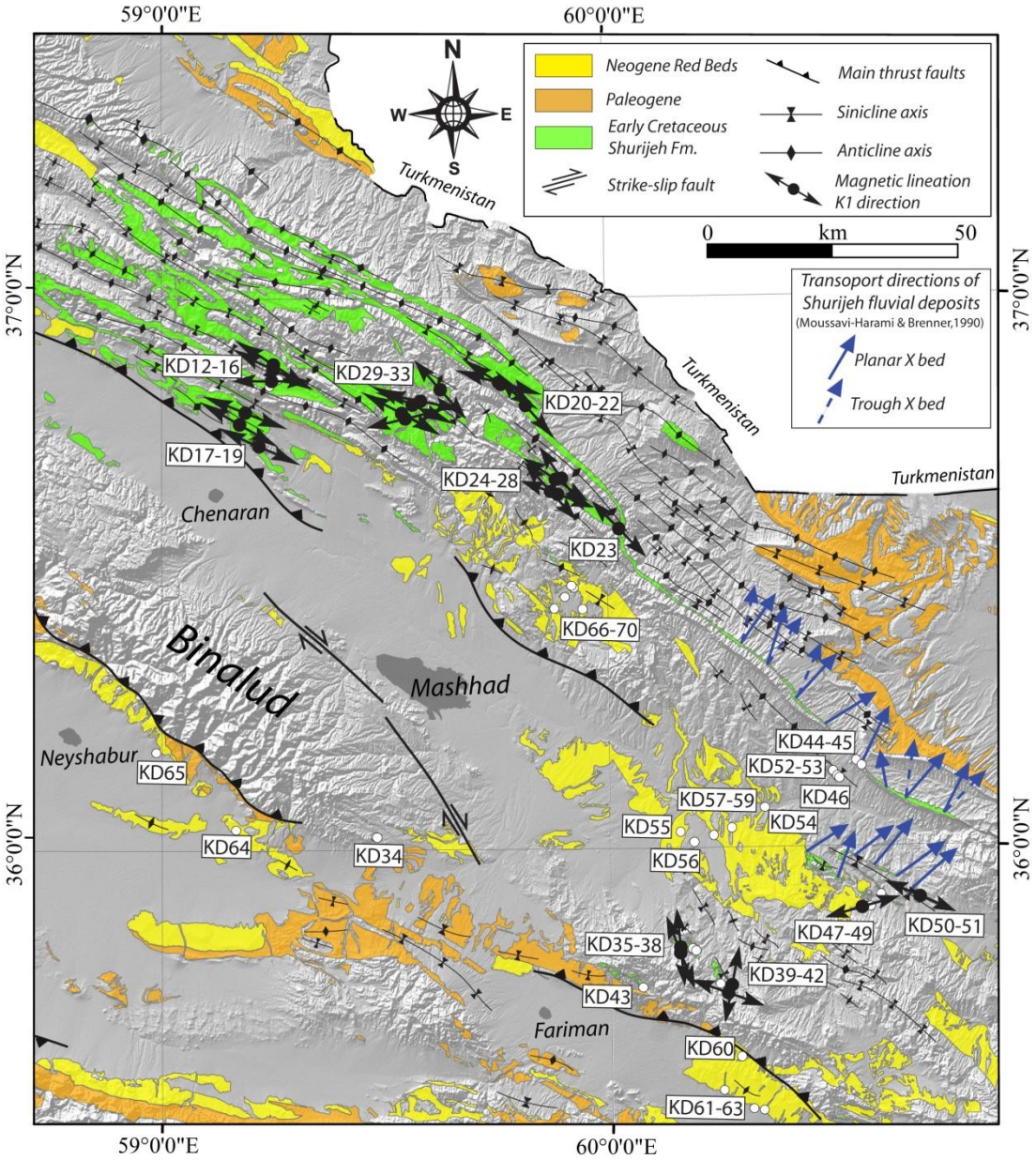

Fig.7.2 *Extract of the simplified geological map of the eastern sector of study area. In the map together with the in situ magnetic lineations are plotted the transport directions (blue arrows) of Shurijeh Fm. fluvial deposits as described by Moussavi-Harami and Brenner (1990).*

As we know, the AMS allows to investigate the alignment of magnetic grains achieved in the final stages of sediment transport, with the maximum susceptibility axis, K_1, and the minimum susceptibility axis, K_3, approximating the preferred orientation of the longest and shortest

magnetic grain axes, respectively (e.g., Jaco H Baas et al., 2007; Borradaile et al., 1999; Felletti et al., 2016; Hamilton and Rees, 1970; Taira and Scholle, 1979; Tarling and Hrouda, 1993).

Naturally, these grains should be proven to be primary (syn-sedimentary) in origin rather than secondary (diagenetic).

When currents are present, hydraulic forces control grains alignment during their deposition (current-induced fabric; Shor et al., 1984). The long shape axis of elongated paramagnetic grains, as well as of large ferromagnetic grains, lines up either parallel or perpendicular to the current direction in case of moderate (<1.2 m/s) or high (>1.2 m/s) hydrodynamic regimes, respectively (Allen, 1984). The magnetic fabric reflects this configuration and consequently, a sedimentary magnetic lineation can develop as revealed by a clustering of the K_1 axes either parallel or perpendicular to the current direction depending on the hydrodynamic boundary conditions.

Considering the studies dealing with magnetic fabrics in deformed rocks (e.g., Borradaile and Tarling, 1984, 1981; Mattei et al., 1995; Parés and Dinarés-Turell, 1993; Sagnotti and Speranza, 1993), as described by Felletti et al. (2016), there seems to be a general agreement about that the first effect of layer-parallel shortening is to group the K_1 axes perpendicular to the shortening direction whereas the K_3 axes tend to remain perpendicular to the bedding plane; with further shortening, the K_3 axes progressively rotate into the tectonic shortening direction, and the magnetic foliation becomes parallel to the flattening plane and mesoscopic cleavage [the sedimentary-to-tectonic fabric progression are provided, for example, by Averbuch et al., (1992), Housen et al., (1995) and Pares et al., (1999)].

Take into account the paleocurrent analysis of cross-bedded Neocomian Shurijeh sandstone units, realized by Moussavi-Harami and Brenner (1990), we known that the fluvial system flowed across the study area (at least for the eastern sector) from the south and southwest (as showed in Fig.7.2). From these observations appears clearly how the fluvial deposits of Shurijeh formation were sourced by the Triassic volcanic units which are exposed in the southern and south-eastern part of Mashhad. As illustrated in Fig.7.2 the transport direction, NE-SW oriented, diverge completely respect to the magnetic lineation detected; in fact as already described, the magnetic fabric configuration outline a perfect adherence with the main structural features observed in the region. In other words, we could consider the AMS fabric of the Early Cretaceous studied samples as induced essentially by tectonic processes, rather than sedimentary (primary) processes, essentially because a strong correlation was observed between the main regional structural features (fold axis, thrusts) and associated AMS fabrics.

7.1.2 Tectonic processes

As already said, the AMS analyses allow to identify the origin of the magnetic fabric of a rock; excluding the sedimentary origin, as just described, the "tectonic hypothesis" appears as the most probable, being in a fold and thrust belt context.

In this work the structural trend of the sampling sites has been evaluated using the orientation of the magnetic lineation defined as the axis of maximum magnetic susceptibility K_1 determined by mean of Anisotropy of Magnetic Susceptibility (AMS) analyses. AMS data have been often used in association with paleomagnetic analyses to investigate the origin of curved orogens (e.g. Weil and Yonkee, 2012). In curved fold and thrust belts the orientation of the magnetic lineation often follows the curvature of the orogen, being therefore representative of its structural trend (Kissel and Laj, 1988; Pares et al., 1999; Sagnotti et al., 1998; Weil and Yonkee, 2009).

With a low to moderate deformation, the principal maximum axis K_1 (magnetic lineation) marks the intersection between LPS and bedding fabrics, placing perpendicular to the shortening direction and aligning sub-parallel to the regional structural trend (Cifelli et al., 2009; Kissel et al., 1986; Mattei et al., 1997; Oliva-Urcia et al., 2009; Parés and Van Der Pluijm, 2002; Sagnotti et al., 1998). This fabric configuration require that K_3 remains perpendicular to the bedding plane, signing the persistence of the primary magnetic fabric. The progressive increase of shortening involves the distribution of K_3 along a girdle parallel to the tectonic shortening direction, with the magnetic ellipsoid that becomes prolate (Kligfield et al., 1983, 1981; Parés and Van Der Pluijm, 2002). As showed by several Authors (Debacker et al., 2009; Hirt et al., 1995; Housen and Pluijm, 1991; Lowrie and Hirt, 1987; Lüneburg et al., 1999) when the evolution of tectonic setting corresponds to an additional shortening, the magnetic fabric's response coincides with the return of the ellipsoid to the flattening field, where the magnetic foliation lies parallel to the flattening plane and to the mesoscopic cleavage, while the magnetic lineation becomes parallel to the stretching direction, developing a purely tectonic magnetic fabric.

The AMS analysis on the Shurijeh Formation has demonstrated the existence at least of three magnetic fabric type, indicating different stage of deformation which affected the Shurijeh red beds deposits. In some sampling sites the magnetic fabric of Shurijeh red beds is still affected by the influence of the original sedimentary fabric, with the magnetic lineation dispersed within the bedding plane (Fig. 5.6 Type1). This kind of ellipsoid configuration characterized few sites, in particular KD14 and KD29 (Table 1), which showing a sedimentary magnetic fabric without a specific geographic distribution. The ellipsoid configuration typical of a composite contribution from sedimentary and tectonic magnetic fabric is the most common among those analyzed; as shown in Fig. 5.3a-b the clusterized distribution of the maximum and intermediate axes (K_1, K_2)

interest most of the Shurijeh Formation sites located in the western and central sectors of the study area (Fig. 5.13-5.14), with K_1 axis clusterized and roughly parallel to the main structural trend.
This configuration together with the diffuse oblate fabrics in almost all sites in the western and central sectors, suggests that magnetic fabric in the Shurijeh Formation represents an intermediate stage between a purely sedimentary and a purely tectonic fabric (Fig. 5.1b and 5.1c; Aubourg et al., 2010; Borradaile and Tarling, 1981; Housen and Pluijm, 1991; Kligfield et al., 1981; Luo et al., 2009; Parés and Van Der Pluijm, 2002; Pares et al., 1999; Richter et al., 1993). In this stage, the orientation of the magnetic fabric is partially controlled by the original sedimentary planar fabric with the bedding planes still recording a preferred orientation of mineral grains. Therefore, in the western and central outcrops of Shurijeh Formation sites, I observe the prevalence of the original sedimentary fabric with the overprinting of a tectonic subfabric. In general, it can be affirm that the parallelism between regional tectonic structures and the orientation of magnetic lineation represents the main features at the regional scale. With the mean value of ~305°N, in the western sector the magnetic lineation (K_1) of the Shurijeh sites is constantly oriented WNW-ESE, which is parallel to the main structural elements of the area (Fig.7.2a). Similar orientation of magnetic lineation was found in the central sector of study area with a ~297°N direction, very consistent with the general structural trend of this portion of the Kopeh Dagh range.
Focusing on the locale scale it's possible to find some deviation of the structural trend at the sampled site from the regional one (e.g. at sites KD12-16 and KD29-33): in these cases the magnetic lineation is also turned and oriented parallel to the local structures demonstrating the good ‘answer’ of magnetic fabric configuration with the structural setting of each sampling site (Kissel and Laj, 1988; Pares et al., 1999; Sagnotti et al., 1998; Weil and Yonkee, 2009).
Moving in the eastern sector, the other Shurijeh sampling sites (from KD35 to KD51 as show in Fig.5.15) come from five different isolated structures, excepted for KD44 and KD45 sites, located along the main Kopeh-Dagh range. Most of the ellipsoids shape (11 of 16 sites as show in Fig.5.4), resulting from AMS analysis, is classified as part of a third magnetic fabric type (Fig. 5.6 Type 3). In this stage, the orientation of the magnetic fabric is mostly controlled by cleavage, with the magnetic foliation plane that results almost orthogonal to the bedding plane. The orientation of the magnetic lineation tracks, in some sites (Fig.5.4), the intersection between cleavage and bedding, suggesting a partial influence of original bedding on the orientation of the magnetic fabric. That configuration, confirmed by the moderately prolate fabrics detected in some sites (KD36 and KD50), suggests as in this sector of the Kopeh Dagh belt the magnetic fabric for the Shurijeh Formation change its shape, loose partially the original sedimentary planar fabric and acquiring a purely tectonic fabric (Fig.5.1 c and d).

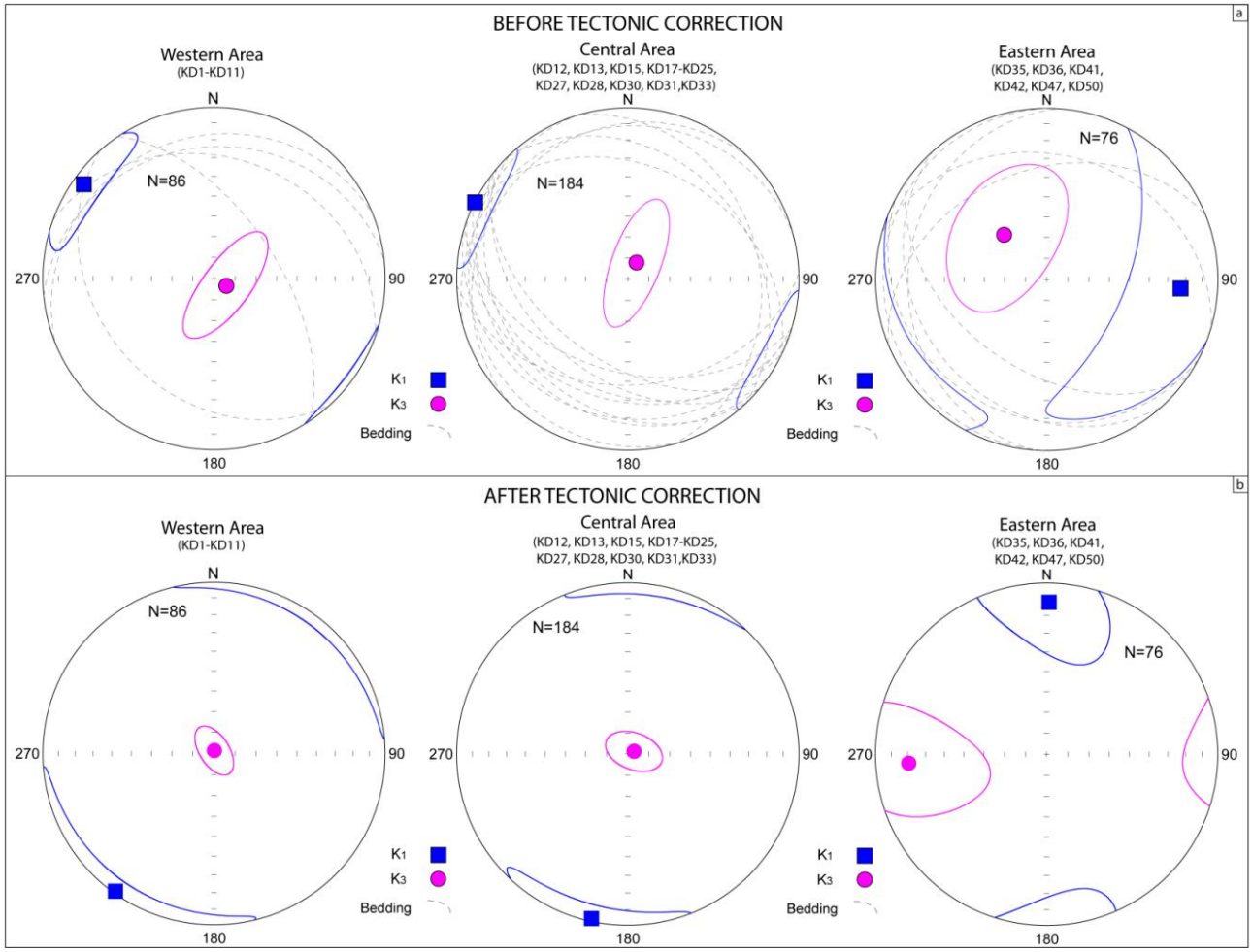

Fig.7.3. *Mean direction of magnetic foliation and magnetic lineation computed for all Shurijeh Fm. sites from the three main sampling areas, compared with bedding directions; a) before and b) after tectonic correction.*

Taking together all the Cretaceous sites according with their position along the range (Fig 7.3a), I observe that in the western and central sector the magnetic foliation is distributed in a girdle with a SW-NE orientation (the mean direction of the K_3 calculated from the western sites is N120,83, and e_{1-2} = 25.7, while in the central sector is N27,86 and e_{1-2} = 24.6). Excluding the sites with a high e_{1-2} value found in the central sector (KD14, KD16, KD26, KD29 and KD32, as show in Tab.5.1), the ellipsoid change little its configuration. In fact in Fig.7.3a, is presented the corrected version, which outlined clearly the perfect concordance between the western and central sector (the mean direction of the K_3 calculated from the western sites is N120,83, and e_{1-2} = 25.7, while in the central sector is N28,81 and e_{1-2} = 23). Appling to the ellipsoids of western and central area (as show in Fig.7.3b) the tectonic correction, a coherent sedimentary configuration is obteined, with the K3 axis located orthogonal to the bedding and foliation plane. This representation (Fig.7.3) confirm the sedimentary origin of magnetic fabric of Shurijeh Fm. in the two first areas (western and central), showing how the recent fold-and-thrust belt deformation had overprint the primary sedimentary magnetic fabric. In fact plotting the results in geographic coordinates the mean values

of magnetic lineation lie on the intersection of the bedding planes, aligned parallel to the fold axes (Fig.7.3a); that demonstrate clearly the existence of a composite sedimentary/tectonic fabric which affect most of the Shurijeh sites sampled in the western and central part of the study area.

The projection of all Cretaceous sites carried out in the eastern sector of study area, shows that the magnetic foliation is distributed in a girdle with a SW-NE orientation (mean direction of the K_3 calculated for all eastern sites is N315,69, and e_{1-2} = 63.4; Fig.7.3a). In this sector the orientation of magnetic lineation diverge from the regional orientation with a mean value of ~94°N.

That mean configuration are affected by an high e_{1-2} value, which invalidate the meaning of the data. If we take into account only the results that present an admissible value of e_{1-2} (<45), the remaining (KD35, KD36, KD41, KD42, KD47 and KD50) show a coherent configuration with the other investigated areas (mean direction of the K_3 calculated for all eastern sites is N316,60, and e_{1-2} = 70; Fig.7.3a).

The eastern sector AMS results for Early Cretaceous Shurijeh Fm. present a different configuration respect to the other sampling area and only from six sites suitable ellipsoids have been obtained with admissible value of e_{1-2} (<45).

This poor reliability of the data could derive from different factors:

a. as identify during the sampling and cutting of the samples of Shurijeh Fm., in the eastern sector the sampled deposits are generally characterized by more coarse sandstones. As illustrated by Moussavi-Harami & Brenner (1990), the fluvial deposits of Shurijeh Fm. consist of three main intervals, relatively coarse-grained the lower and middle parts, finer-grained the upper part. Predominating in the eastern sector those with a medium to coarse grain, this has determined the poor reliability of AMS results;
b. another aspect regards the deformation rate which interests this portion of the range. It's possible to consider the eastern part of Kopeh Dagh range as the ending of the entire fold and thrust belt; here the convergence of Arabian Plate against the Eurasian Plate is bordered on the eastern margin by the Afghan Block. In this particular tectonic setting the deformation rate may be less constant and homogeneous in its action during the time rather than in the central part of the range (western and central areas), where from Cretaceous to Neogene the Arabia-Eurasia convergence acted constantly.

At the regional scale, it can be affirm that in the central part of Kopeh Dagh range as well as in the eastern part of Eastern Alborz Mountains, the mean magnetic fabric configuration of Shurijeh Fm. shows a composite contribution from sedimentary and tectonic processes (Fig. 7.1), with the magnetic foliation and lineation oriented parallel to the fold axes, as resulting by the bedding attitude distribution. Tectonic deformation overprints the primary sedimentary configuration in

almost all sites, but restoring the horizontal bedding for each sampled deposits (tectonic correction) a general sedimentary configuration of magnetic fabric have been obtained, as showed in Fig.7.3b.

Focusing on the Neogene sampled deposits the AMS analysis indicate, at the regional scale, the good agreement between the orientations of magnetic lineation resulting from Upper Red Formation and Shurijeh Formation in the western and central sector (Fig. 5.13-5.14). Both Cretaceous and Neogene mean magnetic lineations show a shortening direction NE-SW oriented. The parallelism to the regional structural trend (NNW-SSE) characterises most of the Neogene sites.

In the eastern sector of the study area, the Neogene magnetic fabric shows a magnetic lineation parallel to the structural trend (Fig. 5.15) in almost all sites. The very good agreement of the Neogene mean magnetic lineation along the range suggest the prevalence of a homogeneous orientation of tectonic shortening, after the deposition of the Neogene Upper Red Formation deposits.

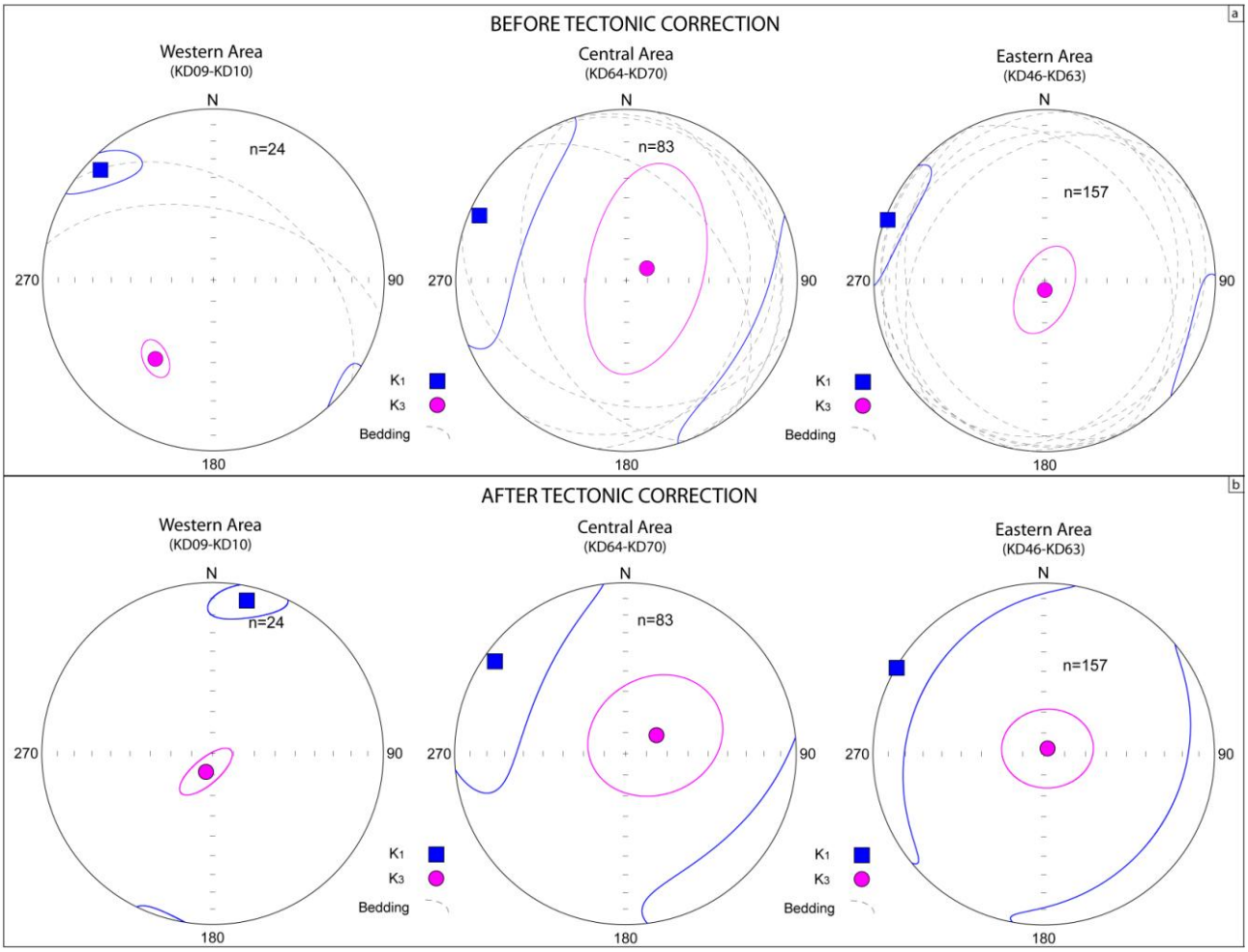

Fig.7.4. *Mean direction of magnetic foliation and magnetic lineation computed for all URF sites compared with bedding directions; a) before and b) after tectonic correction.*

Taking together all the Neogene sites according with their position along the range (Fig 7.4), it has been observed that in the western sector, the mean direction of the K_3 calculated from the only two western sites (KD09 and KD10) is N216,42, and e_{1-2} = 22.2, while in the central sector the magnetic foliation is distributed in a girdle with a SSW-NNE orientation (the mean direction of the K_3 calculated from the central sites is N59,79, and e_{1-2} = 49). The projection of all Neogene sites carried out in the eastern sector of study area, shows a mean direction of the K_3 calculated for all eastern sites is N180, 85, and e_{1-2} = 24 (Fig.7.4a). As made for the Shurijeh mean projection (Fig.7.3), the tectonic correction for each of three sampling areas was applied (as show in Fig.7.4b), obtaining the projection of AMS direction with horizontal bedding. A coherent sedimentary configuration has been acquired, with the K_3 axes located orthogonal to the bedding and foliation plane. This representation (Fig.7.4) confirms the sedimentary origin of magnetic fabric of Neogene URF in all of three areas, showing how the recent fold-and-thrust belt deformation had overprint the primary sedimentary magnetic fabric.

All these observations give strong evidence that the formation of the magnetic fabric has been mainly driven by tectonic processes. The concordance between the magnetic fabric of Neogene deposits and the structural trend of Kopeh Dagh range along all the study area demonstrate how the LPS has been interested by composite contribution of sedimentary and tectonic processes. The western and central sector are characterized by a composite contribution with a predominance of tectonic process (Fig.5.1 c-d), as indicate both by the Cretaceous and Neogene magnetic fabric (Fig.7.3-7.4); the good agreement between the Early Cretaceous and Neogene ellipsoid configurations suggests the dominance of the same shortening direction, which could constantly act on the area from the Cretaceous to the Neogene

In the eastern sector the Cretaceous magnetic fabric (Fig.7.3) shows a different AMS direction respect to the other areas and to the regional trend; in this sector of the range it was revealed that the foliation plane is not parallel to the bedding plane. This difference from the general orientation of Shurijeh fabric along the range can be interpreted as the result of a greater granulometry of the sampled deposits, together with a strongly tectonic stress which interested this portion of the belt before the Neogene; in fact the URF deposits sampled in this area, show a better concordance of magnetic direction with the regional tectonic structure, probably due to a more homogeneous distribution of deformation during the Neogene.

The general concordance between the Early Cretaceous and Neogene AMS ellipsoid configurations along all the Kopeh Dagh range, object of this study, indicate the dominance of the NNE-SSW shortening stress direction which affected this region since starting from the early-to-

middle Oligocene (Berberian and King, 1981; Robert et al., 2014) after the deposition of the terrestrial continental red beds (URF) during Neogene (34-20 Ma).

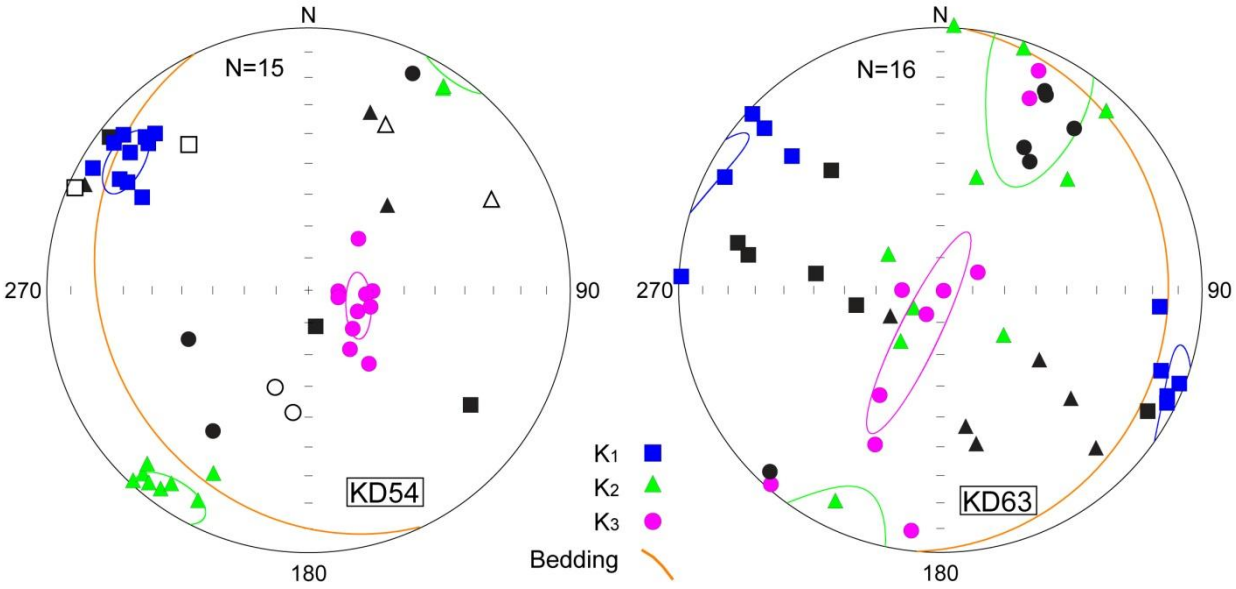

Fig.7.5. *AMS plots of URF Fm. KD54 and KD63 sites. Data are plotted on lower hemisphere, equal-area projections, in geographic coordinates. Coloured squares and circles represent maximum and minimum axes of the outcrops samples, while the black symbols represent maximum and minimum axes of marly clasts. Bedding planes are also represented by the yellow line*

During the sampling of Neogene outcrops, in two sites some samples were carried out in marly clasts incorporated in conglomerate beds, alternating to fine grained marls . These Neogene conglomerates allowed the demonstration of primary origin or not of the ChRM component identified for these rocks, through the so called *Conglomerate Test*. If this characterization works for paleomagnetic studies, its application for AMS analysis is just as interesting.

As show at Fig.7.5 the shape ellipsoid of KD54 and KD63 indicates a magnetic fabric developed with the composite contribution of sedimentary and tectonic processes (Fig.5.1 b-c).

The foliation plane results to be parallel to the bedding plane in each sites (KD54 and KD63) while shows a different orientation in the clastic samples both in KD54 and KD63. This first aspect testify the different sedimentary origin of the marly clasts respect to the outcrop in which it is embedded.

Conversely for the magnetic lineation which result to have the same orientation in the outcrop samples as well as in the clast samples in each analyzed sites. Considering the magnetic foliation as a magnetic parameter directly correlated to the primary sedimentary fabric, the discordance between the "matrix" or outcrop samples and the clast samples as well as the concordance of all magnetic lineation values, demonstrate how the Neogene conglomeratic deposits acquired a

homogenous magnetic lineation after the deposition of conglomerate. This could be the useful target which allows to affirm how the tectonic stress had acted mainly after the deposition of Upper Red Formation during the Neogene. If this hypothesis were true, would mean that the deformation able to re-orient the magnetic fabric in most of the analyzed Cretaceous and Neogene deposits, has acted very recently, overprinting on the sedimentary magnetic fabric.
Generally it can be said that the regional shortening active in this area since from the early-to-middle Oligocene (Berberian and King, 1981; Robert et al., 2014), related to the Arabia-Eurasia collision, modified the magnetic fabric of these deposits without a drastic reorganization of the rocks which maintained partially the original sedimentary planar fabric. Only in the eastern sector the Shurijeh fluvial deposits show a strongly tectonic configuration of AMS ellipsoids due to the coarse granulometry which affect these deposits.

7.2 Paleomagnetic constraints to geodynamic evolution of North Iran

7.2.1 Previous paleomagnetic data in north-eastern Iran and Kopeh Dagh range

As described at the beginning of this thesis, my research project has been focused on the north-eastern sector of Iranian region, trying to answer some pending questions about the relationship of northern margin of Iranian blocks with the Turan and Southern Caspian blocks.
The data collected for this project were integrated with the previous paleomagnetic results from north-eastern Iran and Kopeh-Dagh mountain belt, which are very sparse and limited to data published by Bazhenov (1987) in the Turkmenistan portion of Kopeh-Dagh and in the Rivand and Samghan folds, south of the Allah Dagh range by Mattei et al. (2017).
Paleomagnetic data by Bazhenov (1987), comprised approximately between longitude 37°E and 39°E (Fig. 7.6), are collected from Lower Cretaceous to Paleocene units in the north-western part of the Kopeh-Dagh Mts. (Turkmenistan). In that study, were presented the results of thermal demagnetization, which were interpreted using paleomagnetic directions after the final heating or using great circle intersection technique.

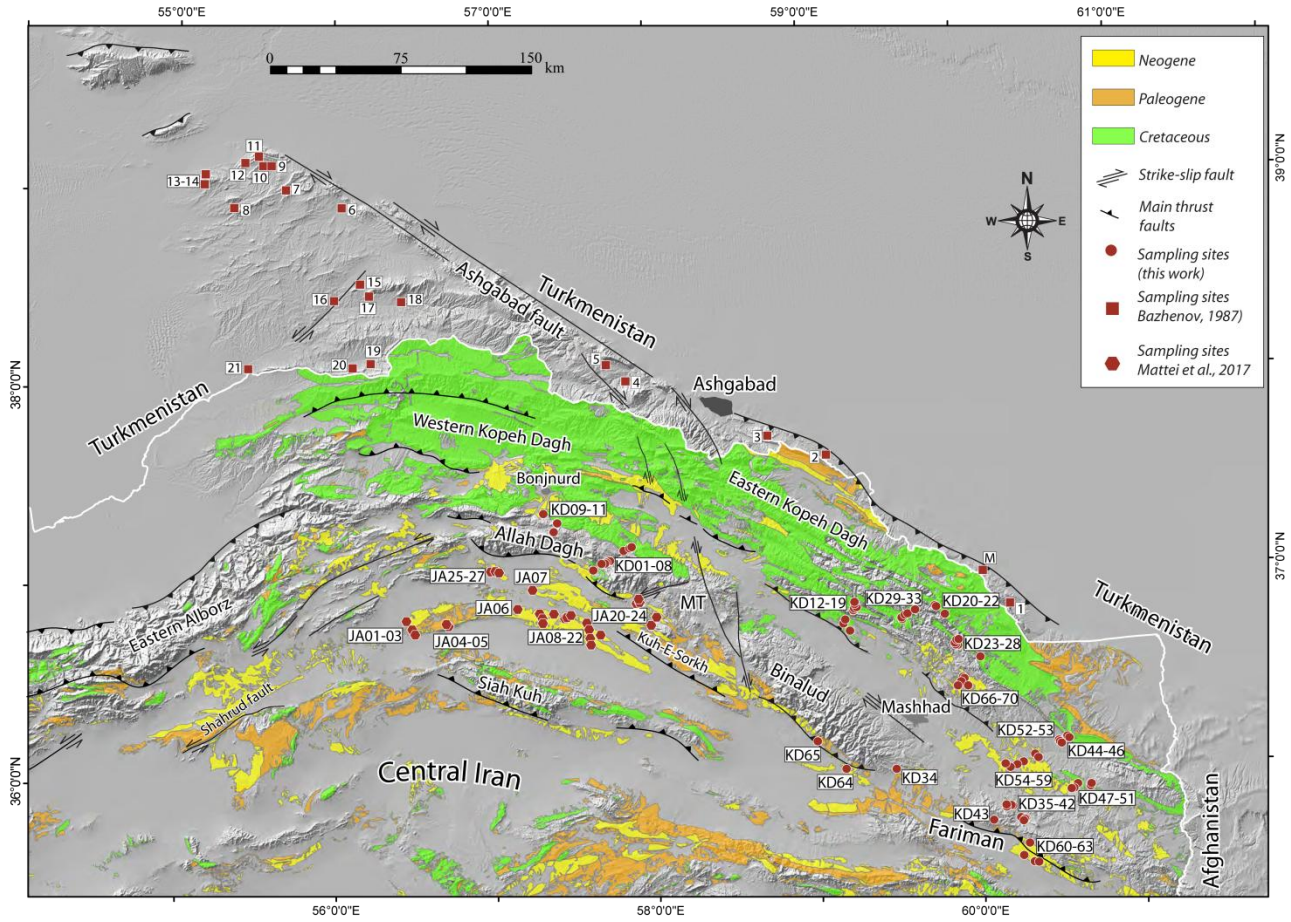

Fig. 7.6 *Main outcrops of Shurijeh Fm. and Neogene sediments of the URF and location of paleomagnetic sampling sites (KD). Numbers are referred to sampling by Bazhenov, 1987, whereas JA sites are from the work by Mattei et al., 2017.*

This method of investigation is now outdated, but nevertheless some directions of the site can be accepted, which appear suitable for tectonic reconstruction, having positive reversal and fold tests. Bazhenov (1987) collected 600 samples in 21 sites, sixteen of them yielding only linear directions, 6 from Cretaceous (Aptian- Cenomanian) units, and 10 from Late Cretaceous-Paleocene deposits (Table 7.1, Fig.7.6).

The mean direction for the six Aptian-Cenomanian sites is declination Dec. = 21.0°, inclination (Inc.) = 54.5°, k = 138.6, α_{95} = 5.7°, whereas the mean direction for the ten Late Cretaceous-Paleocene sites is declination (Dec.) = 22.5°, inclination (Inc.) = 46.4°, k = 37.6, α_{95} = 8.0° (Table 7.1). In order to calculate paleomagnetic rotations, the Aptian-Cenomanian and Late Cretaceous-Paleocene sites have been compared with the 100 Ma (λ (°N) = -80.8°; ϕ (E) = 332.3°; α_{95} = 3.3°) and 70 Ma (λ (°N) = -79.2°; ϕ (E) = 355.7°; α_{95} = 2.5°) Eurasian reference poles, respectively (Torsvik et al., 2012).

Table 7.1. Paleomagnetic directions from the Turkmen Kopeh Dagh

Location					ATC				Tectonic Rotations	
Site	**Lat (°N)**	**Lon(°E)**	**Fm**	**N/n**	**D°**	**I°**	**K**	**α_{95}**	**R (°) ± Err (°)**	**R (°) ± Err (°)**
3	7°04'28.30"	57°37'14.30"	Al-C	15/12	6	54	38	7.1	-5.4±10.0	2.0±6.1
6	37°06'46.00"	57°42'19.90"	Ap-C	19/15	19	57	33	6.8	7.6±10.3	-0.1±5.8
13	37°07'12.80"	57°43'34.30"	Al-C	9/6	34	60	42	8.1	22.6±13.2	-3.9±6.8
14	37°10'16.90"	57°48'51.10"	Al-C	13/10	30	54	24	9.1	18.6±12.6	2.0±7.5
19	37°10'58.10"	57°51'18.90"	Al-C	24/15	18	51	29	6.7	6.6±8.9	5.0±5.8
21	37°11'21.30"	57°51'56.10"	Al-C	18/14	21	49	24	7.7	9.6±9.7	7.0±6.5
Mean			**CRE**	**6**	**21.0**	**54.5**	**138.6**	**5.7**	**9.6±8.3**	**1.5±5.1**
M	37°16'22.00"	57°22'22.10"	Tp	23/20	10	41	7	12.0	-1.2±12.7	10.6±9.6
1	36°07'46.81"	60°30'34.67"	M-Tp	40/26	16	46	14	7.4	4.8±8.6	5.6±6.1
3	36°07'59.66"	60°30'18.79"	St-Tp	13/8	18	43	12	14.4	6.8±15.6	8.6±11.4
6	36°08'33.47"	60°29'44.23"	T-Tp	43/36	10	45	13	6.5	-1.2±7.5	6.6±5.4
9	36°03'36.11"	60°21'41.40"	Cn-Tp	39/31	8	45	23	5.2	-3.2±6.2	6.6±4.6
10	36°00'59.04"	60°11'12.70"	Cn-Tp	46/35	8	47	20	5.4	-3.2±6.6	4.6±4.7
11	36°01'43.86"	60°13'47.42"	Cn-Tp	38/26	15	45	29	5.1	3.8±6.1	6.6±4.5
15	36°02'31.52"	60°16'13.58"	Cp-Tp	18/11	36	41	61	5.2	24.8±5.8	10.6±4.5
16	36°04'38.32"	60°20'36.10"	Cp-Tp	20/14	57	51	43	5.7	45.8±7.4	0.6±4.9
17	35°37'49.37"	60°17'08.77"	Cn-M	17/15	54	46	54	5.2	42.8±6.2	5.6±4.6
Mean			**C-T**	**10**	**22.5**	**46.4**	**37.6**	**8.0**	**11.3±9.4**	**5.2±6.6**

Notes and abbreviations: Fm = Geological Formation; N/n number of demagnetized samples/ number of stable directions at a site; D, I are site-mean declinations and inclinations calculated after tectonic correction; K = precision parameter; α95 = confident limit (statistical parameters after Fisher, 1953); R = rotation and relative error; F = flattening and relative error; Al = Albian; Ap = Aptian; C = Cenomanian; T= Turonian; St = Santonian; Cn = Coniacian;, Cp = Campanian; M = Maastrichtian; Tp = Paleocene; CRE = Cretaceous; C-T = Cretaceous-Tertiary.

Paleomagnetic results from Mattei et al. (2017) are from Middle-Late Miocene URF from the Rivand and Samghan fold structures, located to the southwest of Allah Dagh mountain chain. Here 27 sites have been sampled between ~56°30′E and ~58°E in marls and siltstones of the URF (25 sites) and in Eocene marls and siltstone (2 sites) (Fig.7.6). The sampling sites are distributed in different parallel tectonic structures, among them the Samghan structure is a 100 km-long E–W curved Neogene fold. Here the uplift has been produced by the activity of the north dipping Samghan thrust fault, which borders the structural relief to the south, and is also responsible of the emplacement of small slices of Pre-Cambrian units representing the only pre-Cenozoic units outcropping in the area (Hollingsworth et al., 2010; Mattei et al., 2017). The results from this work show positive fold and reversal test with a mean regional direction (Dec.) = 21.5°, (Inc.) = 43.9°, k= 24.7, α_{95} = 6.9° that, when compared to the 10 Ma reference pole, indicates a CW rotation R = 17.4° ± 7.7° (see Table 1 in Mattei et al., 2017 for further details).

7.2.2 Age and distribution of vertical axis rotations in Kopeh-Dagh, Allah Dagh and Binalud-Fariman mountain belts

Paleomagnetic results from the study areas placed in the Kopeh Dagh, Allah Dagh and Binalud-Fariman mountains (Fig.7.9) demonstrate that north-eastern Iran underwent CW vertical axis rotations. The same directions are, in fact, observed in the Shurijeh Fm. sites from Allah Dagh (D= 33.3°; I=47.0°; k=17.6; α_{95}=14.8°) (Tab.7.2, red part), Kopeh-Dagh (D= 31.2°; I=49.3°; k=44.97; α_{95}=4.5°) (Tab.7.2, blue part) and Fariman (D= 27.2°; I=51.7°; k=53.1; α_{95}=5.7°) (Tab.7.2, green part) suggesting that these structures underwent a similar rotational history.

Table 7.2. Paleomagnetic directions from the Shurijeh Formation

Location						BTC				ATC				Tectonic Rotations	
Site	Lat (°N)	Lon(°E)	Fm	N/n	S0	D°	I°	K	α_{95}	D°	I°	K	α_{95}	R(°)±Er(°)	F(°)±Er(°)
KD01	37°04'28"	57°37'14"	SHU	9/8	354,24	15.1	34.9	45.3	8.3	11.6	12.2	35	11.5	0.3±9.7	42.9±9.3
KD02	37°06'46"	57°42'20"	SHU	12/12	56,60	247.6	67.6	134.2	3.8	48.9	51.8	133.4	3.8	37.6±5.7	3.3±3.9
KD03	37°07'13"	57°43'34"	SHU	11/11	228,32	42.5	32.3	77.4	5.2	37.3	64.1	77.4	5.2	26.0±9.9	-8.9±4.8
KD06	37°10'17"	57°48'51"	SHU	11/11	338,18	53.8	54.9	48.4	6.6	33.3	47.2	48.4	6.6	22.0±8.2	7.9±5.7
KD07	37°10'58"	57°51'19"	SHU	15/13	0,0	27.5	57.9	11.6	12.7	27.5	57.9	11.6	12.7	16.2±19.3	-2.7±10.2
KD08	37°11'21"	57°51'56"	SHU	12/12	0,0	34.9	51.4	36.3	7.3	34.9	51.4	36.3	7.3	23.6±9.6	3.7±6.2
KD11	37°19'00"	57°23'57"	SHU	11/11	20,30	74	61.9	49.9	6.2	49.2	38.7	49.9	6.2	37.9±7.0	16.4±5.5
Mean			**SHU**	**7**		**35.6**	**58**	**8.8**	**21.5**	**33.3**	**47**	**17.6**	**14.8**		
KD12	36°52'04"	59°15'20"	SHU	14/14	226,26	24.9	39.8	108.6	3.8	8.7	62.9	108.6	3.8	-2.6±7.4	-7.9±3.9
KD13	36°52'14"	59°15'20"	SHU	11/11	220,21	26	29.8	158.6	3.6	20.9	50	158.6	3.6	9.6±5.3	4.9±3.8
KD14	36°51'13"	59°16'00"	SHU	11/10	252,8	23.3	44.4	28.3	9.2	25.5	52.2	28.3	9.2	14.2±12.2	2.7±7.6
KD15	36°50'56"	59°15'07"	SHU	8/7	29,28	21.3	45.8	37.7	10	14.1	50.5	37.7	10.0	2.8±12.7	4.4±8.2
KD16	36°50'28"	59°14'50"	SHU	12/12	14,50	144.8	80.5	57	5.8	24.3	45.8	57	5.8	13.0±7.2	9.1±5.1
KD17	36°44'08"	59°13'14"	SHU	10/8	344,12	25.8	51.6	113.2	5.2	17.9	42.1	113.2	5.2	6.6±6.3	12.8±4.8
KD18	36°46'27"	59°10'51"	SHU	14/10	196,20	23.6	29.9	67.3	5.9	26.2	49.7	67.3	5.9	14.9±7.8	5.2±5.3
KD19	36°47'36"	59°11'31"	SHU	11/9	46,28	3.3	69	63.7	6.5	26.1	44.5	63.7	6.5	14.8±7.8	10.4±5.6
KD20	36°48'10"	59°49'09"	SHU	11/11	74,24	23.6	73.3	111.1	4.4	52.3	53.2	111.1	4.4	41.0±6.6	1.6±4.2
KD21	36°50'36"	59°45'57"	SHU	16/16	178,38	26.4	4.3	25.3	7.5	34.7	36.7	25.3	7.5	23.4±8.0	18.3±6.4
KD22	36°50'47"	59°45'42"	SHU	9/4	206,34	22.1	24.8	335.3	5.0	19.3	58.6	335.3	5.0	8.0±8.1	-3.6±4.7
KD23	36°34'49"	60°01'46"	SHU	10/10	200,30	20.9	24.9	70.8	5.8	21.5	54.9	70.8	5.8	10.2±8.5	-6.1±5.2
KD24	36°38'38"	59°53'24"	SHU	9/5	26,34	86.2	84.3	79.8	8.6	34.2	52.9	79.8	8.6	22.9±11.6	2.0±7.2
KD25	36°38'45"	59°52'46"	SHU	10/10	25,39	77	73.2	69.2	5.9	42.1	39.2	69.2	5.9	30.8±6.8	15.7±5.3
KD26	36°39'19"	59°52'31"	SHU	10/9	54,52	274.8	75.5	73.6	6.0	39.8	48.2	73.6	6.0	28.5±7.7	6.7±5.3
KD27	36°40'12"	59°53'06"	SHU	10/10	216,50	28	11.5	25.8	9.7	19.9	60.7	25.8	9.7	8.6±16.0	-5.8±8.0
KD28	36°40'21"	59°53'50"	SHU	11/11	220,42	28.7	1	86.3	4.9	24.7	42	86.3	4.9	13.4±6.0	12.9±4.6
KD29	36°47'15"	59°32'58"	SHU	10/9	36,22	39	55.7	114.9	4.8	38	33.7	114.9	4.8	26.2±5.6	24.1±4.4
KD30	36°47'27"	59°32'53"	SHU	10/10	314,14	34.6	49.3	135.4	4.2	20	45.2	135.4	4.2	8.2±5.7	12.6±4.0
KD31	36°48'25"	59°34'03"	SHU	9/9	0,0	37.5	52.3	130.3	4.5	37.5	52.3	130.3	4.5	25.7±6.6	5.5±4.2
KD32	36°49'55"	59°37'54"	SHU	12/12	42,36	21.9	78.7	45.2	6.5	36.7	43.2	45.2	6.5	24.9±7.7	14.6±5.6
KD33	36°48'47"	59°35'04"	SHU	14/14	197,45	24.4	18.5	215.3	2.7	32.4	62.8	215.3	2.7	20.6±5.7	-5.0±3.2
Mean			**SHU**	**22**		**26.8**	**48.2**	**8**	**11.7**	**28.5**	**49.5**	**60.7**	**4**		

KD35	35°49'32"	60°09'11"	SHU	12/11	208,20	26.8	42.6	56.7	6.1	26.1	62.6	56.7	6.1	14.9±10.8	-8.5±5.4
KD36	35°49'12"	60°09'12"	SHU	10/7	270,5	27.3	46.1	32.4	10.8	22.4	48.2	32.4	10.8	11.2±13.1	5.9±8.8
KD37	35°49'30"	60°10'50"	SHU	12/10	185,5	26	45.4	126.5	3.9	28	50	126.5	3.9	16.8±5.6	4.1±4.0
KD38	35°49'16"	60°11'16"	SHU	15/12	230,16	30.1	37.7	38.2	7.1	23.8	52.4	38.2	7.1	12.6±9.6	1.7±6.1
KD39	35°45'39"	60°14'29"	SHU	11/10	42,22	15.9	76.7	50.1	6.9	31.7	55.6	50.1	6.9	20.5±10.0	-1.5±6.0
KD40	35°44'50"	60°15'26"	SHU	14/13	50,22	32.4	73.9	46.3	6.2	42.1	52.4	46.3	6.2	30.9±8.5	1.7±5.5
KD41	35°45'16"	60°15'45"	SHU	11/10	274,20	17.9	44.7	8.5	17.5	357.4	46	8.5	17.5	-13.8±20.2	8.1±13.1
KD42	35°44'59"	60°15'32"	SHU	12/11	16,28	47.5	69.7	54.1	6.3	30.5	43.6	54.1	6.3	19.3±7.5	10.5±5.6
KD43	35°45'19"	60°04'14"	SHU	12/9	250,14	52.9	48.4	30.6	9.5	42.1	52.4	30.6	9.5	38.9±12.6	1.7±7.8
KD44	36°09'08"	60°33'34"	SHU	14/10	48,64	232.3	65.5	34.2	8.4	45.2	50.4	34.2	8.4	34.0±10.8	3.7±7.0
KD45	36°09'40"	60°32'53"	SHU	13/12	220,65	245.7	24.6	45.7	6.5	248.6	-34.6	45.7	6.5	57.4±6.9	19.5±5.7
KD47	35°53'45"	60°33'36"	SHU	14/13	338,36	66.5	60.2	40	6.6	21.7	44	40	6.6	10.5±7.8	10.1±5.8
KD48	35°53'51"	60°34'30"	SHU	9/9	352,42	73.3	67.2	12.4	15.2	15.9	45	12.4	15.2	4.7±17.3	9.1±12.1
KD49	35°55'09"	60°35'55"	SHU	14/14	52,76	227	56.2	22.9	8.5	56.1	47.6	22.9	8.5	44.9±10.4	6.5±7.1
KD50	35°54'47"	60°40'59"	SHU	11/8	215,46	25.5	6.6	31.9	9.9	19.7	51.7	31.9	9.9	8.5±12.9	2.4±8.1
KD51 *	35°54'35"	60°40'50"	SHU	9/2	230,76	355	40.4	564.9	10.5	280	35.4	564.9	10.5	-91.2±10.5	18.7±8.6
Mean			**SHU**	**17**		**25.5**	**63.1**	**5.4**	**17**	**27.2**	**51.7**	**53.1**	**5.7**		
Mean values of all Shurijeh sampling sites															
						BTC				**ATC**				**Tectonic Rotations**	
			Fm	**N**		**D°**	**I°**	**K**	**α_{95}**	**D°**	**I°**	**K**	**α_{95}**	**R (°)±Er(°)**	**F(°) ± Er(°)**
Mean			**SHU**	**44**		**28.8**	**53.3**	**6.8**	**8.8**	**30.7**	**50**	**38.7**	**3.5**	**19.4±5.2**	**4.6±3.7**

Table 7.3. Paleomagnetic directions from the Upper Red Formation

Location						**BTC**				**ATC**				**Tectonic Rotations**	
Site	**Lat (°N)**	**Lon(°E)**	**Fm**	**N/n**	**S0**	**D°**	**I°**	**K**	**α_{95}**	**D°**	**I°**	**K**	**α_{95}**	**R(°) ± Er(°)**	**F(°) ± Er(°)**
KD09	37°21'50"	57°18'34"	URF	12/12	36,44	118	70.9	8.4	15.9	61.1	40.4	8.4	15.9	56.0±16.5	16.0±12.5
KD10	37°16'22"	57°22'22"	URF	12/11	34,46	55.4	53	26.8	9	46.9	8.7	26.8	9	41.8±7.3	47.7±7.1
KD46	36°07'47"	60°30'35"	URF	11/11	242,6	9.7	37.6	53	6.3	5.7	41	53	6.3	1.6±6.7	14.6±5.1
KD52	36°07'60"	60°30'19"	URF	10/8	0,0	356.1	33.3	46.3	8.2	356.1	33.3	46.3	8.2	-8.0±7.8	22.3±6.5
KD53	36°08'33"	60°29'44"	URF	10/9	280,14	19.8	25.7	37.2	8.5	12.9	27.2	37.2	8.5	8.8±7.7	28.4±6.7
KD54	36°03'36"	60°21'41"	URF	10/8	244,22	222.9	-15	16.8	13.9	218.8	-35.2	16.8	13.9	34.7±13.4	20.4±10.9
KD56	36°00'59"	60°11'13"	URF	10/9	25,6	193.5	-49.9	39.9	8.2	194.7	-44	39.9	8.2	10.6±9.1	10.8±6.5
KD57	36°01'44"	60°13'47"	URF	11/7	145,12	202.5	-27.6	27.7	11.7	208.7	-33.5	27.7	11.7	25.7±11.1	21.3±9.2
KD58	36°02'31"	60°16'14"	URF	11/10	170,8	353.8	27.5	39.3	7.8	354.1	35.5	39.3	7.8	-9.9±7.7	19.3±6.2
KD59	36°04'38"	60°20'36"	URF	10/7	310,28	202.5	-44.9	18.2	14.5	182.4	-31.6	18.2	14.5	-1.6±13.4	23.2±11.4
KD60	35°37'49"	60°17'09"	URF	12/10	105,24	357	44.4	35.4	8.2	22	46.8	35.4	8.2	17.9±9.5	8.0±6.5
KD61	35°34'11"	60°14'51"	URF	11/11	11,21	5.4	41.6	132.4	4	6.5	20.6	132.4	4	2.4±3.7	34.2±3.4
KD62*	35°32'09"	60°18'43"	URF	12/12	333,16	17.4	66.3	3.4	27.7	1	53.2	3.4	27.7	3.0±39.7	1.5±21.6
KD63	35°32'00"	60°20'10"	URF	9/9	95,14	189.5	-56.5	7.8	19.7	208.9	-53	7.8	19.7	24.8±26.6	1.7±15.4
Mean			**URF**	**11**		**12.6**	**37.6**	**22.4**	**9.9**	**9.8**	**41.8**	**19.2**	**14.1**		
KD64	36°02'25"	59°10'15"	URF	11/10	50,42	332	43	80.2	5.4	358.5	23.9	80.2	5.4	2.4±3.7	34.2±3.4
KD65	36°10'50"	58°59'42"	URF	12/12	15,15	217.3	-26.8	29.2	8.2	215.3	-12.8	29.2	8.2	-5.5±4.9	30.9±4.4
KD66	36°26'21"	59°52'52"	URF	9/9	213,11	197.5	-18.9	35.6	8.7	196.1	-29.5	35.6	8.7	12.0±8.0	25.3±6.9
KD68	36°28'31"	59°55'27"	URF	11/10	184,37	199	-31.4	40.1	7.7	216.6	-65.9	40.1	7.7	32.5±15.0	-11.1±6.2
KD69	36°27'32"	59°54'17"	URF	11/8	100,29	359.1	31.4	44.2	8.4	17.6	32.3	44.2	8.4	13.5±7.9	22.5±6.7
KD70	36°26'13"	59°56'36"	URF	10/10	62,12	325.9	61.3	15.4	12.7	347.5	60.3	15.4	12.7	-16.5±20.6	-5.5±10.0
Mean			**URF**	**6**		**6.3**	**37.9**	**10**	**22.3**	**14.9**	**40.2**	**25.9**	**10.3**		

Mean values of all URF sampling sites															
						BTC				ATC				Tectonic Rotations	
			Fm	N		D°	I°	K	α_{95}	D°	I°	K	α_{95}	R (°)±Er(°)	F(°) ± Er(°)
Mean			URF	19		13.7	41.6	11.4	10.4	18.4	37	14.8	9	14.3±9.0	18.3±7.1

Notes and abbreviations: Lat = latitude of the sampled site; Lon = Longitude of the sampled site; Fm = Geological formation; N/n— number of demagnetized samples/ number of stable directions at a site; S_0—bedding attitude (azimuth of the dip and dip values). D°, I°— site mean declinations and inclinations calculated before tectonic correction (BTC) and after tectonic correction (ATC); K—precision parameter; α_{95}—confident limit (statistical parameters after Fisher, 1953); R (°) ± Er (°) =rotation values and relative error; F (°) ± Er (°) = flattening values and relative error. * = sites not considered in further tectonic interpretation; URF = Upper Red Formation; PES = Pestehleigh Formation; SHU = Shurijeh Formation.

Upper Red Formation sites show as well similar rotations in Fariman (D= 14.9°; I=40.2°; k=25.9; α_{95}=10.3°) (Tab.7.3, green part) and Kopeh Dagh (D= 9.8°; I=41.8°; k=19.2; α_{95}=14.1°) (Tab.7.3, blue part) areas. These latter directions are also no statistically different from results obtained by Mattei et al. (2017) in the Rivand and Samghan fold structures (D = 21.5°, I = 43.9°, k = 24.7, α_{95} = 6.9°), south of Allah Dagh (Fig. 7.7).

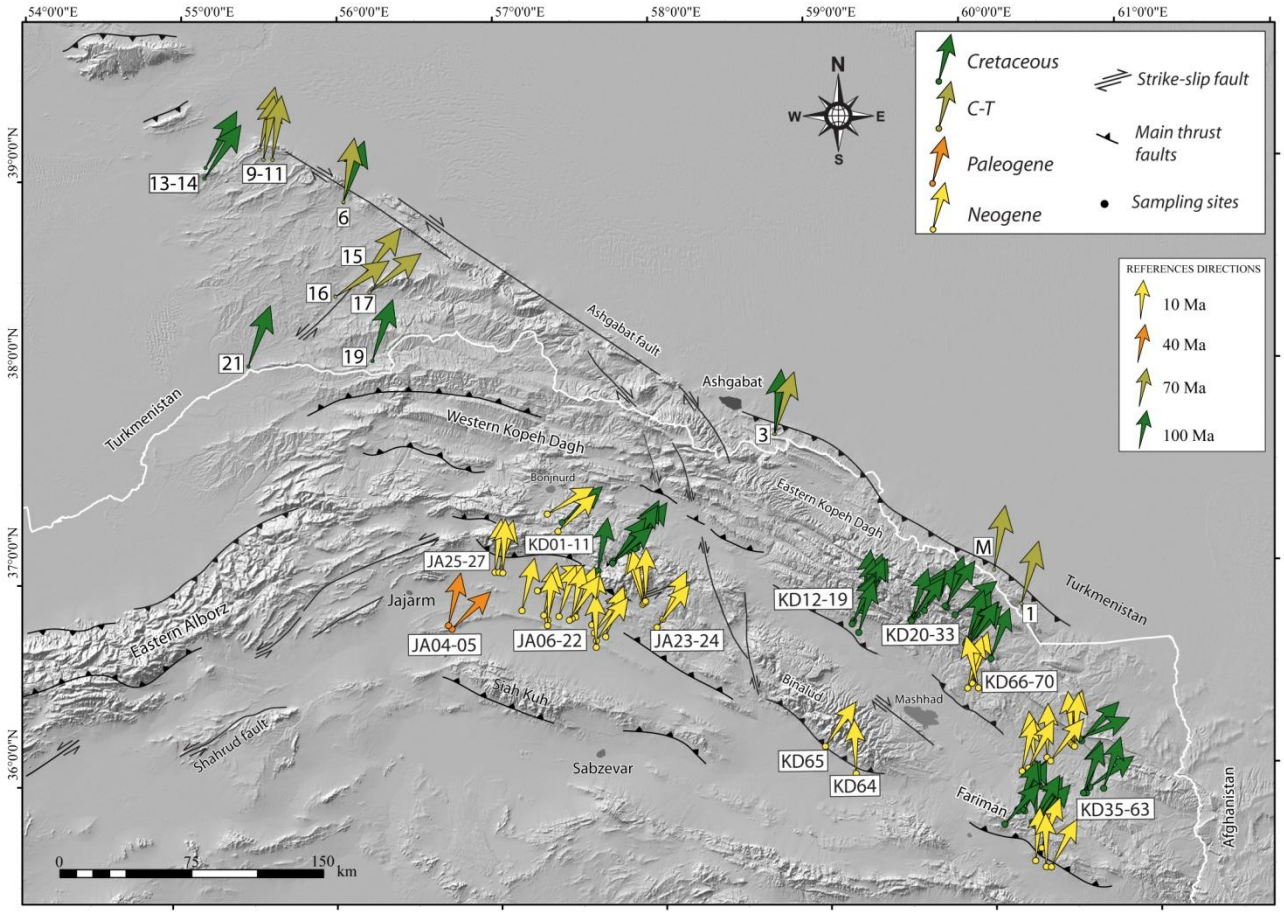

Fig.7.7 *Paleomagnetic rotations from north-eastern Iran and Turkmenistan, calculated comparing the obtained paleo-declinations with the 10 Ma (URF), 70 Ma (C-T) and 100 Ma (SHU and CRE) reference poles (see text and Tables 1 and 2 for details). Green arrows represent paleomagnetic declinations from Cretaceous rocks; orange arrows represent paleomagnetic declination from Eocene (Mattei et al., 2017) and Upper Cretaceous-Paleocene (Bazhenov, 1987) rocks; yellow arrows represent paleomagnetic declination from Middle-Late Miocene URF rocks.*

The amount of CW rotation is statistically comparable in the Upper Jurassic-Lower Cretaceous Shurijeh Fm and in the Middle-Upper Miocene URF (Tab. 7.2-7.3), suggesting that the entire amount of CW rotations measured in the Upper Jurassic-Lower Cretaceous units occurred after Late Miocene, and that north-eastern Iran did not undergo significant vertical axis rotations between Late Cretaceous and Late Miocene. It is worth to note that the amount of paleomagnetic rotations measured in the Shurijeh and URF is also statistically comparable with rotations obtained by Bazhenov (1987) in the Aptian-Cenomanian (9.6° ± 8.3°) and Upper Cretaceous-Paleocene units (11.3° ± 5.2°) from Turkmenistan Kopeh-Dagh (Table 7.1). Paleomagnetic rotations are consistently distributed in the different geological structures of north-eastern Iran (Fig. 7.7).

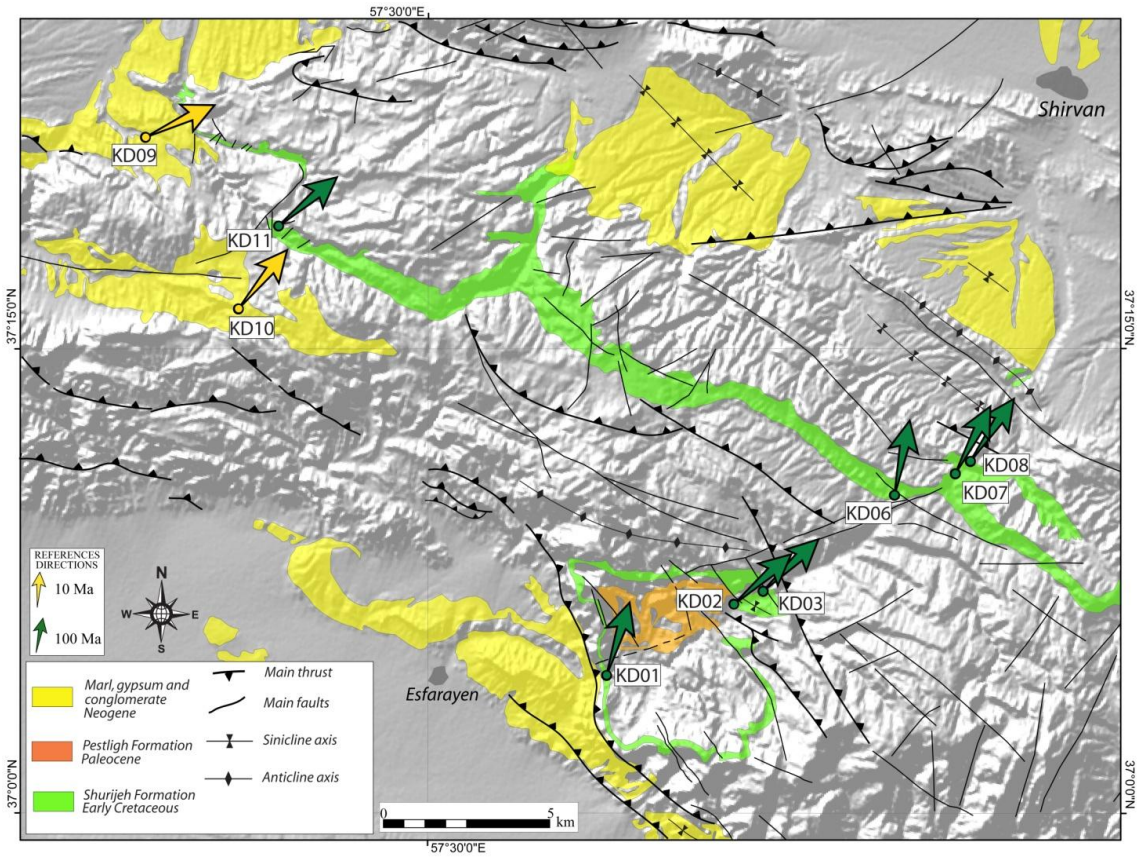

Fig.7.8 *Simplified geological map of the western sector, in the Allah Dagh mountains. Sampling sites and directions of in situ magnetic declination from this area are also reported (green arrows for Early Cretaceous sites and brown arrows for Neogene sites).*

Focusing on the single macro-areas where the samples were collected it's easy to note how the same magnetic declination directions are homogeneous distributed in each areas both for Cretaceous as for Neogene sampling sites (Fig.7.8-7.9-7.10). The resulting amount of vertical axis rotation for each sampling site show a general CW vertical axis rotation trend which regards the Cretaceous and Neogene deposits with the magnetic declination directions in the order of 5-25°.

For some Cretaceous sites were calculated a larger value of CW rotation probably due to specific structural setting of the outcrops; in fact these condition has been recognized randomly in each sampling area: KD02 and KD11 in the first area (Fig.7.8), KD20 and KD25 in the second area (Fig.7.9) and also in the third area where in six sites were founded an high rotation values. As show in Fig.7.10, the third area was interested by a poor distribution of the Shurijeh Fm. which crop-out in few tectonized outcrops, in fact being located at the ending of the oroclinal this area has been subjected to a larger tectonic stress. Responding to these strongly deformation the Cretaceous deposits show a much higher variability in the paleomagnetic directions values (magnetic declination, see Fig.7.10 and Tab.7.2-7.3), as well as in the magneto fabric configuration (as show in Fig. 5.15 and Tab.5.1).

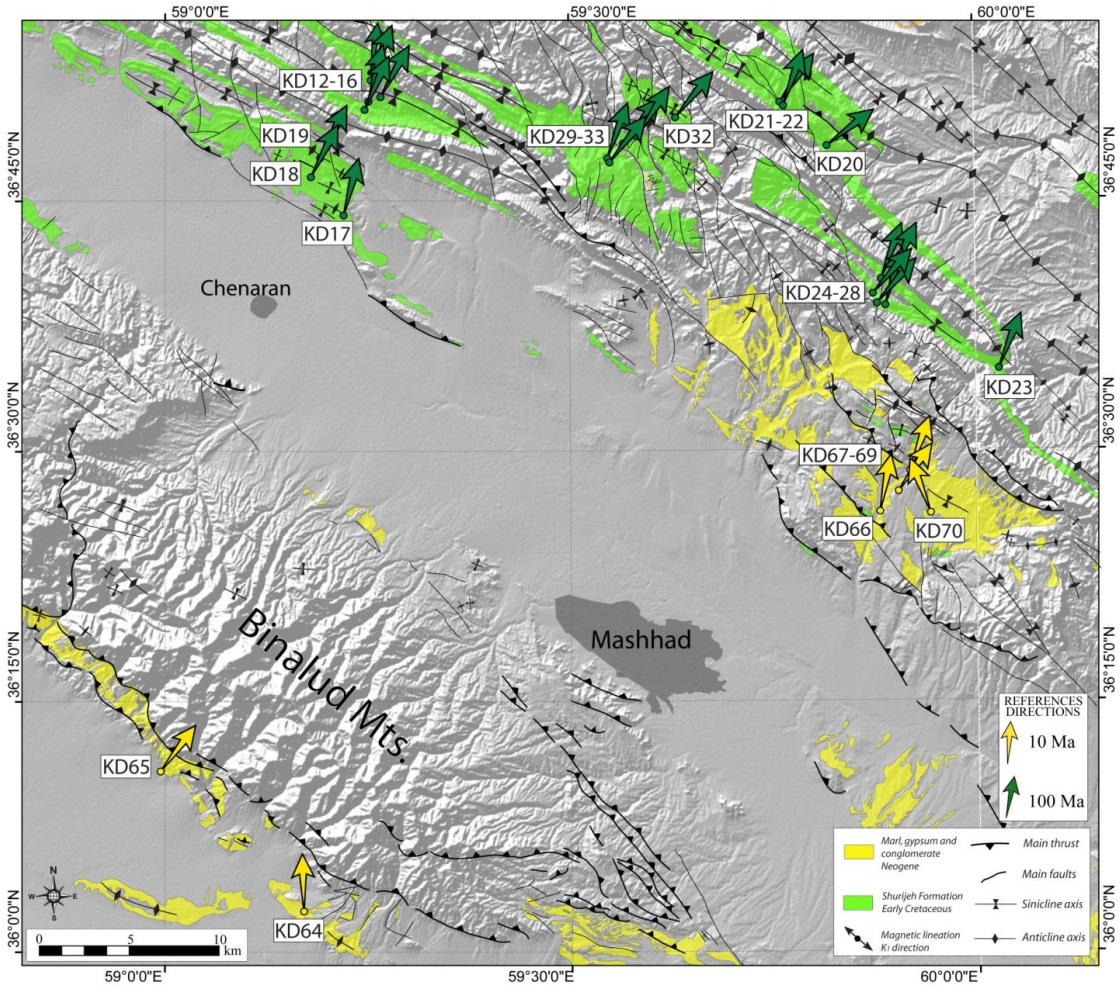

Fig.7.9 *Simplified geological map of the central sector of Kopeh Dagh range and Binalud Mountains. Sampling sites and directions of in situ magnetic declination from this area are also reported (green arrows for Early Cretaceous sites and brown arrows for Neogene sites).*

If few sites show an higher magnetic direction values, in some others are registered lower values, close to zero. These deposits has been probably remagnetized in the recent time, for this reason the actual magnetic field direction are overprinted and the magnetic declination are very low.

In general it can said that most of the Cretaceous and Neogene sampling sites show a common magnetic declination direction coherent with the regional shortening direction, instead the sites characterized by higher or lower values of magnetic declination, may have been interested by a local structural configuration which modified the original configuration, as well as a recent remagnetization processes could be the reason of magnetic declination directions close to zero.

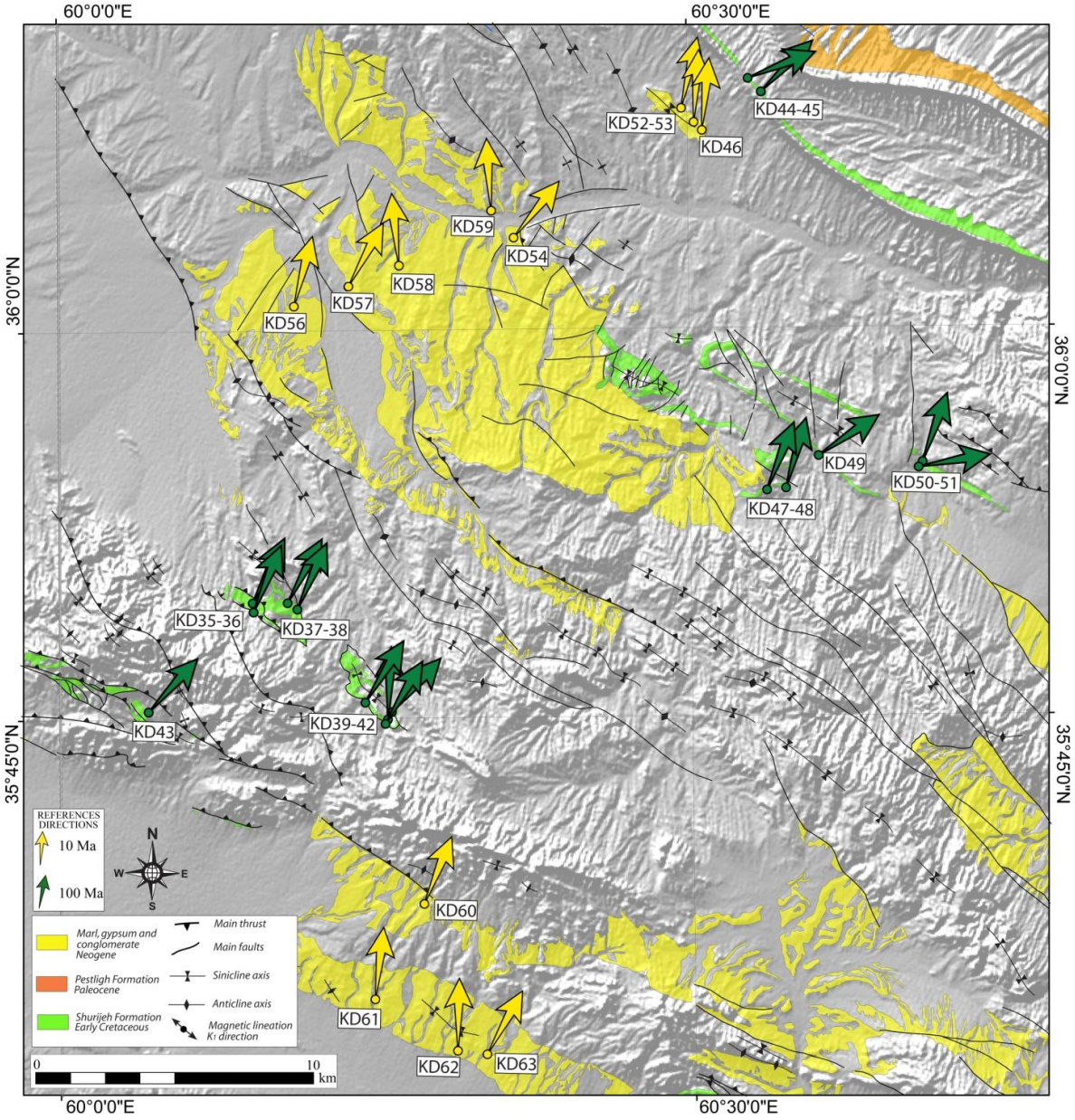

Fig.7.10 *Simplified geological map of the eastern sector along the Fariman metamorphic complex and near Agdarband tectonic window. Sampling sites and directions of in situ magnetic declination from this area are also reported (green arrows for Early Cretaceous sites and brown arrows for Neogene sites).*

7.2.3 Tectonic evolution of north-eastern Iran

The Cenozoic to Present-day tectonic evolution of north-eastern Iran has been widely discussed in the last decades. According to GPS, seismological, geomorphological and structural data two main features characterize the present-day kinematics of north-eastern Iran:

a. the northward motion of Central Iran with respect to Eurasia represent the main geodynamic feature in the region. The convergence motion decreases linearly from ~11 mm/yr at the longitude of Tehran to zero at the eastern margin of Iran (Fig.2.2). This velocity field is consistent with shortening accommodated by active folds and thrusts of northern Iran and with distributed N–S right-lateral shear across north eastern Iran (Mousavi et al., 2013; Vernant et al., 2004).
b. The second feature is represented by the westward extrusion of the South Caspian block, accommodated by dextral strike slip faults along the north-eastern border of Iran and by left-lateral motion along its southern margin (Fig.2.2). The westward motion of this ancient block which starting in the recent time, is still active and affect the tectonic setting of the surrounding areas. Among them the Ashkhabad fault zone, which runs in along the north-eastern margin, is partitioned onto north-vergent thrusts faults and right-lateral straight-slip fault segments, and the Shahrud fault zone in the south-eastern margin, which is a system of discontinuous left lateral faults segments (e.g., Hollingsworth et al., 2008)

Despite the general agreement on these first-order features that characterise the present-day kinematics of north-eastern Iran, the tectonic evolution of the Kopeh-Dagh, Allah Dagh and Binalud mountains, how these structures accommodate the Arabia-Eurasia shortening and the westward extrusion of the South Caspian block, is much more debated and different models have been proposed (Fig. 7.11).

1. A first class of models (Hollingsworth et al., 2010, 2008, 2006; Jackson et al., 2002) subdivides Kopeh Dagh range in three different regions, characterised by different kinematics and style of deformation (Fig. 7.11a). East of 59°E, mountains have the highest peaks and GPS data show 2 mm/yr N-S shortening between Central Iran and Eurasia, which appears to be partitioned into range-parallel thrusts and right-lateral strike-slip faults. West of 57°E, the topography across the Kopeh Dagh decreases gradually and the range is progressively buried by sediments toward the Caspian coast (Lyberis and Manby, 1999; Robert et al., 2014), and the right-lateral Ashkhabad Fault is the dominant tectonic feature of the region. In this area right-lateral slip and slip on

range-parallel thrusts accommodates the motion between Eurasia and the South Caspian block (Jackson et al., 2002). Between 57° E and 59° E, the relative motion of the South Caspian block away from north-eastern Iran causes the central portion of the Kopeh Dagh to experience range-parallel extension in addition to the N-S convergence between Iran and Eurasia that are accommodated by CCW rotation on a series of NNW-striking right-lateral strike-slip faults (Bakhardan-Quchan- Fault Zone) (Hollingsworth et al., 2006).

2. A second class of models (Shabanian et al., 2009a, 2009b) subdivides north-eastern Iran in two blocks with independent kinematics (Fig.7.11b). The two blocks are separated by a NNW-SSE striking strike-slip fault system (Meshkan and Bakhardan-Quchan Fault Zones) that allows the northward movement of Central Iran relative to eastern Iran. In particular, the western Kopeh Dagh movement toward the South Caspian Basin, is taken up by lateral motion on the Ashkhabad Fault and the Shahrud Fault system. In this model, right-lateral strike-slip faults across the Kopeh Dagh range do not rotate but instead accommodate the north-westward translation of Iran relative to Eurasia and represent the eastern border of the South Caspian Block (WKA in Fig. 7.11b).

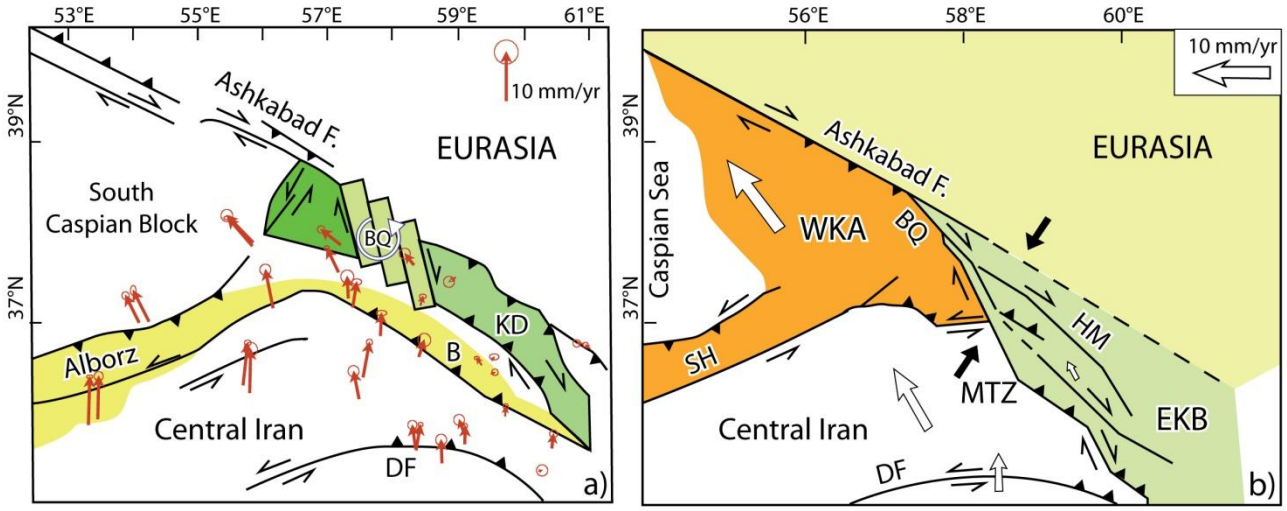

Fig. 7.11 *Tectonic models proposed for north-eastern Iran (modified by* Shabanian et al., 2009a). ***a)*** *Simplified version of the kinematic model proposed by* Hollingsworth et al., (2008). *Red arrows represent GPS velocities in the Eurasian reference frame* (Mousavi et al., 2013). ***b)*** *model of the tectonic configuration in NE Iran proposed by* Shabanian et al., (2009a). *White arrows are GPS velocity vectors in the Eurasian reference frame. Black arrows show the direction of the s1 stress axis. B = Binalud; BQ = Bakharden-Quchan Fault system; DF = Doruneh Fault; EKB= eastern Kopeh Dagh–Binalud tectonic domain; HM = Hezar Masjed Fault system; KD = Kopeh Dagh; MTZ = Meshkan Transfer Zone; SH = Shahrud Fault system; WKA = western Kopeh Dagh–Alborz tectonic domain. The inactive NE margin of the Kopeh Dagh is marked by dashed line.*

Paleomagnetic data from north-eastern Iran, collected both from this work as well as from Bazhenov, (1987) and Mattei et al., (2017), show that Eastern Alborz, Binalud-Fariman Mts. and Kopeh Dagh underwent comparable amount of CW rotations in both Cretaceous, Paleocene and Neogene deposits. This pattern of paleomagnetic rotations is at odd with the present-day kinematics of north-eastern Iran as suggested by GPS data (as show in Fig.7.11a by the red arrows, from Mousavi et al., 2013) that highlight the existence of fault-bounded blocks with different kinematics . In particular, paleomagnetic data do not show differential rotations between Eastern Alborz, which belongs to the South Caspian block according to the Shabanian et al. (2010) model (Fig. 7.11b), and the eastern Kopeh-Dagh, Binalud and Fariman structures, which belong to the EKB block of Figure 7.11b.

On this basis, I propose that the measured pattern of paleomagnetic rotations has occurred in a tectonic regime different from the present-day one, and that the tectonic reorganization of north-eastern Iran is relatively young and therefore its rotational pattern cannot be detected using paleomagnetism. In good agreement with this propose are the results from AMS analysis. The mean values of magnetic lineation directions show a perfect correspondence with the main structure of the range in each of the three sampling areas. In other words as show in Fig.5.12 (Fig.5.13-5.14-5.15), the magnetic fabric configuration detected both for Cretaceous and Neogene units are referred to the Arabia Eurasia collision. The AMS analyzes have shown to be an excellent tool to support paleomagnetic techniques; in fact the AMS fabric components has been compared with vertical axis rotations to document the possible oroclinal bending, assuming that the magnetic lineation is tectonically originated and formed during layer-parallel shortening (LPS) before vertical axis rotations occurred (e.g., Speranza et al., 1997; Weil and Yonkee, 2009).

Using this method it is possible to obtain more precise information than deriving structural directions from large-scale geological maps, overcoming the intrinsic error from this method and reducing all the problem deriving from the estimation of structural direction in that sites where bedding is weakly tilted and/or in structures with a plunging structural axis (Mattei et al., 2017).

In general the data that have been taken into account come from which sites where the orientation of the magnetic lineation is representative of the general structural trend. In these cases, the magnetic lineation is well defined at the basin scale and is oriented almost parallel to the bedding strike, with the magnetic foliation almost parallel to bedding.

The actual setting of the region is progressively characterized by the westward extrusion of the South Caspian block to the west which influenced the regional tectonic setting of area, while to the south-east the shortening must die out against the Afghanistan border, as western Afghanistan is evidently part of Eurasia (Jackson and McKenzie, 1984; Vernant et al., 2004).

This recent evolution of the tectonic setting, as suggested by GPS data (Fig. 7.11a), has not been signed in the rocks, in fact the configurations of rock magnetic fabric are coherent with the N-S convergence due to the Arabia-Eurasia collision.
It is noteworthy that our sampling sites do not cover the Kopeh Dagh region comprised between 57° and 59° E of longitude, where a CCW rotations of fault bounded blocks has been suggested (Fig. 11a) and therefore our data do not give any information on tectonic processes in this area.

7.2.4 Oroclinal bending in Northern Iran

Previous paleomagnetic results in northern Iran (Ballato et al., 2008; Cifelli et al., 2015; Mattei et al., 2017) showed that the WNW-ESE oriented western Alborz and Rivand and Samghan fold belts rotated about 15–20° CW whereas the WSW-ENE oriented central Alborz Mts. rotated about 20°CCW. (Fig. 7.12). This distribution of paleomagnetic rotations has been interpreted as the result of an oroclinal bending process that occurred in the Alborz Mts. after Late Miocene. In fact as described by Mattei et al., (2017), the timing for the curvature of the arc is suggested by:

i) the slope of the best fit line in the paleomagnetic strike test, which indicates an almost 100% secondary rotation since middle-late Miocene;
ii) clockwise rotations between ≈12° and ≈35° of the Cretaceous volcanic rocks from the Western Alborz (Mattei et al., 2015), which are not distinguishable from the rotation values obtained from the Miocene URF in the same area;
iii) detailed magneto-stratigraphic analysis section from Western Alborz that does not show any evidence of a rotation trend throughout the section, suggesting that almost all rotation occurred after the deposition of the URF in the area (Ballato et al., 2008; Cifelli et al., 2015).

Our paleomagnetic results from the Kopeh Dagh, Allah Dagh and Binalud-Fariman ranges confirm that the WNW-ESE oriented structure of north-eastern Iran underwent CW rotations after Late Miocene, supporting the oroclinal bending hypothesis of the whole mountain range. Furthermore, the absence of differential rotations in the Shurijeh Fm. and URF excludes that the oroclinal bending processes started earlier than Late Miocene, as suggested by Hollingsworth et al. (2010).

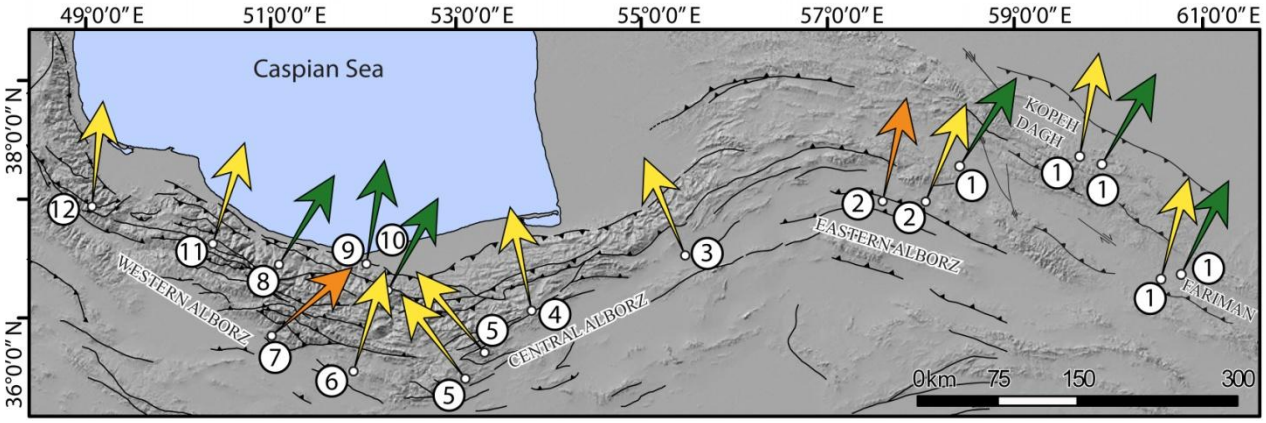

Fig.7.12 *Mean paleomagnetic rotations from the different sectors of North Iran:* ***1)*** *this work;* ***2)*** *Jajarm (Mattei et al., 2017);* ***3-5)*** *Semnan Basin (Mattei et al., 2017);* ***6)*** *Eyvanikey (Ballato et al., 2011; Cifelli et al., 2015);* ***7)*** *Karaj (Bina et al., 1986);* ***8-9)*** *Chalus (Wensink and Varekamp, 1980);* ***10)*** *Haraz River (Wensink and Varekamp, 1980);* ***11)*** *Alamut (Mattei et al., 2017);* ***12)*** *Manjil (Mattei et al., 2017). Arrows' colours are the same of Fig. 7.7.*

Our paleomagnetic data also prove that oroclinal bending and CW rotation in north-eastern Iran are not limited to the Alborz Mts. but also extend to the southeast (Binalud Mts.) and to the outer border of the deformation structures related to the Arabia-Eurasia convergence (Kopeh Dagh Mts.) (Fig.7.12). That confirm the post Late Miocene rotations, which allowed the involvement of all mountain belts during the oroclinal construction.

In Figure 7.13, a paleotectonic reconstruction of Northern Iran from Miocene to Present is proposed, that takes into account the main constraints derived from paleomagnetic data.

Figure 7.13a shows a possible paleotectonic configuration of Northern Iran during the Middle-Late Miocene, before the beginning of the oroclinal bending process.

The main features are:

i) two rigid blocks located along the southern Eurasia margin, separated by a embayment with low-velocity mantle (Maggi and Priestley, 2005). These blocks are the Turan platform to the east, part of the stable Eurasian domain and the South Caspian Basin to the west, a trapped block of rigid crust (probably oceanic), today surrounded by active fold and thrust belts (e.g., Kadinsky-Cade et al., 1981);

ii) the Alborz and Kopeh-Dagh orogenic systems, whose existence during the Middle-Late Miocene is testified firstly by a Late Eocene-Oligocene regional unconformity in the western Kopeh-Dagh (Robert et al., 2014), by regional volcanic dikes dated to 8.7 to 6.7 Ma, which cutting a regional thrust fault system in western Alborz, and finally by rapid exhumation of the Alborz Mts., as testified by a strong cluster of apatite fission track ages around 10–20 Ma (Madanipour et al., 2013; Rezaeian et al., 2012);

iii) the E-W orientation of the Alborz and Kopeh-Dagh mountain ranges derived by paleomagnetic data (Mattei et al., 2017 and results from this work).

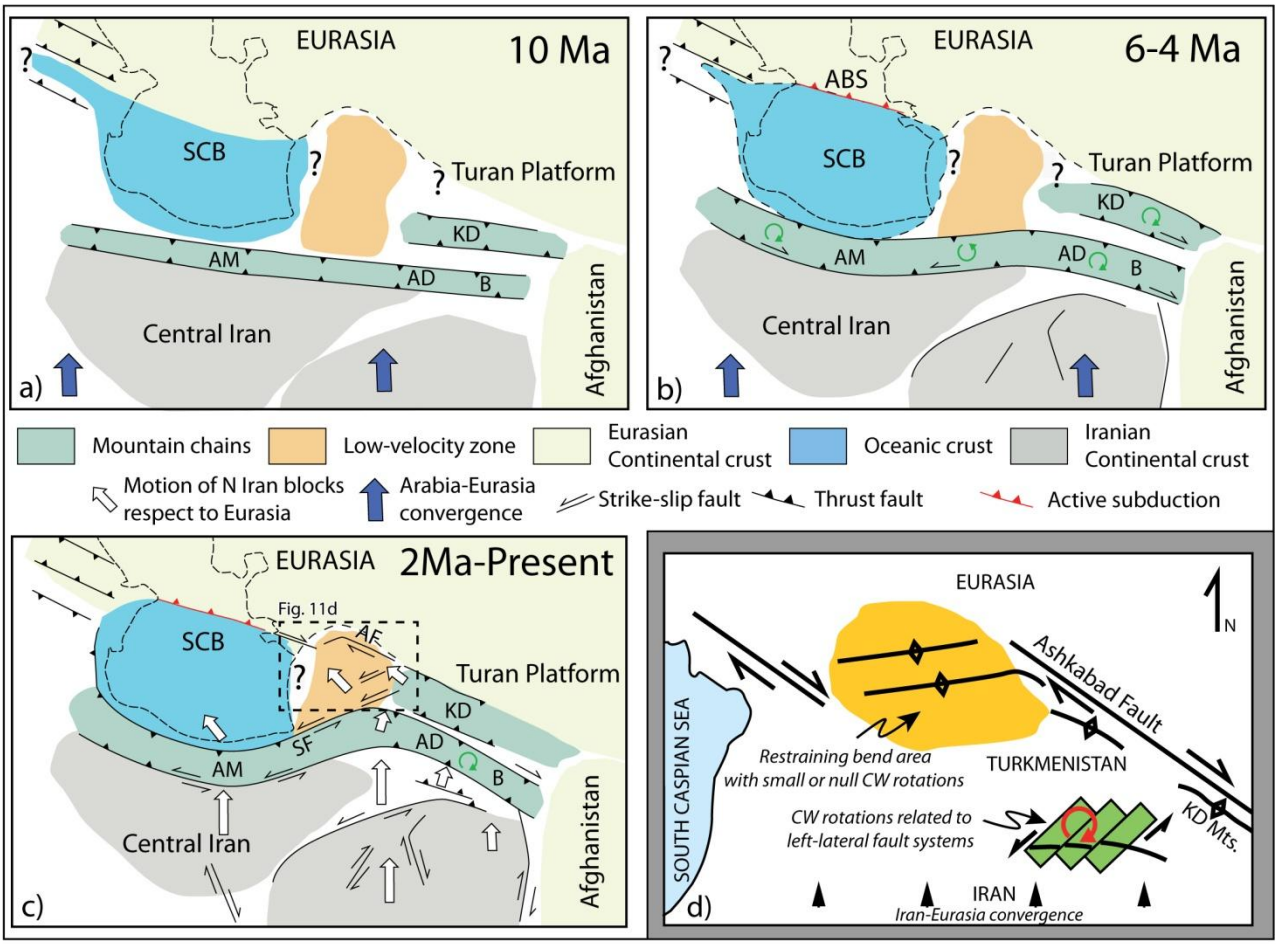

Fig. 7.13. a-c) *Schematic cartoons of the tectonic evolution of Northern Iran from Late Miocene to Present (modified from Mattei et al., 2017):* ***a)*** *Linear W-E orientation of the North Iran mountain belts at 10 Ma, before the collision of the Central Iranian Blocks with the South Caspian Block and with the Turan Platform;* ***b)*** *collision of Central Iran with the South Caspian Block and with the Turan Platform, that caused the internal deformation and the outward migration of the mountain ranges, the initiation of the South Caspian subduction underneath the Aspheron Sill and was accompanied by large vertical axis rotations;* ***c)*** *recent to Present-day kinematics of North Iran with the westward extrusion of the South Caspian Block and the initiation of strike-slip tectonics in the area.* ***d)*** *Tectonic model of the Ashkhabad area in Turkmenistan (inset in fig. 11c) explaining the origin of the differently oriented systems of fold and thrust structures and the CW rotations related to the presence of left-lateral strike slip fault system. AM = Alborz Mts.; B = Binalud Mts.; AD = Allah Dagh Mts.; KD = Kopeh Dagh; SCB = Sothern Caspian Basin; ABS = Aspheron-Balkhan Sill; AF = Ashkhabad Fault.*

Afterwards, as show in Figure 7.13b, the initiation of the oroclinal bending processes in North Iran is shown (about 6-4 Ma), related to the impinging of Central Iran between the South Caspian block and the southern margin of the Turan platform. In particular, the collision of Central Iran with the rigid South Caspian block has produced the present-day curved shape of the Western and Central Alborz mountain chain that progressively wrapped around it with CW and CCW rotations, respectively (Allen et al., 2003; Cifelli et al., 2015; Hollingsworth et al., 2010; Mattei et al., 2017). At the same time, the interaction of Central Iran with the southern margin of the Turan platform caused the progressive CW rotation of the Allah Dagh, Binalud and Kopeh Dagh Mts. The age of

the collision between Central Iran and the South Caspian block is documented by several evidence, among them:

i) the incorporation of middle Miocene sedimentary sequences deposited in the Caspian Sea block (Red Marl Fm.) in the northern side of the Alborz orogenic wedge;
ii) an important phase of exhumation in the Alborz Mts, accompanied by an increase of fold and thrust activities in the internal part of the chain during the late Miocene-Pliocene time (6–4 Ma);
iii) the outward migration of the orogenic wedge frontal thrusts along the southern and northern sides of the mountain range.

In the South Caspian Basin this collisional event is recorded by an increase in the sedimentation rate, recorded by ≈2.4 km of tectonic subsidence since ≈5.5 Ma (Allen et al., 2002). This rapid accumulation of sediments is related to an increase in the basement subsidence, which testifies the beginning of northward subduction of the South Caspian basement under the Aspheron-Balkhan Sill, now imaged by the subcrustal earthquakes with depths down to 80 km (Allen et al., 2003, 2002; Jackson et al., 2002).

Finally, in Figure 7.13c the present-day tectonic configuration of the North Iran is represented, highlighting the major changes in the tectonic regime of Northern Iran related to the initiation of the westward extrusion of the South Caspian block.

According to GPS data, it can be stated that:

i) Western and Central Alborz behave as a single block, moving toward the southwest with respect to Central Iran (Djamour et al., 2010; Mousavi et al., 2013);
ii) the Western Kopeh Dagh motion is coherent with the South Caspian Block and is presently moving toward northwest with respect to Eurasia, whereas the Binalud and Eastern Kopeh Dagh Mts. behave substantially coherently and do not show significant movements with respect to Eurasia (Mousavi et al., 2013).

The age of the beginning of this tectonic regime, associated to the initiation of left-lateral strike slip faulting in the Alborz Mts. (Shahrud Fault system), together with dextral movement along the Ashkhabad fault at the NE boundary with the Eurasia plate has been largely disputed in the recent literature, being proposed at ~10 Ma (Hollingsworth et al., 2008), ~5 Ma (Allen et al., 2002), and ~1.8 Ma ago (Mattei et al., 2017; Ritz et al., 2006).

Paleomagnetic results show a pattern of vertical axis rotations that is inconsistent with the present-day kinematics of the northern Iranian blocks as described by seismicity and GPS data. Therefore, it can be concluded that the tectonic processes responsible for the bending of northern Iran mountain chains are younger than ~7 Ma (younger age of URF) but are no longer active. On this

basis I suggest that the beginning of the westward motion of the South Caspian basin, and therefore the initiation of opposite strike-slip motion along the Ashkhabad and Shahrud faults, occurred very recently (~2 Ma ago), as suggested by Ritz et al. (2006) on the basis of geomorphologic data. As a consequence, I agree with Ritz (2009) and Mattei et al. (2017) that the initiation of the northward subduction of the South Caspian basin below the Apsheron-Balkan Sill (Fig. 7.13b) and the westward extrusion of the South Caspian block (Fig. 7.13c) did not occur at the same time, with the former starting between the late Miocene and the Pliocene, and the latter during the Pleistocene.

7.2.5 Reinterpretation of paleomagnetic rotations in the Turkmen Kopeh Dagh Mts.

Paleomagnetic results from the Turkmenistan part of the Kopeh Dagh Mts. have been published by Bazhenov, (1987). These data were used in this study for calculating the relative vertical axis rotations of Bazhenov's sites with respect to coeval Eurasian poles (Torsvik et al., 2012) (Table 7.1). These sites were sampled in different fold structures whose strike ranges from WSW-ENE to NW-SE, almost orthogonal and parallel to the Ashkhabad Fault, respectively (Fig. 7.7). Paleomagnetic data show that about half of the sites are substantially not rotated, whereas half show a statistically significant CW rotation (Table 7.1). The oroclinal test applied on these paleomagnetic results is negative (Bazhenov, 1987), demonstrating that in this area there is no relationship between the fold axes orientation and the amount of vertical axis rotations, and that the curvature of the fold axis is primary. Therefore, an oroclinal bending mechanism is not applicable to this portion of the Kopeh-Dagh Mts. and the presence of fold and thrust structures with different orientation needs an alternative explanation. The ENE-WSW oriented folds are cored by Cretaceous sediments and form at the northwest termination of the right-lateral Ashkhabad Fault, where the right lateral fault zone steps ~40 km to SW, and continues to northwest toward the Apsheron Balkan Sill (Fig. 7.13c-d) (Bretis et al., 2012; Hollingsworth et al., 2008). It is worth to note that in this area upper Pliocene marine rocks overlie Cretaceous rocks without any significant angular discordance, being clearly folded with the older rocks (Lyberis and Manby, 1999). Therefore, the age of the tectonic uplift and folding of these structure is post-Upper Pliocene and is almost coeval with the activity of the Ashkhabad fault system. On this basis, it is proposed that these folds formed in a restraining bend in correspondence of the sinistral step-over of the Ashkhabad right lateral fault, with their fold axis trending at high angle respect to the WNW-ESE oriented main fault, showing no rotations or a limited amount of CW rotations (Fig. 7.13d and Table 7.1). On the other hand, significant CW rotations are measured by Bazhenov, (1987) at sites 15,16 and 17 (Table 7.1, Fig. 7.7), located in the northwest part of our study area, at

latitude 38°N, where the E-W oriented folds are dissected by a NNE-SSW oriented left-lateral strike-slip fault system (Fig. 3 in Lyberis and Manby, 1999). Therefore it can be hypothesized that such a large CW rotation could be related to the activity of such a fault system which rotates CW to accommodate the N-S component of shortening between the South Caspian Block and Eurasia and the along-strike elongation of the western Kopeh-Dagh respect to the South Caspian block (Fig. 7.13c-d).

8. CONCLUSIONS

The interpretation of magnetic fabric and paleomagnetic data in the Ala-Dagh, Binalud and Kopeh Dagh mountains, along the north-eastern margin of Iran investigated in this PhD thesis, allowed to further contribute to clarifying the tectonic evolution of this region and its role in the accommodation of the deformation related to the Arabia-Eurasia collision.

The intracontinental deformation history of Northern Iran, was dominated by the long-standing convergence history between Eurasia and Perigondwanan terranes. Within this scenario Kopeh Dagh region is a crucial area, which today represents the north-eastern side of the Arabia-Eurasia collision zone, where the convergence is divided into compressional and strike-slip components. This scenario is largely debated by several authors, who mainly focused on active tectonics in the central and eastern part of the chain. This study area had represented a good target for understanding the Post Cimmerian evolution of north-eastern part of the iranian region.

Knowing how the present-day kinematics is not able to explain the curvature of the northern Iran mountain belts, which has been acquired throughout oroclinal bending in a different tectonic regime (Mattei et al., 2017), our investigations confirm that this region represent a key area for defining and for understanding the timing of the tectonic processes which have occurred at the boundary between the Iranian deforming zone and the southern margin of stable Eurasia.

Paleomagnetic results show a homogeneous amount of CW rotations measured in red bed units of both the Lower Cretaceous Shurijeh Fm. and Middle-Late Miocene URF., suggesting that the oroclinal bending process, which occurred in North Iran after the Middle-Late Miocene, also extended to the north-eastern border of the Arabia-Eurasia deforming zone in Iran.

The curvature of the Northern Iran mountain belts is due to the collision of Central Iran with two rigid blocks, the oceanic South Caspian Sea and the continental Turan platform, which represent the southern margin of Eurasia in the area.

Taking together all the data collected in the region (from this work, Bazhenov, 1987; Mattei et al., 2017) it can be affirmed that Eastern Alborz, Binalud-Fariman Mts. and Kopeh Dagh underwent comparable amount of CW rotations in both Cretaceous, Paleocene and Neogene deposits.

The integrations of paleomagnetic analysis with AMS analysis allow to define the tectonic origin of the magnetic lineation in the sampled Formations. In fact, showing the same NW-SE orientation of magnetic lineation, both for Cretaceous and Neogene units, the magnetic fabric investigation confirm how the deformation in the area was dominated mainly by the Arabia-Eurasia collision.

It is proposed that the measured pattern of paleomagnetic rotations has occurred in a tectonic regime different from the present-day one, and that the tectonic reorganization of north-eastern

Iran is relatively young and therefore its rotational pattern cannot be detected using paleomagnetism.

Paleomagnetic rotations occurred between ≈6-4 Ma and ≈2Ma, before the beginning of the westward extrusion of the South Caspian Block caused a drastic change in the tectonic regime of the area. In this reconstruction, the initiation of the northward subduction of the South Caspian Sea underneath the Aspheron Sill (≈ 6-4 Ma) preceded the initiation of strike-slip tectonics in north-eastern Iran (≈ 2Ma), which accompanies the westward movement of the South Caspian block.

Previous paleomagnetic results in northern Iran (Ballato et al., 2008; Cifelli et al., 2015; Mattei et al., 2017) which showed a 15–20° CW rotation for the WNW-ESE oriented western Alborz and Rivand and Samghan fold belts and 20°CCW rotation for the WSW-ENE oriented central Alborz Mts. , has been interpreted as the result of an oroclinal bending process that occurred in the Alborz Mts. after Late Miocene. Our paleomagnetic results from the Kopeh Dagh, Allah Dagh and Binalud-Fariman ranges confirm that the WNW-ESE oriented structure of north-eastern Iran underwent CW rotations after Late Miocene, supporting the oroclinal bending hypothesis of the whole mountain range. Furthermore, the absence of differential rotations in the Shurijeh Fm. and URF excludes that the oroclinal bending processes started earlier than Late Miocene. Our paleomagnetic data also prove that oroclinal bending and CW rotation in north-eastern Iran are not limited to the Alborz Mts. but also extend to the southeast (Binalud Mts.) and to the outer border of the deformation structures related to the Arabia-Eurasia convergence (Kopeh Dagh Mts.)

Another important contribution from this work is represented by the reinterpretation of the previous paleomagnetic data collected by Bazhenov (1987) in the Turkmenistan portion of the Kopeh-Dagh Mountains as part of a new tectonic framework.

No relationships were found between the fold axes orientation and the amount of vertical axis rotations; that absence is interpreted not as a primary curvature of the fold axes but as the consequence of the different tectonic location of the sampled sites. The sites with no or limited amount of CW rotation are located in a restraining bend due to interaction of two segments of the right-lateral Ashkhabad fault, whereas larger CW rotations have been interpreted as the results of block rotations of a left-lateral strike-slip fault system which accommodate the N-S convergence between Iran and Eurasia and the E-W elongation due to the westward extrusion of the South Caspian Block.

REFERENCES

Afshar-Harb, A., 1994. Geology of Kopet Dagh. Treatise Geol. Iran 11, 1–275.

Agard, P., Omrani, J., Jolivet, L., Mouthereau, F., 2005. Convergence history across Zagros (Iran): constraints from collisional and earlier deformation. Int. J. earth Sci. 94, 401–419.

Agard, P., Omrani, J., Jolivet, L., Whitechurch, H., Vrielynck, B., Spakman, W., Monié, P., Meyer, B., Wortel, R., 2011. Zagros orogeny: a subduction-dominated process. Geol. Mag. 148, 692–725.

Aghanabati, A., 2004. Geology of Iran. Geological survey of Iran.

Alavi, M., 1991. Sedimentary and structural characteristics of the Paleo-Tethys remnants in northeastern Iran. Geol. Soc. Am. Bull. 103, 983–992.

Alavi, M., Vaziri, H., Seyed-Emami, K., Lasemi, Y., 1997. The Triassic and associated rocks of the Nakhlak and Aghdarband areas in central and northeastern Iran as remnants of the southern Turanian active continental margin. Geol. Soc. Am. Bull. 109, 1563–1575.

Allen, J.R.L., 1984. Development in sedimentology 30: Sedimentary structures their character and physical basis.

Allen, M., Jackson, J., Walker, R., 2004. Late Cenozoic reorganization of the Arabia-Eurasia collision and the comparison of short-term and long-term deformation rates. Tectonics 23. https://doi.org/10.1029/2003TC001530

Allen, M.B., Blanc, E., Walker, R., Jackson, J., Talebian, M., Ghassemi, M.R., 2006. Contrasting styles of convergence in the Arabia-Eurasia collision: Why escape tectonics does not occur in Iran. Geol. Soc. Am. Spec. Pap. 409, 579–589. https://doi.org/10.1130/2006.2409(26)

Allen, M.B., Ghassemi, M.R., Shahrabi, M., Qorashi, M., 2003. Accommodation of late Cenozoic oblique shortening in the Alborz range, northern Iran. J. Struct. Geol. 25, 659–672.

Allen, M.B., Jones, S., Ismail-Zadeh, A., Simmons, M., Anderson, L., 2002. Onset of subduction as the cause of rapid Pliocene-Quaternary subsidence in the South Caspian basin. Geology 30, 775–778.

Allen, M.B., Kheirkhah, M., Emami, M.H., Jones, S.J., 2011. Right-lateral shear across Iran and kinematic change in the Arabia-Eurasia collision zone. Geophys. J. Int. 184, 555–574. https://doi.org/10.1111/j.1365-246X.2010.04874.x

Ardestani, M.S., Vahidinia, M., Sadeghi, A., Dochev, D., 2012. Integrated biostratigraphy of the Upper Cretaceous Abderaz Formation of the East Kopet Dagh Basin (NE Iran) 21–37.

Aubourg, C., Pozzi, J.-P., Kars, M., 2012. Burial, claystones remagnetization and some consequences for magnetostratigraphy. Geol. Soc. London, Spec. Publ. 371, SP371-4.

Aubourg, C., Smith, B., Eshraghi, A., Lacombe, O., Authemayou, C., Amrouch, K., Bellier, O., Mouthereau, F., 2010. New magnetic fabric data and their comparison with palaeostress markers in the Western Fars Arc (Zagros, Iran): tectonic implications. Leturmy, P., Robin, C. (Eds.), Tecton. Stratigr. Evol. Zagros Makran Dur. Mesozoic–Cenozoic. Geol. Soc. London, Spec. Publ. 330, 97–120. https://doi.org/10.1144/SP330.6

Averbuch, O., de Lamotte, D.F., Kissel, C., 1992. Magnetic fabric as a structural indicator of the deformation path within a fold-thrust structure: a test case from the Corbières (NE Pyrenees, France). J. Struct. Geol. 14, 461–474.

Baas, J.H., Hailwood, E.A., McCaffrey, W.D., Kay, M., Jones, R., 2007. Directional petrological characterisation of deep-marine sandstones using grain fabric and permeability anisotropy: Methodologies, theory, application and suggestions for integration. Earth-Science Rev. 82, 101–142.

https://doi.org/10.1016/j.earscirev.2007.02.003

Bagheri, S., Stampfli, G.M., 2008. The Anarak, Jandaq and Posht-e-Badam metamorphic complexes in central Iran: New geological data, relationships and tectonic implications. Tectonophysics 451, 123–155. https://doi.org/10.1016/j.tecto.2007.11.047

Ballato, P., Nowaczyk, N.R., Landgraf, A., Strecker, M.R., Friedrich, A., Tabatabaei, S.H., 2008. Tectonic control on sedimentary facies pattern and sediment accumulation rates in the Miocene foreland basin of the southern Alborz mountains, northern Iran. Tectonics 27, 1–20. https://doi.org/10.1029/2008TC002278

Ballato, P., Stockli, D.F., Ghassemi, M.R., Landgraf, A., Strecker, M.R., Hassanzadeh, J., Friedrich, A., Tabatabaei, S.H., 2013. Accommodation of transpressional strain in the Arabia-Eurasia collision zone: new constraints from (U-Th)/He thermochronology in the Alborz mountains, north Iran. Tectonics 32, 1–18.

Ballato, P., Uba, C.E., Landgraf, A., Strecker, M.R., Sudo, M., Stockli, D.F., Friedrich, A., Tabatabaei, S.H., 2011. Arabia-Eurasia continental collision: Insights from late Tertiary foreland-basin evolution in the Alborz Mountains, Northern Iran. Bull. Geol. Soc. Am. 123, 106–131. https://doi.org/10.1130/B30091.1

Banerjee, S., Elmore, R.D., Engel, M.H., 1997. Chemical remagnetization and burial diagenesis: testing the hypothesis in the Pennsylvanian Belden Formation, Colorado. J. Geophys. Res. Solid Earth 102, 24825–24842.

Bazhenov, M.L., 1987. Paleomagnetism of Cretaceous and Paleogene sedimentary rocks from the Kopet-Dagh and its tectonic implications. Tectonophysics 136, 223–235. https://doi.org/10.1016/0040-1951(87)90026-6

Berberian, M., 1983. The southern Caspian: a compressional depression floored by a trapped, modified oceanic crust. Can. J. Earth Sci. 20, 163–183.

Berberian, M., King, G.C.P., 1981. Towards a paleogeography and tectonic evolution of Iran. Can. J. Earth Sci. 18, 210–265.

Besse, J., Courtillot, V., 2002. Apparent and true polar wander and the geometry of the geomagnetic field over the last 200 Myr. J. Geophys. Res. Solid Earth 107, EPM-6.

Besse, J., Torcq, F., Gallet, Y., Ricou, L.E., Krystyn, L., Saidi, A., 1998. Late Permian to late Triassic palaeomagnetic data from Iran: constraints on the migration of the Iranian block through the Tethyn Ocean and initial destruction of Pangea. Geophys. J. Int. 135, 77–92. https://doi.org/10.1046/j.1365-246X.1998.00603.x

Bina, M.M., Bucur, I., Prevot, M., Meyerfeld, Y., Daly, L., Cantagrel, J.M., Mergoil, J., 1986. Palaeomagnetism, petrology and geochronology of tertiary magmatic and sedimentary units from Iran. Tectonophysics 121, 303–329.

Blumstein, A.M., Elmore, R.D., Engel, M.H., Elliot, C., Basu, A., 2004. Paleomagnetic dating of burial diagenesis in Mississippian carbonates, Utah. J. Geophys. Res. Solid Earth 109.

Borradaile, G.J., 1988. Magnetic-susceptibility, petrofabrics and strain. Tectonophysics 156, 1–20. https://doi.org/10.1016/0040-1951(88)90279-x

Borradaile, G.J., Fralick, P.W., Lagroix, F., 1999. Acquisition of anhysteretic remanence and tensor subtraction from AMS isolates true palaeocurrent grain alignments. Geol. Soc. London, Spec. Publ. 151, 139–145.

Borradaile, G.J., Henry, B., 1997. Tectonic applications of magnetic susceptibility and its anisotropy. Earth-Science Rev. 42, 49–93.

Borradaile, G.J., Jackson, M., 2004. Anisotropy of magnetic susceptibility (AMS): magnetic petrofabrics of deformed rocks. Geol. Soc. London, Spec. Publ. 238, 299–360.

Borradaile, G.J., Tarling, D., 1984. Strain partitioning and magnetic fabrics in particulate flow. Can. J. Earth Sci. 21, 694–697.

Borradaile, G.J., Tarling, D.H., 1981. The influence of deformation mechanisms on magnetic fabrics in weakly deformed rocks. Tectonophysics 77, 151–168. https://doi.org/10.1016/0040-1951(81)90165-7

Bretis, B., Grasemann, B., Conradi, F., 2012. An active fault zone in the Western Kopeh Dagh (Iran). Austrian J. Earth Sci. 105, 95–107.

Bröcker, M., Rad, G.F., Burgess, R., Theunissen, S., Paderin, I., Rodionov, N., Salimi, Z., 2013. New age constraints for the geodynamic evolution of the Sistan Suture Zone, eastern Iran. Lithos 170, 17–34.

Brunet, M.-F., Korotaev, M. V, Ershov, A. V, Nikishin, A.M., 2003. The South Caspian Basin: a review of its evolution from subsidence modelling. Sediment. Geol. 156, 119–148.

Butler, R., 1998. Paleomagnetism: Magnetic domains to geologic terranes. Electron. Ed. 319. https://doi.org/10.1006/icar.2001.6754

Chadima, M., Hrouda, F., 2006. Remasoft 3.0 a user-friendly paleomagnetic data browser and analyzer. Trav. Géophysiques 27, 20–21.

Cifelli, F., Ballato, P., Alimohammadian, H., Sabouri, J., Mattei, M., 2015. Tectonic magnetic lineation and oroclinal bending of the Alborz range: Implications on the Iran-Southern Caspian geodynamics. Tectonics 34, 116–132.

Cifelli, F., Mattei, M., Chadima, M., Hirt, A.M., Hansen, A., 2005. The origin of tectonic lineation in extensional basins: Combined neutron texture and magnetic analyses on "undeformed" clays. Earth Planet. Sci. Lett. 235, 62–78. https://doi.org/10.1016/j.epsl.2005.02.042

Cifelli, F., Mattei, M., Chadima, M., Lenser, S., Hirt, A.M., 2009. The magnetic fabric in "undeformed clays": AMS and neutron texture analyses from the Rif Chain (Morocco). Tectonophysics 466, 79–88. https://doi.org/10.1016/j.tecto.2008.08.008

Cifelli, F., Mattei, M., Della Seta, M., 2008. Calabrian Arc oroclinal bending: The role of subduction. Tectonics 27.

Cifelli, F., Mattei, M., Hirt, A.M., Günther, A., 2004. The origin of tectonic fabrics in "undeformed" clays: The early stages of deformation in extensional sedimentary basins. Geophys. Res. Lett. 31.

Cifelli, F., Mattei, M., Rashid, H., Ghalamghash, J., 2013. Right-lateral transpressional tectonics along the boundary between lut and tabas blocks (central iran). Geophys. J. Int. 193, 1153–1165. https://doi.org/10.1093/gji/ggt070

Cox, A., Doell, R.R., Dalrymple, G.B., 1963. Geomagnetic polarity epochs and Pleistocene geochronometry. Nature 198, 1049.

Creer, K.M., Irving, E., Runcorn, S.K., 1954. The direction of the geomagnetic field in remote epochs in Great Britain. J. Geomagn. Geoelectr. 6, 163–168.

Debacker, T.N., Hirt, A.M., Sintubin, M., Robion, P., 2009. Tectonophysics Differences between magnetic and mineral fabrics in low-grade , cleaved siliciclastic pelites : A case study from the Anglo-Brabant Deformation Belt (Belgium). Tectonophysics 466, 32–46. https://doi.org/10.1016/j.tecto.2008.09.039

Dercourt, J., Zonenshain, L.P., Ricou, L.E., Kazmin, V.G., Le Pichon, X., Knipper, A.L., Grandjacquet, C., Sbortshikov, I.M., Geyssant, J., Lepvrier, C., Pechersky, D.H., Boulin, J., Sibuet, J.C., Savostin, L.A.,

Sorokhtin, O., Westphal, M., Bazhenov, M.L., Lauer, J.P., Biju-Duval, B., 1986. Geological evolution of the tethys belt from the atlantic to the pamirs since the LIAS. Tectonophysics 123, 241–315. https://doi.org/10.1016/0040-1951(86)90199-X

Djamour, Y., Vernant, P., Bayer, R., Nankali, H.R., Ritz, J.-F., Hinderer, J., Hatam, Y., Luck, B., Le Moigne, N., Sedighi, M., 2010. GPS and gravity constraints on continental deformation in the Alborz mountain range, Iran. Geophys. J. Int. 183, 1287–1301.

Dubey, A.K., 2014. Anisotropy of magnetic susceptibility, in: Understanding an Orogenic Belt. Springer, pp. 17–34.

Dunlop, D.J., 1972. Magnetic mineralogy of unheated and heated red sediments by coercivity spectrum analysis. Geophys. J. R. Astron. Soc. 27, 37–55.

Dunlop, D.J., Özdemir, Ö., 2001. Rock magnetism: fundamentals and frontiers. Cambridge university press.

Eldredge, S., Bachtadse, V., Van der Voo, R., 1985. Paleomagnetism and the orocline hypothesis. Tectonophysics 119, 153–179.

Ellwood, B.B., 1980. Induced and remanent magnetic properties of marine sediments as indicators of depositional processes. Mar. Geol. 38, 233–244. https://doi.org/10.1016/0025-3227(80)90061-4

Felletti, F., Dall'Olio, E., Muttoni, G., 2016. Determining flow directions in turbidites: An integrated sedimentological and magnetic fabric study of the Miocene Marnoso Arenacea Formation (northern Apennines, Italy). Sediment. Geol. 335, 197–215. https://doi.org/10.1016/j.sedgeo.2016.02.009

Ferré, B., Honarmand, A., Ghaderi, A., Vahidinia, M., 2016. Saccocomid remains (Crinoidea, Roveacrinida, Saccocomidae) in the uppermost Santonian-Campanian deposits (Abtalkh Formation) from the Kopet-Dagh Range (NE Iran), in: Annales de Paléontologie. Elsevier, pp. 69–77.

Fisher, R.A., 1953. Dispersion on a sphere. Proc. R. Soc. Lond. A 217, 295–305.

Freund, R., 1970. Rotation of strike slip faults in Sistan, southeast Iran. J. Geol. 78, 188–200.

Fuller, M., 1969. Magnetic orientation of borehole cores. Geophysics 34, 772–774.

Fürsich, F.T., Wilmsen, M., Seyed-Emami, K., Cecca, F., Majidifard, M.R., 2005. The upper Shemshak Formation (Toarcian–Aalenian) of the Eastern Alborz (Iran): Biota and palaeoenvironments during a transgressive–regressive cycle. Facies 51, 365–384.

Fürsich, F.T., Wilmsen, M., Seyed-Emami, K., Majidifard, M.R., 2009a. Lithostratigraphy of the Upper Triassic–Middle Jurassic Shemshak Group of Northern Iran. Geol. Soc. London, Spec. Publ. 312, 129–160. https://doi.org/10.1144/SP312.6

Fürsich, F.T., Wilmsen, M., Seyed-Emami, K., Majidifard, M.R., 2009b. The Mid-Cimmerian tectonic event (Bajocian) in the Alborz Mountains, Northern Iran: evidence of the break-up unconformity of the South Caspian Basin. Geol. Soc. London, Spec. Publ. 312, 189–203. https://doi.org/10.1144/SP312.9

Fürsich, F.T., Wilmsen, M., Seyed-Emami, K., Schairer, G., Majidifard, M.R., 2003. Platform-basin transect of a Middle to Late Jurassic large-scale carbonate platform system (Shotori Mountains, Tabas area, east-central Iran). Facies 48, 171.

Ganser, A., Huber, H., 1962. Geological observations in the central Elburz, Iran, Schweiz miner. Petrogy. Mitt 42, 583–630.

Garzanti, E., Gaetani, M., 2002. Unroofing history of Late Paleozoic magmatic arcs within the '" Turan Plate "' (Tuarkyr , Turkmenistan) 151, 67–87.

Ghasemi, A., Talbot, C.J., 2006. A new tectonic scenario for the Sanandaj – Sirjan Zone (Iran) 26, 683–693. https://doi.org/10.1016/j.jseaes.2005.01.003

Gough, D.I., 1956. A study of the palaeomagnetism of the Pilansberg dykes. Geophys. Suppl. to Mon. Not. R. Astron. Soc. 7, 196–213.

Graham, J.W., 1966. Significance of Magnetic Anisotropy in Appalachian Sedimentary Rocks 10, 627–648. https://doi.org/10.1029/GM010p0627

Graham, J.W., 1954. Rock magnetism and the earth's magnetic field during Paleozoic time. J. Geophys. Res. 59, 215–222.

Graham, J.W., 1949. The stability and significance of magnetism in sedimentary rocks. J. Geophys. Res. 54, 131–167.

Guest, B., Axen, G.J., Lam, P.S., Hassanzadeh, J., 2006a. Late Cenozoic shortening in the west-central Alborz Mountains, northern Iran, by combined conjugate strike-slip and thin-skinned deformation. Geosphere 2, 35–52.

Guest, B., Stockli, D.F., Grove, M., Axen, G.J., Lam, P.S., Hassanzadeh, J., 2006b. Thermal histories from the central Alborz Mountains, northern Iran: Implications for the spatial and temporal distribution of deformation in northern Iran. Geol. Soc. Am. Bull. 118, 1507–1521.

Hadavi, F., Khodadadi, L., 2013. Nannostratigraphy and palaeoecology of uppermost Mozduran Formation in the Kopeh-Dagh range (NE Iran). https://doi.org/10.1007/s12517-013-0839-z

Hamilton, N., Rees, A.I., 1970. The use of magnetic fabric in paleocurrent estimation. Palaeogeophysics 445, 464.

Heidari, A., Shokri, N., Ghasemi-Nejad, E., Gonzales, L., Ludvigson, G., 2015. Application of petrography, major and trace elements, carbon and oxygen isotope geochemistry to reconstruction of diagenesis of carbonate rocks of the Sanganeh Formation (Lower Cretaceous), East Kopet-Dagh Basin, NE Iran. Arab. J. Geosci. 8, 4949–4967.

Heirtzler, J.R., Dickson, G.O., Herron, E.M., Pitman, W.C., Le Pichon, X., 1968. Marine magnetic anomalies, geomagnetic field reversals, and motions of the ocean floor and continents. J. Geophys. Res. 73, 2119–2136.

Hirt, M., Evans, F., Engelder, T., 1995. Correlation between magnetic anisotropy and fabric for Devonian shales on the Appalachian Plateau 247, 121–132.

Hollingsworth, J., Fattahi, M., Walker, R., Talebian, M., Bahroudi, A., Bolourchi, M.J., Jackson, J., Copley, A., 2010. Oroclinal bending, distributed thrust and strike-slip faulting, and the accommodation of Arabia-Eurasia convergence in NE Iran since the Oligocene. Geophys. J. Int. 181, 1214–1246. https://doi.org/10.1111/j.1365-246X.2010.04591.x

Hollingsworth, J., Jackson, J., Walker, R., Nazari, H., 2008. Extrusion tectonics and subduction in the easter South Caspian region since 10 Ma. Geology 36, 763–766. https://doi.org/10.1130/G25008A.1

Hollingsworth, J., Jackson, J., Walker, R., Reza Gheitanchi, M., Javad Bolourchi, M., 2006. Strike-slip faulting, rotation, and along-strike elongation in the Kopeh Dagh mountains, NE Iran. Geophys. J. Int. 166, 1161–1177. https://doi.org/10.1111/j.1365-246X.2006.02983.x

Horton, B.K., Hassanzadeh, J., Stockli, D.F., Axen, G.J., Gillis, R.J., Guest, B., 2008. Detrital zircon provenance of Neoproterozoic to Cenozoic deposits in Iran : Implications for chronostratigraphy and collisional tectonics 451, 97–122. https://doi.org/10.1016/j.tecto.2007.11.063

Housen, B.A., Pluijm, B.A., 1991. Slaty cleavage development and magnetic anisotropy fabrics. J. Geophys. Res. Solid Earth 96, 9937–9946.

Housen, B.A., Van Der Pluijm, B.A., Essene, E.J., 1995. Plastic behavior of magnetite and high strains obtained from magnetic fabrics in the Parry Sound shear zone, Ontario Grenville Province. J. Struct. Geol. 17, 265–278.

Hrouda, F.E.K., 1982. MAGNETIC ANISOTROPY OF ROCKS AND ITS APPLICATION 5, 37–82.

Ihmlé, P.F., Hirt, A.M., Lowrie, W., Dietrich, D., 1989. Inverse magnetic fabric in deformed limestones of the Morcles Nappe, Switzerland. Geophys. Res. Lett. 16, 1383–1386.

Irving, E., 1964. Paleomagnetism and its application to geological and geophysical problems. Wiley.

Irving, E., 1957. Rock magnetism: a new approach to some palaeogeographic problems. Adv. Phys. 6, 194–218.

Irving, E., 1956. Palaeomagnetic and palaeoclimatological aspects of polar wandering. Pure Appl. Geophys. 33, 23–41.

Ising, G., 1943. On the Magnetic Properties of Varved Clay: Line of Investigations. Almqvist & Wiksells.

Jackson, J., Jackson, J., Priestley, K., Priestley, K., Allen, M., Allen, M., Berberian, M., Berberian, M., 2002. Active tectonics of the South Caspian Basin. Geophys. J. Int. 214–245.

Jackson, J., McKenzie, D., 1984. Active tectonics of the Alpine—Himalayan Belt between western Turkey and Pakistan. Geophys. J. Int. 77, 185–264.

Jackson, M., Tauxe, L., 1991. Anisotropy of Magnetic Susceptibility and Remanence: Developments in the Characterization of Tectonic, Sedimentary and Igneous Fabric. Rev. Geophys. Natl. Rep. To Int. Union Geod. Geophys. 371–376. https://doi.org/10.1002/rog.1991.29.s1.371

Jelinek, V., 1981. Characterization of the magnetic fabric of rocks. Tectonophysics 79, 63–67. https://doi.org/10.1016/0040-1951(81)90110-4

Jelínek, V., Pokorný, J., 1997. Some new concepts in technology of transformer bridges for measuring susceptibility anisotropy of rocks. Phys. Chem. Earth 22, 179–181.

Jezek, J., Hrouda, F., 2004. Determination of the orientation of magnetic minerals from the anisotropy of magnetic susceptibility. Geol. Soc. London, Spec. Publ. 238, 9–20.

Kadinsky-Cade, K., Barazangi, M., Oliver, J., Isacks, B., 1981. Lateral variations of high-frequency seismic wave propagation at regional distances across the Turkish and Iranian plateaus. J. Geophys. Res. Solid Earth 86, 9377–9396.

Kalanat, B., Vahidinia, M., Vaziri-moghaddam, H., 2017. Journal of African Earth Sciences Benthic foraminiferal response to environmental changes across Cenomanian / Turonian boundary (OAE2) in the northeastern Tethys , Kopet-Dagh basin. J. African Earth Sci. 134, 33–47. https://doi.org/10.1016/j.jafrearsci.2017.05.019

Kalantari, A., 1987. Biofacies map of Kopet Dagh region. NIOC Explor. Prod. 1.

Katz, B., Elmore, R.D., Cogoini, M., Ferry, S., 1998. Widespread chemical remagnetization: Orogenic fluids or burial diagenesis of clays? Geology 26, 603–606.

Kavoosi, M.A., Lasemi, Y., Sherkati, S., Moussavi-harami, R., 2009. Facies analysis and depositional sequences of the Upper Jurassic Mozduran Formation, a carbonate reservoir in the Kopet Dagh Basin, NE Iran. J. Pet. Geol. 32, 235–259. https://doi.org/10.1111/j.1747-5457.2009.00446.x

Kavoosi, M.A.L.I., 2015. Depositional systems and sequence stratigraphy analysis of the Upper Callovian to Tithonian sediments in the Central and Western Kopet-Dagh Basin , Northeast Iran. https://doi.org/10.1002/gj.2648

Kent, D. V, 1985. Thermoviscous remagnetization in some Appalachian limestones. Geophys. Res. Lett. 12, 805–808.

Kent, D. V, Irving, E., 2010. Influence of inclination error in sedimentary rocks on the Triassic and Jurassic apparent pole wander path for North America and implications for Cordilleran tectonics. J. Geophys. Res. Solid Earth 115.

Kissel, C., 1986. the main compressive stress • 1 inferred from previous 5, 769–781.

Kissel, C., Barrier, E., Laj, C., Lee, T., 1986. Magnetic fabric in "undeformed" marine clays from compressional zones. Tectonics 5, 769–781.

Kissel, C., Laj, C., 1988. The Tertiary geodynamical evolution of the Aegean arc: a paleomagnetic reconstruction. Tectonophysics 146, 183–201.

Kissel, C., Laj, C., Mazaud, A., Dokken, T., 1998. Magnetic anisotropy and environmental changes in two sedimentary cores from the Norwegian Sea and the North Atlantic 164, 617–626.

Kligfield, R., Lowrie, W., Hirt, A., Siddans, A.W.B., 1983. Effect of progressive deformation on remanent magnetization of Permian redbeds from the Alpes Maritimes (France). Tectonophysics 98, 59–85.

Kligfield, R., Owens, W.H., Lowrie, W., 1981. Magnetic susceptibility anisotropy, strain, and progressive deformation in Permian sediments from the Maritime Alps (France) Roy Kligfield 1,2, W.H. Owens 3 and W. Lowrie 2 55, 181–189.

Langereis, C.G., Krijgsman, W., Muttoni, G., Menning, M., 2010. Magnetostratigraphy–concepts, definitions, and applications. Newsletters Stratigr. 43, 207–233.

Lanza, R., Meloni, A., 2006. The Earth's magnetism. Springer.

Larrasoaña, J.C., Pueyo, E.L., Parés, J.M., 2004. An integrated AMS, structural, palaeo-and rock-magnetic study of Eocene marine marls from the Jaca-Pamplona basin (Pyrenees, N Spain); new insights into the timing of magnetic fabric acquisition in weakly deformed mudrocks. Geol. Soc. London, Spec. Publ. 238, 127–143.

Lasemi, Y., 1995. Platform carbonates of the Upper Jurassic Mozduran Formation in the Kopet Dagh basin, NE Iran—facies, palaeoenvironments and sequences. Sediment. Geol. 99, 151–164.

Lee, T.-Q., Kissel, C., Laj, C., Horng, C.-S., Lue, Y.-T., 1990. Magnetic fabric analysis of the Plio-Pleistocene sedimentary formations of the Coastal Range of Taiwan. Earth Planet. Sci. Lett. 98, 23–32.

Lowrie, W., 2007. Fundamentals of geophysics. Cambridge university press.

Lowrie, W., 1990. Identification of ferromagnetic minerals in a rock by coercivity and unblocking temperature properties. Geophys. Res. Lett. 17, 159–162. https://doi.org/10.1029/GL017i002p00159

Lowrie, W., Hirt, A.M., 1987. Anisotropy of magnetic susceptibility in the Scaglia Rossa pelagic limestone ~ Stumps 82, 349–356.

Lowrie, W., Hirt, A.M., 1986. Paleomagnetism in arcuate mountain belts, in: Developments in Geotectonics. Elsevier, pp. 141–158.

Lüneburg, C.M., Lampert, S.A., Lebit, H.D., Hirt, A.M., Casey, M., Lowrie, W., 1999. Magnetic anisotropy, rock fabrics and finite strain in deformed sediments of SW Sardinia (Italy). Tectonophysics 307, 51–74.

Luo, L., Jia, D., Li, H., Li, Y., Deng, F., Chen, Z., Jia, Q., Sun, S., Zhang, Y., 2009. Magnetic fabric investigation in the northwestern Sichuan Basin and its regional inference. Phys. Earth Planet. Inter.

173, 103–114. https://doi.org/10.1016/j.pepi.2008.11.004

Lyberis, N., Manby, G., 1999. Oblique to orthogonal convergence across the Turan block in the post-Miocene. Am. Assoc. Pet. Geol. Bull. 83, 1135–1160.

Madanipour, S., Ehlers, T.A., Yassaghi, A., Rezaeian, M., Enkelmann, E., Bahroudi, A., 2013. Synchronous deformation on orogenic plateau margins: Insights from the Arabia–Eurasia collision. Tectonophysics 608, 440–451.

Maggi, A., Priestley, K., 2005. Surface waveform tomography of the Turkish–Iranian plateau. Geophys. J. Int. 160, 1068–1080.

Mahboubi, A., Moussavi-Harami, R., Lasemi, Y., Brenner, R.L., 2001. Sequence stratigraphy and sea level history of the upper Paleocene strata in the Kopet-Dagh basin, northeastern Iran. Am. Assoc. Pet. Geol. Bull. 85, 839–860.

Marshak, S., 1988. Kinematics of orocline and arc formation in thin-skinned orogens. Tectonics 7, 73–86.

Mattei, M., Cifelli, F., Alimohammadian, H., Rashid, H., Winkler, A., Sagnotti, L., 2017. Oroclinal bending in the Alborz Mountains (Northern Iran): New constraints on the age of South Caspian subduction and extrusion tectonics. Gondwana Res. 42, 13–28. https://doi.org/10.1016/j.gr.2016.10.003

Mattei, M., Cifelli, F., Muttoni, G., Rashid, H., 2015. Post-Cimmerian (Jurassic-Cenozoic) paleogeography and vertical axis tectonic rotations of Central Iran and the Alborz Mountains. J. Asian Earth Sci. 102, 92–101. https://doi.org/10.1016/j.jseaes.2014.09.038

Mattei, M., Cifelli, F., Muttoni, G., Zanchi, A., Berra, F., Mossavvari, F., Eshraghi, S.A., 2012. Neogene block rotation in central Iran: Evidence from paleomagnetic data. Bull. Geol. Soc. Am. 124, 943–956. https://doi.org/10.1130/B30479.1

Mattei, M., Funiciello, R., Kissel, C., 1995. Paleomagnetic and structural evidence for Neogene block rotations in the Central Apennines, Italy. J. Geophys. Res. Solid Earth 100, 17863–17883.

Mattei, M., Muttoni, G., Cifelli, F., 2014. A record of the Jurassic massive plate shift from the Garedu Formation of central Iran. Geology 42, 555–558. https://doi.org/10.1130/G35467.1

Mattei, M., Petrocelli, V., Lacava, D., Schiattarella, M., 2004. Geodynamic implications of Pleistocene ultrarapid vertical-axis rotations in the Southern Apennines, Italy. Geology 32, 789–792.

Mattei, M., Sagnotti, L., Faccenna, C., Funiciello, R., 1997. Magnetic fabric of weakly deformed clay-rich sediments in the Italian peninsula: relationship with compressional and extensional tectonics. Tectonophysics 271, 107–122.

Mattei, M., Speranza, F., Argentieri, A., Rossetti, F., Sagnotti, L., Funiciello, R., 1999. Extensional tectonics in the Amantea basin (Calabria, Italy): a comparison between structural and magnetic anisotropy data. Tectonophysics 307, 33–49.

Matuyama, M., 1929. On the direction of magnetisation of basalt in Japan, Tyosen and Manchuria. Proc. Imp. Acad. 5, 203–205.

McClusky, S., Balassanian, S., Barka, A., Demir, C., Ergintav, S., Georgiev, I., Gurkan, O., Hamburger, M., Hurst, K., Kahle, H., Kastens, K., Kekelidze, G., King, R., Kotzev, V., Lenk, O., Mahmoud, S., Mishin, A., Nadariya, M., Ouzounis, A., Paradissis, D., Peter, Y., Prilepin, M., Reilinger, R., Sanli, I., Seeger, H., Tealeb, A., Toksöz, M.N., Veis, G., 2000. Global Positioning System constraints on plate kinematics and dynamics in the eastern Mediterranean and Caucasus. J. Geophys. Res. Solid Earth 105, 5695–5719. https://doi.org/10.1029/1999JB900351

McDougall, I., Tarling, D.H., 1963. Dating of polarity zones in the Hawaiian Islands. Nature 200, 54.

McElhinny, M.W., McFadden, P.L., 1999. Paleomagnetism: continents and oceans. Academic Press.

McKenzie, D., Jackson, J., 1986. A block model of distributed deformation by faulting. J. Geol. Soc. London. 143, 349–353.

Mercanton, P.-L., 1926. Inversion de l'inclinaison magnétique terrestre aux âges géologiques. J. Geophys. Res. 31, 187–190.

Moheghy, M.A., Hadavi, F., 2014. Nannostratigraphy and Palaeoecology of the Uppermost Mozduran Formation in the Jozak Section in West Kopet-Dagh (NE Iran) 2014, 12–19.

Moheghy, M.A., Hadavi, F., Rahimi, B., 2013. Investigation of the Boundary between Abderaz and Kalat Formations Based on Calcareous Nannofossils in West Kopet-Dagh (NE IRAN) 2013, 178–186. https://doi.org/10.4236/ojg.2013.33021

Morris, A., 2003. A palaeomagnetic and rock magnetic glossary. Tectonophysics 377, 211–228.

Mortazavi, M., Moussavi-Harami, R., Mahboubi, A., Nadjafi, M., 2014. Geochemistry of the Late Jurassic–Early Cretaceous shales (Shurijeh Formation) in the intracontinental Kopet-Dagh Basin, northeastern Iran: implication for provenance, source weathering, and paleoenvironments. Arab. J. Geosci. 7, 5353–5366. https://doi.org/10.1007/s12517-013-1081-4

Mousavi, Z., Walpersdorf, A., Walker, R.T., Tavakoli, F., Pathier, E., Nankali, H., Nilfouroushan, F., Djamour, Y., 2013. Global Positioning System constraints on the active tectonics of NE Iran and the South Caspian region. Earth Planet. Sci. Lett. 377, 287–298.

Moussaid, B., El Ouardi, H., Casas-Sainz, A., Villalaín, J.J., Román-Berdiel, T., Oliva-Urcia, B., Soto, R., Torres-López, S., 2013. Magnetic fabrics in the Jurassic–Cretaceous continental basins of the northern part of the Central High Atlas (Morocco): Geodynamic implications. J. African Earth Sci. 87, 13–32.

Moussavi-Harami, R., Brenner, R.L., 1992. Geohistory Analysis and Petroleum Reservoir Characteristics of Lower Cretaceous (Neocomian) Sandstones, Eastern Kopet-Dagh Basin, Northeastern Iran (1). Am. Assoc. Pet. Geol. Bull. 76, 1200–1208.

Moussavi-Harami, R., Brenner, R.L., 1990. Lower cretaceous (Neocomian) fluvial deposits in eastern Kopet-Dagh Basin, northeastern Iran. Cretac. Res. 11, 163–174. https://doi.org/10.1016/S0195-6671(05)80031-X

Moussavi-Harami, R., Mahboubi, A., Nadjafi, M., Brenner, R.L., Mortazavi, M., 2009. Mechanism of calcrete formation in the Lower Cretaceous (Neocomian) fluvial deposits, northeastern Iran based on petrographic, geochemical data. Cretac. Res. 30, 1146–1156. https://doi.org/10.1016/j.cretres.2009.04.003

Moussavi-Harami, R., Brenner, R.L., 1993. Diagenesis of Non-Marine Petroleum Reservoirs: the Neocomian (Lower Cretaceous) Shurijeh Formation, Kopet-Dagh Basin, Ne Iran. J. Pet. Geol. 16, 55–72. https://doi.org/10.1111/j.1747-5457.1993.tb00730.x

Muttoni, G., Dallanave, E., Channell, J.E.T., 2013. The drift history of Adria and Africa from 280 Ma to Present, Jurassic true polar wander, and zonal climate control on Tethyan sedimentary facies. Palaeogeogr. Palaeoclimatol. Palaeoecol. 386, 415–435.

Muttoni, G., Erba, E., Kent, D. V, 2005. Mesozoic Alpine facies deposition as a result of past latitudinal plate motion 59–63. https://doi.org/10.1038/nature03310.1.

Muttoni, G., Gaetani, M., Kent, D. V., Sciunnach, D., Angiolini, L., Berra, F., Garzanti, E., Mattei, M., Zanchi, A., 2009a. Opening of the Neo-tethys ocean and the pangea B to pangea A transformation during the permian. GeoArabia 14, 17–48.

Muttoni, G., Mattei, M., Balini, M., Zanchi, A., Gaetani, M., Berra, F., 2009b. The drift history of Iran

from the Ordovician to the Triassic. Geol. Soc. London, Spec. Publ. 312, 7–29. https://doi.org/10.1144/SP312.2

Nur, A., Ron, H., 1987. Block rotations, fault domains and crustal deformation, in: Annales Tectonicae. pp. 40–47.

Nur, A., Ron, H., Scotti, O., 1989. Mechanics of distributed fault and block rotation, in: Paleomagnetic Rotations and Continental Deformation. Springer, pp. 209–228.

Oldow, J.S., Channell, J.E.T., Catalano, R., D'argenio, B., 1990. Contemporaneous thrusting and large-scale rotations in the western Sicilian fold and thrust belt. Tectonics 9, 661–681.

Oliva-Urcia, B., Larrasoaña, J.C., Pueyo, E.L., Gil, A., Mata, P., Parés, J.M., Schleicher, A.M., Pueyo, O., 2009. Disentangling magnetic subfabrics and their link to deformation processes in cleaved sedimentary rocks from the Internal Sierras (west central Pyrenees, Spain). J. Struct. Geol. 31, 163–176.

Opdyke, M.D., Channell, J.E.T., 1996. Magnetic stratigraphy. Academic press.

Opdyke, N.D., 1995. Paleomagnetism, polar wandering, and the rejuvenation of crustal mobility. J. Geophys. Res. Solid Earth 100, 24361–24366.

Opdyke, N.D., Henry, K.W., 1969. A test of the dipole hypothesis. Earth Planet. Sci. Lett. 6, 139–151.

Owens, W.H., Bamford, D., 1976. A Discussion on natural strain and geological structure-Magnetic, seismic, and other anisotropic properties of rock fabrics. Phil. Trans. R. Soc. Lond. A 283, 55–68.

Parés, J.M., 2004. How deformed are weakly deformed mudrocks? Insights from magnetic anisotropy. Geol. Soc. London, Spec. Publ. 238, 191–203.

Parés, J.M., Dinarés-Turell, J., 1993. Magnetic fabric in two sedimentary rock-types from the southern Pyrenees. J. Geomagn. Geoelectr. 45, 193–205.

Parés, J.M., Van Der Pluijm, B.A., 2002. Evaluating magnetic lineations (AMS) in deformed rocks. Tectonophysics 350, 283–298.

Pares, J.P., Van Der Pluijm, B.A., Dinarès-Turell, J., 1999. Evolution of magnetic fabric during incipient deformation of mudrock (Pyrenees, northen Spain). Tectonophysics 307, 1–14.

Paterson, S.R., Yu, H., Oertel, G., 1995. Primary and tectonic fabric intensities in mudrocks 247, 105–119.

Philip, H., Cisternas, A., Gvishiani, A., Gorshkov, A., 1989. The Caucasus: an actual example of the initial stages of continental collision. Tectonophysics 161, 1–21.

Pierre, F. Dela, Ghisetti, F., Lanza, R., Vezzani, L., 1992. Palaeomagnetic and structural evidence of Neogene tectonic rotation of the Gran Sasso range (central Apennines, Italy). Tectonophysics 215, 335–348.

Piper, J.D.A., Elliot, M.T., Kneller, B.C., 1996. Anisotropy of magnetic susceptibility in a Palaeozoic flysch basin: The Windermere Supergroup, northern England. Sediment. Geol. 106, 235–258. https://doi.org/10.1016/S0037-0738(96)00011-5

Poursoltani, M.R., Moussavi-Harami, R., Gibling, M.R., 2007. Jurassic deep-water fans in the Neo-Tethys Ocean: the Kashafrud Formation of the Kopet-Dagh basin, Iran. Sediment. Geol. 198, 53–74.

Pueyo Anchuela, Ó., Ramajo Cordero, J., Gil Imaz, A., Meléndez Hevia, G., 2013. Analysis of anisotropy of magnetic susceptibility in iron-oolitic beds: A potential tool for paleocurrent identification. Int. J. Earth Sci. 102, 1131–1149. https://doi.org/10.1007/s00531-012-0848-2

Raisossadat, N., Moussavi-Harami, R., 2000. Lithostratigraphic and facies analyses of the Sarcheshmeh Formation (Lower Cretaceous) in the eastern Kopet Dagh Basin, NE Iran. Cretac. Res. 21, 507–516. https://doi.org/10.1006/cres.2000.0216

Raisossadat, S.N., 2006. The ammonite family Parahoplitidae in the Sanganeh Formation of the Kopet Dagh Basin , north-eastern Iran 27. https://doi.org/10.1016/j.cretres.2006.04.003

Rees, A.I., 1965. THE USE OF ANISOTROPY OF MAGNETIC SUSCEPTIBILITY IN THE ESTIMATION OF SEDIMENTARY FABRIC 1. Sedimentology 4, 257–271.

Rezaeian, M., Carter, A., Hovius, N., Allen, M.B., 2012. Cenozoic exhumation history of the Alborz Mountains, Iran: New constraints from low-temperature chronometry. Tectonics 31.

Richter, C., van der Pluijm, B.A., Housen, B.A., 1993. The quantification of crystallographic preferred orientation using magnetic anisotropy. J. Struct. Geol. 15, 113–116. https://doi.org/10.1016/0191-8141(93)90082-L

Ritz, J.-F., 2009. Extrusion tectonics and subduction in the eastern South Caspian region since 10 Ma: COMMENT. Geology 37, e191–e191.

Ritz, J.-F., Nazari, H., Ghassemi, A., Salamati, R., Shafei, A., Solaymani, S., Vernant, P., 2006. Active transtension inside central Alborz: A new insight into northern Iran–southern Caspian geodynamics. Geology 34, 477–480.

Rivandi, B., Vahidinia, M., Nadjafi, M., Mahboubi, A., Sadeghi, A., 2013. Biostratigraphy and Sequence Stratigraphy of Paleogene Deposits in Central Kopet-Dagh Basin (NE of Iran) 2013.

Robert, A.M.M., Letouzey, J., Kavoosi, M.A., Sherkati, S., Müller, C., Vergés, J., Aghababaei, A., 2014. Structural evolution of the Kopeh Dagh fold-and-thrust belt (NE Iran) and interactions with the South Caspian Sea Basin and Amu Darya Basin. Mar. Pet. Geol. 57, 68–87. https://doi.org/10.1016/j.marpetgeo.2014.05.002

Robertson, A.H.F., 2000. Mesozoic-Tertiary tectonic-sedimentary evolution of a south Tethyan oceanic basin and its margins in southern Turkey. Geol. Soc. London, Spec. Publ. 173, 97–138.

Rochette, P., 1987. Magnetic susceptibility of the rock matrix related to magnetic fabric studies. J. Struct. Geol. 9, 1015–1020. https://doi.org/10.1016/0191-8141(87)90009-5

Rochette, P., Fillion, G., 1988. Identification of multicomponent anisotropies in rocks using various field and temperature values in a cryogenic magnetometer. Phys. Earth Planet. Inter. 51, 379–386.

Rochette, P., Jackson, M., Aubourg, C., 1992. Rock magnetism and the interpretation of anisotropy of magnetic susceptibility. Rev. Geophys. 30, 209–226.

Ron, H., Freund, R., Garfunkel, Z., Nur, A., 1984. Block rotation by strike-slip faulting: Structural and paleomagnetic evidence. J. Geophys. Res. Solid Earth 89, 6256–6270.

Ron, H., Nur, A., Eyal, Y., 1990. Multiple strike-slip fault sets: A case study from the Dead Sea Transform. Tectonics 9, 1421–1431.

Rossetti, F., Nasrabady, M., Vignaroli, G., Theye, T., Gerdes, A., Razavi, M.H., Vaziri, H.M., 2010. Early Cretaceous migmatitic mafic granulites from the Sabzevar range (NE Iran): implications for the closure of the Mesozoic peri-Tethyan oceans in central Iran. https://doi.org/10.1111/j.1365-3121.2009.00912.x

Rusnak, G.A., 1957. The Orientation of Sand Grains under Conditions of" Unidirectional" Fluid Flow: 1. Theory and Experiment. J. Geol. 65, 384–409.

Ruttner, A.W., 1993. Southern borderland of Triasic Laurasia in NE Iran. Geol. Rundschau 82, 110–120.

Ruttner, A.W., 1991. Geology of the Aghdarband Area (Kopet Dagh, NE-lran), The Triassic of Aghdarband (AqDarband), NE-Iran, and its Pre-Triassic Frame.

Saccani, E., Delavari, M., Beccaluva, L., Amini, S., 2010. Petrological and geochemical constraints on the origin of the Nehbandan ophiolitic complex (eastern Iran): Implication for the evolution of the Sistan Ocean. Lithos 117, 209–228.

Sagnotti, L., Speranza, F., 1993. Magnetic fabric analysis of the Plio-Pleistocene clayey units of the Sant'Arcangelo Basin, southern Italy. Phys. Earth Planet. Inter. 77, 165–176.

Sagnotti, L., Speranza, F., Winkler, A., Mattei, M., Funicello, R., 1998. Magetic fabric of clay sediments from the external northen Apennines (Italy). Phys. Earth Planet. Inter. 105, 73–93.

Schreurs, G., 1994. Experiments on strike-slip faulting and block rotation. Geology 22, 567–570.

Sengor, A.M., 1979. C. 1979. Mid-Mesozoic closure of Permo-Triassic Tethys and its implications. Nature 279, 590–593.

Şengör, A.M.C., Yılmaz, Y., Sungurlu, O., 1984. Tectonics of the Mediterranean Cimmerides: nature and evolution of the western termination of Palaeo-Tethys. Geol. Soc. London, Spec. Publ. 17, 77–112. https://doi.org/10.1144/GSL.SP.1984.017.01.04

Seyed-Emami, K., Fürsich, F.T., Wilmsen, M., 2003. Documentation and significance of tectonic events in the northern Tabas Block (east-central Iran) during the Middle and Late Jurassic. Riv. Ital. di Paleontol. e Stratigr. (Research Paleontol. Stratigr. 110.

Shabanian, E., 2012. Active tectonic study in northeast Iran: contribution of the Kopeh Dagh and Binalud mountains to the accommodation of the Arabia-Eurasia convergence 1–310.

Shabanian, E., Bellier, O., Abbassi, M.R., Siame, L., Farbod, Y., 2010. Plio-quaternary stress states in NE Iran: Kopeh Dagh and Allah Dagh-Binalud mountain ranges. Tectonophysics 480, 280–304.

Shabanian, E., Bellier, O., Siame, L., Arnaud, N., Abbassi, M.R., Cochemé, J.J., 2009a. New tectonic configuration in NE Iran: Active strike-slip faulting between the Kopeh Dagh and Binalud mountains. Tectonics 28, 1–29. https://doi.org/10.1029/2008TC002444

Shabanian, E., Siame, L., Bellier, O., Benedetti, L., Abbassi, M.R., 2009b. Quaternary slip rates along the northeastern boundary of the Arabia-Eurasia collision zone (Kopeh Dagh Mountains, Northeast Iran). Geophys. J. Int. 178, 1055–1077. https://doi.org/10.1111/j.1365-246X.2009.04183.x

Sharafi, M., Mahboubi, A., Ashuri, M., Rahimi, B., 2013. Journal of Asian Earth Sciences Sequence stratigraphic significance of sedimentary cycles and shell concentrations in the Aitamir Formation (Albian – Cenomanian), Kopet-Dagh Basin , northeastern Iran. J. Asian Earth Sci. 67–68, 171–186. https://doi.org/10.1016/j.jseaes.2013.02.025

Sheikholeslami, M.R., Kouhpeyma, M., 2012. Structural analysis and tectonic evolution of the eastern Binalud Mountains, NE Iran. J. Geodyn. 61, 23–46. https://doi.org/10.1016/j.jog.2012.06.010

Shor, A.N., Kent, D. V, Flood, R.D., 1984. Contourite or turbidite?: Magnetic fabric of fine-grained Quaternary sediments, Nova Scotia continental rise. Geol. Soc. London, Spec. Publ. 15, 257–273.

Soffel, H.C., Davoudzadeh, M., Rolf, C., 1989. Palaeomagnetic investigations on Phanerozoic formations from Iran: Reinterpretation of measurements between 1972 and 1982. Muenchner Geophys. Mitteilungen, Münchner Univers. Schriften 4, 23–56.

Soffel, H.C., Schmidt, S., Davoudzadeh, M., Rolf, C., 1996. New palaeomagnetic data from Central Iran and a Triassic palaeoreconstruction. Geol. Rundschau 85, 293–302. https://doi.org/10.1007/BF02422235

Soto, R., Kullberg, J.C., Oliva-Urcia, B., Casas-Sainz, A.M., Villalaín, J.J., 2012. Switch of Mesozoic extensional tectonic style in the Lusitanian basin (Portugal): Insights from magnetic fabrics. Tectonophysics 536, 122–135.

Soto, R., Larrasoaña, J.C., Arlegui, L.E., Beamud, E., Oliva-Urcia, B., Simón, J.L., 2009. Reliability of magnetic fabric of weakly deformed mudrocks as a palaeostress indicator in compressive settings. J. Struct. Geol. 31, 512–522.

Speranza, F., Sagnotti, L., Mattei, M., 1997. Tectonics of the Umbria-Marche-Romagna arc (central northern Apennines, Italy): New paleomagnetic constraints. J. Geophys. Res. Solid Earth 102, 3153–3166.

Stampfli, G.M., Borel, G.D., 2002. A plate tectonic model for the Paleozoic and Mesozoic constrained by dynamic plate boundaries and restored synthetic oceanic isochrons. Earth Planet. Sci. Lett. 196, 17–33.

Stern, D.P., 2002. A millennium of geomagnetism. Rev. Geophys. 40.

Stöcklin, J., 1974. Possible Ancient Continental Margins in Iran. Geol. Cont. Margins 873–887. https://doi.org/10.1007/978-3-662-01141-6_64

Taheri, J., Fürsich, F.T., Wilmsen, M., 2009. Stratigraphy, depositional environments and geodynamic significance of the Upper Bajocian–Bathonian Kashafrud Formation, NE Iran. Geol. Soc. London, Spec. Publ. 312, 205–218. https://doi.org/10.1144/SP312.10

Taira, a, 1989. Magnetic fabrics and depositional processes. Sediment. Facies Act. Plate Margin.

Taira, A., Scholle, P.A., 1979. Deposition of resedimented sandstone beds in the Pico Formation, Ventura Basin, California, as interpreted from magnetic fabric measurements. Geol. Soc. Am. Bull. 90, 952–962.

Tait, J.A., Bachtadse, V., Soffel, H., 1996. Eastern Variscan fold belt: paleomagnetic evidence for oroclinal bending. Geology 24, 871–874.

Tarling, D., Hrouda, F., 1993. Magnetic anisotropy of rocks. Springer Science & Business Media.

Tatar, M., Jackson, J., Hatzfeld, D., Bergman, E., 2007. The 2004 May 28 Baladeh earthquake (M w 6.2) in the Alborz, Iran: Overthrusting the South Caspian Basin margin, partitioning of oblique convergence and the seismic hazard of Tehran. Geophys. J. Int. 170, 249–261.

Tauxe, L., 2010. Essentials of paleomagnetism. Univ of California Press.

Terres, R.R., Luyendyk, B.P., 1985. Neogene tectonic rotation of the San Gabriel region, California, suggested by paleomagnetic vectors. J. Geophys. Res. Solid Earth 90, 12467–12484.

Torsvik, T.H., Cocks, L.R.M., Torsvik, T.H., Cocks, L.R.M., 2012. Geological Society , London , Special Publications The Palaeozoic palaeogeography of central Gondwana service Subscribe The Palaeozoic palaeogeography of central Gondwana. https://doi.org/10.1144/SP357.8

Vahidinia, M., Ardestani, M.S., 2017. Biostratigraphy of the Abderaz Formation Based on Heterohelicids , at Six Stratigraphical Sections in East and Center of the Kopeh-Dagh Sedimentary Basin , Northeastern of Iran 2017, 623–645. https://doi.org/10.4236/ijg.2017.84034

Van der Voo, R., 2005. Paleomagnetism of the Atlantic, Tethys and Iapetus oceans. Cambridge University Press.

Van Der Voo, R., Torsvik, T.H., 2012. The history of remagnetization of sedimentary rocks: deceptions, developments and discoveries. Geol. Soc. London, Spec. Publ. 371, SP371-2.

Vernant, P., Nilforoushan, F., Hatzfeld, D., Abbassi, M.R., Vigny, C., Masson, F., Nankali, H., Martinod, J., Ashtiani, A., Bayer, R., Tavakoli, F., Chéry, J., 2004. Present-day crustal deformation and plate kinematics in the Middle East constrained by GPS measurements in Iran and northern Oman. Geophys. J. Int. 157, 381–398. https://doi.org/10.1111/j.1365-246X.2004.02222.x

Walker, R., Jackson, J., 2004. Active tectonics and late Cenozoic strain distribution in central and eastern Iran. Tectonics 23, 1–24. https://doi.org/10.1029/2003TC001529

Walker, R., Jackson, J., Baker, C., 2003. Surface expression of thrust faulting in eastern Iran : source parameters and surface deformation of the 1978 Tabas and 1968 Ferdows earthquake sequences 749–765.

Walters, R.J., Elliott, J.R., Li, Z., Parsons, B., 2013. Rapid strain accumulation on the Ashkabad fault (Turkmenistan) from atmosphere-corrected InSAR 118, 3674–3690. https://doi.org/10.1002/jgrb.50236

Weil, A.B., Sussman, A.J., 2004. Classifying curved orogens based on timing relationships between structural development and vertical-axis rotations. Orog. curvature Integr. Paleomagn. Struct. Anal. 383, 1–16.

Weil, A.B., Yonkee, A., 2009. Anisotropy of magnetic susceptibility in weakly deformed red beds from the Wyoming salient, Sevier thrust belt: Relations to layer-parallel shortening and orogenic curvature. Lithosphere 1, 235–256. https://doi.org/10.1130/L42.1

Weil, A.B., Yonkee, W.A., 2012. Layer-parallel shortening across the Sevier fold-thrust belt and Laramide foreland of Wyoming: Spatial and temporal evolution of a complex geodynamic system. Earth Planet. Sci. Lett. 357–358, 405–420. https://doi.org/10.1016/j.epsl.2012.09.021

Wells, R.E., Hillhouse, J.W., 1989. Paleomagnetism and tectonic rotation of the lower Miocene Peach Springs Tuff: Colorado Plateau, Arizona, to Barstow, California. Geol. Soc. Am. Bull. 101, 846–863.

Wensink, H., 1982. Tectonic inferences of paleomagnetic data from some Mesozoic formations in central Iran. J. Geophys. FUR Geophys. 51, 12–23.

Wensink, H., Varekamp, J.C., 1980. Paleomagnetism of basalts from Alborz: Iran part of Asia in the Cretaceous. Tectonophysics 68, 113–129.

Wilmsen, M., Fürsich, F.T., Majidifard, M.R., 2015. An overview of the Cretaceous stratigraphy and facies development of the Yazd Block, western Central Iran. J. Asian Earth Sci. 102, 45–72. https://doi.org/10.1016/j.jseaes.2014.07.015

Wilmsen, M., Fürsich, F.T., Majidifard, M.R., 2013. The Shah Kuh Formation, a latest Barremian - Early Aptian carbonate platform of Central Iran (Khur area, Yazd Block). Cretac. Res. 39, 183–194. https://doi.org/10.1016/j.cretres.2012.02.013

Wilmsen, M., Fürsich, F.T., Seyed-Emami, K., Majidifard, M.R., 2009a. An overview of the stratigraphy and facies development of the Jurassic System on the Tabas Block, east-central Iran. Geol. Soc. London, Spec. Publ. 312, 323–343. https://doi.org/10.1144/SP312.15

Wilmsen, M., Fürsich, F.T., Seyed-Emami, K., Majidifard, M.R., Taheri, J., 2009b. The Cimmerian Orogeny in northern Iran: Tectono-stratigraphic evidence from the foreland. Terra Nov. 21, 211–218. https://doi.org/10.1111/j.1365-3121.2009.00876.x

Wilmsen, M., Fürsich, F.T., Taheri, J., 2009c. The Shemshak Group (Lower–Middle Jurassic) of the Binalud Mountains, NE Iran: stratigraphy, depositional environments and geodynamic implications. Geol. Soc. London, Spec. Publ. 312, 175–188. https://doi.org/10.1144/SP312.8

Wilmsen, M., Wiese, F., Seyed-Emami, K., Fürsich, F.T., 2005. First record and significance of Turonian ammonites from the Shotori Mountains, east-central Iran. Cretac. Res. 26, 181–195.

https://doi.org/10.1016/j.cretres.2004.10.004

Witte, W.K., Kent, D. V, 1991. Tectonic implications of a remagnetization event in the Newark Basin. J. Geophys. Res. Solid Earth 96, 19569–19582.

Yeats, R., 2012. Active faults of the world. Cambridge University Press.

Zanchetta, S., Berra, F., Zanchi, A., Bergomi, M., Caridroit, M., Nicora, A., Heidarzadeh, G., 2013. The record of the Late Palaeozoic active margin of the Palaeotethys in NE Iran: Constraints on the Cimmerian orogeny. Gondwana Res. 24, 1237–1266. https://doi.org/10.1016/j.gr.2013.02.013

Zanchetta, S., Zanchi, A., Villa, I., Poli, S., Muttoni, G., 2009. The Shanderman eclogites: a Late Carboniferous high-pressure event in the NW Talesh Mountains (NW Iran). Geol. Soc. London, Spec. Publ. 312, 57–78. https://doi.org/10.1144/SP312.4

Zanchi, A., Berra, F., Mattei, M., Ghassemi, M.R., Sabouri, J., 2006. Inversion tectonics in central Alborz, Iran. J. Struct. Geol. 28, 2023–2037.

Zanchi, A., Malaspina, N., Zanchetta, S., Berra, F., Benciolini, L., Bergomi, M., Cavallo, A., Javadi, H.R., Kouhpeyma, M., 2015. The Cimmerian accretionary wedge of Anarak, Central Iran. J. Asian Earth Sci. 102, 45–72. https://doi.org/10.1016/j.jseaes.2014.08.030

Zanchi, A., Zanchetta, S., Balini, M., Ghassemi, M.R., 2016. Oblique convergence during the Cimmerian collision: Evidence from the Triassic Aghdarband Basin, NE Iran. Gondwana Res. 38, 149–170. https://doi.org/10.1016/j.gr.2015.11.008

Zanchi, A., Zanchetta, S., Berra, F., Mattei, M., Garzanti, E., Molyneux, S., Nawab, A., Sabouri, J., 2009a. The Eo-Cimmerian (Late? Triassic) orogeny in North Iran. Geol. Soc. London, Spec. Publ. 312, 31–55. https://doi.org/10.1144/SP312.3

Zanchi, A., Zanchetta, S., Garzanti, E., Balini, M., Berra, F., Mattei, M., Muttoni, G., 2009b. The Cimmerian evolution of the Nakhlak–Anarak area, Central Iran, and its bearing for the reconstruction of the history of the Eurasian margin. Geol. Soc. London, Spec. Publ. 312, 261–286. https://doi.org/10.1144/SP312.13

Zand-moghadam, H., Moussavi-harami, R., Mahboubi, A., Aghaei, A., 2016. Journal of African Earth Sciences Lithofacies and sequence stratigraphic analysis of the Upper Jurassic siliciclastics in the eastern Kopet-Dagh Basin , NE Iran. J. African Earth Sci. 117, 48–61. https://doi.org/10.1016/j.jafrearsci.2016.01.021

Zijderveld, J.D.A., 1967. The natural remanent magnetizations of the Exeter Volcanic Traps (Permian, Europe). Tectonophysics 4, 121–153. https://doi.org/10.1016/0040-1951(67)90048-0